

Spring 7-10-2017

Design and Experimental Investigation of 500kV Current Transformer Seismic Retrofit Utilizing Structure Rocking and Supplemental Damping with Self-Centering

Ilya S. Palnikov
Portland State University

Follow this and additional works at: https://pdxscholar.library.pdx.edu/open_access_etds



Part of the [Civil and Environmental Engineering Commons](#)

Let us know how access to this document benefits you.

Recommended Citation

Palnikov, Ilya S., "Design and Experimental Investigation of 500kV Current Transformer Seismic Retrofit Utilizing Structure Rocking and Supplemental Damping with Self-Centering" (2017). *Dissertations and Theses*. Paper 3673.

<https://doi.org/10.15760/etd.5557>

This Thesis is brought to you for free and open access. It has been accepted for inclusion in Dissertations and Theses by an authorized administrator of PDXScholar. Please contact us if we can make this document more accessible: pdxscholar@pdx.edu.

Design and Experimental Investigation of 500kV Current Transformer Seismic Retrofit
Utilizing Structure Rocking and Supplemental Damping with Self-Centering

by
Ilya S. Palnikov

A thesis submitted in partial fulfillment of the
requirements for the degree of

Master of Science
in
Civil and Environmental Engineering

Thesis Committee:
Peter Dusicka, Chair
Franz Rad
Leon Kempner
Evan Kristof

Portland State University
2017

ABSTRACT

Electrical substations perform a key role in electrical transmission and distribution; the ability for a substation to remain functional during and after a seismic event contributes significantly to the resilience of the clients supplied. Many legacy components currently installed in the main grid substations were designed with minimal consideration of lateral loads and are not qualified per IEEE693. One of the more critical high-voltage substation components that are vulnerable to earthquake damage is the 500kV freestanding current transformer (CT). The CT is particularly vulnerable due to the slenderness and mass distribution of the component. Current transformers are typically constructed from a combination of aluminum and brittle porcelain. Two novel retrofit measures were investigated utilizing base rocking and supplemental damping to reduce the seismic amplification in the CT while also potentially providing post-earthquake self-centering capability. The retrofit measures utilize both shift in system frequency and energy dissipation through supplemental damping to reduce seismic demands on the CT. The purpose of the research was to conceptually develop, detail design, analyze and experimentally validate the retrofit measures. A desired feature of the retrofit measures was for minimal or no residual displacement following the seismic event, which was implemented in the retrofit through a preloaded centering mechanism. Based on the analyses and experiments, the proposed retrofit measures exhibited significantly decreased demands on the CT and true self-centering.

ACKNOWLEDGEMENTS

I would first like to thank my advisor and committee chair, Dr. Peter Duscika for the experience and knowledge which was gained through the time spent in the iStar Laboratory. For the opportunity to get involved in research and contributing to society. Also, I would like to thank Dr. Peter Dusicka for assisting with funding through a GRA.

The research team acknowledges Bonneville Power Administration for making the research possible through their funding, input and expertise. Particularly we would like to thank Mr. Michael Riley and Dr. Leon Kempner for their guidance, suggestions, and technical contributions.

I would like to acknowledge Dr. Franz Rad and Evan Kristoff, J.D., for their questions and suggestions used to improve this thesis.

Additional appreciation is due to the staff and faculty at the University of Nevada, Reno (UNR) for accommodating part of the work to be conducted at their facility. We would like to thank Dr. Patrick Laplace for technical assistance and Dr. Sherif Elfass for administrative assistance at UNR. Also, we would like to thank Todd Lyttle and Chad Lyttle from UNR as well as Aaron Smith from PSU for lab floor assistance during the experimental portion at the University of Nevada, Reno.

Finally, I would like to thank my family for the support, love, care and guidance during my studies at Portland State University. I am thankful for their contributions to my success and support in both my undergrad and graduate studies. I am thankful for my wife's love and encouragement during the course of my entire education.

TABLE OF CONTENTS

Abstract	i
Acknowledgements	ii
Table of Contents	iii
List of Tables	vi
List of Figures	viii
1.0 Introduction.....	1
1.1 Research Objectives	5
1.2 Literature Review.....	5
1.2.1 Design Procedure for Controlled Rocking of Self-Centering Steel Frames.....	5
1.2.2 Displacement-Based Design of Precast Walls with Additional Dampers	7
1.2.3 Post-Tensioned Moment Connections with a Bottom Flange Device for Seismic Resistant Self-Centering MRFs.....	9
1.2.4 Self-Centering Seismic Lateral Force Resisting System: High Performance Structures for the City of Tomorrow	10
1.2.5 Mechanism of Energy Absorption in Special Devices for use in Earthquake Resistant Structures.....	12
1.2.6 Experimental/Numerical Study of U-Shape Flexural Plate (UFP) Dissipaters	14
2.0 Retrofit Back ground.....	18
3.0 Retrofit Configurations	24
3.1 Pre-Tension Members	25
3.2 Energy Dissipaters	28
4.0 U-Shape Design	31
4.1 UFP Theory and Application	31
5.0 General Numerical Model.....	35
5.1 Pedestal Modeling.....	35
5.2 Upper CT Mass	36
5.3 Foundation and Friction Modeling	38
5.4 Pre-Tension Model Application.....	40
5.5 Hysteretic Device Modeling	42
5.6 Viscous Damper Modeling	46
6.0 Parametric Study on Hysteretic Retrofit Parameters	49
6.1 Pre-Tension Force	49
6.2 Rocking Stiffness	50
7.0 Proof of Concept	52

8.0 Proof of Concept Test-Setup.....	53
9.0 Proof of Concept Results	55
10.0 Full-Scale Mass System Design.....	57
11.0 Full-scale Retrofit Design	60
11.1 Hysteretic Device	60
11.1.1 Elastic PT Member Design	60
11.1.2 PT Load Design	62
11.1.3 Hysteretic Device Design	67
11.1.4 SAP2000 Hysteretic Device Calibration	69
11.2 Viscous Damper Design.....	71
12.0 Full-scale Test Setup	78
12.1 Instrumentation.....	78
12.2 Fabricated Pedestal.....	84
12.3 Viscous Damper Configuration.....	85
12.4 Hysteretic Damper Configuration	86
12.5 Non-Retrofitted Configuration.....	88
13.0 Full-Scale Test Results	89
13.1 System Properties	89
13.2 Test Matrix	91
13.3 Viscous Damper Retrofit Results	92
13.3.1 Viscous Damper Table Response Spectrum.....	92
13.3.2 Viscous Damper System Damping & Free Vibration	95
13.3.3 Viscous Damper System Response	96
13.4 Hysteretic Device	106
13.4.1 Hysteretic Device Table Response Spectrum.....	106
13.4.2 Hysteretic Device System Damping & Free Vibration	109
13.4.3 Hysteretic Device System Response	110
13.5 Non-Retrofitted	126
13.5.1 Non-Retrofitted Table Response Spectrum.....	126
13.5.2 Non-Retrofitted System Damping & Free Vibration.....	128
13.5.3 Non-Retrofitted System Response.....	129
14.0 Numerical Model vs. Experimental Results	134
14.1 Viscous Damper Experimental Comparison to Numerical	134
14.2 Hysteretic Experimental Comparison to Numerical	136
14.3 Non-Retrofitted Experimental Comparison to Numerical	138

15.0 Economic Comparison.....	140
16.0 Full-scale Retrofit Comparison and Summary	142
17.0 Recommendations	146
18.0 References	147
19.0 Appendix A.....	150
20.0 Appendix B	152
21.0 Appendix C	157
22.0 Appendix D.....	162
23.0 Appendix E	178
24.0 Appendix F.....	182
25.0 Appendix G.....	189
26.0 Appendix H.....	197
27.0 Appendix I.....	210
28.0 Appendix J	218
29.0 Appendix K	235
30.0 Appendix L	239

LIST OF TABLES

Table 11-1: Viscous Damper “c” Factor Study w/ $\alpha=1.0$ 74

Table 11-2: Viscous Damper “c” Factor Study w/ $\alpha=0.7$ 76

Table 12-1: Accelerometer and String Pot Locations 83

Table 13-1: Current Transformer Properties..... 90

Table 13-2: Pedestal Properties..... 90

Table 13-3: System Properties 91

Table 13-4: Viscous Damper -- Retrofit Damping and Fundamental Frequency.... 96

Table 13-5: Viscous Damper – System X Absolute Maximum Acceleration 97

Table 13-6: Viscous Damper – System Y Absolute Maximum Acceleration 98

Table 13-7: Viscous Damper – System Z Absolute Maximum Acceleration 98

Table 13-8: Viscous Damper – System Absolute Maximum Reactions..... 99

Table 13-9: Viscous Damper – System Maximum Displacement 20-65% Motions
..... 100

Table 13-10: Viscous Damper – System Maximum Displacement 70-100% Motions
..... 100

Table 13-11: Viscous Damper – System Residual Displacement 20-65% Motions
..... 100

Table 13-12: Viscous Damper – System Residual Displacement 70-100% Motions
..... 101

Table 13-13: Viscous Damper – Pedestal Absolute Maximum Strain 101

Table 13-14: Viscous Damper – Pedestal Residual Strain 102

Table 13-15: Viscous Damper – Damper Absolute Maximum Displacement 102

Table 13-16: Viscous Damper – Damper Residual Displacement 102

Table 13-17: Viscous Damper – Damper Maximum Force..... 103

Table 13-18: Viscous Damper – Damper Bracket Slip 104

Table 13-19: Viscous Damper – Maximum PT Force..... 104

Table 13-20: Viscous Damper – % PT Force Loss Post Motion..... 105

Table 13-21: Viscous Damper – Pedestal Rocking Uplift..... 105

Table 13-22: Viscous Damper – Maximum Base Plate Slip 106

Table 13-23: Viscous Damper – Relative Base Plate Movement Pre-Post Motion
..... 106

Table 13-24: UFP Retrofit Damping and Fundamental Frequency 110

Table 13-25: Hysteretic Device – System X Absolute Maximum Acceleration ... 111

Table 13-26: Hysteretic Device – System Y Absolute Maximum Acceleration ... 112

Table 13-27: Hysteretic Device – System Z Absolute Maximum Acceleration ... 114

Table 13-28: Hysteretic Device – 20-65% System Absolute Maximum Reactions
..... 116

Table 13-29: Hysteretic Device – 70-100% System Absolute Maximum Reactions
..... 117

Table 13-30: Hysteretic Device – System Maximum Displacement 20-70% Motions
..... 118

Table 13-31: Hysteretic Device – System Maximum Displacement 75-100%
Motions 118

Table 13-32: Hysteretic Device – System Residual Displacement 20-70% Motions	118
Table 13-33: Hysteretic Device – System Residual Displacement 75-100% Motions	119
Table 13-34: Hysteretic Device – Pedestal Absolute Maximum Strain	119
Table 13-35: Hysteretic Device – Pedestal Residual Strain	120
Table 13-36: Hysteretic Device – UFP Bracket Slip	120
Table 13-37: Hysteretic Device – UFP Absolute Maximum Displacement	121
Table 13-38: Hysteretic Device – UFP Residual Displacement	121
Table 13-39: Hysteretic Device – UFP Set Maximum Force	122
Table 13-40: Hysteretic Device – Maximum PT Force	122
Table 13-41: Hysteretic Device – % PT Force Loss Post Motion	123
Table 13-42: Hysteretic Device – Pedestal Rocking Uplift	124
Table 13-43: Hysteretic Device – Maximum Base Plate Slip	124
Table 13-44: Hysteretic Device – Relative Base Plate Movement Pre-Post Motion	125
Table 13-45: Non-Retrofitted System Damping and Fundamental Frequency	129
Table 13-46: Non-Retrofitted – System X Absolute Maximum Acceleration	129
Table 13-47: Non-Retrofitted – System Y Absolute Maximum Acceleration	130
Table 13-48: Non-Retrofitted – System Z Absolute Maximum Acceleration	130
Table 13-49: Non-Retrofitted – 20-50% System Absolute Maximum Reactions .	131
Table 13-50: Non-Retrofitted – System Maximum Displacement 20-50% Motions	131
Table 13-51: Non-Retrofitted – System Residual Displacement 20-50% Motions	132
Table 13-52: Non-Retrofitted – Pedestal Absolute Maximum Strain	132
Table 13-53: Non-Retrofitted – Pedestal Residual Strain	132
Table 13-54: Initial Anchor Loads	133
Table 13-55: Maximum Anchor Loads	133
Table 15-1: Viscous Damper Retrofit Cost Summary	140
Table 15-2: Hysteretic Device Retrofit Cost Summary	141
Table 16-1: Damping and Fundamental Frequency Comparison	142

LIST OF FIGURES

Figure 1-1: 500kV Current Transformer.....	2
Figure 1-2: IEEE693-0.5g PGA Design Spectrum (IEEE, 2006).....	4
Figure 1-3: Rocking Shear Wall Theoretical Diagram.....	8
Figure 1-4: Self-Centering MRF w/ Friction Damping.....	10
Figure 1-5: Life Time of Double Strip Test Apparatus (UFP).....	14
Figure 1-6: NZ2014 Testing Configuration and Results.....	15
Figure 1-7: NZ2014 Numerical and Experimental UFP Results.....	16
Figure 2-1: Theoretical Elastic Rocking.....	19
Figure 2-2: UFP Theoretical Hysteretic Behavior.....	21
Figure 2-3: Theoretical Rocking w/ Supplemental Damping.....	22
Figure 3-1: Rendering of Provided CT Pedestal.....	24
Figure 3-2: Proposed CFRP Configuration.....	26
Figure 3-3: Arrangement of Belleville Washers.....	27
Figure 3-4: BeS Stiffness and Displacement Relationship.....	27
Figure 3-5: Belleville Washer Dimensional Specifications.....	28
Figure 3-6: Base Retrofit w/ Taylor Viscous Dampers.....	29
Figure 3-7: Hysteretic Device Base Retrofit.....	29
Figure 3-8: Typical UFP Assembly.....	30
Figure 4-1: UFP Section Definition.....	32
Figure 4-2: Shear Couple and Plastic Moment.....	33
Figure 5-1: Pedestal SAP2000 Shell Model.....	35
Figure 5-2: Stick Model.....	36
Figure 5-3: Scaled Complete System Model.....	37
Figure 5-4: Full-scale Complete System Model.....	37
Figure 5-5: Restraints to Avoid Global Instability in SAP2000.....	38
Figure 5-6: Gap Link Properties.....	39
Figure 5-7: Gap Link Locations.....	39
Figure 5-8: Elastic PT Modeling Properties.....	40
Figure 5-9: PT Location on SAP2000 Model.....	41
Figure 5-10: Device Locations on SAP2000 Model.....	42
Figure 5-11: Wen-link Property Data.....	43
Figure 5-12: CSI Example 6-008 Wen-link Definition.....	44
Figure 5-13: Wen-link Directional Properties.....	45
Figure 5-14: Wen Model Calibration for PSU System.....	46
Figure 5-15: Damper- Exponential Link Properties.....	47
Figure 5-16: D-E Link Directional Properties.....	48
Figure 6-1: PT Force Influence on System Behavior.....	50
Figure 6-2: Rocking Stiffness Influence on System Behavior.....	51
Figure 7-1: Scaled Mass System.....	52
Figure 8-1: Scaled Mass System Test Setup.....	54
Figure 10-1: Mass Plate Mounting Detail.....	58
Figure 10-2: Designed Mass System.....	59
Figure 10-3: 500kV CT.....	59
Figure 11-1: Belleville Washers.....	61

Figure 11-2: Installed BeS	62
Figure 11-3: Rocking Initiation	63
Figure 11-4: PT Force Contribution	64
Figure 11-5: Hysteretic Device Response.....	64
Figure 11-6: Self-Centering System Response	65
Figure 11-7: a/b Ratio Comparison.....	66
Figure 11-8: Hysteretic Device Design Procedure	68
Figure 11-9: Full-Scale Wen-link Properties	70
Figure 11-10: Full-Scale Model Wen-link Response	70
Figure 11-11: Viscous Damper α Influence of Device Force.....	72
Figure 11-12: Viscous Damper "c" Factor Study w/ $\alpha=1.0$	73
Figure 11-13: Viscous Damper "c" Comparison w/ $\alpha=1.0$	74
Figure 11-14: Viscous Damper "c" Factor Study w/ $\alpha=0.7$	75
Figure 11-15: Viscous Damper "c" Comparison w/ $\alpha=0.7$	76
Figure 11-16: Viscous Damper Design Procedure	77
Figure 12-1: LVDT Locations on Pedestal Base	79
Figure 12-2: Strain Gauge Placement	81
Figure 12-3: Lumped Mass Method	82
Figure 12-4: Accelerometer & String Pot Locations	82
Figure 12-5: Instrumented Specimen.....	84
Figure 12-6: Viscous Damper Instrumentation.....	84
Figure 12-7: Hysteretic UFP Instrumentation.....	84
Figure 12-8: NW Viscous Damper	85
Figure 12-9: Retrofitted Base w/ Taylor Viscous Dampers.....	86
Figure 12-10: Installed Hysteretic UFP	87
Figure 12-11: Retrofitted Base w/ Hysteretic Device	87
Figure 12-12: Non-Retrofitted Base	88
Figure 13-1: Response Spectrum X (Viscous Damper).....	93
Figure 13-2: Response Spectrum Y (Viscous Damper).....	94
Figure 13-3: Response Spectrum Z (Viscous Damper).....	95
Figure 13-4: 100% 0.5g IEEE693 Y-System Response w/ Viscous Dampers	103
Figure 13-5: Hysteretic Device – Response Spectrum X	107
Figure 13-6: Hysteretic Device – Response Spectrum Y	108
Figure 13-7: Hysteretic Device – Response Spectrum Z.....	108
Figure 13-8: Hysteretic Device – System X Absolute Maximum Acceleration Plot	112
Figure 13-9: Hysteretic Device – System Y Absolute Maximum Acceleration Plot	113
Figure 13-10: Hysteretic Device – System Y Absolute Maximum Acceleration Plot	115
Figure 13-11: Non-Retrofitted – Response Spectrum X.....	127
Figure 13-12: Non-Retrofitted– Response Spectrum Y.....	127
Figure 13-13: Non-Retrofitted– Response Spectrum Z.....	128

Figure 14-1: Viscous Damper – 100% - X Experimental vs. Numerical Comparison	135
Figure 14-2: Viscous Damper –100% -Y Experimental vs. Numerical Comparison	136
Figure 14-3: Hysteretic Device – 100% - X Experimental vs. Numerical Comparison	137
Figure 14-4: Hysteretic Device – 100% - Y Experimental vs. Numerical Comparison	138
Figure 14-5: Non-Retrofitted – 40% - X Experimental vs. Numerical Comparison	139
Figure 14-6: Non-Retrofitted – 40% - Y Experimental vs. Numerical Comparison	139
Figure 15-1: Viscous Damper Retrofit Cost	140
Figure 15-2: Hysteretic Device Retrofit Cost	141
Figure 16-1: X - Retrofitted System Compared to Non-Retrofitted System	143
Figure 16-2: Y - Retrofitted System Compared to Non-Retrofitted System	144
Figure 19-1: Trench Support Pedestal	150
Figure 19-2: 226-293 Trench 500k V Current Transformer Specifications	151
Figure 25-1: Viscous Damper Retrofit X-Damping 20-50%	189
Figure 25-2: Viscous Damper Retrofit X-Damping 60-75%	190
Figure 25-3: Viscous Damper Retrofit X-Damping 85-95%	191
Figure 25-4: Viscous Damper Retrofit X-Damping 100%	192
Figure 25-5: Viscous Damper Retrofit Y-Damping 20-50%	193
Figure 25-6: Viscous Damper Retrofit Y-Damping 60-75%	194
Figure 25-7: Viscous Damper Retrofit Y-Damping 80-95%	195
Figure 25-8: Viscous Damper Retrofit Y-Damping 100%	196
Figure 26-1: 20% 0.5g IEEEE693 X-System Response w/ Viscous Dampers	197
Figure 26-2: 20% 0.5g IEEEE693 Y-System Response w/ Viscous Dampers	197
Figure 26-3: 20% 0.5g IEEEE693 NE Viscous Damper Response	198
Figure 26-4: 20% 0.5g IEEEE693 SE Viscous Damper Response	198
Figure 26-5: 20% 0.5g IEEEE693 SW Viscous Damper Response	199
Figure 26-6: 20% 0.5g IEEEE693 NW Viscous Damper Response	199
Figure 26-7: 50% 0.5g IEEEE693 X-System Response w/ Viscous Devices	200
Figure 26-8: 50% 0.5g IEEEE693 Y-System Response w/ Viscous Devices	200
Figure 26-9: 50% 0.5g IEEEE693 NE Viscous Damper Response	201
Figure 26-10: 50% 0.5g IEEEE693 SE Viscous Damper Response	201
Figure 26-11: 50% 0.5g IEEEE693 SW Viscous Damper Response	202
Figure 26-12: 50% 0.5g IEEEE693 NW Viscous Damper Response	202
Figure 26-13: 75% 0.5g IEEEE693 X-System Response w/ Viscous Devices	203
Figure 26-14: 75% 0.5g IEEEE693 Y-System Response w/ Viscous Devices	203
Figure 26-15: 75% 0.5g IEEEE693 NE Viscous Damper Response	204
Figure 26-16: 75% 0.5g IEEEE693 SE Viscous Damper Response	204
Figure 26-17: 75% 0.5g IEEEE693 SW Viscous Damper Response	205
Figure 26-18: 75% 0.5g IEEEE693 NW Viscous Damper Response	205
Figure 26-19: 100% 0.5g IEEEE693 X-System Response w/ Viscous Dampers	206

Figure 26-20: 100% 0.5g IEEEE693 Y-System Response w/ Viscous Dampers	206
Figure 26-21: 100% 0.5g IEEEE693 X-System Response w/ Viscous Dampers	207
Figure 26-22: 100% 0.5g IEEEE693 Y-System Response w/ Viscous Dampers	207
Figure 26-23: 100% 0.5g IEEEE693 NE Viscous Damper Response	208
Figure 26-24: 100% 0.5g IEEEE693 SE Viscous Damper Response	208
Figure 26-25: 100% 0.5g IEEEE693 SW Viscous Damper Response	209
Figure 26-26: 100% 0.5g IEEEE693 NW Viscous Damper Response	209
Figure 27-1: Hysteretic Device Retrofit X-Damping 20-50%	210
Figure 27-2: Hysteretic Device Retrofit X-Damping 60-75%	211
Figure 27-3: Hysteretic Device Retrofit X-Damping 80-95%	212
Figure 27-4: Hysteretic Device Retrofit X-Damping 100%	213
Figure 27-5: Hysteretic Device Retrofit Y-Damping 20-50%	214
Figure 27-6: Hysteretic Device Retrofit Y-Damping 60-75%	215
Figure 27-7: Hysteretic Device Retrofit Y-Damping 80-95%	216
Figure 27-8: Hysteretic Device Retrofit Y-Damping 100%	217
Figure 28-1: 20% 0.5g IEEEE693 X-System Response w/ Hysteretic Device	218
Figure 28-2: 20% 0.5g IEEEE693 X-System Response w/ Hysteretic Device	218
Figure 28-3: 20% 0.5g IEEEE693 NE Hysteretic Device Response	219
Figure 28-4: 20% 0.5g IEEEE693 SE Hysteretic Device Response	219
Figure 28-5: 20% 0.5g IEEEE693 SW Hysteretic Device Response	220
Figure 28-6: 20% 0.5g IEEEE693 NW Hysteretic Device Response	220
Figure 28-7: 50% 0.5g IEEEE693 X-System Response w/ Hysteretic Device	221
Figure 28-8: 50% 0.5g IEEEE693 Y-System Response w/ Hysteretic Device	221
Figure 28-9: 50% 0.5g IEEEE693 NE Hysteretic Device Response	222
Figure 28-10: 20% 0.5g IEEEE693 SE Hysteretic Device Response	222
Figure 28-11: 50% 0.5g IEEEE693 SW Hysteretic Device Response	223
Figure 28-12: 50% 0.5g IEEEE693 NW Hysteretic Device Response	223
Figure 28-13: 75% 0.5g IEEEE693 X-System Response w/ Hysteretic Device	224
Figure 28-14: 75% 0.5g IEEEE693 Y-System Response w/ Hysteretic Device	224
Figure 28-15: 75% 0.5g IEEEE693 NE Hysteretic Device Response	225
Figure 28-16: 75% 0.5g IEEEE693 SE Hysteretic Device Response	225
Figure 28-17: 75% 0.5g IEEEE693 SW Hysteretic Device Response	226
Figure 28-18: 75% 0.5g IEEEE693 NW Hysteretic Device Response	226
Figure 28-19: 100% 0.5g IEEEE693 X-System Response w/ Hysteretic Device	227
Figure 28-20: 100% 0.5g IEEEE693 X-System Response w/ Hysteretic Device	227
Figure 28-21: 100% 0.5g IEEEE693 Y-System Response w/ Hysteretic Device	228
Figure 28-22: 100% 0.5g IEEEE693 Y-System Response w/ Hysteretic Device	228
Figure 28-23: 100% 0.5g IEEEE693 NE Hysteretic Device Response	229
Figure 28-24: 100% 0.5g IEEEE693 SE Hysteretic Device Response	229
Figure 28-25: 100% 0.5g IEEEE693 SW Hysteretic Device Response	230
Figure 28-26: 100% 0.5g IEEEE693 NW Hysteretic Device Response	230
Figure 28-27: 100% 0.5g IEEEE693 X-System Response w/ Virgin Hysteretic Device	231
Figure 28-28: 100% 0.5g IEEEE693 X-System Response w/ Virgin Hysteretic Device	231

Figure 28-29: 100% 0.5g IEEE693 Y-System Response w/ Virgin Hysteretic Device	232
Figure 28-30: 100% 0.5g IEEE693 Y-System Response w/ Virgin Hysteretic Device	232
Figure 28-31: 100% 0.5g IEEE693 NE Virgin Hysteretic Device Response	233
Figure 28-32: 100% 0.5g IEEE693 SE Virgin Hysteretic Device Response	233
Figure 28-33: 100% 0.5g IEEE693 NE SW Virgin Hysteretic Device Response	234
Figure 28-34: 100% 0.5g IEEE693 NW Virgin Hysteretic Device Response	234
Figure 29-1: Non- Retrofitted X-Damping 20-50%	235
Figure 29-2: Non- Retrofitted X-Damping 50%	236
Figure 29-3: Non-Retrofitted Y-Damping 20-50%	237
Figure 29-4: Non- Retrofitted Y-Damping 50%	238
Figure 30-1: 20% 0.5g IEEE693 Non-Retrofitted X-System Response	239
Figure 30-2: 20% 0.5g IEEE693 Non-Retrofitted Y-System Response	239
Figure 30-3: 40% 0.5g IEEE693 Non-Retrofitted X-System Response	240
Figure 30-4: 40% 0.5g IEEE693 Non-Retrofitted Y-System Response	240

1.0 INTRODUCTION

The ability for a substation to function prior, during, and after a seismic event significantly influences individual consumers. Resilience of substations in a seismic event allows the consumers to utilize electricity rapidly after a natural disaster. Previous analysis of the individual components in the 115kV, 230kV, and 500kV substations indicated that the current transformers used in the 500kV main grid substations was extremely vulnerable to lateral forces. As part of the main grid system, interruption in service would affect many individual consumers. Current transformers typically have long lead times and are expensive to replace if damaged. Shown in Figure 1-1 is a typical 500kV current transformer used in a substation located in Wilsonville, Oregon. Typically, a 500kV CT weighs 5000 l.-7000 lb and has a total height of 27 ft-30 ft when assembled on a pedestal. The center of gravity of a typical 500kV CT is 20 ft -24 ft from the pedestal base.

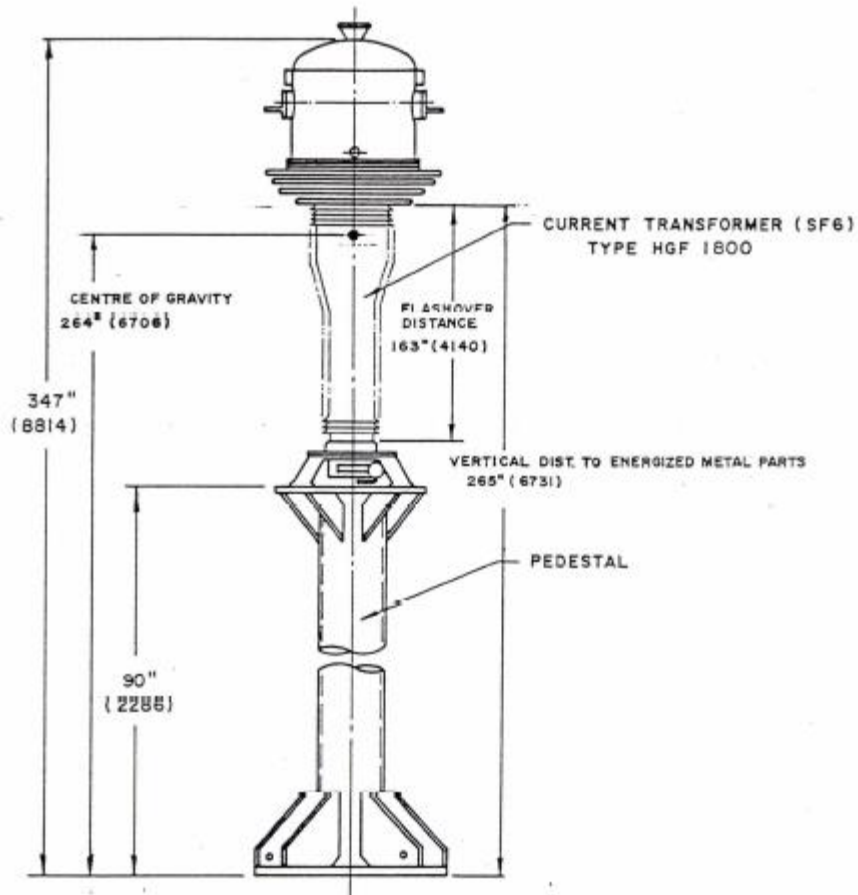
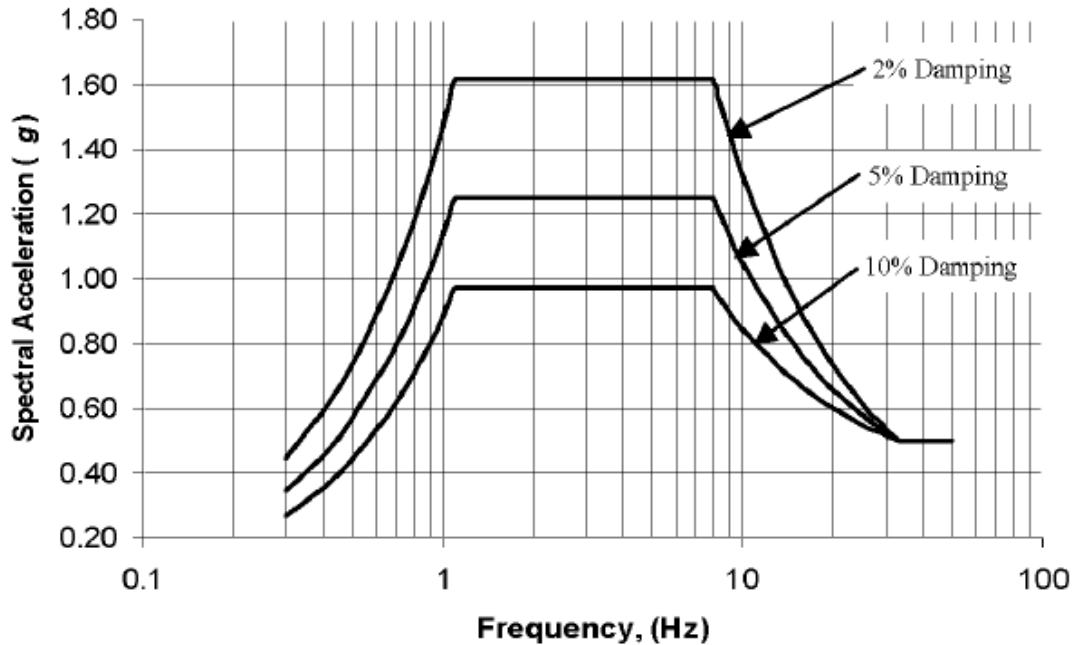


Figure 1-1: 500kV Current Transformer

If an as-built 500kV CT is exposed to IEEE693 qualification motion, the forces transmitted to the base of the bolted structure base will result in pedestal yielding and likely cause porcelain fracture. Various studies on rocking reinforced concrete shear walls, steel braced frames, and various forms of beam-column connections have shown promising results by decreasing forces. A combination of rocking, self-centering, and energy dissipation is proposed as a retrofit measure to mitigate structure damage. Rocking is utilized to shorten the natural frequency (elongate the period) of the system. As the system becomes more flexible due to base rocking, energy dissipaters are introduced to the system to control displacements of the structure. Pre-tensioning added

to the base of the CT allows the system to plumb after the motion has seized if all components are sized properly. As gaps form from the movement of the base plate, the system stiffness reduces and frequency shortens. By softening the global stiffness, the fundamental frequency of the system could be reduced and the demands decreased. Examining the 0.5g PGA IEEE693 design spectrum shown in Figure 1-2, reveals how decreasing the frequency below 1.1 Hz leads to sudden decreases in spectral acceleration. Likewise, additional damping further reduces the spectral acceleration of the system. Throughout the work described, 0.5g PGA IEEE693 motion is referred to as the 100% IEEE693 motion.



Spectral Accelerations, S_a (g), for Frequencies, f (Hz):

$$S_a = 1.144 \beta f \quad \text{for } 0.0 \leq f \leq 1.1$$

$$S_a = 1.25 \beta \quad \text{for } 1.1 \leq f \leq 8.0$$

$$S_a = (13.2 \beta - 5.28) / f - 0.4 \beta + 0.66 \quad \text{for } 8.0 \leq f \leq 33$$

$$S_a = 0.5 \quad \text{for } f > 33$$

$\beta = (3.21 - 0.68 \ln(d)) / 2.1156$, where d is the percent damping (2, 5, 10, etc.) and $d \leq 20\%$.

Figure 1-2: IEEE693-0.5g PGA Design Spectrum (IEEE, 2006)

The research conducted evaluates the effectiveness of a self-centering rocking system with supplemental damping. Two primary phases of the research were conducted; the initial phase was a scaled concept validation on a single directional shake table at Portland State University (PSU). The second phase of the work was performed on a full-scale representative CT model at the University of Nevada, Reno (UNR) on a 6 degree-of-freedom shake table (6-DOF). Two types of damping devices were investigated, viscous dampers and a hysteretic device. Taylor Devices fluid viscous dampers designed to the specific application were utilized as the first device type. The hysteretic device

used was u-shaped flexural plate (UFP). Component level modeling, global modeling, scaled testing, and full-scale testing was conducted to validate the proposed retrofit concepts.

1.1 Research Objectives

The primary objective of the research performed is to improve the seismic performance of the 500kV current transformers by reducing the demands on the CT components. BPA personnel would like the system to have no residual displacement after the seismic event. Two types of energy dissipating devices for the CT retrofit were considered; viscous and hysteretic. The retrofit measure aimed to reduce foundation anchor loads, decrease acceleration of the equipment, reduce forces on the pedestal, and reduce forces at the CT interface.

1.2 Literature Review

Discussed in this section are previous studies and publication on similar controlled rocking self-centering systems. Many studies and implementations of rocking systems have been complete on braced frames and shear wall in order to prevent structural damage and decrease demand on the system.

1.2.1 Design Procedure for Controlled Rocking of Self-Centering Steel Frames

The study (Eatherton, 2014) consisted of multiple experimental and computational phases in order to develop a self-centering rocking braced frame. The work summarizes the results obtained from the experimental and computation studies into design concept recommendations. Various arrangements of the pre-tension strands, fuses, and gap opening were shown for various height buildings. The authors state that as frame height

increases and slenderness decreases the higher modes will have a larger impact on structure response to seismic events.

The proposed design procedure for the fuse and PT design consider the first mode typically controlling base overturning for low-rise and midrise structures. The primary design parameter is the system overturning where the moment due to lateral loading must be less than the resisting PT and fuse resisting force. Key parameters and recommended considerations in design include initial uplift, fuse yielding, PT yielding, loss of self-centering capacity, and overall strength degradation.

Self-centering is the ability for a system to have minimal residual drift after the inertial loads are no longer present on the system. The authors introduce a self-centering ratio which is a ratio of the moment associated with rocking initiation to the fuse yielding moment. The ratio must be greater than unity for self-centering to occur. Although the ratio provides a metric for determining if self-centering occurs, it neglects effects of increasing PT force during loading and additional moment due to fuse hardening.

The author's design recommendations discuss a global uplift limit state that must be checked to ensure that global uplift will not occur. Global uplift is prevented when the total vertical load, including the PT force and dead load are greater than the upward force from the fuses.

The authors discuss the recommended minimum energy dissipation to avoid strength degradation and excessive structure drift. The energy dissipation ratio is defined as the ratio of the fuse moment to the bi-linear elastic system moment. The author states that previous research (Seo, 2005) suggests that the ductility demands between an elastic

perfectly plastic system and inelastic flag-shaped hysteretic system depend on the post-yield stiffness of the flag shape system. For system with a post-yield stiffness of 10% and 20% of the initial stiffness and energy dissipation ratios of 25% and 12.5% respectively, resulted in similar ductility demands to conventional systems. Previous research also suggested that for energy dissipation (ED) ratios above 25% of the peak drift was less sensitive to ED ratio. The author suggest using a minimum energy dissipation ratio of 25% unless the analysis to determine the drift demand explicitly considers damping.

Next, the authors discuss PT yield and fracture. The author suggests considering initial preloading of the member along with the expected uplift assuming rigid body motion to determine the strain in the members.

The authors state that the rocking typically only effects the first mode of the system and causes the forces to be reduced. Higher modes are not impacted by the rocking system and must be considered to properly estimate base shears and moments. In previous work on bridges, rocking columns had a significant impact on the system loading due to the high mass of the system, since the high weight of the bridge resulted in both lateral and vertical inertial effects with rocking columns. The authors state that for buildings the vertical inertial effects are less significant since the vertical mass contribution is less than bridges.

1.2.2 Displacement-Based Design of Precast Walls with Additional Dampers

The research by Pennucci (2009) tailors previously proposed displacement based design procedures to rocking precast walls with additional energy dissipating devices.

The proposed procedure is applied to multiple scenarios and validated through numerical analyses.

In order to limit costs of structure retrofit associated with damage due to seismic events in conventional construction, an alternative form of construction with precast concrete walls post-tensioned with partially unbounded cables is discussed in this work. Conventional construction typically results in permanent drift, structural damage, and high repair costs. A comparison between the system response in conventional construction, rocking structure, and rocking structure with supplemental damage is shown in Figure 1-3.

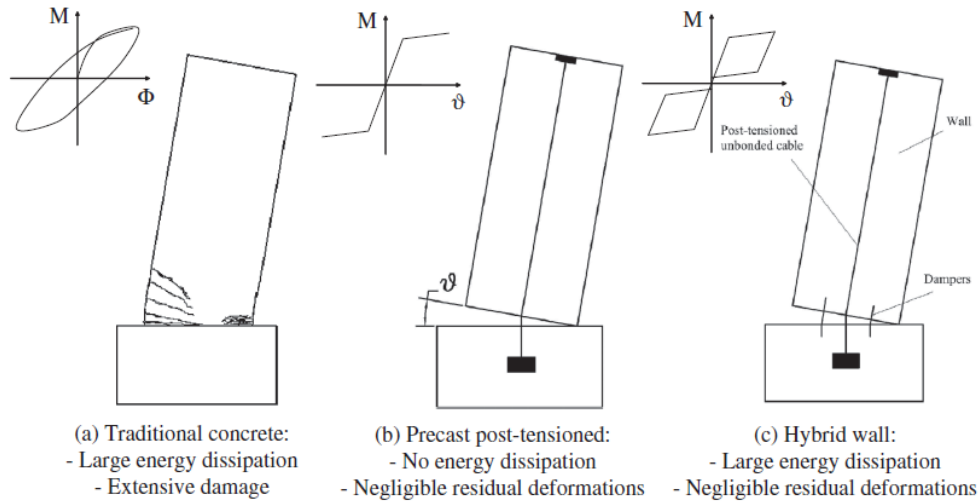


Figure 1-3: Rocking Shear Wall Theoretical Diagram

Rocking systems avoid plastic hinge formation and allow for concentration of inelasticity in replaceable fuses. The research conducted considers the use of steel dependent yielding dampers. The procedure includes the following steps: select design drift, define equivalent SDOF system, determine equivalent elastic damping, obtain design loads, and design based on capacity. The researchers refer to an a/b metric which

compares the restoring moment to the device moment used to characterize a systems self-centering capabilities (defined in Figure 11-7). The authors developed a damping-ductility curve for $\lambda=a/b=1.25$ used for estimating the equivalent viscous damping of the system. Although the maximum dissipation ratio occurs when $a/b=1.0$ or when the fuse and the restoring moment are equal, previous research indicated suggests that 1.25 be used to account for material over strength. The authors validated the recommended design procedure through numerical modeling and obtained similar results. The researchers recommend additional investigations on the systems response with three-dimensional excitation.

1.2.3 Post-Tensioned Moment Connections with a Bottom Flange Device for Seismic Resistant Self-Centering MRFs

Lehigh, Princeton, and Purdue Universities collaborated in development of a new earthquake-resistant structural steel moment resisting frame (MRF) through experimental and analytical research (Ricles, 2006). The work consisted of developing a self-centering moment resisting frame (SC-MRF) with additional energy dissipation through a friction device at the bottom beam flange. The authors state that in traditional MRFs, damage occurs to the structure and an alternative to weld construction is discussed.

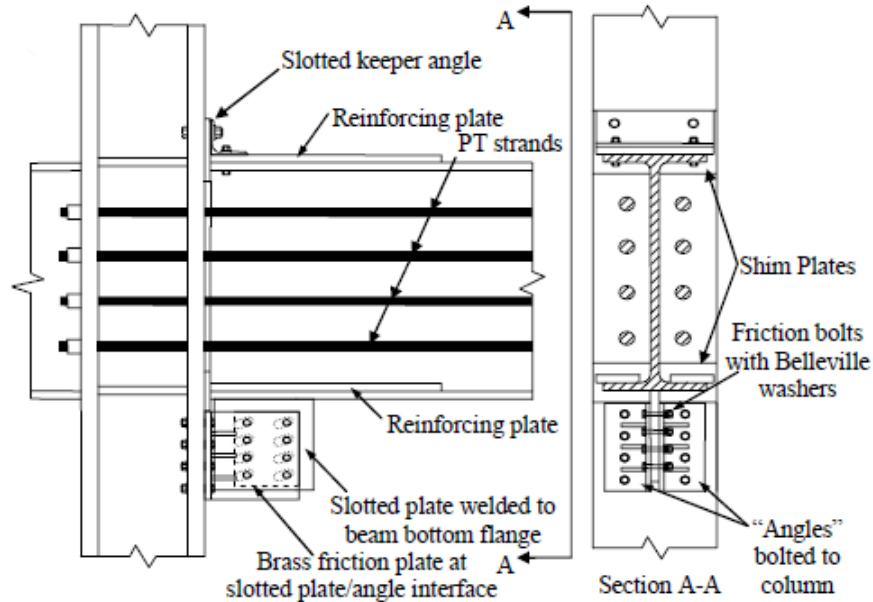


Figure 1-4: Self-Centering MRF w/ Friction Damping

The authors utilized AST B-19 UNS cartridge brass as the friction material which was positioned between two steel angles. The angle-brass friction interfaces were pre-compressed using Belleville disk spring washers. The self-centering mechanism was achieved through conventional PT strands as shown in Figure 1-4. Rotation at the connection leads to gap opening and displacement in the bottom flange friction device (BFFD). The authors used recommendations made by (Seo, 2005) and used an energy dissipation ratio of 0.25. The SC-MRF with a bottom flange friction device demonstrated sufficient energy dissipation and self-centering capabilities. Self-centering was achieved without residual drift when the PT strains remained elastic.

1.2.4 Self-Centering Seismic Lateral Force Resisting System: High Performance Structures for the City of Tomorrow

Four authors from three educational institutions explain self-centering seismic lateral force resisting systems and discussing the current challenges with self-centering system in (Chancellor, 2014). The authors discuss lateral force resisting systems that

reduce structural damage by softening the system through gap opening. Yielding devices or friction devices are used to dissipate energy through relative movement due to the gap opening.

The authors discuss conventional lateral systems which rely on damage of structural components in order to dissipate energy. For various conventional system, energy dissipation is achieved through plastic hinge formation, buckling of braces, or crushing and yielding in reinforced structures. Traditional lateral systems typically result in residual displacements after lateral loads are removed and structure damage. The authors discuss the large economic impact that the 6.3 magnitude earthquake had on Christchurch, New Zealand in 2011. The authors claim that the estimated repair costs are \$40 billion (NZD) not accounting for any economic losses associated with business downtime.

The authors state that conventional design approaches are inefficient in limiting structural damage and residual drift. Introduced by the researchers are the key components for a self-centering seismic lateral resisting system. The academics discuss the restoring force and gap opening mechanisms typically used in self-centering systems, which provide bilinear elastic self-centering but no energy dissipation. Previous research indicates that minimal energy dissipation is required to limit drift in a self-centering system to those of conventional elastic-plastic systems. Most self-centering systems have four limit states outlined by the authors: (1) PT decompression coupled energy dissipating device; (2) PT yielding; (3) limited damage to structural elements; and (4) severe damage to structural elements.

The investigators discuss four main challenges with self-centering systems, including component compatibility, higher mode effects, collapse assessment, and strategic implementation of self-centering. Due to the gap opening associated with rocking in self-centering system, detailing is of extreme importance for all components of the system. The authors discuss floor diaphragms and other connection complications associated with rocking systems. Limited research and knowledge is known on the effect of higher modes on self-centering systems. The authors state that base rocking only reduces forces in the first mode and additional softening locations along the length of the structure. The authors state that the approach appears promising but additional research must be conducted to determine the effectiveness of a multi-rocking system. The investigators also state that although self-centering systems are designed to reduce forces and minimize residual displacements, extreme earthquakes may cause permanent damage to the restoring mechanism and safety collapse assessments must be completed. The research also suggests performing life-cycle costs analysis to determine whether a self-centering system is worth the premium detail and construction costs compared to those of conventional systems.

1.2.5 Mechanism of Energy Absorption in Special Devices for use in Earthquake Resistant Structures

A paper by Kelly, Skinner, and Heine (1972) investigated methods for designing structures that dissipate kinetic energy due to ground motion. The authors state concern regarding conventional design where damage to structural components results in member capacity reductions. The authors propose adding additional members into structures for

the sole purpose of energy absorption. The academics explore rolling strips, torsion of square and rectangular bars, and the flexure of short thick beams.

The authors state that torsion was the most effective energy dissipating mechanism. Plastic strains from 3% to 12% and energy dissipation of 2000 lb in/in³ -7500 lb in/in³ per cycle was achieved in plastic torsion of mild steel. The devices dissipating energy through plastic torsion had lifespan within 100 cycles to 1000 cycles. In addition, the researchers stated that the torsional device had a gradual decay failure. The authors state that rolling strips and flexure of short thick beams dissipate less energy and are less reliable. The devices dissipated 500 lb -2000 lb in/in³ per cycle and had lifespans between 20 to 200 cycles. The rolling strips and flexure of short thick beams are more compact than the torsional devices.

The researchers tested a range of steel strip geometries made of mild steel and stainless steel. The strips were all 9 mm (0.354 in.) wide and ranged in thickness from 0.75 mm (0.029 in.) to 2.0 mm (0.079 in.). Four diameters were used for the bent strips, 9 mm (0.354 in.), 11mm (0.43 in.), 13 mm (0.511 in.), and 15 mm (0.59 in.). All plates were cold rolled and tested under displacement control. The devices would kink and then completely fracture. The academics state that the stroke and the level of maximum strain dictate the lifespan of the device. Device stroke should be near πR to maximum the energy dissipation, but should not exceed πR . A summary provided by the authors relates the maximum strain, normalized stroke and lifespan shown in Figure 1-5. The researchers also discuss the results obtained from torsional and flexural dissipaters which are not

implemented in the research discussed due to the required compactness of the energy dissipating devices.

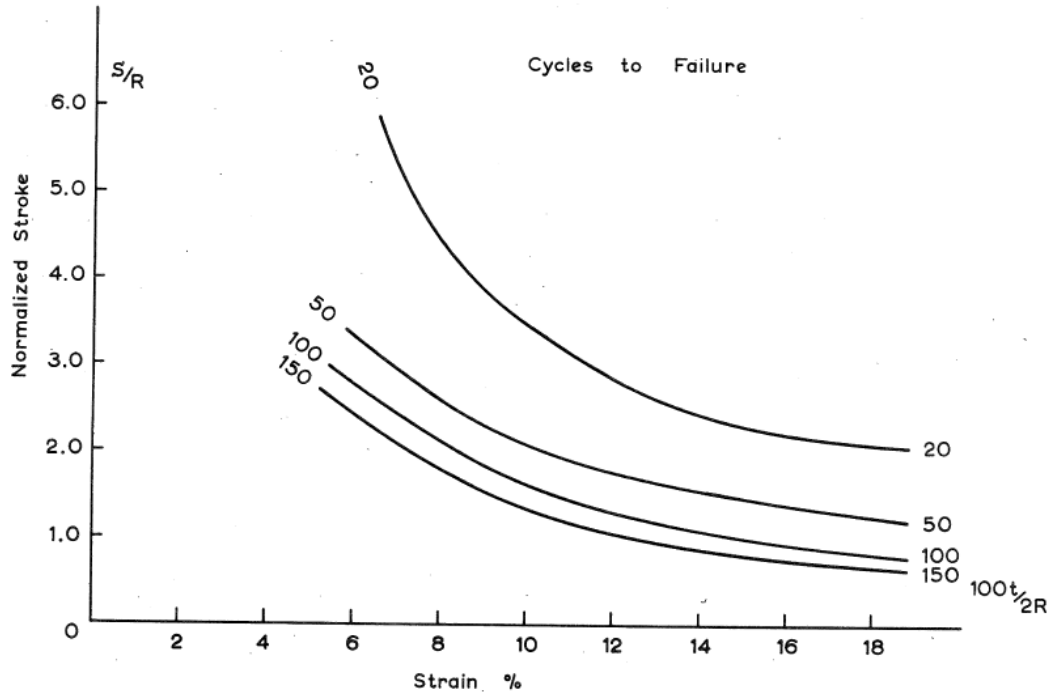


Figure 1-5: Life Time of Double Strip Test Apparatus (UFP)

1.2.6 Experimental/Numerical Study of U-Shape Flexural Plate (UFP) Dissipaters

The Christchurch earthquake resulted in increase in interest in structures that have low damage according to (Baird, 2014). Low damage structures minimize the need of repairs after events and allow for immediate occupancy. Low damage structures concentrate all non-linear behavior into replaceable components rather than relying on structural member yielding for energy dissipation. The authors use U-shape flexural plate (UFP) dissipaters because they are simple to design, inexpensive, versatile, and replaceable. The researchers state that limited information on UFPs is available regarding initial and post-yield stiffness. The author summarizes the work performed in Kelly,

Skinner, and Heine (1972) where the equations for UFP capacity and max strain were derived.

The authors apply Castigliano's Second Theorem in order to derive the initial stiffness of a UFP. Shown in (1) is the derived equation the author presents.

$$k_0 = \frac{F_y}{\Delta_y} = \frac{16Eb_u}{27\pi} \left(\frac{t_u}{D_u}\right)^3 \quad (1)$$

The academics performed a series of experimental tests using ACI loading recommendations. The loading protocol consisted of multiple amplitude displacements, three cycles at each amplitude and a maximum amplitude of 82.5mm. The experimental results were compared to the model outputs developed in the research. The UFPs had the following properties $d_i=120$ mm, $b=8$ mm, $F_y=6.4$ kN, $F_p=9.6$ kN and a leg length of 100 mm. The maximum strain for the UFP geometry was determined to be 6.3%. The authors state that they expected more than 150 cycles for the specified geometry based on the limited data summarized in Kelly, Skinner, and Heine (1972). Testing Configuration and Results are shown in Figure 1-6.

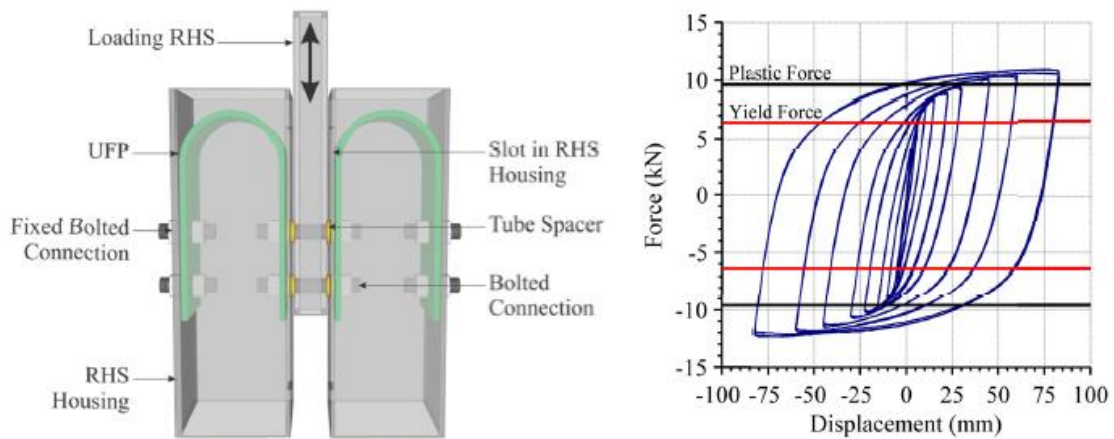


Figure 1-6: NZ2014 Testing Configuration and Results

ABAQUS finite element models were constructed with similar geometries to the experimental UFPs. The model utilized tetrahedral elements with isotropic yielding and cyclic hardening. The model material properties were based on a tensile coupon of the steel used for the UFPs. Shown in Figure 1-7 are the results obtained by the researchers. The authors accurately modeled the post-yield stiffness and maximum forces in the UFP. The model did not accurately capture the Bauschinger effect in the steel, resulting in a larger energy area than determined from experimental results.

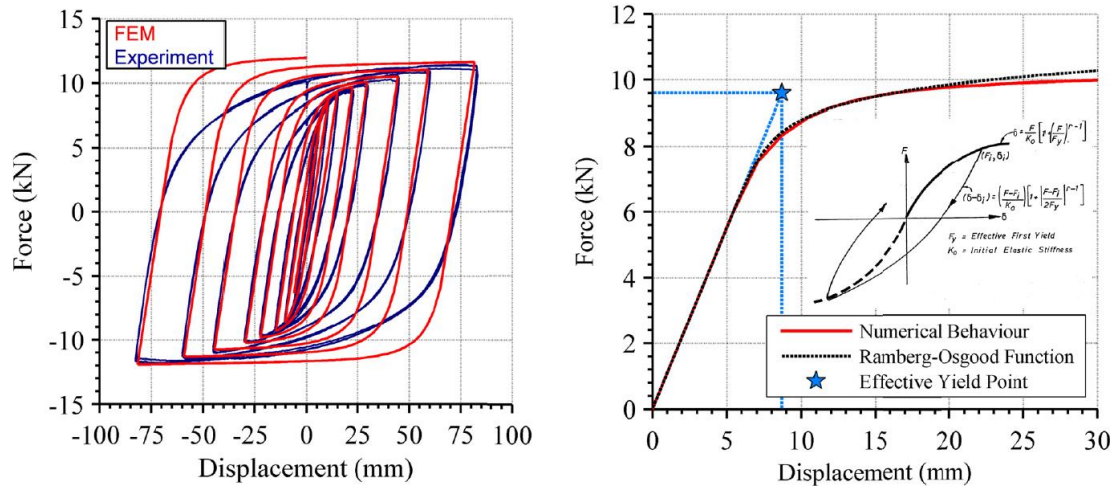


Figure 1-7: NZ2014 Numerical and Experimental UFP Results

A UFP parametric investigation was conducted using finite element modeling that was developed based on the experimental results. Plate thickness and diameter of the UFP were investigated to determine the influence on yield force, yield displacement, initial stiffness and post-yield stiffness. The Ramberg-Osgood function was used to fit the results and found to have an excellent representation of the behavior as shown in Figure 1-7. Based on the results obtained from numerical analysis, the author suggests the relationship shown in (2) for defining the Ramberg-Osgood R factor.

$$R = 7.1 \ln \left(\frac{t_u}{D_u} \right) + 29.5 \quad (2)$$

The researchers state that high levels of accuracy were observed between the experimental and numerical results. Also, the post-yield stiffness was well represented with the Ramberg-Osgood function and the recommend function is proposed for determine the R factor.

2.0 RETROFIT BACKGROUND

Based on the objectives of this research, a self-centering rocking system with supplemental damping is proposed to reduce demands on the 500kV Current Transformers. The proposed system utilizes reduction in stiffness, energy dissipation, and elastic pre-tensioned members (PT) to reduce demands on the CT while eliminating residual displacements.

The retrofitted CT consists of three primary components: elastic structure, elastic pre-tensioned members, and energy dissipating device which significantly influence the behavior of the system during a seismic event.

Understanding the fundamentals of the elastic and non-linear components is the key to designing a self-centering rocking system. Illustrated in Figure 2-1, is the idealized bilinear elastic load-deformation curve of a rocking system's response. When a system is pre-tensioned with elastic members, the system stiffness could be assumed to be equal to the bolted stiffness structure until uplift occurs. The initial stiffness, K_f , is the flexural stiffness of the bolted structure shown in the diagram from (a) to (b) and on the reversal cycle from (g) to (i). Before the pre-tensioned components are decompressed, the flexural stiffness controls the system response. The force required for uplift to occur is controlled by adjusting the pre-tension force. For the work conducted, two metrics were used to determine the decompression load, wind load and target maximum acceleration. Once the decompression force is overcome, any additional load causes uplift and results in system frequency shift. When uplift occurs (b), the stiffness reduces to K_{PT} based on the stiffness of the pre-tension members. By reducing the global stiffness, the demand on the structure's components is reduced, but displacements increase. The equivalent stiffness of

the system varies with displacement, typically equivalent stiffness decreases as the displacement increases.

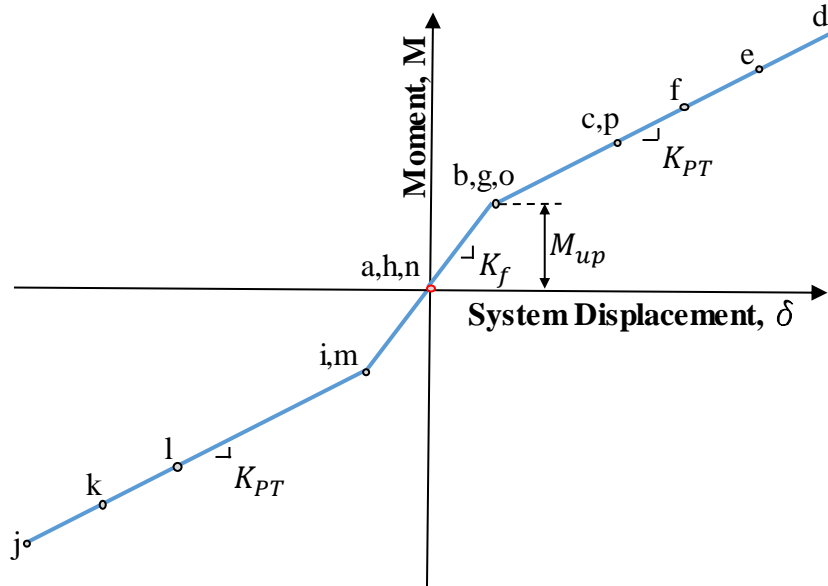


Figure 2-1: Theoretical Elastic Rocking

As the equivalent stiffness of the structure decreases, the displacement of the system increases. Energy dissipating devices are introduced to reduce system displacements and concentrate the non-linearities of the systems response into the energy dissipating devices. Two types of energy dissipating devices were investigated, Taylor Devices fluid viscous dampers and hysteretic yielding devices.

A fluid viscous damper dissipates energy by forcing fluid through orifices from one chamber to another. As the fluid travels through the orifices, the kinetic energy from the relative velocity is converted to thermal energy which is absorbed and dissipated by the damper. The size of the orifices control the amount of force produced. Viscous dampers are velocity dependent, the force developed is proportional to the relative velocity of the damper end constrains. Viscous damper coefficients are based on three main parameters,

velocity at the location of the device, global displacement, and device force at max velocity. Each parameter is interconnected and the properties are typically iterated until a desirable medium is met for all the design parameters. General equation used for determining the force in the device is defined in (3).

$$F = C \cdot v^\alpha \tag{3}$$

F = Damper Force (lb)

C = Damping Constant (lb-sec/in)

v = Velocity (in/sec)

α = Velocity Exponent ($0.3 < \alpha < 1.0$)

After a seismic event, when relative velocity is near zero, self-centering could be achieved by the pre-tensioned members. Viscous dampers act out of phase to the structure's displacement. Unlike velocity dependent viscous dampers, hysteretic devices develop residual forces in the devices after the lateral inertial loads are no longer present, due to elasto-plastic deformation, which must be considered when designing the self-centering system. Also, when removing yielded devices, the developed residual forces must be considered.

Hysteretic devices use material non-linearity, yielding of material to dissipate energy. Many forms of hysteretic devices have been evaluated for stable and repeatable properties. Used in the research, are u-shape flexural plates which yield when relative displacement between the two legs occurs, the plate steel is rolled and energy is dissipated.

The UFP is designed based on the initial pre-tension force and structure weight to ensure self-centering after a seismic event. If the hysteretic device capacity is larger than

initiates. From (b) to (c) the stiffness of the system is a combination of damper yield stiffness (K_d) and PT stiffness(K_{PT}) defined as K_2 . From (c) to (d) the plastic damper deforms with stiffness (K_y) and PT elongates elastically (K_{PT}) defined as K_3 . UFPs typically present relatively low post-yield stiffness compared to their initial stiffness.

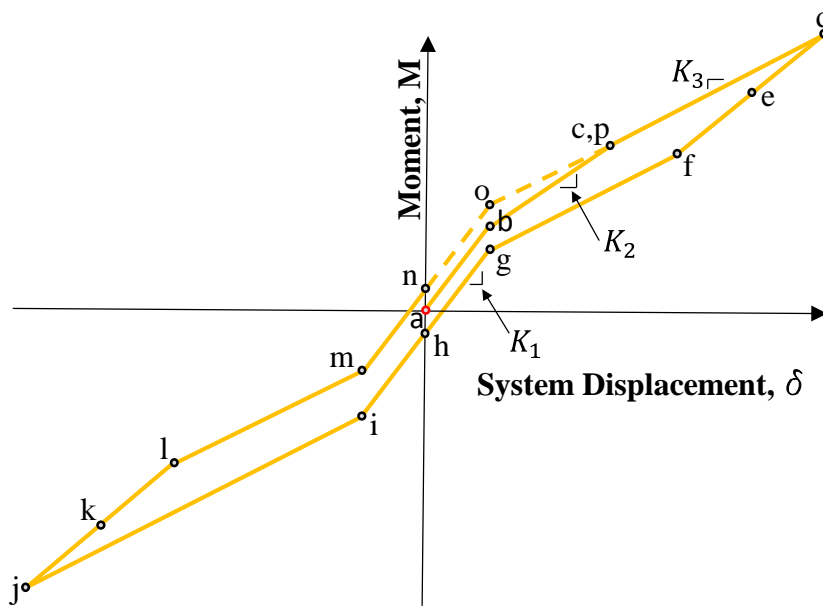


Figure 2-3: Theoretical Rocking w/ Supplemental Damping

When the system is unloaded, (d) to (f), the system deforms following K_2 . Once the damper has yielded in the opposite direction (f), the system follows K_3 until the base plate and damper are in their initial positions (g). The system then is allowed to recover its flexural deformation (g) to (h) following K_1 . Although no external force is present at (h) the hysteretic devices produce locked-moments in the system when returned to its initial position by the PT members.

The moment produced by the PT elements must always be greater than the moment required to yield the dampers back to their original position. If the elastic moment is less

than the moment required to yield the fuse elements back to their original position, the system will not plumb.

Two main differences are expected in the dynamic characteristics of the viscous dampers and the hysteretic devices. While both devices are expected to reduce displacement of the system, the viscous devices are expected to be more effective at small levels of excitation. At low excitations, the hysteretic devices will remain elastic and are expected to minimally contribute to damping. Taylor viscous dampers dissipate energy whenever any relative velocity is present on the shaft. Another important difference is viscous dampers are out of phase with structural stresses. Out of phase damping typically leads to lower demand on structural members.

3.0 RETROFIT CONFIGURATIONS

Legacy current transformers are typically installed on pedestals supplied by the manufacturer of the electrical component. Both the pedestal and the porcelain CT were designed with minimal considerations to lateral loads. The proposed retrofit aims to reduce demand on all components of the current transformer. Reduced demand in anchors, support pedestal, and porcelain members are expected from the retrofitted CT.

Supplied by BPA was a typical support pedestal used to install 500kV CTs, complete details on the pedestal are shown in Figure 19-1. The support structure has a 1-1/8" base plate that is 30" square. Each corner of the base plate has 1-15/16" holes drilled for anchoring the support. Two stiffeners are located 4" apart from each other. Shown in Figure 3-1, is the type of CT pedestal provided. The pedestal has 8 existing stiffeners which are utilized for mounting brackets for both the viscous and hysteretic devices. The retrofit method could be applied to other pedestal geometries although custom brackets and other modifications to the retrofit will be required.

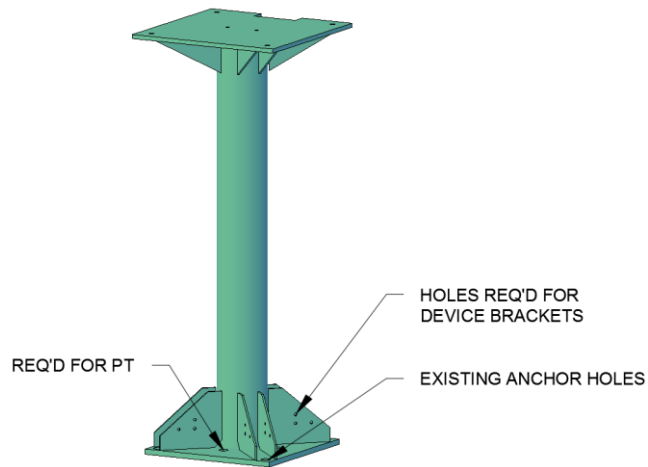


Figure 3-1: Rendering of Provided CT Pedestal

3.1 Pre-Tension Members

Numerous material types were considered for the elastic self-centering mechanism of the CT retrofit. Factors that dictated the material or device used to generate the system restoring force included the pedestal geometry, stiffness of the material, and ease of application. Conventional pre-tensioning strands were initially investigated but their high stiffness and maximum elongation did not meet the desirable traits for the application. A desired characteristic of the elastic self-centering device is low stiffness while accommodating the displacement demands of the system.

Next, Carbon Fiber Reinforced Polymer (CFRP) Bar Aslan 200/250 series pre-tension bars were investigated because of two specific properties that the material exhibits: the high ultimate stress and the modulus of elasticity. A high ultimate stress along with a lower modulus of elasticity allows for a smaller area of PT to be used and longer material elongation to occur. The smaller area allows for a reduced axial stiffness and overall reduction in stiffness once the system begins to rock. Aslan 200/250 material has a modulus of elasticity of 18,000 ksi, ultimate strain of 1.67%-1.75% and a guaranteed tensile strength of 300 ksi-315 ksi (Aslan FRP, 2011).

Typically, steel PT strands could reach strains of 0.8-1% at yield and have a modulus of elasticity of 27,000 ksi-28,000 ksi. The CFRP material could handle forces of 24% more than steel with similar axial stiffness; likewise, the CFRP members could elongate 12% more than an equivalently stiff steel member assuming a yield strain of 0.008 for steel pre-tension strands. Shown in Figure 3-2 was the original retrofit concept utilizing CFRP.

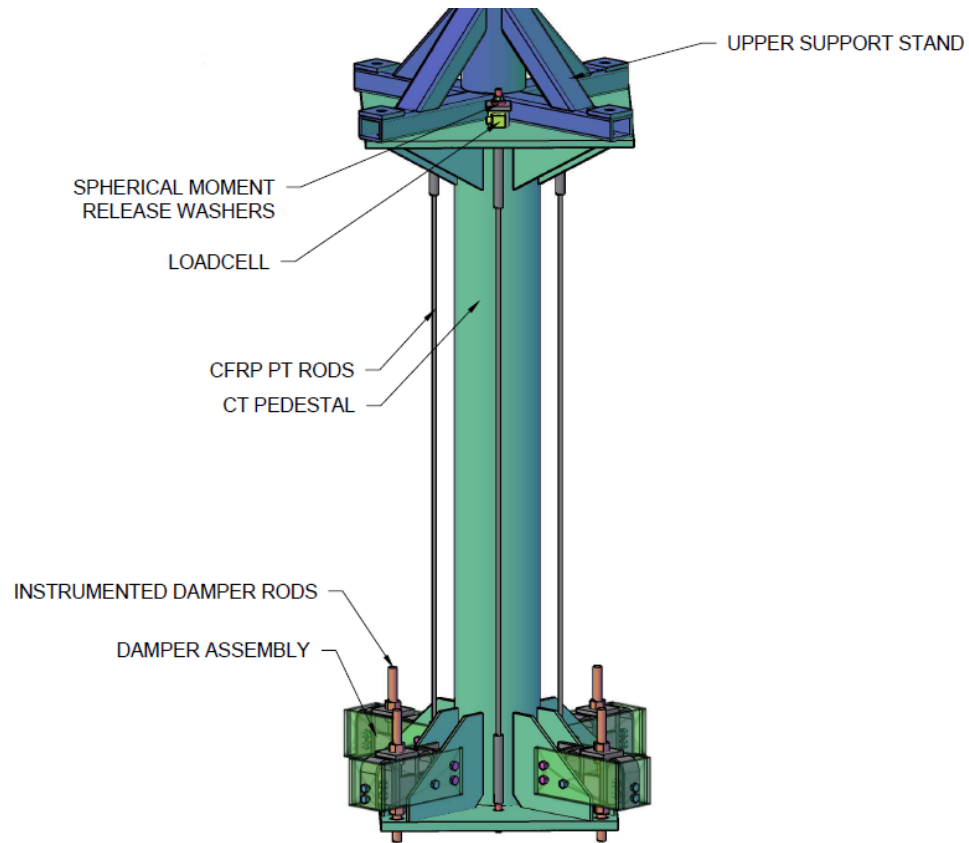


Figure 3-2: Proposed CFRP Configuration

CFRP presented two properties which made CFRP an unattractive choice for the retrofit, brittle behavior and difficulty of implementation. Belleville Spring Washers (BeS) were chosen as the restoring device for the retrofit because of their stiffness and displacement versatility and ease of application in the design. BeS washers are spherically shaped washers which could be arranged in parallel or series arrangements to achieve the desired stroke and stiffness. Obtained from the Solon Manufacturing Co. catalog is Figure 3-3 and Figure 3-4 which shows the various arrangements of Belleville Spring Washers to achieve the desirable stiffness. Solon also provides design guides for using Belleville Spring Washers to maintain bolt preload.

- A. Single, one spring.
- B. Parallel, all springs stacked the same way.
- C. Series, all springs stacked opposing each other.
- D. Parallel-Series, a combination of the two.

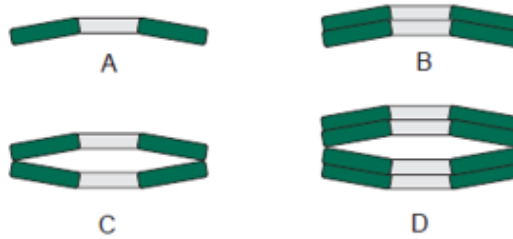


Figure 3-3: Arrangement of Belleville Washers

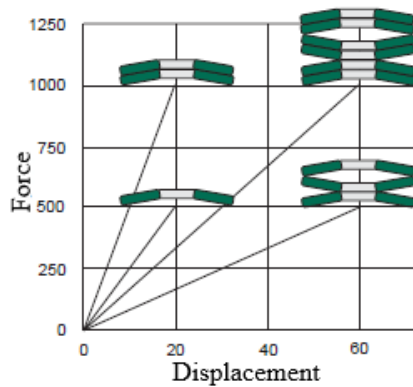


Figure 3-4: BeS Stiffness and Displacement Relationship

Belleville Spring Washers are linear for 90% of their total flat load. After 90%, the stiffness of the washer set starts to increase until the flat load is achieved. At the flat load the threaded rod which is used to transfer the load to the foundation will feel the load directly. Stiffness of the system significantly increases if the system experiences displacements larger than the BeS could occupy. One major advantage of the BeS system compared to the CFRP strands is that collapse is prevented when the displacement exceeds the designed displacement. Typical specifications for Belleville washers are shown in Figure 3-5 obtained from Solon Mfg.

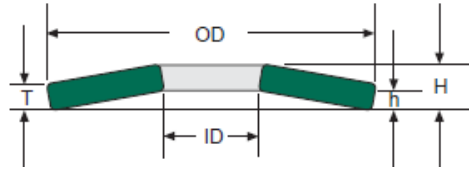


Figure 3-5: Belleville Washer Dimensional Specifications

3.2 Energy Dissipaters

Once rocking initiates, the elastic member's pre-tension force is surpassed, the pedestal will exhibit relative displacement to the anchors used in the fixed base condition. Relative displacement between the existing anchors and the pedestal allows for energy dissipation. Dampers and UFPs are activated, providing supplemental damping, i.e. energy dissipation, as the relative displacement occurs.

The self-centering concept developed for potential retrofit of CT equipment concentrates non-linear energy dissipating devices on each corner of the existing pedestal. Shown in Figure 3-6 is the proposed viscous device arrangement which was evaluated in this research. When rocking occurs, relative displacement between the anchors and the pedestal cause movement in the damper's shaft and energy dissipation occurs. Detailed drawings of the viscous damper application are located in Appendix B. When uplift occurs, the base plate reacting on the bottom of the BeS washers compresses the washers and stores elastic energy. The stored elastic energy is used to plumb the system after the motion has seized.

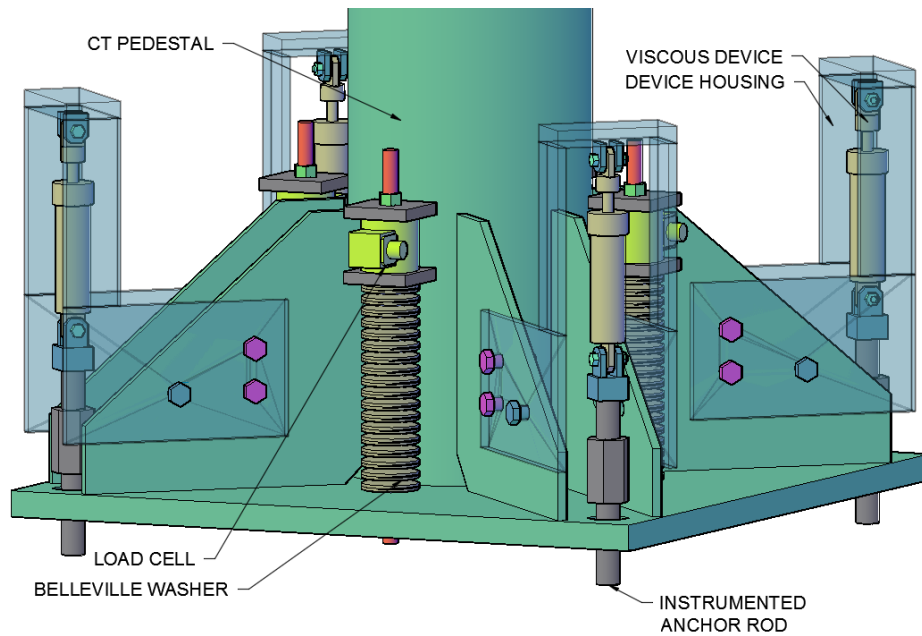


Figure 3-6: Base Retrofit w/ Taylor Viscous Dampers

Illustrated in Figure 3-7 is the proposed position and application of the second type of energy dissipating device, u-shape flexural plates. The proposed orientation shown in Figure 3-7 is composed of device sets at each corner of the pedestal.

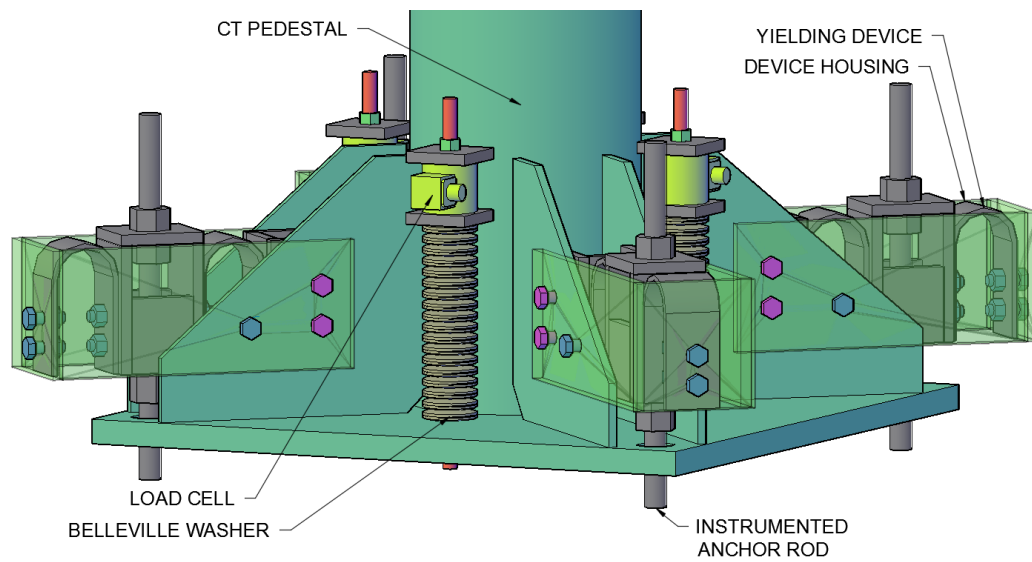


Figure 3-7: Hysteretic Device Base Retrofit

A set is comprised of two u-shape flexural plates and is positioned so the reaction block utilizes the existing anchoring holes in the CT pedestal base plate. Shown in Figure 3-8 is a subassembly of a UFP set. The reaction block has a nut and washer on both the top and the bottom of the top plate. The top plate is welded to the sides of the reaction block; the UFPs are slip-critically bolted to the reaction block. The dual-nut arrangement allows for the u-shapes to be yielded in both directions of motion. Detailed drawings and dimensions of the retrofit are located in Appendix C.

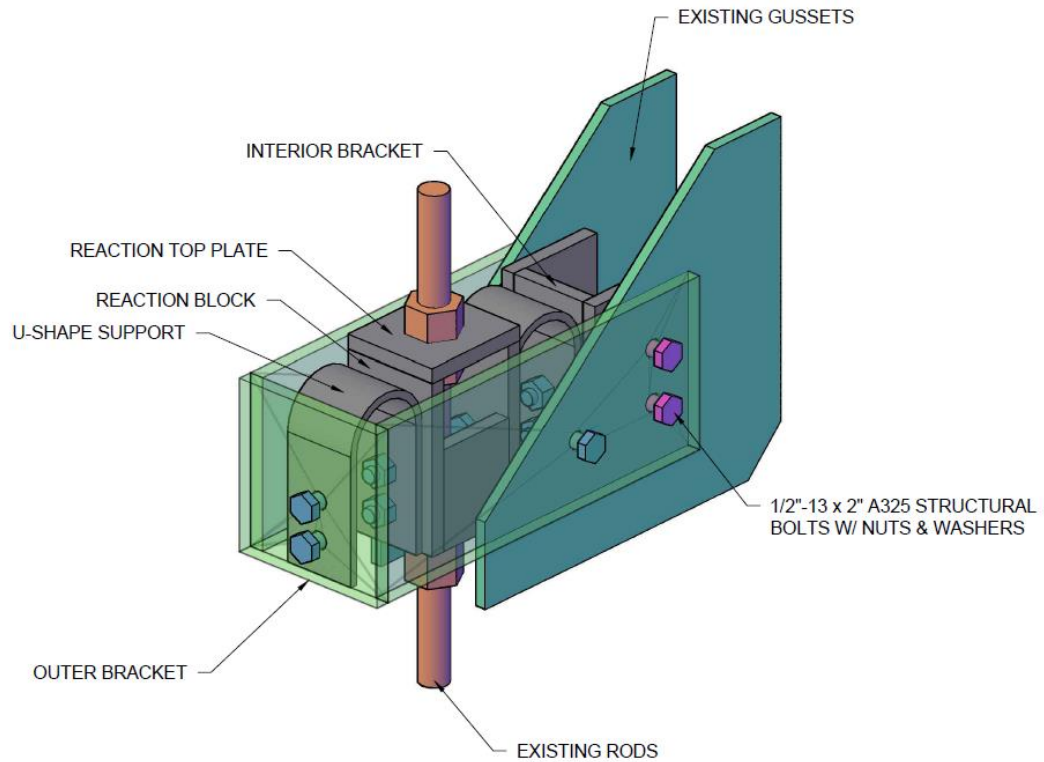


Figure 3-8: Typical UFP Assembly

4.0 U-SHAPE DESIGN

4.1 UFP Theory and Application

Various researchers have studied energy dissipation through u-shape flexural plates where mechanical strains are the primary source of dissipated energy. The advantage of UFP elements is their ability to undergo large deformations while maintaining a similar capacity. Fabrication of UFPs requires little specialty skills and allow for effective energy dissipation at a low cost. The UFPs are positioned in a location where a stiffer member allows the radius to roll as the sides of the UFP move parallel to each other. The member forms two plastic hinges at the location of contact with the stiffer elements. The capacity of the damper could be calculated by relating the plastic moment to the shear force required to cause the entire section to yield. Typical parameters used to define the shape of the UFP are presented in Figure 4-1.

As defined in the figure:

t_u = thickness of the steel plate

D_u = diameter to the center of the plate

r_u = radius to the center of the plate

b_u = width of the plate

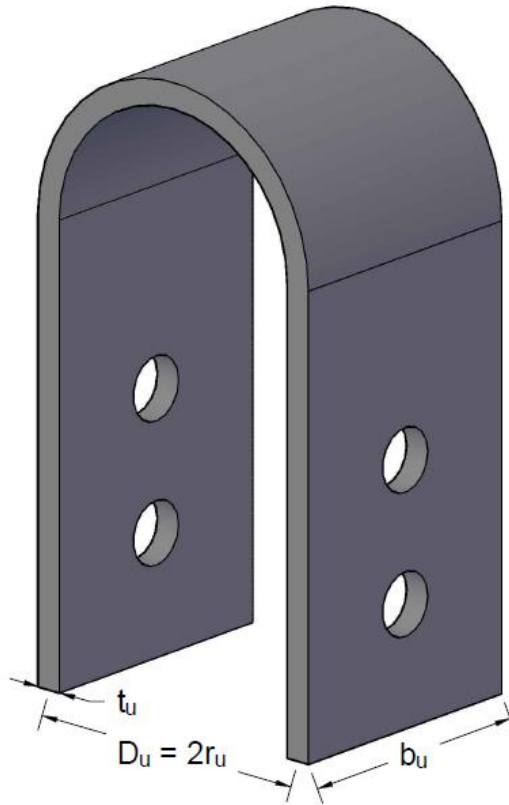


Figure 4-1: UFP Section Definition

The plastic moment, where the entire rectangular section has yielded can be defined by (4). The capacity of the UFP was analytically derived by researchers in the early 1970's by relating the shear couple to the plastic moment (Kelly, Skinner, & Heine, 1972).

$$M_p = \sigma_y Z_{URP} = \frac{\sigma_y b_u t_u^2}{4} \quad (4)$$

Illustrated in Figure 4-2 is the shear couple which must be equal to $2M_p$ in order for rolling of the plate to occur. Using the previously derived plastic moment (4) and summing the moments we could relate the shear force to the plastic moment as presented in (5).

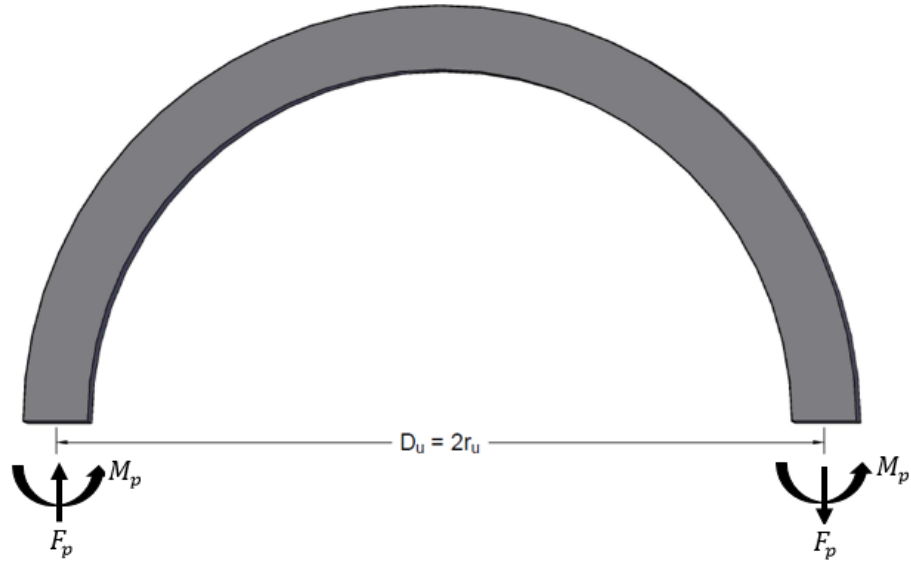


Figure 4-2: Shear Couple and Plastic Moment

$$F_p = \frac{2}{D_u} \cdot M_p = \frac{2}{D_u} \cdot \frac{\sigma_y b_u t_u^2}{4} = \frac{\sigma_y b_u t_u^2}{2D_u} \quad (5)$$

The same approach could be utilized to determine the yield force and yield moment of the UFP. For a rectangular section, the elastic section modulus shown in (6), could replace the plastic section modulus to determine the yield force and yield moment. Following the same methodology as described above for plastic properties, (7) to (10) show the relationship between shear couple, yield moment, and yield force. For a rectangular UFP section, the yield moment and plastic moment are related by a 2/3 factor. Shown in (10) is the derivation for the relationship between yield force and plastic force of the UFP.

$$S_{UFP} = \frac{b_u t_u^2}{6} \quad (6)$$

$$M_y = \sigma_y S_{URP} = \frac{\sigma_y b_u t_u^2}{6} \quad (7)$$

$$2M_y = D_u F_y \quad (8)$$

$$F_y = \frac{2}{D_u} \cdot M_y = \frac{2}{D_u} \cdot \frac{\sigma_y b_u t_u^2}{6} = \frac{\sigma_y b_u t_u^2}{3D_u} \quad (9)$$

$$\frac{F_y}{F_p} = \frac{\frac{\sigma_y b_u t_u^2}{3D_u}}{\frac{\sigma_y b_u t_u^2}{2D_u}} = \frac{2}{3} \quad (10)$$

Recent research on UFP application have been conducted using u-shape devices for energy dissipation in Cross Laminated Timber (CLT) walls (Gu, Pang, & Schiff, 2015) and precast concrete panel systems (Schultz, R., Tadros, & Huo, 1994). Similar approaches utilizing URPs are to be extended in the research outline. The benefits of rocking, along with supplemental damping with UFPs, are to be explored for the vulnerable current transformer.

5.0 GENERAL NUMERICAL MODEL

5.1 Pedestal Modeling

The actual Trench current transformer, model: 226-293 used as basis for the work performed has a fundamental frequency of 3.78Hz. A shell model of the pedestal was constructed in SAP2000 to determine the flexibility of the support structure, Figure 5-1. The shell model incorporated the base and stiffeners of the support structure. Joints were shared between the stiffeners and the mounting plates to account for the stiffness increase due to the stiffeners.

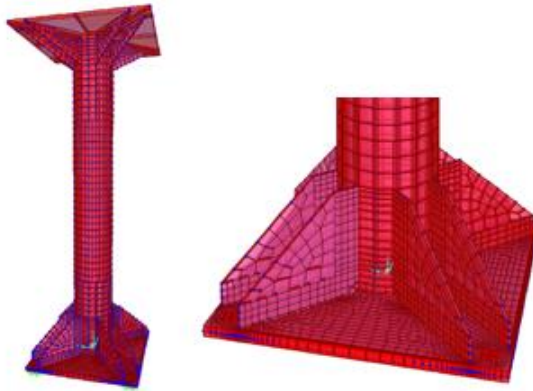


Figure 5-1: Pedestal SAP2000 Shell Model

In order to reduce the runtime of a non-linear direct integration model, an equivalent stick model was constructed. Stiffeners were modeled by rigidity end length offsets. A rigid zone factor of 1 was used along with the appropriate stiffener length to account for the significant increase in stiffness at the stiffener locations. To properly model the stiffener's contribution to the base plate stiffness, the stick model contained x-beams at the top and bottom of the pedestal which were calibrated by the shell model. After similar stiffness was achieved by the two models, additional masses were added to the top and bottom of the stick model to account for the plate weight. Shown in Figure

5-2 is the representative stick model of the CT pedestal. After combining the 3.78Hz CT with the 20.37Hz pedestal, the system fundamental frequency was 1.22Hz.

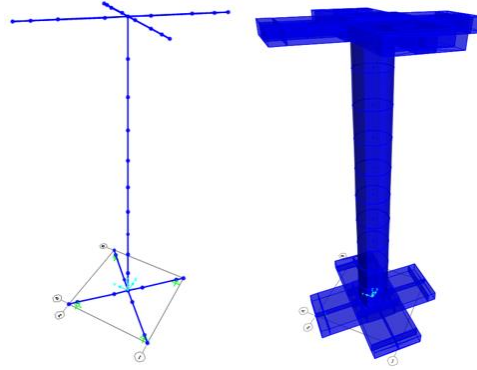


Figure 5-2: Stick Model

5.2 Upper CT Mass

Scaled system CT mass was constructed in SAP2000 using beam elements along with lumped masses. A single lumped mass concentrated the mass plates at the proper location. Since the initial phases of the research focused on a SDOF system, no mass distribution was required to properly size the dampers and UFP. The retrofit devices were only sized for the full-scale system due to the limited project funds. Shown in Figure 5-3 is the SAP2000 model used to estimate the system response prior to testing. The scaled system was designed with a 5000 lbs. lumped mass at 12 ft. from the structures base.

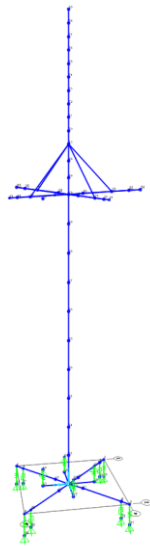


Figure 5-3: Scaled Complete System Model

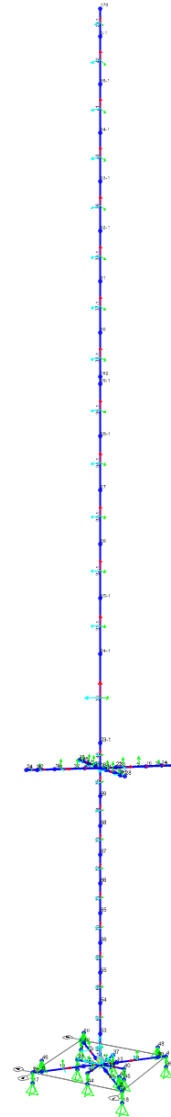


Figure 5-4: Full-scale Complete System Model

The full-scale system considered distributed masses corresponding to the seismic qualification of the 226 Trench current transformer and the designed mass system. Discussed in section 10.0, Full-Scale Mass System Design, is the procedure used to design the mass which was applied to the SAP2000 model. The model was iterated until the proper mass distribution was achieved. Shown in Figure 5-4 is the model constructed in SAP2000 to represent the full-scale system.

5.3 Foundation and Friction Modeling

With a rocking system, base sliding has to be controlled or eliminated in order to avoid global instability. In addition, z-displacement only could occur in one direction when the system undergoes uplift. SAP2000 does not have the capabilities to model friction between surfaces or components. Hand calculations were performed to verify that rocking or tipping would occur prior to base sliding. Next, in order to have a proper response in SAP2000 not allowing sliding at the base, u1, u2, and r3 degrees of freedom were restrained at the base center. Shown in Figure 5-5 is the node definition to eliminate global instability.

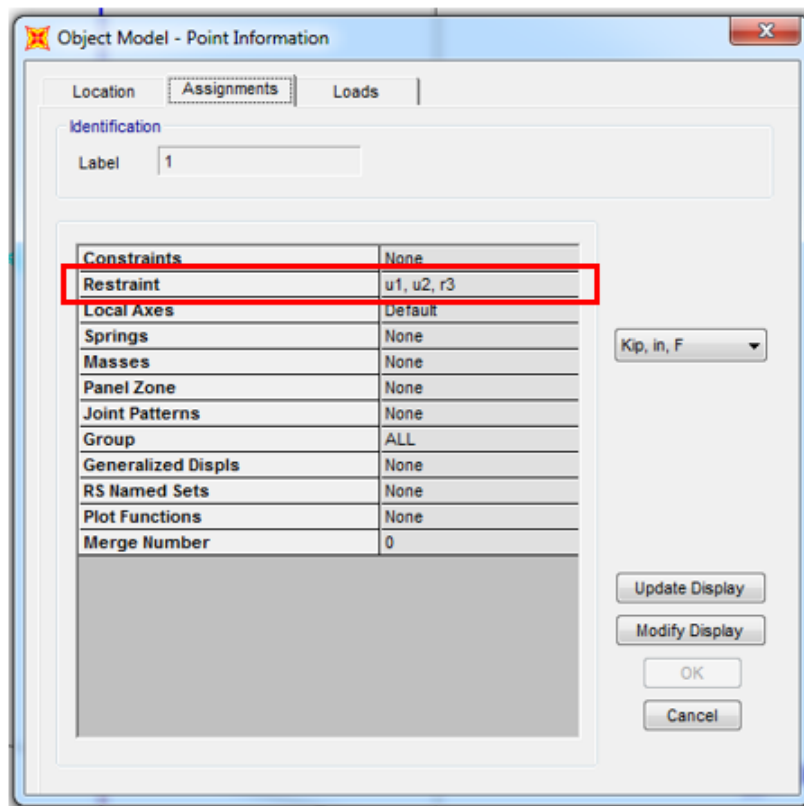


Figure 5-5: Restraints to Avoid Global Instability in SAP2000

To model the base support plate/foundation interface of the structure, non-linear gap elements were defined and implemented. Gap links are compression-only acting

springs. The gap elements were defined to act in the u1 direction along the link element and had a high stiffness in order to avoid any downward displacement along the edges of the structure. Generally, a minimum of 10 times the stiffness of the stiffest element is recommended to define a gap element. Shown in Figure 5-6 are the properties used to define the gap elements and Figure 5-7 shows the location of the gap elements on the model.

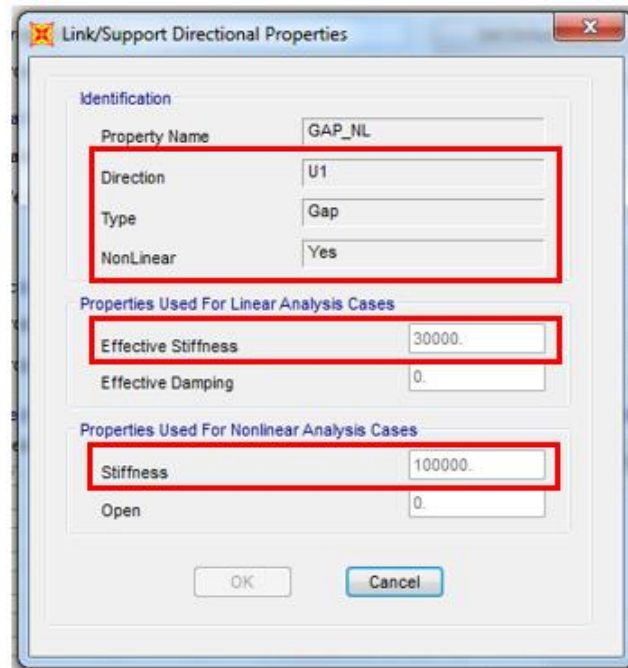


Figure 5-6: Gap Link Properties

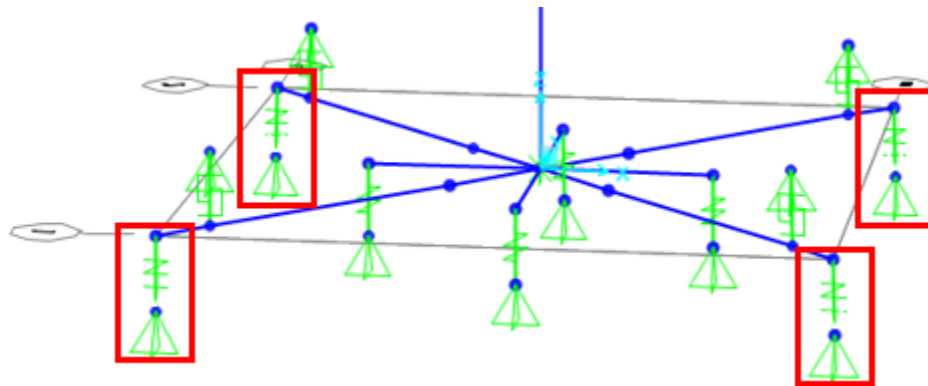


Figure 5-7: Gap Link Locations

5.4 Pre-Tension Model Application

Belleville springs, used for pre-tensioning the pedestal base, were modeled using linear link elements. Properties for the linear link were defined in the u1 direction along the length of the link. Using the determined linear load and linear displacement based on the specified type/number of BeS washers, the stiffness of the linear PT could be determined and defined in the model. The type/number defines the configuration, capacity, and stiffness. Based on the full-scale system, a linear stiffness for the PT was determined to be 7.395kips/in. Shown in Figure 5-8 are the properties specified for the PT elastic elements. Discussed in 11.1.1, Elastic PT Member Design, are the assumptions made in determining the required BeS configuration and stiffness.

The screenshot shows the 'Linear Link/Support Directional Properties' dialog box. The 'Directional Control' section has the 'U1' checkbox checked. The 'Stiffness Values Used For All Load Cases' section has 'Stiffness Is Uncoupled' selected, and the 'U1' text box contains the value '7.395'. The 'Damping Values Used For All Load Cases' section has 'Damping Is Uncoupled' selected, and the 'U1' text box contains the value '0'. The 'Units' dropdown menu is set to 'Kip, in, F'. The 'OK' and 'Cancel' buttons are at the bottom.

Figure 5-8: Elastic PT Modeling Properties

PT was positioned near the center of the base plate to maximize the contribution of each BeS stack, limit the required stroke, and minimize post-rocking stiffness. When rocking occurs about an edge or corner, the BeS stack located furthest from the rocking point will experience the largest displacement. PT members were placed at a 8" radius from the base center point at each quadrant. The center node of the pedestal base plate was utilized to connect rigid links from the PT location to the base center as shown in Figure 5-9. Rigid links were utilized because negligible base plate deformation was expected. The pre-tension application point lies between the base plate stiffeners and the HSS pedestal, increasing the flexural stiffness of the base plate significantly.

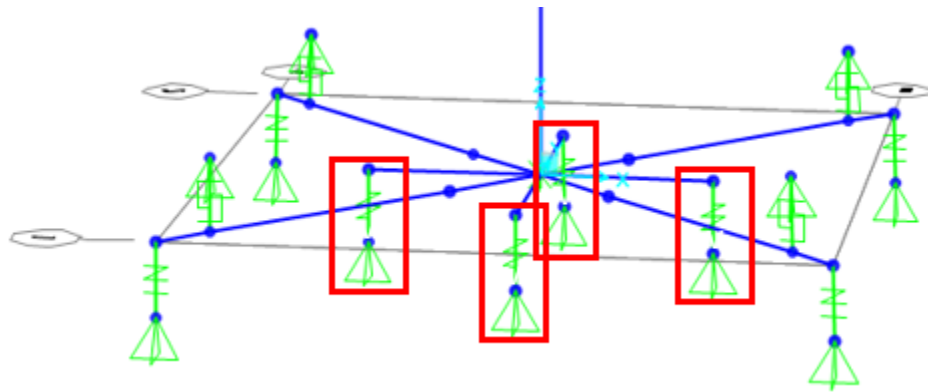


Figure 5-9: PT Location on SAP2000 Model

The model defines the BeS system without bounds or limits which must be considered post analysis. The maximum BeS linear displacement must not be exceeded in order to obtain representative results. Linear link elements have an infinite stroke and improper use of the model could lead to significant error in system response.

5.5 Hysteretic Device Modeling

Hysteretic UFP sets were modeled in SAP2000 using non-linear Wen-links. The location of the UFPs are shown in Figure 5-10, the same locations were used for the viscous model retrofit.

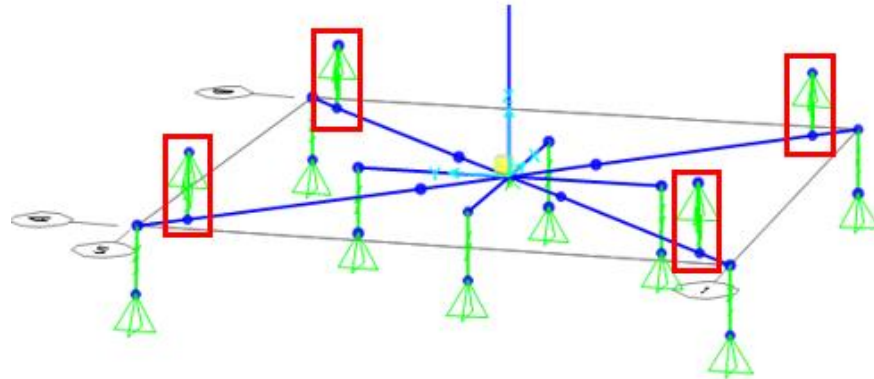


Figure 5-10: Device Locations on SAP2000 Model

The Wen-link defines uniaxial plasticity through 6 core properties. Wen-link definition includes effective stiffness, effective damping, stiffness, yield strength, post yield stiffness ratio, and yielding exponent. Shown in Figure 5-11 and Figure 5-13 are the required property specifications.

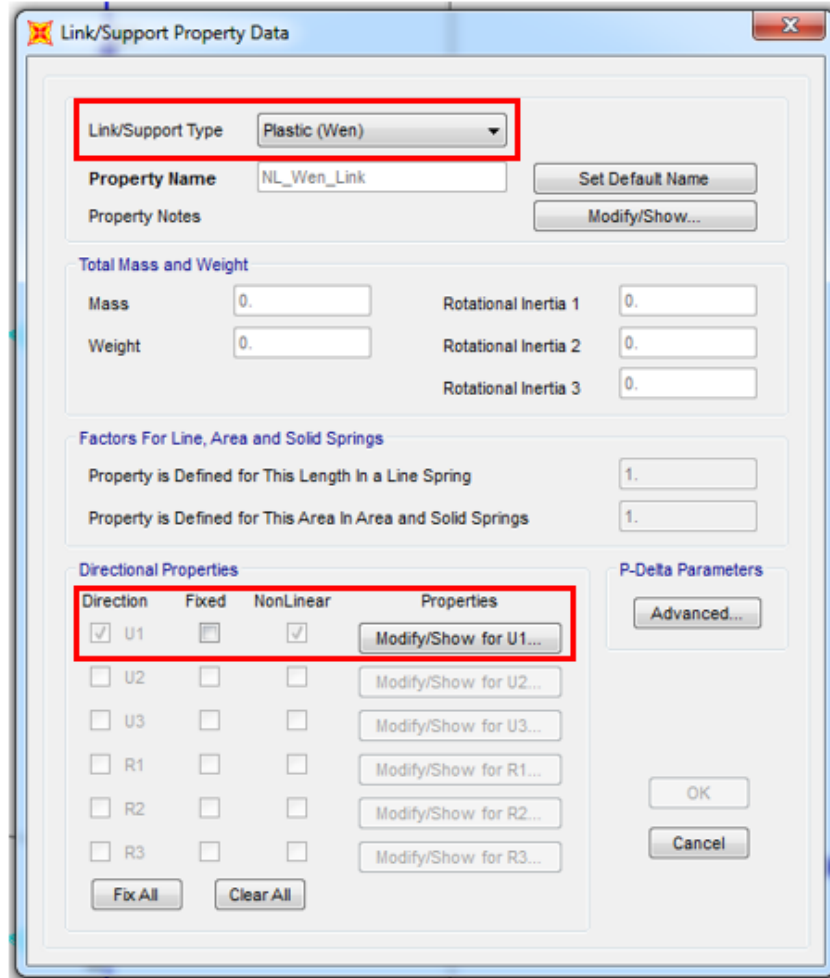


Figure 5-11: Wen-link Property Data

Directional properties for the retrofit were defined for each UFP set. A UFP set was comprised of two UFP members at each quadrant. The UFP members were positioned in parallel with each other and their stiffness and strength properties were cumulative. Based on the geometry of the UFP, the initial stiffness and yield strength could be determined using the methods discussed in section 4.0, U-Shape Design. The Wen-link definition required amplified yield strength to properly model the UFP of interest. Obtained from (CSI, 2016) is the CSI definition of the Wen-link shown in Figure 5-12. Yield strength is defined as the slope transition point “y” and the yield exponent “e”

dictates how rapid the transition occurs. Listed in section 4.0, U-Shape Design, is the equation to determine the yield force of a single UFP. The yield force is defined as the initial yield or the transition point from linear to non-linear in section 4.0. Since the CSI and theoretical definitions of the yield force are inconsistently defined, the true yield force must be amplified to properly define the Wen-link.

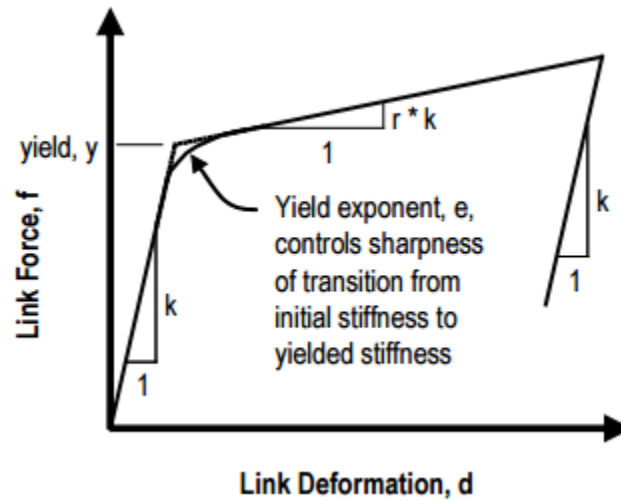


Figure 5-12: CSI Example 6-008 Wen-link Definition

Initially, iterations on the yielding exponent were conducted to match component level test behavior to the component model output. After the shape of the transition was properly defined, iterations of the yield strength were conducted to match the ultimate strength at the required displacement. The post-yield stiffness ratio was determined from scaled component level testing and used for both system models. Also, Wen-links have no fatigue properties, stroke limitations, or maximum force definitions so the final output of the model must fall within the design limitations of the hysteretic device.

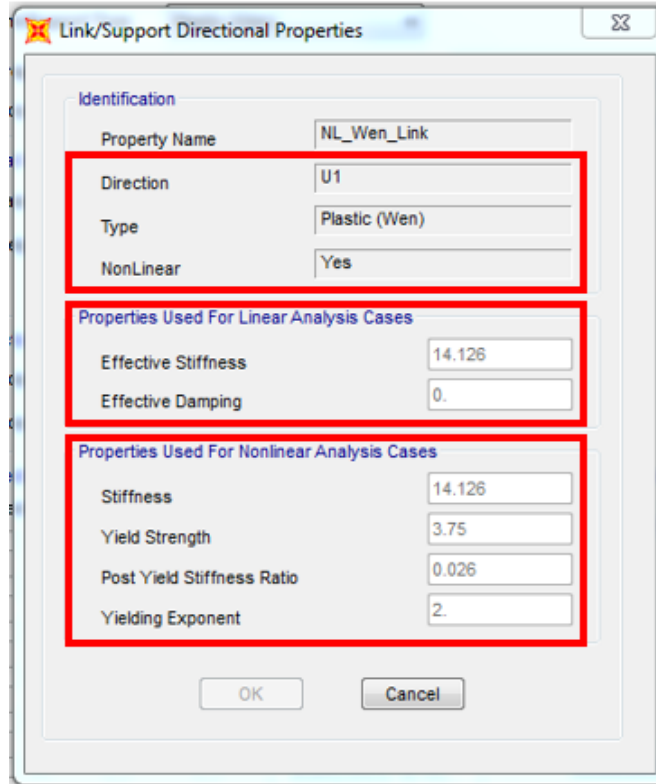


Figure 5-13: Wen-link Directional Properties

Component level testing was completed utilizing FEMA461 and IEEE693 seismic protective device protocol. The component level test results were used to calibrate the Wen-link as previously described. The backbone constructed from the component hysteresis results was used to define the Wen-link. Shown in Figure 5-14 are the component level test results, backbone curve, and SAP2000 Wen-link response for the PSU system UFP set.

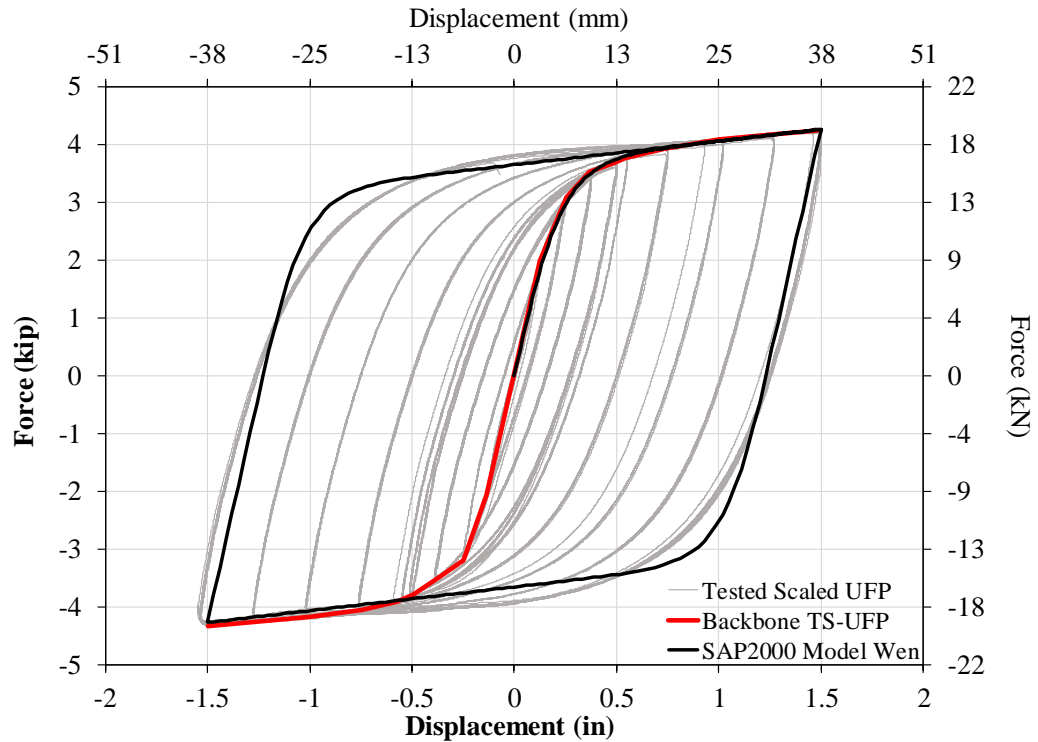


Figure 5-14: Wen Model Calibration for PSU System

5.6 Viscous Damper Modeling

Viscous dampers are modeled in SAP2000 using damper-exponential non-linear links. Depending on the orientation of the link element, the directional properties could be specified. A sample property assignment of the damper-exponential link is shown in Figure 5-15 and Figure 5-16. The designer typically specifies the exponent and force constant and the device stiffness is obtained from the manufacturer. Only one damper type was utilized in the work performed and was designed based on the full-scale system. Discussed in 11.2, Viscous Damper Design, are the methods for determining the specified damper design for the retrofit.

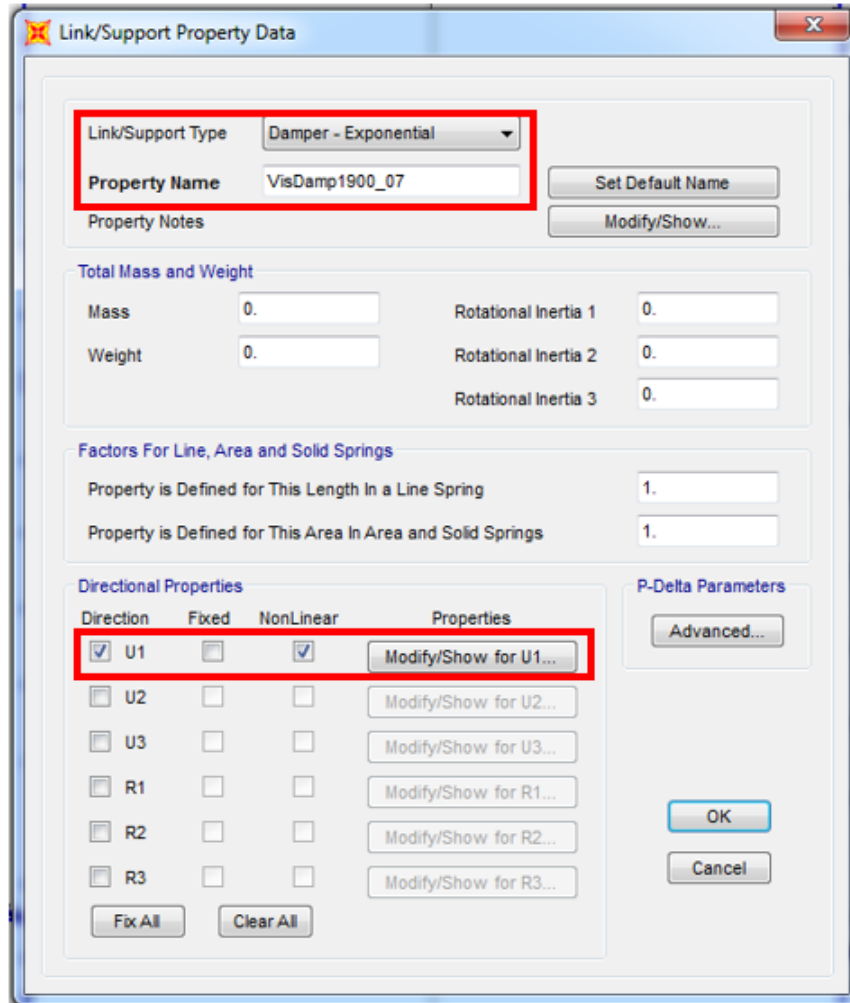


Figure 5-15: Damper- Exponential Link Properties

Link/Support Directional Properties

Identification

Property Name: VisDamp1900_07

Direction: U1

Type: Damper - Exponential

NonLinear: Yes

Properties Used For Linear Analysis Cases

Effective Stiffness: 140.

Effective Damping: 0.

Properties Used For Nonlinear Analysis Cases

Stiffness: 140.

Damping Coefficient: 1.9

Damping Exponent: 0.7

OK Cancel

Figure 5-16: D-E Link Directional Properties

6.0 PARAMETRIC STUDY ON HYSTERETIC RETROFIT PARAMETERS

Parametric studies were performed on an early design of the rocking system. The trends obtained show the influence of the initial pre-tensioning force and the rocking stiffness. Although the stiffness of the actual CT is not represented in this parametric study, the trends and influence of important factors are demonstrated.

A model was constructed in SAP2000 using the scaled system geometry to explore how each component of the retrofit influences the behavior of the system. The parametric studies investigated pre-tension force and rocking stiffness independently to supplement full-scale system design. When investigating each parameter, the parameter of interest was varied throughout a range while all other system properties were held constant.

6.1 Pre-Tension Force

Pre-tension force controls when rocking initiates and contributes significantly to the systems equivalent stiffness. As the pre-tension force is increased, the system experiences less uplift. If the pre-tension force produces a moment larger than the moment due to lateral seismic loading, the system will be non-rocking and effectively will have a bolted base stiffness. Figure 6-1 shows the influence of varying the PT force from 1kip-7 kips on a rocking system with hysteretic devices. Generally, the pre-tension force had the largest influence on system displacement. The system experiences similar magnitude base shear values for all the PT force values investigated. For a case where the base does not experience rocking, the base shear will be significantly higher following the initial stiffness throughout the entire duration of the displacement. When uplift occurs, device displacement and yielding occurs. When PT force is lower, lesser load is required to cause uplift and rocking.

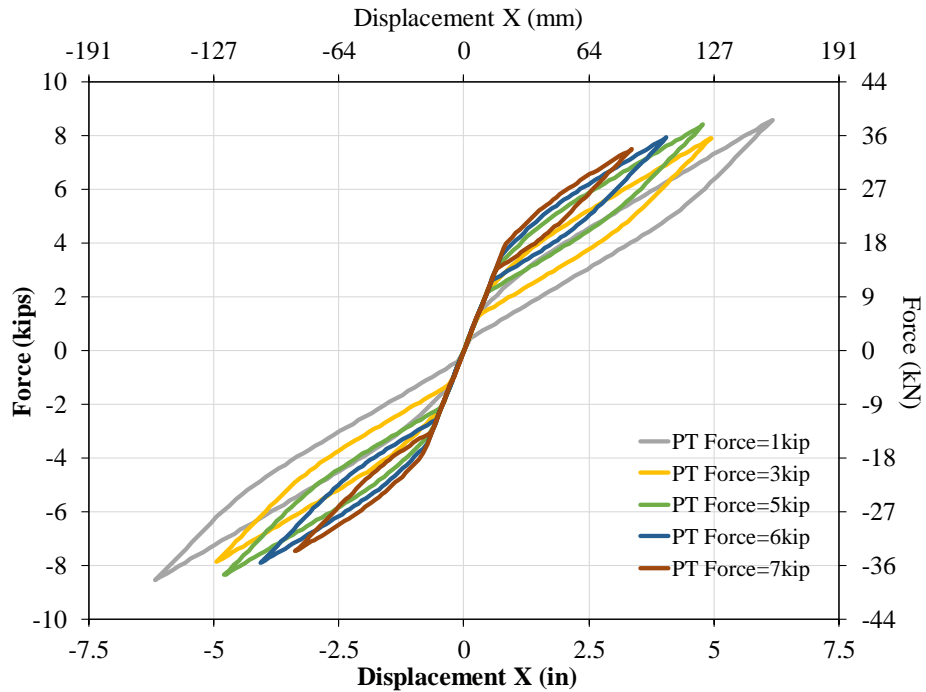


Figure 6-1: PT Force Influence on System Behavior

6.2 Rocking Stiffness

Next, the influence of rocking stiffness was investigated. Rocking stiffness could be varied multiple ways: change in elastic PT stiffness, change in PT location, and change in base size. For the parametric study, the base size or rocking location was altered in order to see how rocking stiffness influences system behavior. Reducing rocking stiffness caused the system to have larger displacements. The base shear trends were not clear and no conclusions could be obtained. For the full-scale system, rocking stiffness is expected to have a greater impact on the systems base shear. The spectral acceleration would shift off the response spectrum plateau, due to the lower fundamental frequency, and demands would decrease significantly. Shown in Figure 6-2 are the results obtained from SAP2000 for the base size variation parametric study. The results shown are push-over results, using the maximum displacement obtained from a time history analysis of each case. The

push-over results allow for clearer representation of trends while capturing maximum displacements from the time history analysis.

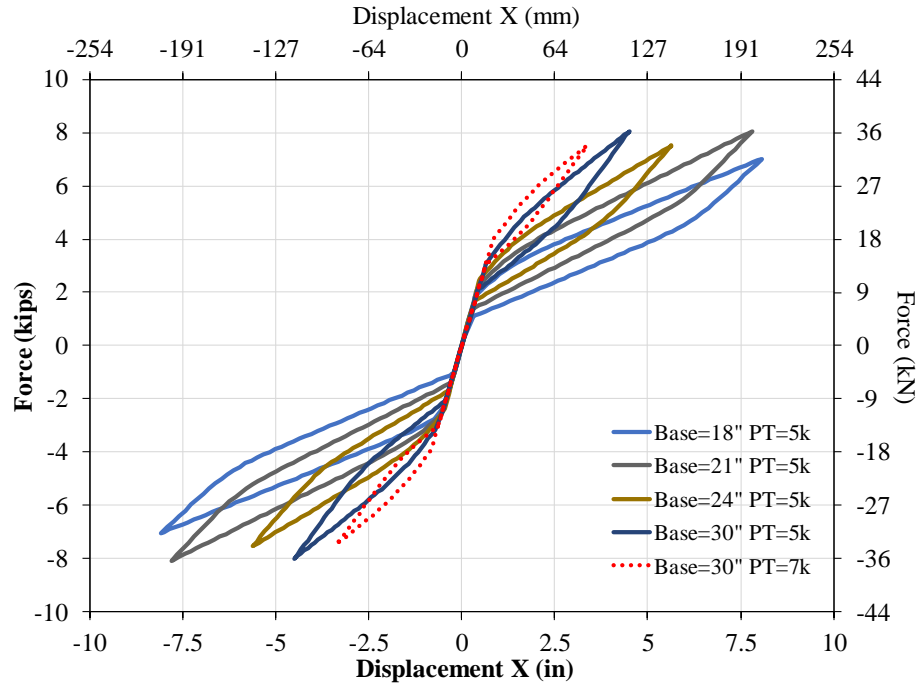


Figure 6-2: Rocking Stiffness Influence on System Behavior

7.0 PROOF OF CONCEPT

After completing numerical analysis and testing on individual components of the retrofit system, a set of proof of concept tests were conducted to validate the retrofit method. A scaled model system was designed and tested on a single-directional shake table at the iStar Laboratory located at the Portland State University campus. Laboratory height limitations allowed a maximum CT mass system height of 12 feet.

Due to the height limitation and flexibility of the system, a system with a similar property to the actual CT could not be achieved. To achieve a similar fundamental frequency, the required section would have insufficient strength. Using the maximum allowable lab clearance and a reduced mass of 5000 lbs., an upper support was designed based on strength. The system tested had a fundamental frequency of 2.93Hz and a concentrated 5000 lb. mass located 12 feet above the CT base. The designed system located on the shake table is shown in Figure 7-1. A complete set of fabrication drawings for the scaled upper mass is located in Appendix D.

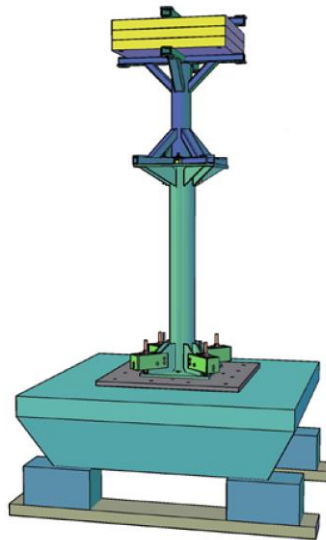


Figure 7-1: Scaled Mass System

8.0 PROOF OF CONCEPT TEST-SETUP

Due to the costs associated with testing components on a 6-DOF shake table, and procuring energy dissipation devices, a scaled mass was tested to ensure proper system performance prior to performing full-scale system research. The scaled system utilized PT and viscous dampers from the full-scale system design which were not tailored to the specific dynamic properties of the scaled system. Two key differences between the scaled system and the full-scaled system were the fundamental frequency and mass distribution. As previously mentioned, the benefits of the retrofit were expected to be significantly greater in the full-scale system based on the definition of the IEEE693 design spectrum and system frequency.

Design of the PT force and UFP include the same procedures outlined for the full-scale system in 11.1.2, PT Load Design, and 11.1.3, Hysteretic Device Design, respectively. The final PT load was determined to be 2.35 kips for each BeS stack. The final UFP had the following properties: $F_y = 0.96$ kips, $F_p = 1.43$ kips, $F_u = 1.86$ kips, and an initial stiffness of $k = 7.91$ kips/in. Detailed drawings for the u-shape geometry used for testing with the scaled mass are shown in Appendix D. Since the system was a SDOF system, the key metrics for comparison were acceleration at C.G. and displacement at C.G.. Other instrumentation capturing device displacement, base uplift, and strains at the pedestal were implemented during tests, but have little meaningful value when comparing to the full-scale system. The proof of concept aimed to show reduced demand on the structure while maintaining reasonable displacements. Also, the proof of concept was implemented to identify potential problems with instrumentation application and retrofit

tolerances. Presented in Figure 8-1 is the test setup with hysteretic devices and a safety catch system.



Figure 8-1: Scaled Mass System Test Setup

9.0 PROOF OF CONCEPT RESULTS

As previously stated, the BeS PT configuration and viscous dampers were designed for the full-scale system. The results obtained were used primarily to show that structure demands could be decreased through the designed retrofit approach. Based on the data obtained, the 100% IEEE693 motion response of each of the systems are discussed. Also, 55% IEEE693 motions is discussed since the non-retrofitted system could only be tested at 55% due to the high demand on the pedestal.

The rocking system with viscous dampers had a maximum C.G. displacement of 3.28 inches when exposed to the 100% 0.5g IEEE693 motion. The C.G. acceleration was 0.67g and the maximum pedestal strain was $601\mu\epsilon$. For the 55% motion the system had a maximum C.G. displacement of 1.65 inches and a maximum acceleration of 0.45g. The maximum strain of $405\mu\epsilon$ was measured in the north quadrant of the system.

Next, results obtained for the scaled system with hysteretic energy dissipating devices and self-centering are discussed. For the 100% motion, the system experienced a relative displacement of 6.25 inches and a maximum C.G. acceleration of 0.93g. The higher accelerations at the mass location caused larger strains in the pedestal also. The largest pedestal strain was $825\mu\epsilon$. When the 55% 0.5g IEEE693 motion excited the system, the system experienced 3.25 inches of displacement at C.G.. The C.G. acceleration was 0.7g causing $690\mu\epsilon$ in the extreme location of the pedestal.

Lastly, the non-retrofitted scaled system with a 55% 0.5g IEEE693 input motion is discussed. The excitation resulted in 2.32 inches of displacement at the C.G. of the system. The C.G. experienced 2.04g of accelerations and the pedestal $1422\mu\epsilon$.

Comparing the three scenarios for the 55% 0.5g IEEE693 excitation, the viscous damper resulted in the lowest system demand and displacements. The viscous dampers along with the self-centering mechanism reduced the displacement by 30% compared to the non-retrofitted case. While the viscous dampers reduced the system displacement, the hysteretic devices were unable to tame the displacements and a 40% increase in displacements was present in the system response.

Both retrofit methods resulted in significant decreases of acceleration at the mass location and pedestal strains. The viscous damper retrofit case presented a 78% reduction in mass acceleration while the hysteretic devices reduced the mass acceleration by 54%. For all retrofit cases, the system presented repeatable self-centering capabilities.

10.0 FULL-SCALE MASS SYSTEM DESIGN

A full-scale representative mass was designed to validate the rocking retrofits. Using a completely steel mass system eliminated the safety concerns associated with testing brittle porcelain. In order to simulate an actual current transformer, the center of mass, mass distribution, height, and fundamental frequency were targeted for the mass system.

BPA substations contain a wide variety of 500kV CT models. Each model varies in mass, mass distribution, and height. Generally, 500kV current transformers are roughly 7000lb, 20 ft.-22 ft. in height, and sit on a 90 inch pedestal. A 226-293 Trench CT was used as the basis for the work performed and a representative mass was designed based on the seismic qualification and drawings of the 226-293 CT.

Current Transformer Type HGF 1800 Model 226-293 has a mass of 3280 kg (7231 lb.) and a fundamental frequency of 3.78Hz without the pedestal. According to Trench, the Center of Gravity is 3870mm (152.36 in.) from the pedestal-CT assembly base. Based on pedestal specification drawings, the pedestal C.G. was determined to be 43.24 inches from the base. Using the manufacturer provided CT-pedestal C.G. of 152.36 inches, CT-pedestal weight of 8257 lbs., and calculated pedestal C.G. of 43.24 inches and a weight of 1026 lbs., the CT C.G. was determined. The CT only weight of 7231 lbs. was determined to act at 217.63 inches from the pedestal base.

A circular section was used to provide the similar stiffness properties in all directions of the equivalent CT mass. Mass was distributed based on geometry of the CT and distribution was iterated until the C.G. location was near 152.36 inches. After the

final iteration, the C.G. location of the designed mass system was 149.74 inches, total weight of 7240 lb., and a fundamental frequency of 3.79Hz. An HSS16x0.375 was used to achieve the stiffness and the mass was considered to provide no stiffness contribution to the HSS section. The mass consisted of steel plates attached to the HSS sections with plate washer spacers. The plate washer spacers allowed flexure in the HSS section without having the mass plates bear on the circular section. The gap provided by the plate washers was intended to eliminate any stiffness contribution of the mass plates. Shown in Figure 10-1 is a diagram showing the method used to attach the mass plates to the HSS section.

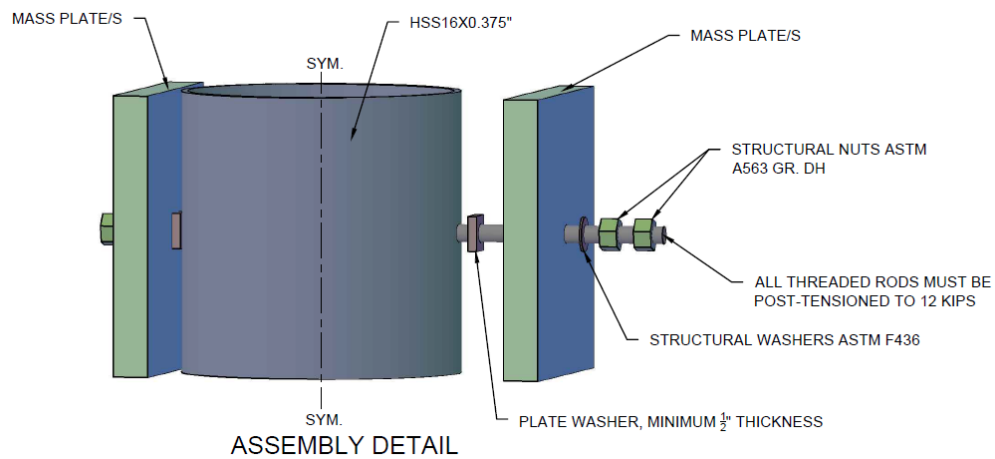


Figure 10-1: Mass Plate Mounting Detail

After completing the final iteration of the mass system, SAP2000 analysis indicated that the combined 3.79Hz representative CT and the 20.37Hz pedestal resulted in a system frequency of 1.25Hz. Complete details on the designed mass system are located in Appendix F. Shown in Figure 10-2 is the designed mass system. A schematic showing the plate locations, number of plates at each location, and details is shown in Appendix F.

The mass distribution was determined using a combination of the CT profile and the location of the C.G. Figure 10-3 shows a typical CT, the shown current transformer is not the exact model used to construct the representative mass system, but shows the vast nature of the CT.

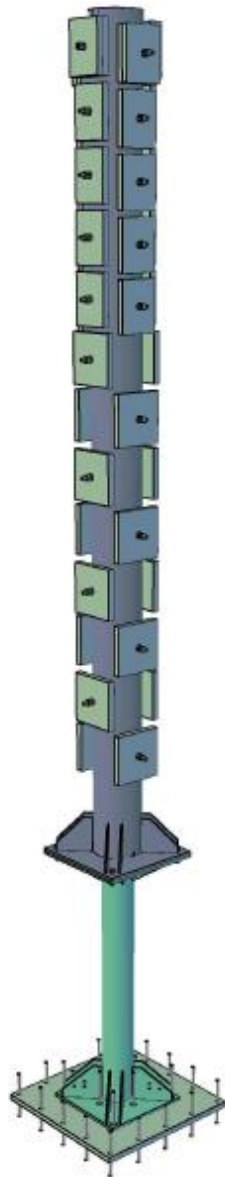


Figure 10-2: Designed Mass System



Figure 10-3: 500kV CT

11.0 FULL-SCALE RETROFIT DESIGN

When designing a rocking system, many considerations must be made to achieve self-centering with a sufficient amount of energy dissipation. Key parameters that dictate the behavior of the system are: base geometry, BeS pre-tension force, restoring forces, and resisting forces. As previously mentioned, the viscous devices have little influence on not achieving self-centering because they are velocity dependent. Altering the pre-tensions load in the viscous configuration will change the equivalent stiffness of the system as it undergoes motion because the amount of force required to initiate rocking will change. Hysteretic devices must be deformed to their initial position by the PT and self-weight in order to achieve self-centering.

11.1 Hysteretic Device

The key components, elastic PT types, preload in PT members, and hysteretic devices, must be properly designed for a rocking system with hysteretic energy dissipaters to be self-centering. Discussed are the methods used to design the tested self-centering system and recommended procedure.

11.1.1 Elastic PT Member Design

Design of the PT system must be completed prior to designing the energy dissipating devices to ensure the restoring moment is greater than the resisting moment in the system. In a rocking system, a low stiffness is desired to minimize the increase in load on the system after rocking is initiated. The BeS system must have the displacement capacity due to initial PT load and displacement due to rocking. Converting the IEEE693 design spectrum to a displacement spectrum, the displacement of the non-retrofitted system could be determined. Assuming the displacement of the elastic system is equal to

the retrofitted system the amount of uplift at the base could be determined. A displacement of 10.1 inches at C.G. was determined based on the displacement spectrum, frequency of the system, and 2% damping. Using the system geometric properties, a maximum uplift of 1.07 inches was calculated at the location of the PT.

Using 6H187177 stainless Belleville Washers, a design uplift of 1.75 inches was used to determine the required amount of elastic washers. Based on the linear displacement of the 6H187177 BeS and total stroke required, it was determined that 36 Belleville washers were required in each stack to accommodate 1.728 inches. Shown in Figure 11-1 are the washers required for the retrofit. Based on the BeS type, the flat load could be obtained from the manufacture and the stiffness of the BeS stack could be determined. For the 6H187177 BeS the linear load is 12,780 lb. The stiffness of the BeS stack is 7.4 kip/in used for the PT system. Next, the PT load was determined and remaining stroke after pre-tensioning must be determined. Shown in Figure 11-2 is the elastic-restoring system installed on the pedestal base.



Figure 11-1: Belleville Washers

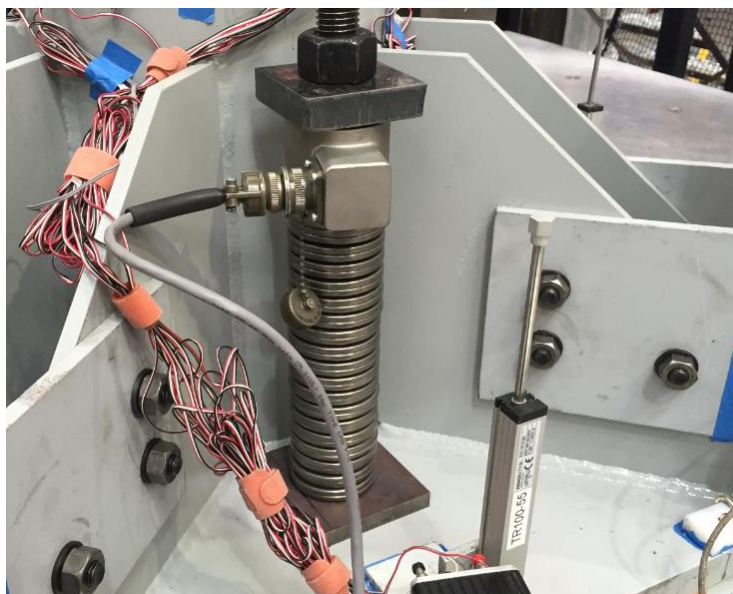


Figure 11-2: Installed BeS

11.1.2 PT Load Design

The second consideration that must be made in design of the PT system is the lateral force which causes uplift. Premature uplift is undesirable because premature displacement in the hysteretic devices may cause fatigue in the hysteretic fuse.

Three criteria were established to determine the load at which uplift initiation would occur. The first criteria limited the allowable C.G. displacement to the expected displacement in the non-retrofitted elastic system exerted to 0.5g IEEE693 motion. The second criterion was a target C.G. acceleration of 0.5g under the 0.5g IEEE693 motion. Since period shift occurs during the rocking, reducing the frequency would result in a significant decrease in spectral acceleration but slight amplification is still expected. And finally, the retrofit PT was designed so that rocking does not occur at lateral loads at and below the retrofit design wind load. Figure 11-3 summarizes the three conditions used to determine the rocking force. Shown in the figure are two rocking forces, each rocking force (F_R) are found independently using the lateral wind and 0.5g criteria along with the

expected elastic displacement (Δ_{Total}). The stiffness of the PT and elastic structure must be known to determine the rocking force. The larger of F_{R1} and F_{R2} calculated is recommended to be used for design. For the lateral wind loading case, the F_R load is known from the wind load calculation and the final load is determined. For the 0.5g seismic case, the final load is known and the rocking load must be determined. It is important to note that all stiffness values must be at the global scale applied at the C.G.. The figure shows the contributions of the elastic system, not the non-linear devices, which are considered separately for design.

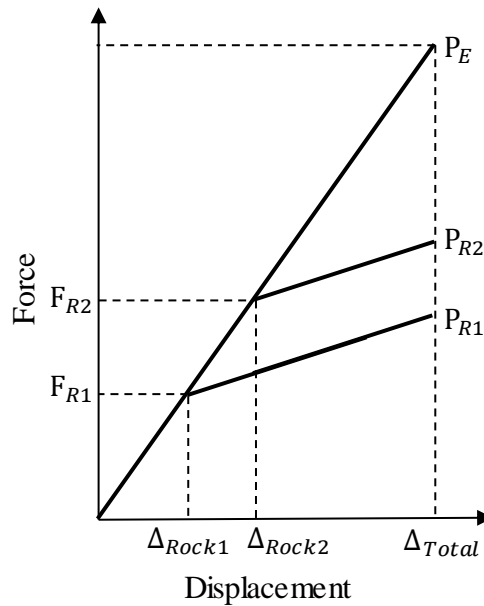


Figure 11-3: Rocking Initiation

The 0.5g seismic criterion is controlled by two factors, force contribution of the elastic system and device force contribution. Hysteretic devices could be sized in such a manner that insufficient energy dissipation occurs or where the device force is too large and self-centering cannot be achieved. Similar to Figure 11-3, Figure 11-4 shows the

contribution of the PT to global force. Denoted “a” on the figure is the maximum force due to PT at the expected displacement.

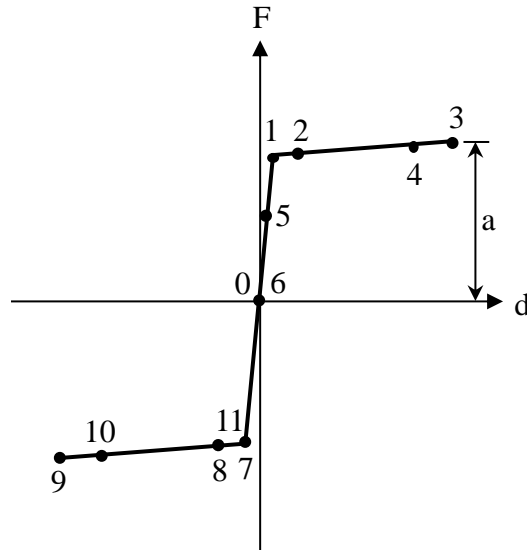


Figure 11-4: PT Force Contribution

The idealized bi-linear behavior of the hysteretic device response due to uplift is shown in Figure 11-5. Shown in the figure as “b” is the maximum force due to the hysteretic devices at maximum uplift.

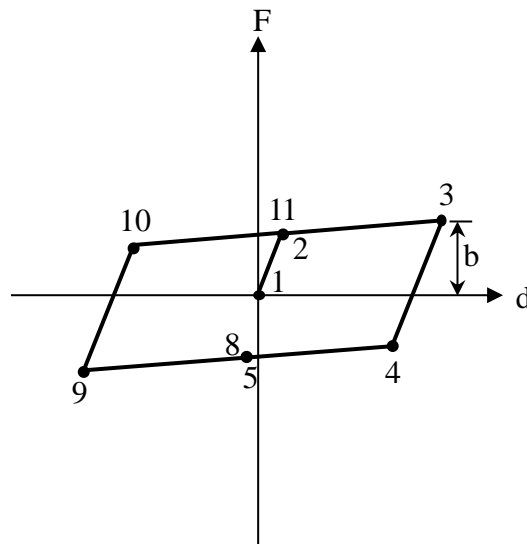


Figure 11-5: Hysteretic Device Response

Combining the contribution of the PT and the UFP response is shown in Figure 11-6. The maximum force of the system is a combination of the elastic system's force and device force. The ratio of a/b is a self-centering ratio used to relate the contribution of the non-linear system to the elastic system. Any system with an a/b ratio less than unity will not self-center.

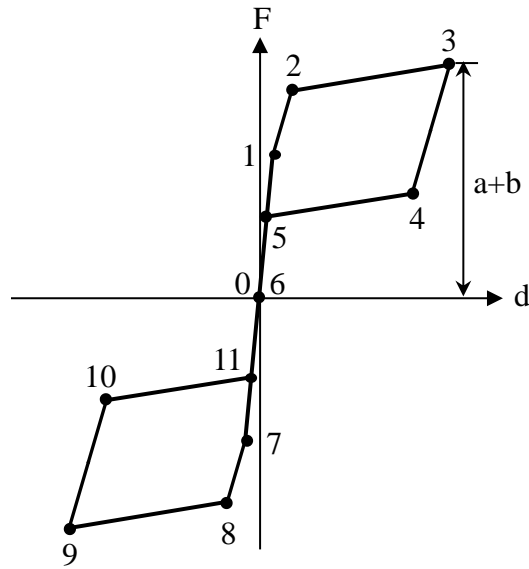


Figure 11-6: Self-Centering System Response

Based on previous work conducted on rocking systems, Pampanin suggests an (a/b) ratio of 1.25 for rocking systems (Pampanin, 2001). Figure 11-7 compares how the a/b ratio changes the amount of energy dissipation and self-centering ability. When the flag shape is eliminated, the system is no longer self-centering.

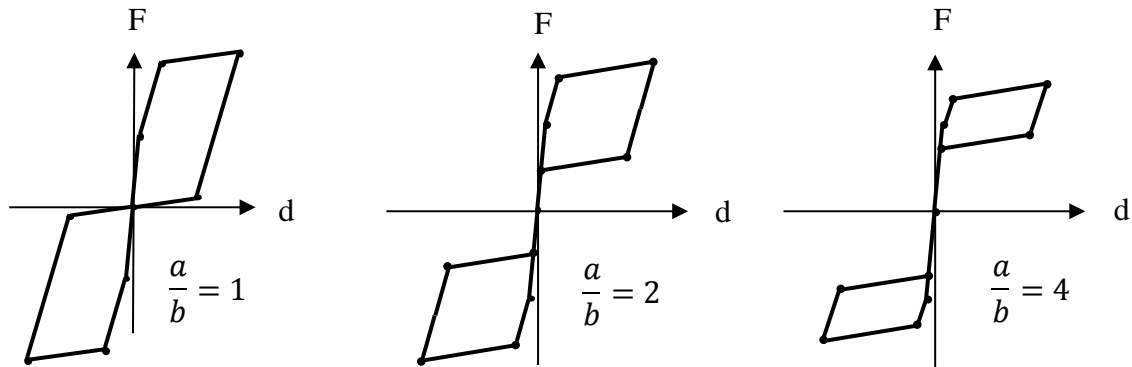


Figure 11-7: a/b Ratio Comparison

Using the recommended $a/b=1.25$, the contribution of moment due to PT for the 0.5g seismic criteria could be determined. Also, the wind load lateral force could be determined using typical ASCE procedures. The greater of the two values will control the uplift force. The uplift force could be calculated using the PT locations and assuming rocking about the base edge. Assuming the base plate does not deform, the force in each PT member is proportional to the distance away from the rocking location.

Based on the pedestal and system geometry an equivalent force at the C.G. was determined for both uplift criterions. For the 0.5g criteria, the equivalent force was 1028 lbs. and for the wind criteria 648 lbs. The moment produced by the larger force was used to determine the required pre-tension force based on the 4 BeS stack locations. A pre-tension force of 3.73 kips was determined to eliminate rocking prior to the design wind loading and achieve near 0.5g acceleration in the system. Using the BeS stack stiffness of 7.4 kip/in, a total of 0.5 inch is expected to be lost in the BeS stack stroke due to initial pre-tensioning. A total stroke of 1.73 inches is available in the elastic washers, allowing for 1.2 inches of uplift to occur. Based on the rigid body calculations, the system

demands 1.07 inches of uplift which could be achieved with the specified BeS stack. Rocking is expected to occur slightly above the design load due to self-weight. Self-weight is neglected in the restoring force because large displacements will result in minimal contribution of self-weight in restoring moment. Considering self-weight and the elastic mechanism, a force of 1.6 kips must be applied at the C.G. to initiate rocking.

11.1.3 Hysteretic Device Design

UFP design consists of many assumptions and could be conducted many ways. The described method uses a SDOF approach and iterates with a numerical model in order to fine-tune the device properties. Summarized in Figure 11-8 is the proposed design iteration for initial hysteretic device sizing.

Hysteretic Device Proposed Design Method

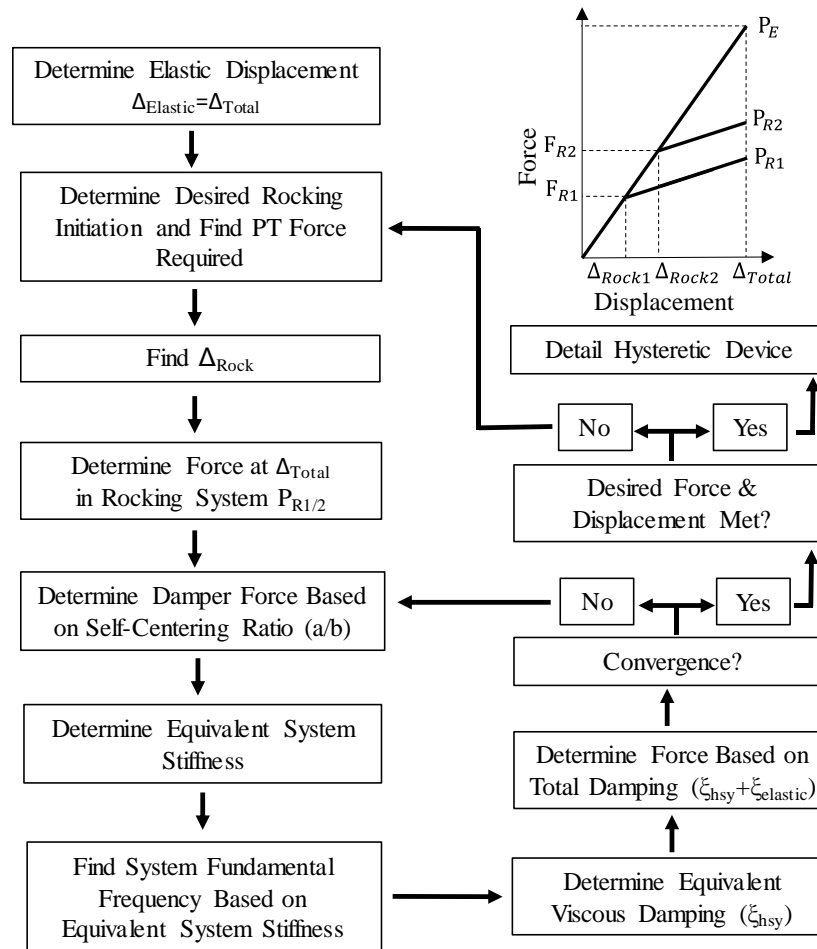


Figure 11-8: Hysteretic Device Design Procedure

The initial 4 steps in the design procedure are discussed in 11.1.1 and 11.1.2. Previous research conducted by Pampanin suggest an a/b ratio of 1.25 for sufficient energy dissipation is recommend to account for material over-strength (Pampanin, 2001). Next, the system rocking stiffness and fixed base stiffness must be determined. Using the determined preload force the amount of deflection prior to rocking could be determined. Assuming the elastic system displaces the same amount as the rocking system, the rocking displacement could be calculated. The PT moment at the expected maximum

displacement could be determined. After calculating the PT contribution to moment resistance, the a/b ratio could be utilized to compute the device moment resistance. The equivalent stiffness could be determined at the maximum displacement in order to estimate the rocking frequency. Using the values obtained, calculate equivalent viscous damping and iterate using the new frequency and damping ratio. Continue iterations until system displacements converge. Using the location of the devices and the required moment contributions from the devices, assume all devices are at their maximum capacity and determine the required capacity of each UFP.

11.1.4 SAP2000 Hysteretic Device Calibration

UFP modeling for the full-scale system utilized the methods discussed in 5.5, Hysteretic Device Modeling, and 11.1.3, Hysteretic Device Design. Shown in Figure 11-9 are the properties used to define the Wen-link used for modeling the full-scale testing. The UFP for the full-scale system had a width of 2.25 inches, an outer diameter of 3.25 inches, a plate thickness of 5/16 inch, and fabricated from ASTM A572 Gr.50 steel. Theoretically, the designed UFP should have the following nominal properties: $F_y=1.37$ kips, $F_p=2.06$ kips, $F_u=2.67$ kips, and $k_{initial}=14.8$ kip/in. Shown in Figure 11-10 is the output from the calibrated SAP2000 model for a UFP set comprised of 2 UFP devices. The final UFP design was designed for a/b ratio of 1.5 rather than 1.25 because the model results showed little flag shape behavior.

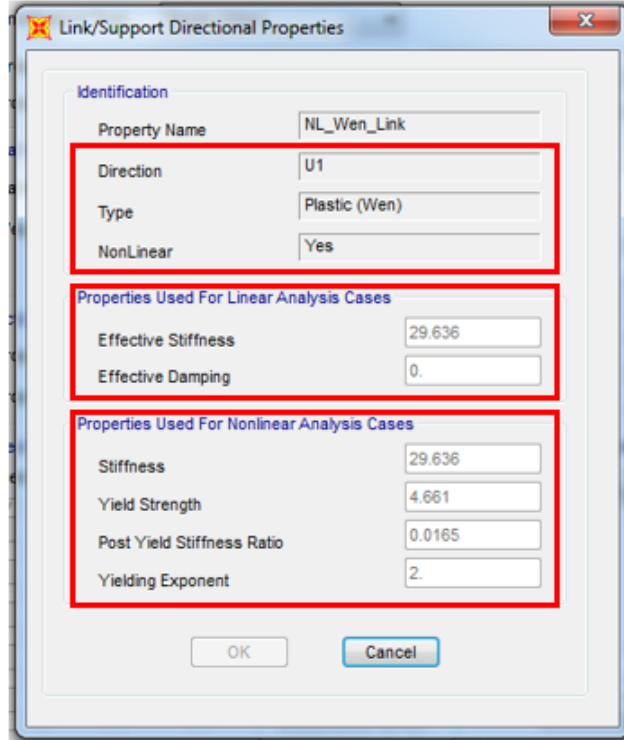


Figure 11-9: Full-Scale Wen-link Properties

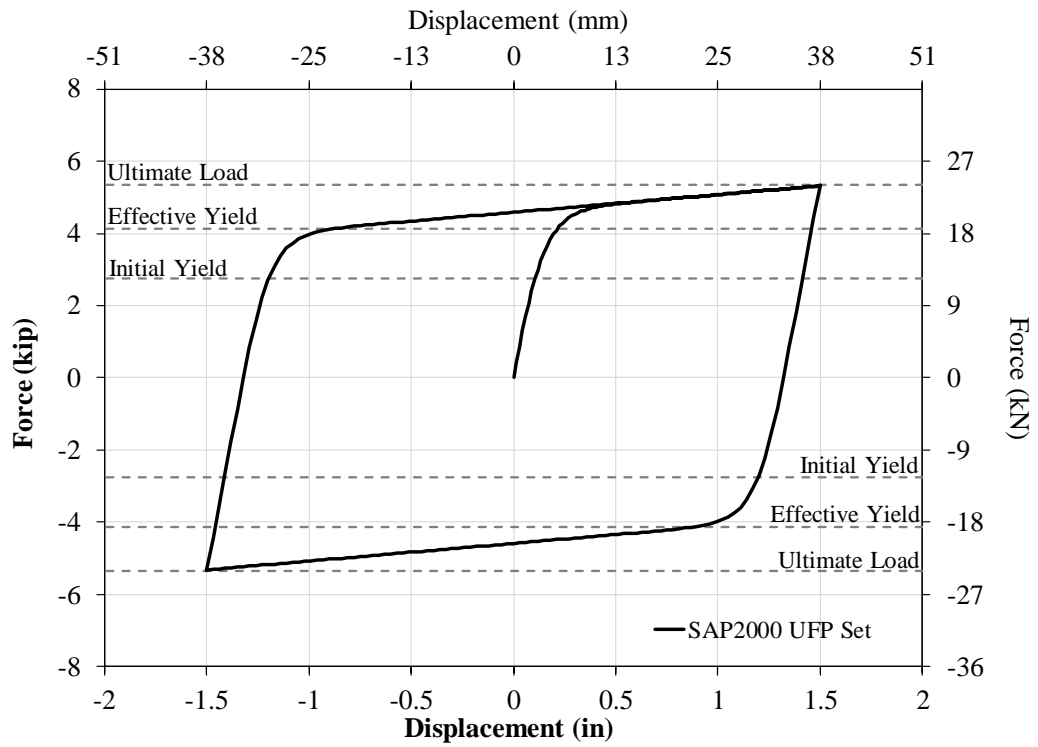


Figure 11-10: Full-Scale Model Wen-link Response

11.2 Viscous Damper Design

Various methods could be used to determine the required properties of the viscous dampers. All methods include approximating the maximum damper velocity and the desired output force at the maximum velocity. Due to the costs associated with rebuilding and procuring viscous dampers, only one set of Taylor Devices viscous dampers was purchased based on the full-scale requirements. The full-scale dampers were utilized at the scaled testing conducted at the iStar Laboratory to verify that all components were properly functioning and no tolerance or constructability issues were present in the designed base retrofit.

Typically, linear viscous dampers are not used in seismic mitigations because the force continues to increase linearly with increases in velocity. Uncertainties in damper velocities could cause overloading in structural members. With non-linear dampers, $0.3 \leq \alpha < 1$, the force in the damper increases rapidly at low velocities but levels off at higher velocities. Figure 11-11 shows comparison between a linear damper and two non-linear dampers. Taylor Device's recommends initial iterations of damper properties based on a linear damper. After initial properties are established, refinements with lower exponents could be made to optimize system performance.

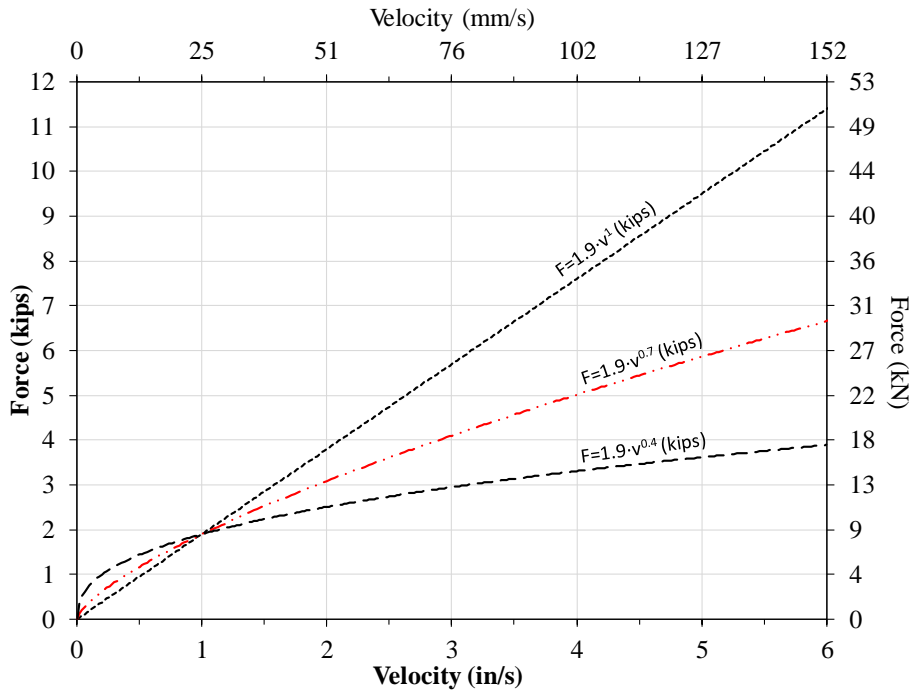


Figure 11-11: Viscous Damper α Influence of Device Force

General application of damper-exponential link elements is described in 5.0, General Numerical Model section. Using the properties of the D-series double acting stainless steel Taylor Devices damper with a total stroke of 2 inches, iterations were conducted to determine the optimal alpha and “c” factor for the full-scale retrofit configuration. Taylor Devices stated that the units have a stiffness of 140 kips/in and an alpha factor of 0.6 to 1 is recommended for the units.

Shown in Figure 11-12 is the systems response to a linear viscous damper with varying “c” variable. A snapshot of two “c” values (800 and 1600) from Figure 11-12 is shown in Figure 11-13. Increasing the “c” value led to decrease in system displacements for the cases investigated. A summary table of system parameters for the various “c” values for $\alpha=1.0$ is shown in Table 11-1.

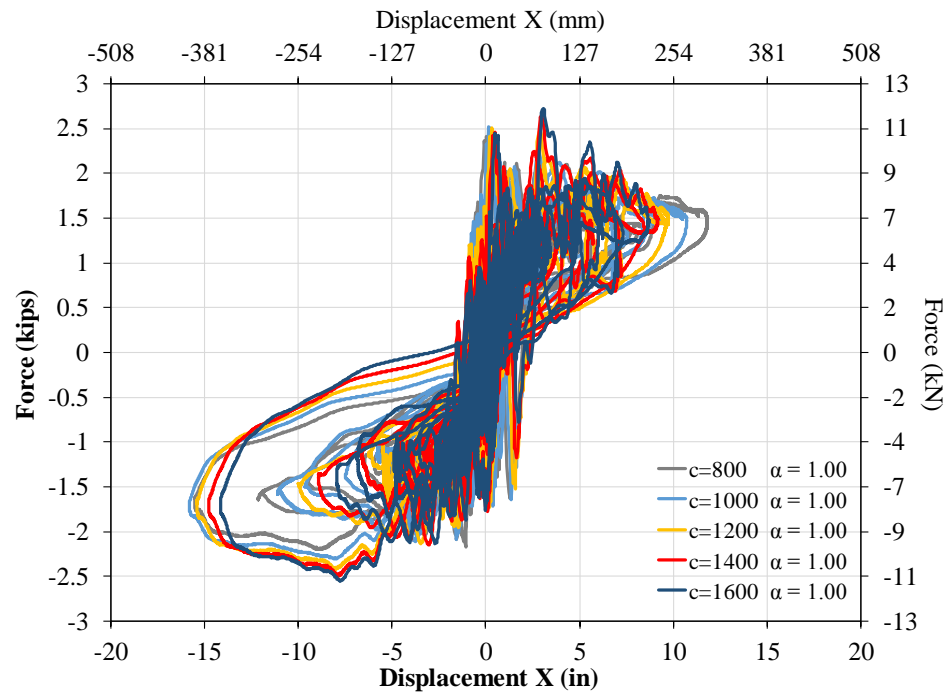


Figure 11-12: Viscous Damper "c" Factor Study w/ $\alpha=1.0$

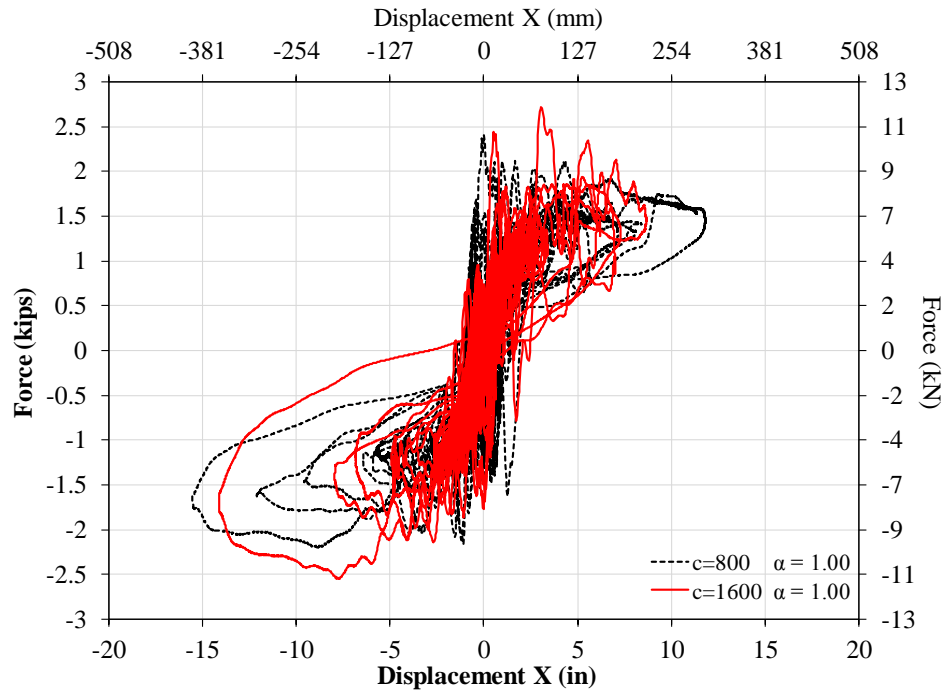


Figure 11-13: Viscous Damper "c" Comparison w/ $\alpha=1.0$

Table 11-1: Viscous Damper "c" Factor Study w/ $\alpha=1.0$

F=c.v ^{α} (lb)		Results from SAP2000 Models						
α	c	Damper-v _{max} (in/s)	Damper-F _{max} (lb)	Damper- δ _{max} (in)	B.S. F _{max} (kip)	C.G. d _{max} (in.)	C.G. a _{max} (in/s ²)	C.G. a _{max} (g)
1	800	5.33	3769	0.89	2.41	15.55	397	1.03
1	1000	4.89	4211	0.80	2.52	15.83	404	1.05
1	1200	4.52	4516	0.71	2.51	15.41	387	1.00
1	1400	3.96	4763	0.66	2.64	14.78	440	1.14
1	1600	3.50	5005	0.62	2.72	14.15	371	0.96

Note: B.S. is the base shear

Similar to the figures presented for linear viscous dampers, Figure 11-14 is a summary of the influence the "c" factor has on the systems base shear and C.G. displacement when $\alpha=0.7$.

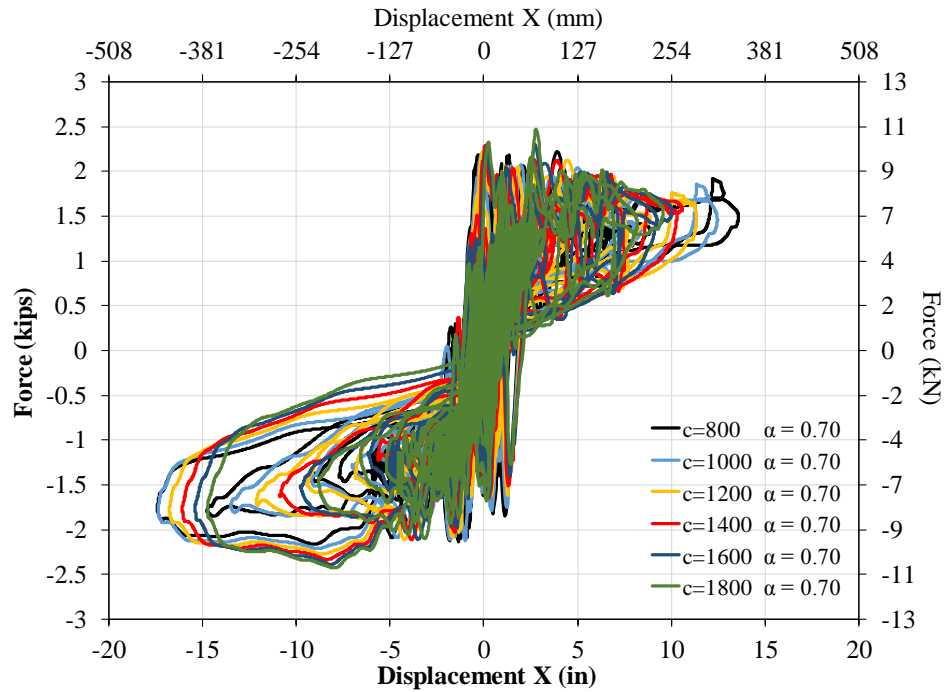


Figure 11-14: Viscous Damper "c" Factor Study w/ $\alpha=0.7$

A complete table of key system parameters is presented in Table 11-2. To show the trends more clearly, a reduced data set, only $c=1000$ and $c=1800$, is shown in Figure 11-15. Between the tabulated results and the figures of the response, increasing the “c” value generally results in smaller system displacements. Also, as “c” increases the maximum velocity seen in the system also reduces. Maximum force developed in the device increased as “c” values were increased. C.G. acceleration tended to decrease with the increase in “c” value, but base shear slightly increased 2.22kips for $c=800$ and 2.48kips for $c=1800$.

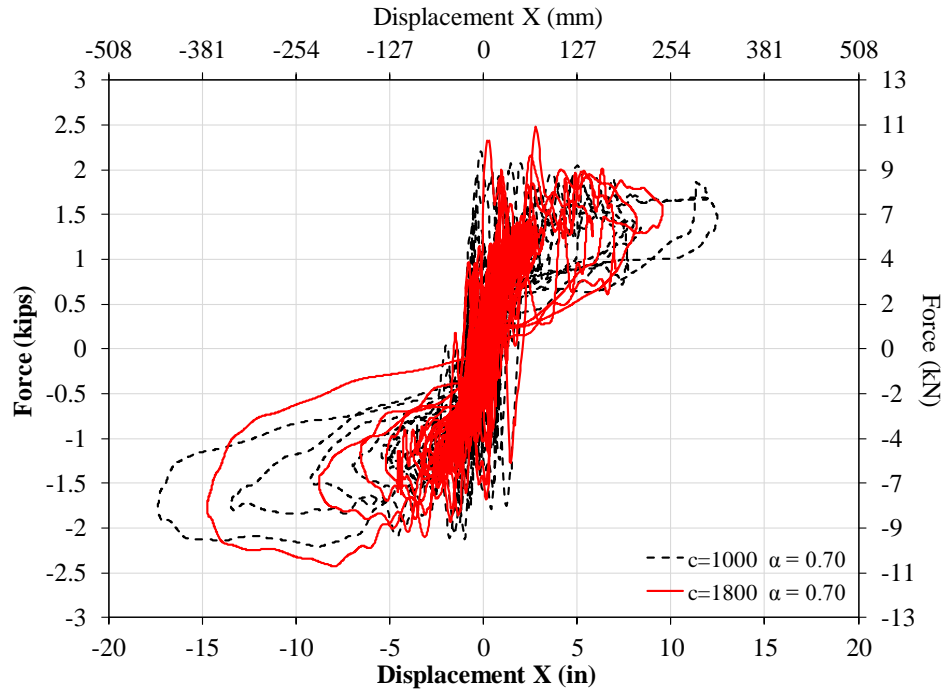


Figure 11-15: Viscous Damper "c" Comparison w/ $\alpha=0.7$

Table 11-2: Viscous Damper "c" Factor Study w/ $\alpha=0.7$

$F=c \cdot v^\alpha$ (lb)		Results from SAP2000 Models						
α	c	Damper- v_{max} (in/s)	Damper- F_{max} (lb)	Damper- δ_{max} (in)	B.S. F_{max} (kip)	C.G. d_{max} (in.)	C.G. a_{max} (in/s ²)	C.G. a_{max} (g)
0.7	800	6.03	2754	1.01	2.22	17.43	427	1.11
0.7	1000	5.56	3212	0.94	2.21	17.39	424	1.10
0.7	1200	5.15	3591	0.85	2.27	16.78	414	1.07
0.7	1400	4.79	3920	0.78	2.33	16.08	400	1.04
0.7	1600	4.46	4209	0.71	2.39	15.39	379	0.98
0.7	1800	4.13	4449	0.69	2.48	14.73	369	0.96

Note: B.S. is the base shear

Comparing the values obtained for the linear and non-linear viscous damper investigated, generally the linear viscous damper resulted in higher base shear forces, damper forces, and acceleration. A non-linear viscous damper with a $\alpha=0.7$ was used for the specified damper for the retrofit application. Taylor devices recommended $\alpha=0.6$ to $\alpha=1.0$ for the specific damper. The damper obtained for the retrofit had the following properties: $c=1900$ lbs, $\alpha=0.7$, 2-inch total stroke, double acting, and slack-free moment-

free ends. The damper was to exert 5015 lbs. at 4in/sec and had a safety factor of 1.4 at 7500 lbs. Approved drawings for the specified viscous damper are attached in Appendix B.

Shown in Figure 11-16 is a summary of the design procedure used to size the viscous damper. Approaches are available that estimate the velocity of a system prior to numerical iterations but the method shown uses modeling technique to converge on an optimal device.

Viscous Damper Design Method

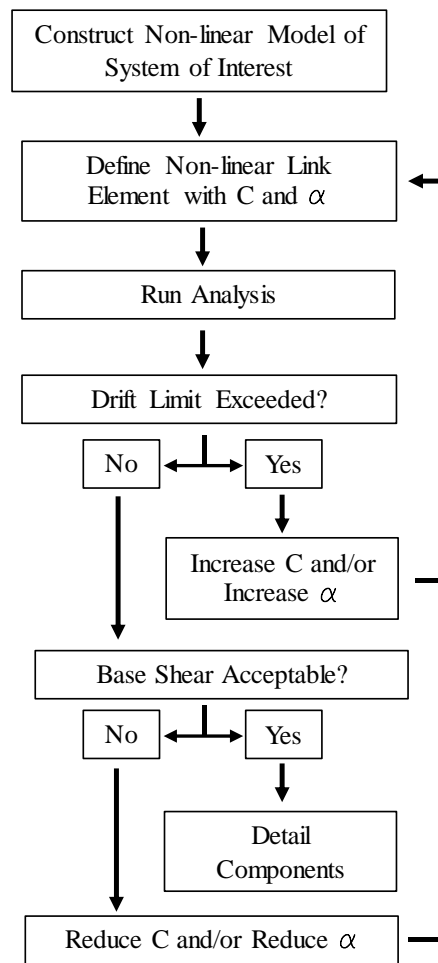


Figure 11-16: Viscous Damper Design Procedure

12.0 FULL-SCALE TEST SETUP

12.1 Instrumentation

Full-scale testing of the CT representative mass model was conducted at the University of Nevada, Reno (UNR), on a 6 degree-of-freedom (6-DOF) shake table. The tQke IEEE693 motion in X, Y, and Z directions was utilized to evaluate the effectiveness of the retrofit. A total of 155 instrumentation channels were used to monitor the behavior of the system. The instrumentation included 29 displacement transducers, 8 load cells, 8 strain gauges, 16 3-D accelerometers, and 62 6-DOF table transducers.

Key metrics captured by the instrumentation included: relative global displacement of the system, uplift on each side of the base plate, device force and displacement, anchor loads, and shear/moment at various locations of the specimen. In addition to the instrumentation, a total of 7 video cameras were used for visual observations of the system behavior.

Relative displacement determined at 3 key locations was computed for each test case. The locations of interest were top of the assembly, C.G. of the assembly, and top of the pedestal. At each location X and Y relative displacements were obtained by taking the difference in the measured displacement and the table displacement.

LVDTs located on each side of the base plate measured base plate uplift. All base plate LVDTs were placed with minimal distance between the base plate and the transducer in order to eliminate measurement corrections. Also, each device mounting assembly was instrumented with three LVDTs to measure the displacement of the device relative to the shake table and slip in the bracket connected to the pedestal. Two LVDTs

were used on each mounting assembly in order to calculate the true displacement of the energy dissipating device due to tri-axial excitation. Shown in Figure 12-1 is a diagram showing the locations of the transducers.

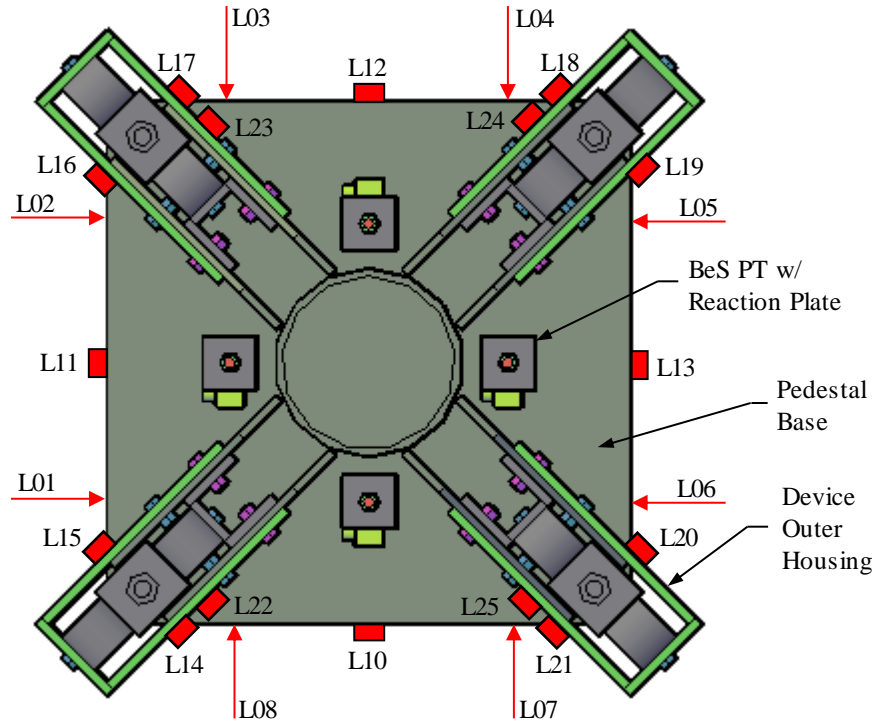


Figure 12-1: LVDT Locations on Pedestal Base

Labeled L01-L08 are LVDTs which measured horizontal movement of the pedestal base. Denoted L10-L13 are LVDTs measuring vertical uplift of the pedestal base. Instruments labeled L14-L21 were used to determine the displacement in the device. Each pair of LVDTs on the device assemblies (L14 & L15, L16 & L17, L18 & L19, L20 & L21) were used to determine the displacement at the location of the anchoring rod. L14-L21 measured relative displacement between the device outer housing and the shake table. Also, slip in the bracket relative to the pedestal was measured using L22-L25. Shown in Figure 12-1 are the instruments installed on the hysteretic retrofit case, the

same instrumentation was implemented on the viscous device retrofit. The non-retrofitted base consisted of the same instrumentation less any device transducers, L14-L25.

Load cells were used to measure forces in foundation anchors. Between the various test cases the anchors were used for various applications. For the retrofitted cases, the 1” anchor rods were used to transfer load from the energy dissipation devices to the foundation. Also, additional anchors are required for the retrofitted case for the PT load to transfer to the foundation. Load cells monitored PT loads, device loads, and bolt yielding during testing.

The CT is a multi-degree of freedom (MDOF) system requiring a higher quantity of sensors to accurately capture the reactions due to the structure dynamics. Shear and moment at key components on the test specimen allow for a simple comparison between the various test cases. Base moment was determined using two independent methods.

The first method utilized 8 strain gauges located 16 inches from the base plate on the HSS pedestal. Four primary gauges were located on the X and Y axis. An additional gauge was placed at four points between the quarter point gauges. Shown in Figure 12-2 are the locations of the strain gauges used to determine moment in the pedestal. A calibration factor between moment and strain was determined and used to determine base moment from the strain gauge readings. The CT representative mass was bolted to the shake table adaptor plate and lateral loads were applied at the top of the specimen. The cantilever load and strain was measured directly, the moment was determined and a calibration factor for each strain gauge was determined. Since only 8 strain gauges were

instrumented on the specimen, only base moment could be obtained from the strain gauge data.

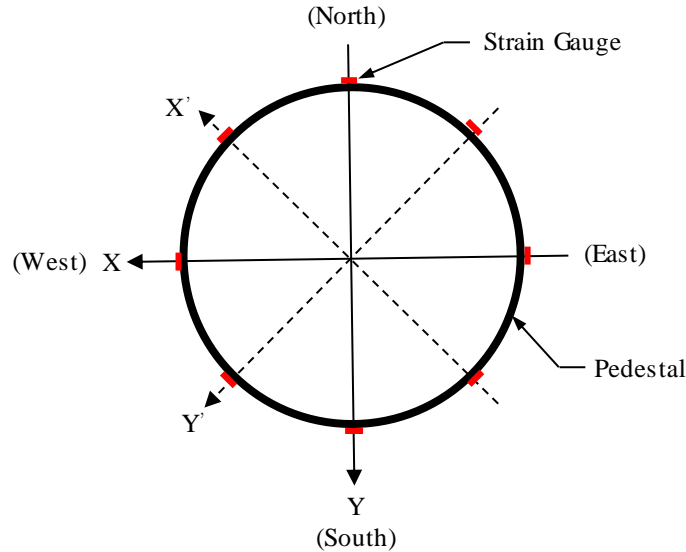


Figure 12-2: Strain Gauge Placement

The second more versatile method used for determining shear and moment on the specimen was acceleration data. A total of 16 tri-axial accelerometers were distributed along the test specimen. Figure 12-4 shows the location of the accelerometers used to determine moment and shear. Figure 12-4 could be used in conjunction with Table 12-1 to determine the exact location of specific accelerometers and string pots. Shear and moment were determined by lumping masses at each accelerometer location. The lumped masses were multiplied by the accelerometer reading in order to obtain the lateral force at the location of interest. Shear and moment at any location along the specimen could be determined by summing the contributions of each node above the location of interest. Figure 12-3 graphically shows the lumped mass method tailored to the test specimen. Although the described method is not exact, the results at the base yielded almost identical results to those obtained from the direct strain gauge reading.

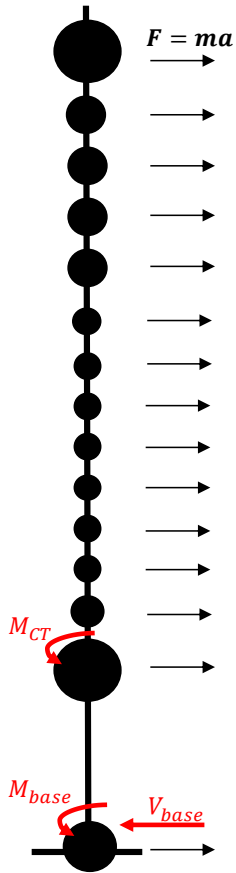


Figure 12-3: Lumped Mass Method

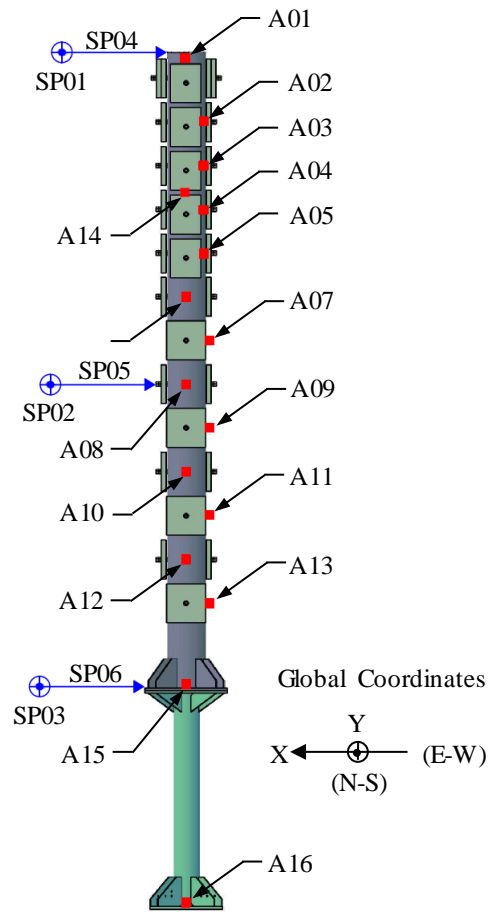


Figure 12-4: Accelerometer & String Pot Locations

Table 12-1: Accelerometer and String Pot Locations

	Instrument	Location (in.)	Measured Direction		
			X	Y	Z
Accelerometer	A01	351	x	x	x
	A02	322	x	x	x
	A03	304.5	x	x	x
	A04	285.5	x	x	x
	A05	268.5	x	x	x
	A06	254	x	x	x
	A07	235	x	x	x
	A08	214.5	x	x	x
	A09	199	x	x	x
	A10	182	x	x	x
	A11	163	x	x	x
	A12	146	x	x	x
	A13	127	x	x	x
	A14	294.5	x	x	x
	A15	91	x	x	x
	A16	1.125	x	x	x
String Pot.	SP01	352.5		x	
	SP02	216.5		x	
	SP03	91.5		x	
	SP04	352.5	x		
	SP05	215	x		
	SP06	91.5	x		

Shown in Figure 12-5 is a completely instrumented specimen. Accelerometers could be clearly seen in the image along the length of the CT representative mass.

Illustrated in Figure 12-6 and Figure 12-7 is the base instrumentation for the viscous and hysteretic retrofitted cases.



Figure 12-5: Instrumented Specimen

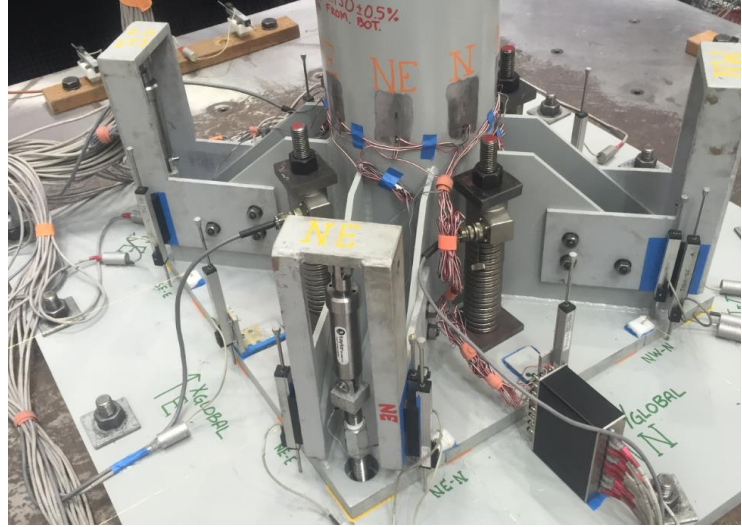


Figure 12-6: Viscous Damper Instrumentation

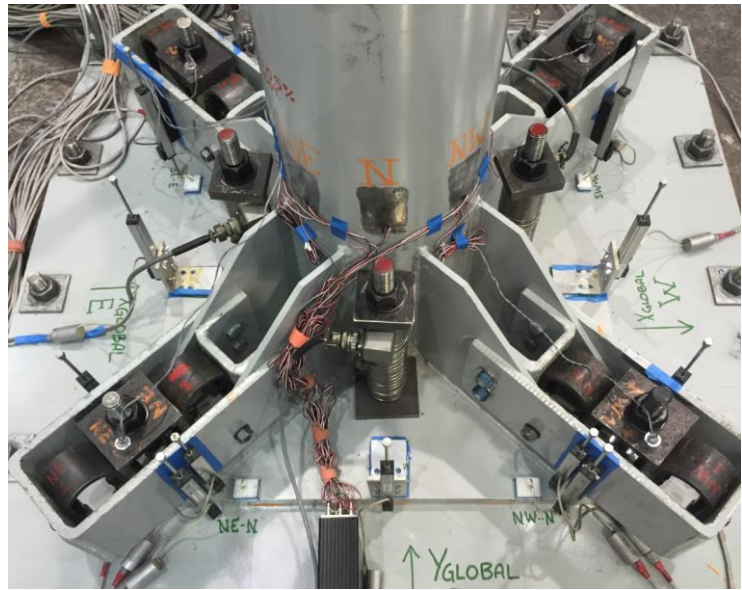


Figure 12-7: Hysteretic UFP Instrumentation

12.2 Fabricated Pedestal

A pedestal was fabricated for full-scale testing which included all the additional holes required for the retrofit. The retrofit requires 24 holes to be drilled in order to attach the device housing to the stiffeners. Also, 4 holes are required in the base plate for the

elastic-self-centering mechanism. A pedestal manufactured by Trench was used in conjunction with the manufacturer's specifications to make detailed drawings of the required modified pedestal. Provided in Appendix A are the Trench drawings for the pedestal provided. Detailed fabrication draws for the modified pedestal are located in Appendix D.

12.3 Viscous Damper Configuration

Installed Taylor viscous dampers are shown in Figure 12-8 and Figure 12-9. In order to measure the load in the damper, an instrumented coupler was used to obtain device force readings. Reduced rod length and coupler elimination is suggested in field installation to reduce bending in the anchoring rods.



Figure 12-8: NW Viscous Damper

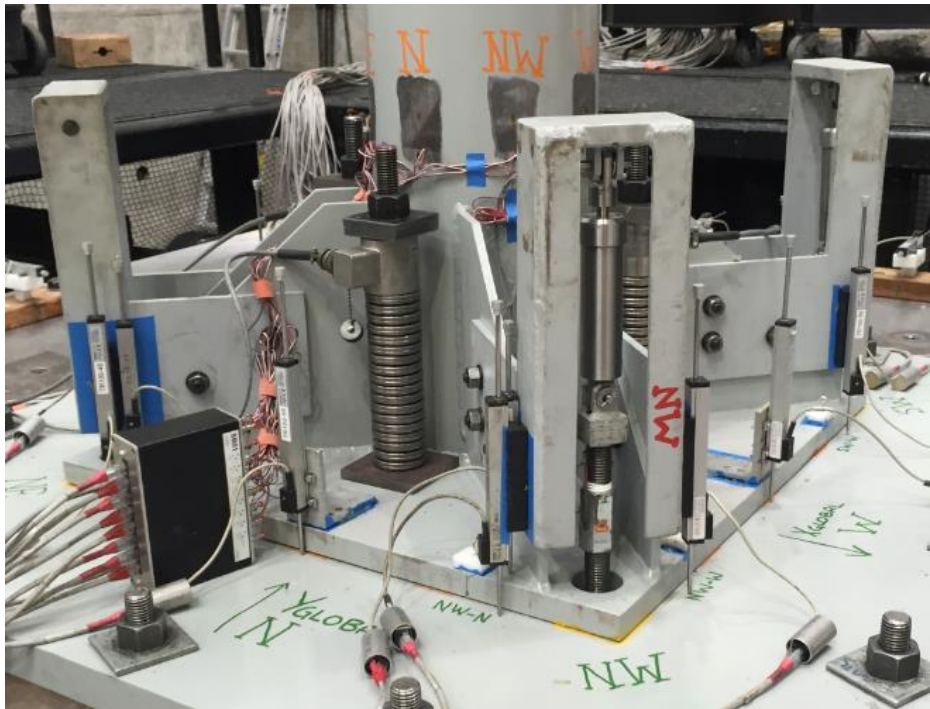


Figure 12-9: Retrofitted Base w/ Taylor Viscous Dampers

12.4 Hysteretic Damper Configuration

Application of the UFP system is shown in Figure 12-10 and Figure 12-11. It is important that all sides of the device are able to displace without reacting on the outer walls of the assembly. Centering the UFP unit is recommended when installing the device. Also, all connections must be slip-critical to maximize energy dissipation and minimize slip in the system.



Figure 12-10: Installed Hysteretic UFP

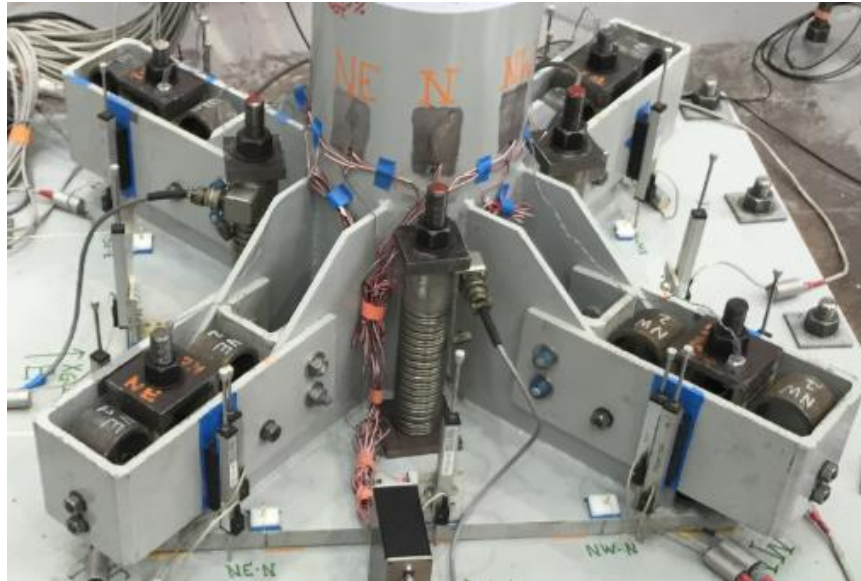


Figure 12-11: Retrofitted Base w/ Hysteretic Device

12.5 Non-Retrofitted Configuration

Shown in Figure 12-12 is the pedestal base without any retrofit devices. The additional holes required for the retrofitted cases were considered to have minimal influence on the dynamic properties of the non-retrofitted case.

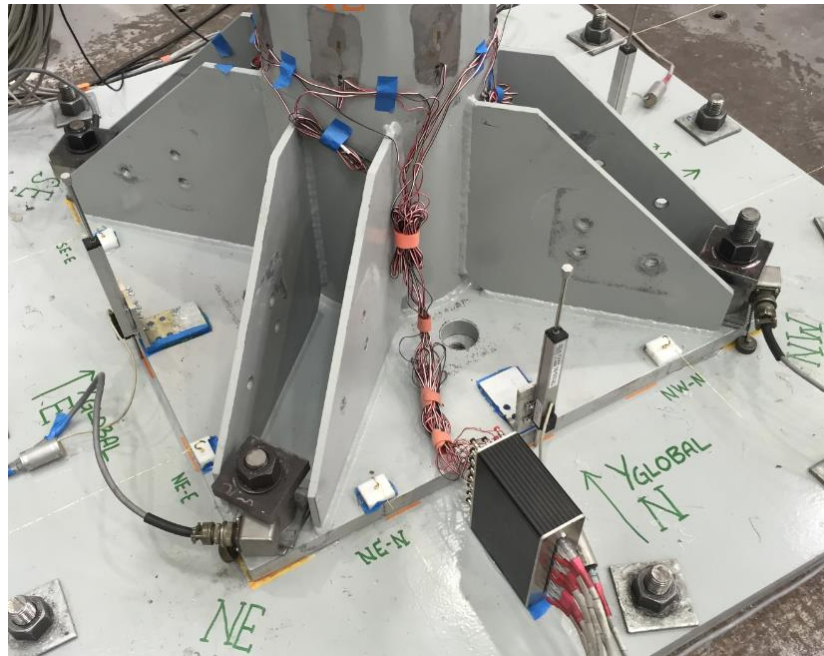


Figure 12-12: Non-Retrofitted Base

13.0 FULL-SCALE TEST RESULTS

After the experimental portion of the full-scale mass system was complete, trends, benefits, and conclusions were determined from the data obtained. Summarized in the following section is the system's response to both types of energy dissipating devices investigated, viscous and hysteretic. In addition, the non-retrofitted base case results are compared to show how acceleration, base reactions, and anchor loads compare to the retrofitted cases.

13.1 System Properties

Prior to testing the retrofitted system, the "as-built" system properties were compared to design and equipment properties. Summarized in Table 13-1, Table 13-2, and Table 13-3 are comparisons between the "as-built" mass system, design values, and manufacturer specifications for the actual CT.

Comparing the values for the current transformer, the most variation was in the system weight, shown in Table 13-1. The "as-built" mass system had a weight of 6752 lbs. while the actual 226-293 Type 1800 CT had a weight of 7231 lbs. The estimated weight of the designed CT mass was 7240 lbs., which is 6.7% more than the "as-built" weight of the system. The center of gravity varies by 1.7% between the actual CT and the "as-built" mass system. The largest difference occurred in the natural frequency of the "as-built" mass system, 18% difference between the manufacturer seismic qualification and the free vibration of the upper mass. Proper anchoring of the upper mass was hard to achieve because the CT mass had a hole spacing different than the lab floor spacing. The clamping likely caused more flexibility in the mass system reducing the fundamental frequency of the "as-built" mass system. Comparing the "as-built" CT-pedestal

properties, the combined system exhibited behaviors that were very similar to the actual CT on a pedestal.

Table 13-1: Current Transformer Properties

Current Transformer 226-293 Type HGF 1800 Properties			
Property	Manufacture Spec of Actual Equipment	Calculated for Mass System	"As-Built" Mass System
Center of Gravity (in.)	152.36	149.74	149.75
Weight of CT (lb)	7231	7240	6752
Natural Frequency (Hz)	3.78	3.79	3.10

Next, the pedestal weight and center of gravity was determined and compared to the values specified by the manufacturer drawings. The manufacturer only provides an estimated pedestal weight but center of mass is not specified. Based on the pedestal drawings, a center of mass was calculated, 43.24 inches from the pedestal base. The “as-built” pedestal had a C.G. that was 0.6% less than the calculated C.G.. The weight of the pedestal differed by 2.4% between the “as-built” and manufacture drawings specifications.

Table 13-2: Pedestal Properties

Pedestal Properties			
Property	Manufacture Spec	Calculated	"As-Built"
Center of Gravity (in.)	N/A	43.24	43
Weight of Pedestal (lb.)	1035	1026	1010

After assembling the pedestal and upper mass, the systems properties were compared to the results obtained from SAP2000 modeling. The manufacture of the current transformer did not specify a pedestal-CT fundamental frequency that could be compared to the “as-built” system. Using individual component C.G. and mass values, a system C.G. of 217.6 inches was determined for the pedestal-CT system. The “as-built” system had a C.G. of 215.25 inches resulting in a 1% difference. The combined pedestal-

CT “as-built” system had a 6% smaller mass than the sum of the component weights specified by the manufacturer.

Table 13-3: System Properties

CT-Pedestal System				
Property	Manufacture Spec	Calculated based on Manf. Components	Calculated Designed System	"As-Built"
System C.G. (in.)	N/A	217.63	213.78	215.25
System Total Weight (lb.)	N/A	8256.55	7840	7762
Natural Frequency (Hz)	N/A	N/A	1.24	1.24

Minor differences were observed between the manufacturer’s specifications and field properties. All the difference presented by the “as-built” system is considered negligible. Elastic damping of the actual CT is unknown and is likely higher than that of the steel mass system damping. Based on the properties obtained, the designed mass system demonstrates similar properties to the actual 226-293 Type 1800 CT Trench current transformer.

13.2 Test Matrix

Each retrofit device was evaluated using 20-100% of the 0.5g IEEE693 motion. Prior to each motion, implementation of a system identification series provided the ability for detecting undesired system deterioration and alteration. The system identification series consisted of X-pulse, Y-pulse, Z-pulse, and XYZ white noise. Two increment steps were used in motions scaling, for low amplitude motions up to 60%, 10% increments were utilized. After the 60% motions, 5% increment steps were used until 100% 0.5g motions were achieved.

An extended test matrix was implemented on the hysteretic device retrofit. In order to determine if the repeated increases in amplitude effected the device performance an

additional test with virgin hysteretic devices was conducted at 100% 0.5g IEEE693. Also, actual ground records for a crustal and subduction earthquake were used to excite the system. The 6.4 magnitude subduction record that centered in Curicó, Maule, Chile was utilized in 100%, 120%, 140%, 160%, and 200% amplitudes. Next, a crustal input motion then excited the pedestal-CT system. The Capitola, California earthquake record was scaled by 100%, 120% and 140%.

13.3 Viscous Damper Retrofit Results

13.3.1 Viscous Damper Table Response Spectrum

Prior to evaluating the effects of the retrofit, a comparison between the shake table feedback and IEEE693 design spectrum was conducted. For equipment seismic qualification, the ground motion must envelope the design spectrum. The retrofits introduced aimed to reduce structure demands and not necessarily qualify the equipment. Shown in Figure 13-1,

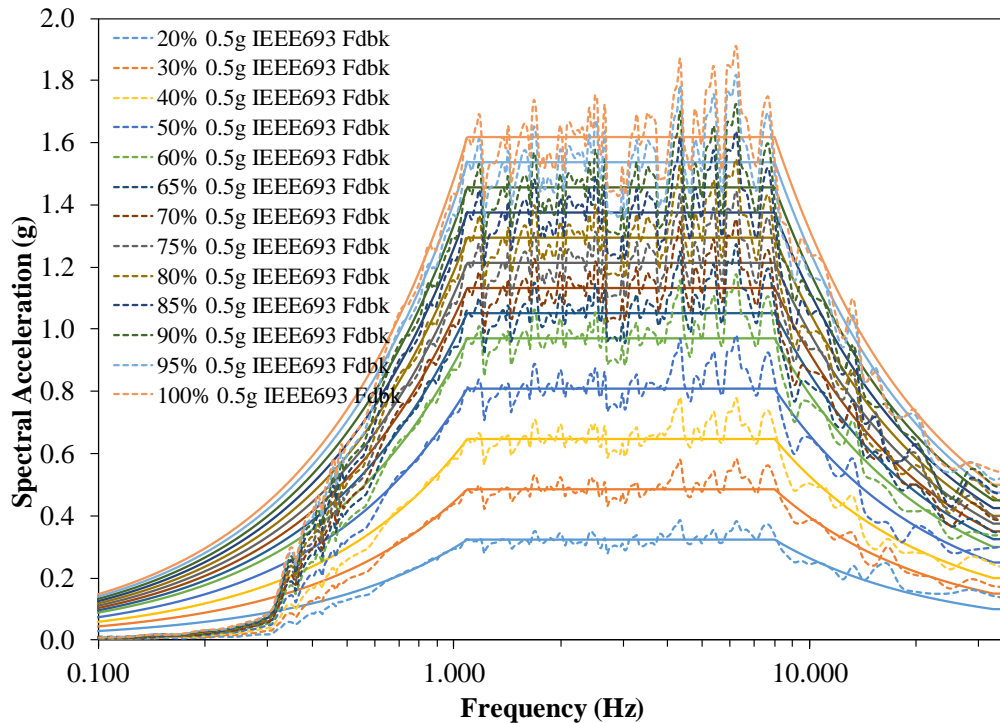


Figure 13-2, and Figure 13-3 is the table response and design spectrum. Low frequencies are considerably undershot in all directions of the motion. For the two

horizontal directions, X and Y, only frequencies between 0.5Hz-1.3Hz are of importance.

The non-retrofitted system has a fundamental frequency of 1.24Hz; reduction in frequency results from system rocking in the retrofitted cases is expected.

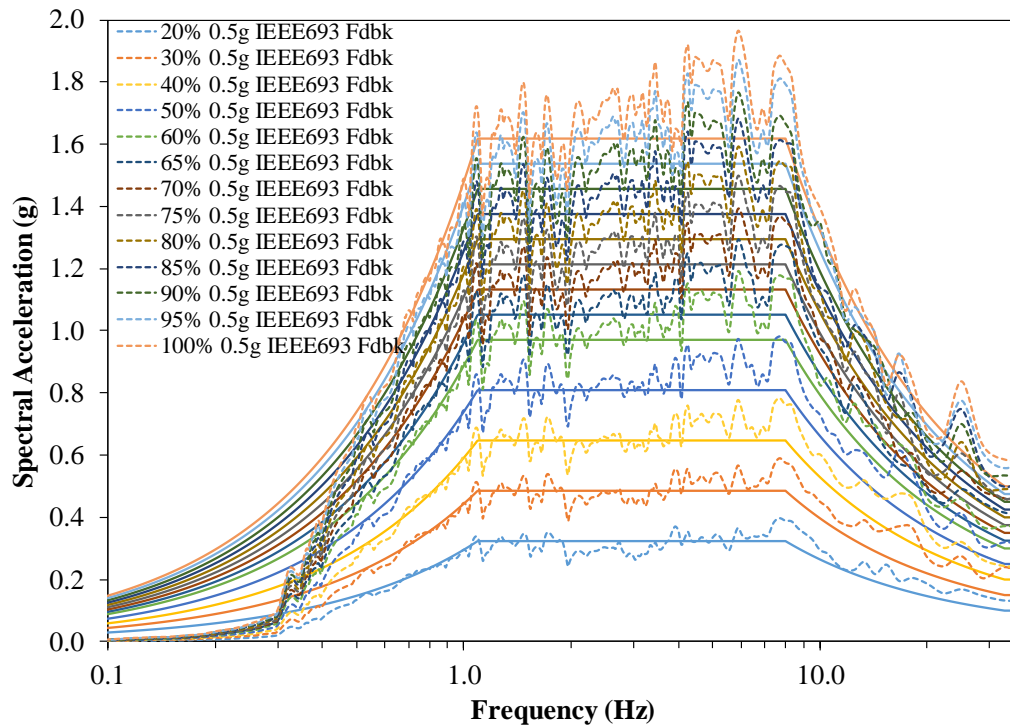


Figure 13-1: Response Spectrum X (Viscous Damper)

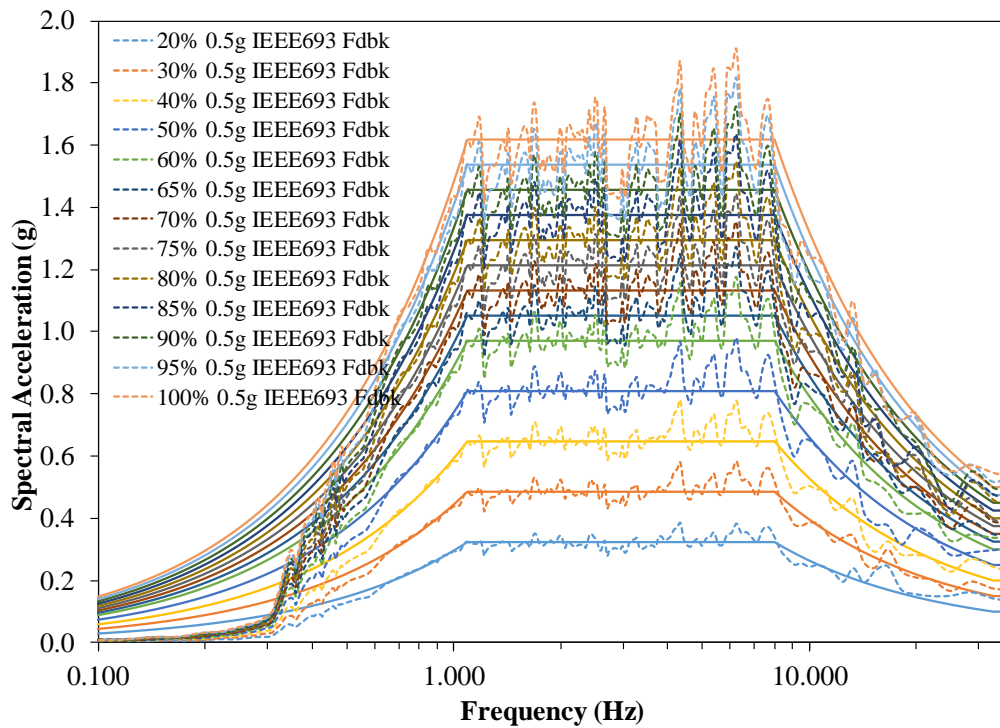


Figure 13-2: Response Spectrum Y (Viscous Damper)

For the Z direction of the motion, all low frequency content is significantly undershot. All frequencies below 10Hz are of little importance for the system because of its high vertical stiffness. The table response envelopes the 0.5g IEEE693 spectrum at all frequencies from 10Hz and above.

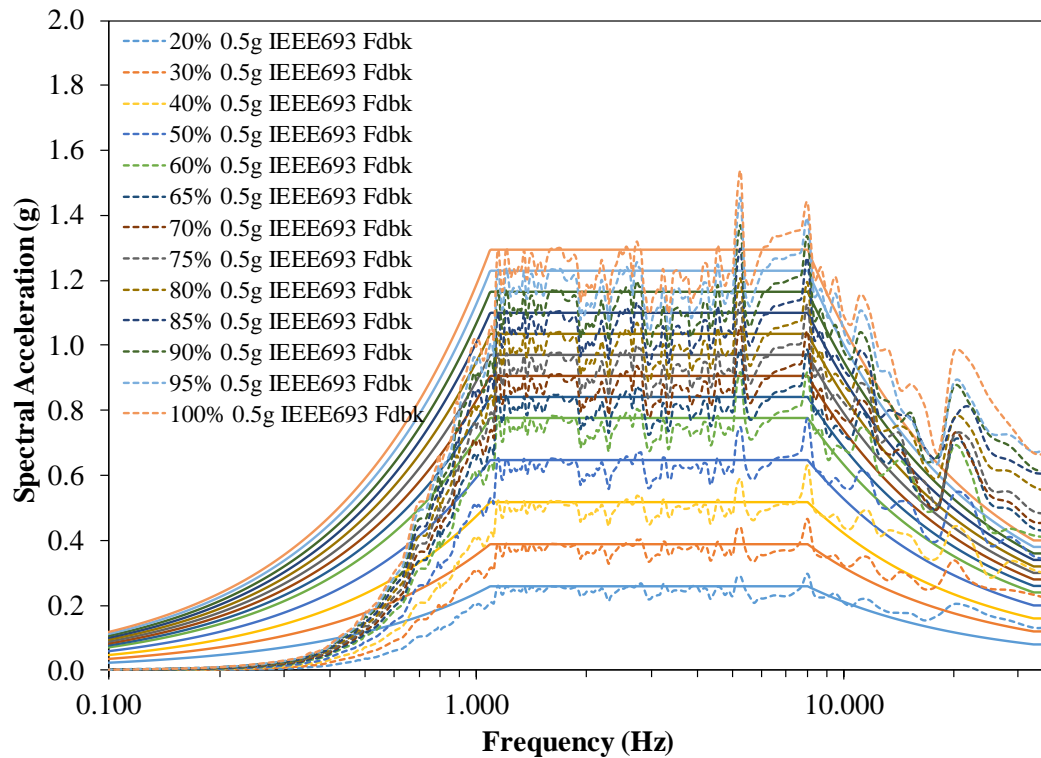


Figure 13-3: Response Spectrum Z (Viscous Damper)

13.3.2 Viscous Damper System Damping & Free Vibration

Utilizing pulse and white noise excitations, system properties were determined prior to each ground motion. Using Fourier analysis the fundamental frequency was determined and recorded in Table 13-4. In addition, elastic damping was calculated using logarithmic decrement and recorded in Table 13-4. Free vibration plots for each test case are located in Appendix G. The system with viscous dampers had an average fundamental frequency of 0.86Hz in the X-direction and 0.75Hz in the Y-direction. The system had 1%-2.5% damping in the horizontal directions with an average of 1.22% in the X-direction and 1.84% in the Y-direction.

Table 13-4: Viscous Damper -- Retrofit Damping and Fundamental Frequency

	% Motion	Motion Name	Retrofit Device	Pulse Free Vibration				White Noise		
				Fundamental Frequency (Hz)		Elastic Damping		Fundamental Frequency (Hz)		
				x	y	x	y	x	y	z
Pre	20	0.5g IEEEE693 tQke	Viscous	0.89	0.80	1.14%	2.33%	0.89	0.80	24.49
Pre	30	0.5g IEEEE693 tQke	Viscous	0.80	0.80	1.07%	1.11%	0.89	0.80	24.49
Pre	40	0.5g IEEEE693 tQke	Viscous	0.88	0.77	0.98%	1.69%	0.88	0.80	24.97
Pre	50	0.5g IEEEE693 tQke	Viscous	0.87	0.77	1.12%	1.59%	0.87	0.87	24.97
Pre	60	0.5g IEEEE693 tQke	Viscous	0.88	0.77	1.30%	1.96%	0.87	0.87	24.97
Pre	65	0.5g IEEEE693 tQke	Viscous	0.86	0.76	1.24%	2.11%	0.84	0.73	27.38
Pre	70	0.5g IEEEE693 tQke	Viscous	0.85	0.76	0.79%	1.56%	0.82	0.74	27.38
Pre	75	0.5g IEEEE693 tQke	Viscous	0.86	0.74	1.11%	1.64%	0.83	0.71	27.24
Pre	80	0.5g IEEEE693 tQke	Viscous	0.86	0.74	1.29%	1.93%	0.84	0.73	27.38
Pre	85	0.5g IEEEE693 tQke	Viscous	0.86	0.73	1.18%	1.46%	0.84	0.71	27.38
Pre	90	0.5g IEEEE693 tQke	Viscous	0.86	0.72	1.47%	2.15%	0.83	0.71	27.24
Pre	95	0.5g IEEEE693 tQke	Viscous	0.87	0.70	1.46%	1.89%	0.83	0.63	27.24
Pre	100	0.5g IEEEE693 tQke	Viscous	0.88	0.68	1.66%	2.53%	0.83	0.63	27.38
Average Response				0.86	0.75	1.22%	1.84%	0.85	0.75	26.35

13.3.3 Viscous Damper System Response

Summarized in this section is the system response to various amplitudes of the 0.5g IEEEE693 synthetic ground motion. Metrics of importance include maximum accelerations along the specimen, system forces, and system displacements. In initial phases of the retrofit development, utilizing a SDOF approach simplified calculations and the design procedure. Evaluating the full-scale system's response, solely considering a lumped mass misrepresents the system's behavior.

A summary of the maximum accelerations measured along the specimen length are reported in Table 13-5, Table 13-6, and Table 13-7. The tables present absolute maximum accelerations for each tested IEEEE693 amplitude. Maximum acceleration magnitudes are reported for each accelerometer location along the specimen's length. Generally, the viscous damper retrofitted system experienced no vertical amplifications. The input vertical excitation was equal to the amplitude of the response acceleration at

the top of the specimen. Amplification trends are present in the lateral components of the acceleration data. Throughout the data obtained for the viscous retrofit case, the top three accelerometer nodes present higher acceleration magnitudes than the rest of the system. For all accelerometers located below 304-1/2 inches, the acceleration magnitudes were similar with exception of the base accelerometer.

Table 13-5: Viscous Damper – System X Absolute Maximum Acceleration

		% of IEEE693 0.5g Motion													
		20%	30%	40%	50%	60%	65%	70%	75%	80%	85%	90%	95%	100%	
X - Absolute Maximum Acceleration (g)		0.23	0.37	0.47	0.58	0.66	0.67	0.71	0.84	0.85	0.82	0.85	0.78	1.02	351
		0.18	0.29	0.37	0.42	0.49	0.51	0.56	0.61	0.59	0.58	0.62	0.64	0.82	322
		0.16	0.26	0.34	0.38	0.45	0.47	0.49	0.56	0.53	0.54	0.59	0.60	0.75	304 1/2
		0.14	0.24	0.30	0.35	0.41	0.43	0.44	0.46	0.45	0.50	0.56	0.57	0.69	285 1/2
		0.15	0.21	0.27	0.34	0.40	0.42	0.43	0.46	0.45	0.51	0.56	0.59	0.72	268 1/2
		0.14	0.22	0.28	0.34	0.39	0.44	0.45	0.50	0.47	0.52	0.57	0.58	0.72	254
		0.15	0.25	0.29	0.35	0.43	0.42	0.46	0.52	0.45	0.56	0.66	0.64	0.69	235
		0.16	0.23	0.28	0.38	0.38	0.44	0.45	0.55	0.46	0.60	0.71	0.62	0.71	214 1/2
		0.17	0.25	0.31	0.39	0.40	0.44	0.46	0.57	0.47	0.62	0.77	0.66	0.66	199
		0.18	0.24	0.30	0.42	0.43	0.46	0.48	0.61	0.48	0.67	0.88	0.67	0.68	182
		0.17	0.24	0.30	0.39	0.47	0.47	0.50	0.58	0.54	0.68	0.95	0.73	0.69	163
		0.16	0.22	0.29	0.41	0.48	0.47	0.50	0.52	0.56	0.69	0.88	0.73	0.72	146
		0.17	0.21	0.30	0.42	0.49	0.47	0.50	0.51	0.59	0.64	0.81	0.84	0.81	127
		0.18	0.22	0.32	0.41	0.45	0.48	0.51	0.53	0.68	0.71	0.92	0.89	0.81	91
	0.14	0.18	0.24	0.30	0.35	0.39	0.41	0.44	0.47	0.49	0.51	0.53	0.63	1 1/8	
	0.12	0.18	0.24	0.29	0.34	0.37	0.40	0.44	0.45	0.48	0.49	0.52	0.55	0	

Location (in), See Fig. 12-4 & Table 12-1

Table 13-6: Viscous Damper – System Y Absolute Maximum Acceleration

% of IEEE693 0.5g Motion														
20%	30%	40%	50%	60%	65%	70%	75%	80%	85%	90%	95%	100%		
0.31	0.41	0.49	0.57	0.67	0.73	0.82	0.82	1.01	1.15	1.04	1.06	1.06	351	Location (in), See Fig. 12-4 & Table 12-1
0.26	0.36	0.41	0.51	0.54	0.60	0.62	0.70	0.77	0.92	0.87	0.83	0.80	322	
0.23	0.31	0.39	0.45	0.48	0.53	0.58	0.61	0.62	0.73	0.72	0.70	0.70	304 1/2	
0.20	0.28	0.35	0.41	0.45	0.49	0.51	0.53	0.51	0.60	0.61	0.61	0.65	285 1/2	
0.18	0.26	0.32	0.39	0.42	0.45	0.48	0.50	0.50	0.57	0.57	0.57	0.65	268 1/2	
0.18	0.26	0.33	0.37	0.40	0.42	0.46	0.49	0.51	0.55	0.59	0.56	0.67	254	
0.19	0.26	0.34	0.36	0.44	0.45	0.49	0.52	0.53	0.61	0.62	0.55	0.67	235	
0.19	0.27	0.34	0.39	0.51	0.54	0.58	0.53	0.59	0.61	0.65	0.62	0.76	214 1/2	
0.19	0.28	0.33	0.39	0.49	0.54	0.59	0.51	0.57	0.66	0.61	0.60	0.67	199	
0.20	0.28	0.33	0.41	0.52	0.57	0.64	0.51	0.54	0.66	0.65	0.62	0.67	182	
0.19	0.27	0.33	0.41	0.52	0.58	0.62	0.51	0.58	0.68	0.61	0.63	0.68	163	
0.19	0.27	0.33	0.40	0.52	0.57	0.60	0.55	0.55	0.64	0.59	0.58	0.65	146	
0.18	0.27	0.32	0.42	0.53	0.53	0.61	0.60	0.64	0.73	0.62	0.57	0.68	127	
0.17	0.22	0.32	0.41	0.45	0.52	0.59	0.71	0.67	0.74	0.78	0.72	0.76	91	
0.14	0.18	0.24	0.30	0.35	0.39	0.35	0.39	0.44	0.43	0.44	0.47	0.57	1 1/8	
0.11	0.14	0.20	0.24	0.30	0.32	0.35	0.35	0.39	0.40	0.43	0.44	0.46	0	

Table 13-7: Viscous Damper – System Z Absolute Maximum Acceleration

% of IEEE693 0.5g Motion														
20%	30%	40%	50%	60%	65%	70%	75%	80%	85%	90%	95%	100%		
0.13	0.20	0.27	0.33	0.40	0.43	0.49	0.52	0.55	0.57	0.64	0.65	0.67	351	Location (in), See Fig. 12-4 & Table 12-1
0.13	0.21	0.28	0.33	0.41	0.45	0.50	0.51	0.56	0.59	0.64	0.66	0.67	322	
0.13	0.22	0.28	0.33	0.44	0.44	0.46	0.51	0.58	0.59	0.63	0.64	0.67	304 1/2	
0.13	0.21	0.28	0.34	0.41	0.45	0.50	0.51	0.56	0.58	0.63	0.65	0.66	285 1/2	
0.14	0.21	0.28	0.33	0.42	0.45	0.47	0.51	0.57	0.60	0.64	0.65	0.67	268 1/2	
0.13	0.20	0.28	0.33	0.40	0.44	0.49	0.51	0.55	0.57	0.64	0.64	0.68	254	
0.14	0.21	0.29	0.34	0.42	0.45	0.49	0.51	0.56	0.59	0.64	0.66	0.68	235	
0.13	0.20	0.29	0.33	0.41	0.44	0.49	0.50	0.55	0.58	0.64	0.65	0.69	214 1/2	
0.13	0.21	0.28	0.33	0.40	0.44	0.49	0.51	0.55	0.58	0.63	0.65	0.68	199	
0.13	0.20	0.28	0.34	0.41	0.45	0.49	0.52	0.55	0.59	0.64	0.64	0.69	182	
0.15	0.21	0.28	0.33	0.40	0.45	0.48	0.51	0.54	0.58	0.64	0.64	0.68	163	
0.14	0.19	0.28	0.33	0.41	0.46	0.51	0.51	0.55	0.58	0.63	0.66	0.68	146	
0.13	0.19	0.28	0.34	0.39	0.45	0.50	0.51	0.53	0.57	0.62	0.65	0.67	127	
0.14	0.21	0.28	0.33	0.39	0.43	0.48	0.51	0.54	0.57	0.60	0.65	0.67	91	
0.13	0.20	0.27	0.33	0.38	0.41	0.45	0.46	0.50	0.54	0.56	0.60	0.64	1 1/8	
0.12	0.19	0.26	0.31	0.37	0.40	0.44	0.46	0.50	0.53	0.56	0.60	0.64	0	

Using the methods discussed in 12.1, Instrumentation, accelerometer measurements allowed for base shear and moment at specific locations of the system to be determined. Summarized in Table 13-8 are moment and shear values at two locations

on the specimen. The first area of interest is the maximum moment in the pedestal base and the second location of interested is the pedestal-CT interface. The maximum moment seen between both measurement methods was 1079 kip-in. for the 100% 0.5g IEEE693 motion. Only the acceleration methods discussed in 12.1, Instrumentation, allowed calculating base shear in the specimen because of the strain gauge orientation on the specimen. The maximum base shear in the primary direction was 4 kips associated with a moment of 1039 kip-in. A base shear of 5.2 kips is estimated in the X'-direction associated with the maximum moment. Based on the section modulus and standard 42ksi grade steel, the expected nominal yield moment is 1205 kip-in. The maximum moment exerted on the CT interface was 681 kip-in.

Table 13-8: Viscous Damper – System Absolute Maximum Reactions

Absolute Max Reaction	Method	% of IEEE693 0.5g Motion												
		20%	30%	40%	50%	60%	65%	70%	75%	80%	85%	90%	95%	100%
Base Moment X	Strain	205	335	429	502	581	597	614	613	647	674	751	761	835
Base Moment Y	Strain	285	407	513	577	625	650	692	700	731	762	786	823	853
Base Moment X'	Strain	273	458	559	676	734	763	811	827	850	900	951	992	1079
Base Moment Y'	Strain	166	230	302	412	400	448	516	593	603	669	690	672	690
Base Moment X	Accel.	226	355	455	551	628	626	646	661	719	796	919	916	1039
Base Moment Y	Accel.	299	422	536	603	655	696	719	759	780	819	835	901	902
Base Shear X	Accel.	0.9	1.4	1.9	2.2	2.4	2.5	2.7	2.8	3.3	3.6	3.8	3.7	4.0
Base Shear Y	Accel.	1.2	1.8	2.2	2.5	2.8	3.0	3.2	3.3	3.5	3.5	3.5	3.7	3.8
Moment CT Interface X	Accel.	148	240	304	354	417	423	444	487	482	524	578	588	681
Moment CT Interface Y	Accel.	205	288	355	407	442	478	500	521	534	592	586	583	589
Shear CT Interface X	Accel.	0.8	1.3	1.7	2.0	2.2	2.3	2.4	2.6	2.7	2.8	3.3	3.2	3.7
Shear CT Interface Y	Accel.	0.7	1.1	1.5	1.8	2.1	2.3	2.6	2.5	2.7	2.9	3.3	3.4	3.5

Moment (kip-in); Shear (kips)

(See Figure 12-2, Strain Gauge Placement for (X,Y) & (X',Y'))

System relative displacement was another important factor used for determining the effectiveness of the retrofit measure. Shown in Table 13-9 and Table 13-10 are the relative displacements between the point of interest and the shake table. Top of Pedestal,

modeled CT C.G., and top of specimen measurements are reported. For the 100% motion, the top of the modeled CT experienced a 21.7 inch maximum displacement.

Table 13-9: Viscous Damper – System Maximum Displacement 20-65% Motions

Location	Location from Base (in.)	% of IEEE693 0.5g Motion						Displacement (in.)
		20%	30%	40%	50%	60%	65%	
Top of Pedestal X	91 1/2	0.610	0.947	1.291	1.769	2.163	2.130	
Top of Pedestal Y	91 1/2	0.862	1.205	1.687	2.012	2.492	2.812	
CG X	215	1.628	2.565	3.468	4.657	5.601	5.698	
CG Y	216 1/2	2.335	3.287	4.536	5.371	6.413	7.207	
Top Displacement X	352 1/2	2.814	4.498	5.933	7.988	9.584	9.798	
Top Displacement Y	352 1/2	4.009	5.696	7.779	9.203	10.846	12.161	

Table 13-10: Viscous Damper – System Maximum Displacement 70-100% Motions

Location	Location from Base (in.)	% of IEEE693 0.5g Motion							Displacement (in.)
		70%	75%	80%	85%	90%	95%	100%	
Top of Pedestal X	91 1/2	2.202	2.847	3.493	3.876	4.508	4.738	5.137	
Top of Pedestal Y	91 1/2	3.024	3.441	3.867	4.119	4.421	4.638	4.945	
CG X	215	5.899	7.155	8.710	9.669	11.210	11.759	12.819	
CG Y	216 1/2	7.757	8.785	9.875	10.510	11.293	11.847	12.612	
Top Displacement X	352 1/2	10.139	12.186	14.766	16.360	18.970	19.867	21.707	
Top Displacement Y	352 1/2	13.078	14.827	16.690	17.741	19.048	19.985	21.239	

To investigate the true self-centering abilities of the designed retrofit, post-motion system position is reported in Table 13-11 and Table 13-12. The largest residual displacements of 0.22 inch is present for the 100% motion. The residual displacement equates to a 0.035° angle. The tested system with viscous dampers presented true self-centering with negligible residual displacements.

Table 13-11: Viscous Damper – System Residual Displacement 20-65% Motions

Location	Location from Base (in.)	% of IEEE693 0.5g Motion						Displacement (in.)
		20%	30%	40%	50%	60%	65%	
Top of Pedestal X	91 1/2	-0.008	0.005	-0.005	0.002	0.016	0.023	
Top of Pedestal Y	91 1/2	0.002	0.008	0.009	0.015	0.006	0.011	
CG X	215	-0.032	0.039	-0.010	0.014	0.038	0.056	
CG Y	216 1/2	-0.005	0.030	0.005	0.020	0.006	0.016	
Top Displacement X	352 1/2	-0.048	0.068	0.000	0.022	0.065	0.078	
Top Displacement Y	352 1/2	-0.034	0.046	-0.018	0.009	0.003	-0.010	

Table 13-12: Viscous Damper – System Residual Displacement 70-100% Motions

Location	Location from Base (in.)	% of IEEE693 0.5g Motion								Displacement (in.)
		70%	75%	80%	85%	90%	95%	100%		
Top of Pedestal X	91 1/2	0.019	0.000	-0.002	0.020	0.051	0.055	0.069		
Top of Pedestal Y	91 1/2	0.016	0.013	0.006	0.017	0.008	0.000	0.010		
CG X	215	0.033	0.015	0.008	0.022	0.131	0.101	0.129		
CG Y	216 1/2	0.026	0.018	0.017	0.039	0.022	0.020	0.022		
Top Displacement X	352 1/2	0.042	0.013	0.036	0.029	0.213	0.163	0.220		
Top Displacement Y	352 1/2	-0.008	0.021	0.017	-0.005	0.007	-0.001	0.019		

Pedestal strain gauges allow for determining yielding initiation in the support pedestal. Nominal yielding is to occur at 42ksi or 1450 micro strain in extreme fibers of the pedestal. All motions over 90% caused strains in the pedestal beyond 1450 micro strain in at least a single strain gauge on the pedestal. A complete summary of absolute maximum strain readings are presented in Table 13-13.

Table 13-13: Viscous Damper – Pedestal Absolute Maximum Strain

Pedestal Strain ($\mu\epsilon$)	% of IEEE693 0.5g Motion												
	20%	30%	40%	50%	60%	65%	70%	75%	80%	85%	90%	95%	100%
North Gauge	358	525	666	731	789	822	872	877	873	877	896	947	1011
South Gauge	296	448	570	626	730	766	819	886	966	1002	1026	1076	1109
NE Gauge	219	285	356	485	620	663	723	714	735	924	1091	1061	1072
SW Gauge	235	320	458	653	620	702	820	943	960	1072	1112	1056	1087
East Gauge	190	308	429	519	595	578	586	617	705	729	814	813	894
West Gauge	257	435	558	658	755	781	805	804	762	693	769	795	870
SE Gauge	393	722	883	1013	1115	1135	1205	1243	1266	1308	1409	1474	1635
NW Gauge	410	672	865	1068	1165	1205	1279	1305	1346	1426	1508	1575	1726

Residual strain from each ground motion provides a metric for comparing the demand exerted on the pedestal during the motion with the specific retrofit. Shown in Table 13-14 are the residual strains in the pedestal for each ground motion. All motions under 90% had residual strains up to $8\mu\epsilon$. The slight shift in strain readings is likely due to slight reposition in the mass positions after each ground motion.

Table 13-14: Viscous Damper – Pedestal Residual Strain

Pedestal Strain ($\mu\varepsilon$)	% of IEEE693 0.5g Motion												
	20%	30%	40%	50%	60%	65%	70%	75%	80%	85%	90%	95%	100%
North Gauge	2	-6	3	2	0	0	3	2	1	5	7	10	16
South Gauge	-4	4	1	6	-1	2	1	5	9	10	6	6	12
NE Gauge	9	-6	2	-1	-2	-2	-2	-1	2	2	9	0	7
SW Gauge	-6	12	2	5	2	1	2	4	2	1	-3	2	4
East Gauge	7	-6	0	-5	5	1	0	2	3	5	11	6	8
West Gauge	-6	10	1	6	6	4	7	6	3	4	4	7	14
SE Gauge	3	-4	0	0	3	3	3	6	7	5	11	13	24
NW Gauge	-2	4	4	9	7	4	8	5	4	8	12	16	28

Maximum uplift of the damper was determined for each ground motion, Table 13-15. The largest uplift experienced by the NW viscous damper measured 1.29 inches. All quadrants of the base had similar magnitude uplift values ranging from 1.07 inches - 1.29 inches. In all cases, the system returned to its initial position and the devices had no residual displacements, Table 13-16.

Table 13-15: Viscous Damper – Damper Absolute Maximum Displacement

Device Displacement	% of IEEE693 0.5g Motion												
	20%	30%	40%	50%	60%	65%	70%	75%	80%	85%	90%	95%	100%
NE	0.12	0.15	0.25	0.35	0.51	0.59	0.64	0.76	0.87	0.92	1.01	1.04	1.11
SE	0.12	0.19	0.31	0.44	0.58	0.62	0.68	0.73	0.81	0.90	1.02	1.08	1.18
SW	0.13	0.18	0.29	0.36	0.44	0.47	0.51	0.55	0.71	0.80	0.97	1.00	1.07
NW	0.14	0.20	0.32	0.45	0.58	0.65	0.70	0.81	0.92	0.99	1.11	1.19	1.29

Table 13-16: Viscous Damper – Damper Residual Displacement

Device Displacement	% of IEEE693 0.5g Motion												
	20%	30%	40%	50%	60%	65%	70%	75%	80%	85%	90%	95%	100%
NE	0.00	0.00	0.00	0.00	0.00	0.00	0.00	0.00	0.00	0.00	0.01	0.01	0.01
SE	0.00	0.00	0.00	0.00	0.00	0.00	0.00	0.00	0.00	0.00	0.01	0.01	0.01
SW	0.00	0.00	0.00	0.00	0.00	0.00	0.00	0.00	0.00	0.00	-0.01	-0.01	-0.01
NW	0.00	0.00	0.00	0.00	0.00	0.00	0.00	0.00	0.01	0.01	0.00	0.01	0.01

Also, force displacement curves were constructed for 20%, 50%, 75%, and 100% motions. Shown in Figure 13-4 is a force-displacement hysteresis for the Y-direction of

the 100% test case. The system presents frequency reduction shift due to stiffness reduction after rocking is initiated, energy dissipation, and self-centering. A complete set of force-displacement curves for each device on the retrofit is located in Appendix H. The largest damper force was present in the NW device, 7.43 kips. Since the viscous devices are velocity dependent and non-linear, the load is not directly proportional to the displacement felt by the device.

Table 13-17: Viscous Damper – Damper Maximum Force

Device Force (kips)	% of IEEE693 0.5g Motion												
	20%	30%	40%	50%	60%	65%	70%	75%	80%	85%	90%	95%	100%
NE Device	1.87	2.42	3.02	3.62	4.44	4.70	5.14	5.27	5.73	6.06	6.02	6.21	6.42
SE Device	1.70	1.97	2.78	3.60	4.26	4.47	4.70	4.98	5.19	4.97	5.46	5.40	5.39
SW Device	1.71	2.15	2.85	3.40	3.84	4.04	4.44	4.51	4.65	4.77	5.72	5.70	6.26
NW Device	2.14	3.16	3.51	4.25	4.99	5.41	6.35	6.74	7.70	7.23	7.80	7.30	7.43

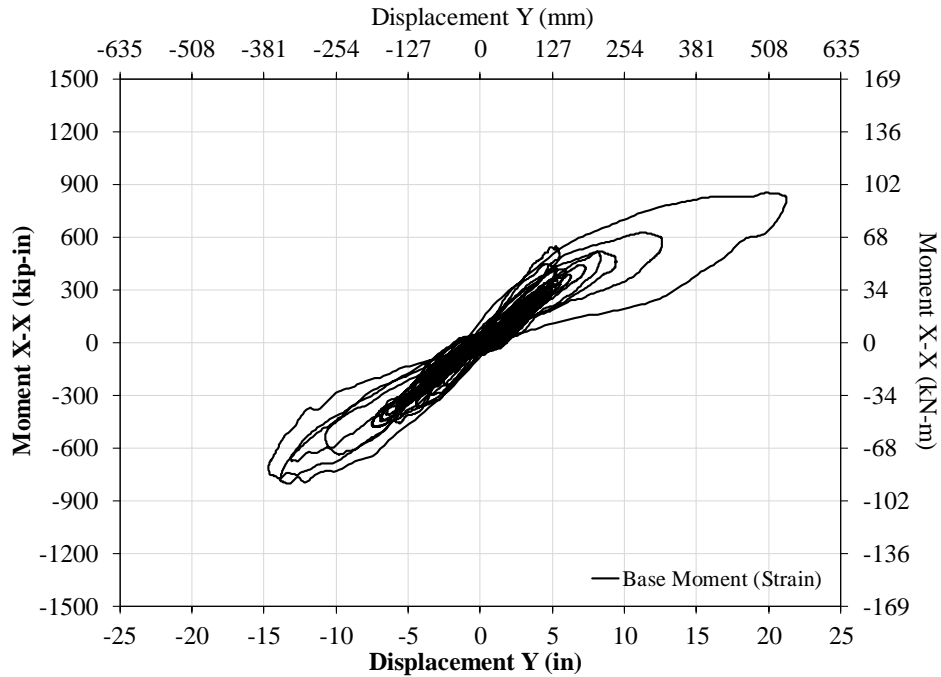


Figure 13-4: 100% 0.5g IEEE693 Y-System Response w/ Viscous Dampers

All device assembly bracket connections are designed to be slip-critical, slip is undesirable because slip reduces the relative displacement between the energy-dissipating device and the rocking structure. The reduced relative displacement decreases the effectiveness of the device and typically leads to larger accelerations and global displacements. Summarized in Table 13-18 is the maximum slip in the device assembly bracket which occurred during the ground motion. All slip values were minimal but re-torquing bolts between motions could have reduced slip magnitudes.

Table 13-18: Viscous Damper – Damper Bracket Slip

Device Slip (in.)	% of IEEE693 0.5g Motion												
	20%	30%	40%	50%	60%	65%	70%	75%	80%	85%	90%	95%	100%
NE-N	0.001	0.002	0.003	0.005	0.011	0.013	0.015	0.018	0.022	0.025	0.025	0.024	0.026
SE-S	0.002	0.003	0.005	0.006	0.007	0.008	0.010	0.011	0.013	0.013	0.018	0.017	0.020
SW-S	0.064	0.003	0.072	0.075	0.008	0.010	0.012	0.011	0.010	0.011	0.010	0.013	0.013
NW-N	0.002	0.003	0.005	0.004	0.006	0.007	0.012	0.017	0.024	0.023	0.031	0.029	0.033

Each BeS set was preloaded to 3.73 kips as previously discussed in the full-scale design section. During each motion, the maximum force transferred through the elastic springs into the foundation was determined and reported in Table 13-19. The maximum force transferred through the pre-tensioning was 11.4 kips, which was below 12.8 kip maximum linear load.

Table 13-19: Viscous Damper – Maximum PT Force

PT Force (kips)	% of IEEE693 0.5g Motion												
	20%	30%	40%	50%	60%	65%	70%	75%	80%	85%	90%	95%	100%
PT North	4.07	4.34	5.32	6.01	6.89	7.51	7.51	8.65	9.29	9.61	10.12	10.33	11.38
PT East	4.18	4.49	4.84	5.57	6.23	6.37	6.59	6.54	6.91	7.29	8.07	8.53	9.16
PT South	4.45	4.76	5.50	6.13	6.76	7.00	7.48	7.64	7.98	8.23	8.51	8.71	9.13
PT West	4.15	4.59	4.89	5.68	6.24	6.06	6.33	7.29	8.36	9.01	10.13	10.83	11.44

Loss in pre-tensioning force is of extreme importance because of its influence on rocking initiation, self-centering, and system behavior. Percent of force variation between

the initial pre-tension load and the final pre-tension load are shown in Table 13-20. Pre-tension force loss was usually below 2%, some cases presented pre-tension force decreases ranging from 4% - 7%. Two instances showed a pre-tension member losing roughly 7% of the force after excitation.

Table 13-20: Viscous Damper – % PT Force Loss Post Motion

PT Force Loss (kips)	% of IEEE693 0.5g Motion												
	20%	30%	40%	50%	60%	65%	70%	75%	80%	85%	90%	95%	100%
PT North	0.2%	-0.4%	-0.8%	-0.8%	-1.4%	-1.0%	-1.7%	-1.8%	-1.2%	-6.8%	-1.7%	-1.9%	-4.0%
PT East	-0.8%	0.4%	0.0%	-1.2%	-1.0%	0.0%	-1.4%	-0.4%	-0.4%	-3.7%	0.6%	-0.4%	0.2%
PT South	-0.9%	0.0%	-1.3%	-1.2%	-0.6%	-0.2%	-1.9%	-0.6%	-0.6%	-4.8%	-1.0%	-2.3%	-1.9%
PT West	-1.3%	-0.9%	-0.4%	-1.5%	-1.5%	-0.4%	-1.6%	-1.7%	-2.1%	-7.1%	-4.3%	-4.0%	-4.0%

As the motion amplitude increased, the system rocking and displacement also increased. Displayed in Table 13-21 are the maximum uplifts experienced by each side of the pedestal base plate. The largest uplift occurred on the north side of the base plate for the 0.5g IEEE693 motion. The system experienced 1.326 inches of vertical displacement on the north side of the pedestal base.

Table 13-21: Viscous Damper – Pedestal Rocking Uplift

Uplift (in.)	% of IEEE693 0.5g Motion												
	20%	30%	40%	50%	60%	65%	70%	75%	80%	85%	90%	95%	100%
Base PL Uplift N	0.139	0.180	0.304	0.423	0.599	0.693	0.747	0.874	0.996	1.069	1.177	1.233	1.326
Base PL Uplift E	0.093	0.160	0.226	0.356	0.476	0.501	0.512	0.505	0.498	0.567	0.706	0.757	0.863
Base PL Uplift S	0.140	0.206	0.335	0.442	0.562	0.606	0.659	0.688	0.737	0.774	0.824	0.847	0.906
Base PL Uplift W	0.101	0.171	0.235	0.369	0.477	0.447	0.440	0.664	0.851	0.957	1.148	1.207	1.304

In order to anchor the system to the shake table, a steel adaptor plate was utilized to attach all foundation anchors. Usually, steel-to-steel contact provides less surface friction than a steel-to-concrete interface. The friction force developed in actual implementation of the retrofit is expected to be greater than that presented in the experimental stages of this study. The largest base slip exhibited by the system was 0.17

inch. The maximum residual base slip displacement was 0.12 inch manifesting in the 100% motion. A report of the maximum and residual base plate slip results are presented in Table 13-22 and Table 13-23.

Table 13-22: Viscous Damper – Maximum Base Plate Slip

Device Uplift (in.)	% of IEEE693 0.5g Motion												
	20%	30%	40%	50%	60%	65%	70%	75%	80%	85%	90%	95%	100%
Base PL Slip NE-X	0.01	0.01	0.02	0.04	0.05	0.05	0.06	0.05	0.06	0.08	0.08	0.12	0.13
Base PL Slip SE-X	0.01	0.03	0.03	0.04	0.06	0.08	0.08	0.08	0.08	0.09	0.12	0.13	0.13
Base PL Slip SW-X	0.01	0.02	0.03	0.03	0.04	0.06	0.06	0.06	0.08	0.07	0.11	0.14	0.16
Base PL Slip NW-X	0.01	0.02	0.03	0.05	0.07	0.06	0.07	0.08	0.11	0.13	0.15	0.16	0.15
Base PL Slip NE-Y	0.02	0.03	0.04	0.05	0.06	0.08	0.09	0.10	0.12	0.13	0.14	0.14	0.16
Base PL Slip SE-Y	0.02	0.02	0.03	0.04	0.05	0.05	0.05	0.06	0.07	0.09	0.11	0.17	0.17
Base PL Slip SW-Y	0.02	0.02	0.04	0.06	0.07	0.08	0.09	0.10	0.11	0.10	0.11	0.12	0.14
Base PL Slip NW-Y	0.02	0.02	0.03	0.04	0.05	0.05	0.06	0.06	0.08	0.11	0.10	0.14	0.17

Table 13-23: Viscous Damper – Relative Base Plate Movement Pre-Post Motion

Device Uplift (in.)	% of IEEE693 0.5g Motion												
	20%	30%	40%	50%	60%	65%	70%	75%	80%	85%	90%	95%	100%
Base PL Slip NE-X	0.00	0.00	0.00	-0.01	-0.01	-0.02	-0.03	-0.01	-0.01	-0.08	-0.06	-0.11	-0.12
Base PL Slip SE-X	0.00	0.00	0.00	0.01	0.01	0.00	0.00	0.02	0.05	0.06	0.08	0.11	0.11
Base PL Slip SW-X	0.00	0.00	0.00	-0.01	-0.01	0.00	0.00	-0.02	-0.05	-0.06	-0.08	-0.11	-0.11
Base PL Slip NW-X	0.00	0.00	0.00	0.01	0.01	0.02	0.03	0.01	0.01	0.07	0.05	0.10	0.12
Base PL Slip NE-Y	0.00	-0.01	-0.01	0.00	0.01	0.00	0.01	0.01	0.03	0.05	0.07	0.11	0.10
Base PL Slip SE-Y	0.00	0.01	0.01	0.00	-0.01	0.00	-0.01	-0.01	-0.03	-0.06	-0.08	-0.13	-0.12
Base PL Slip SW-Y	0.00	0.00	0.01	0.02	0.01	0.01	0.02	0.02	0.02	0.08	0.06	0.10	0.12
Base PL Slip NW-Y	0.00	-0.01	-0.01	-0.02	-0.01	-0.01	-0.02	-0.02	-0.03	-0.08	-0.07	-0.11	-0.12

13.4 Hysteretic Device

13.4.1 Hysteretic Device Table Response Spectrum

A response spectrum for each IEEE693 input motion was constructed to show the discrepancies between the design spectrum and the table feedback. As previously mentioned, the work conducted aimed to reduce component demands and not necessarily seismically qualify the equipment. For the two horizontal directions, X and Y, only frequencies between 0.5Hz-1.3Hz are of importance. The non-retrofitted system has a fundamental frequency of 1.24Hz; reduction in frequency due to rocking is expected in

the retrofitted cases. Shown in Figure 13-5 and Figure 13-6 are the horizontal component response spectrums. Both horizontal components have minor undershooting when comparing the table response to the design spectrum. Shown in Figure 13-3 is the response spectrum for the vertical direction, which envelopes all high frequencies of interest.

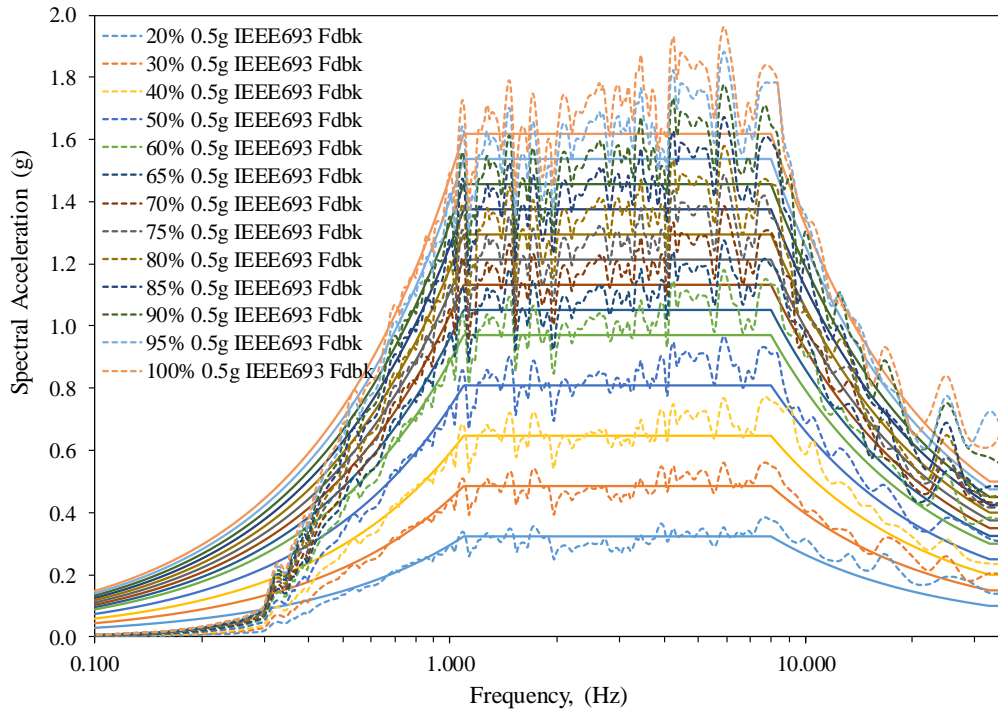


Figure 13-5: Hysteretic Device – Response Spectrum X

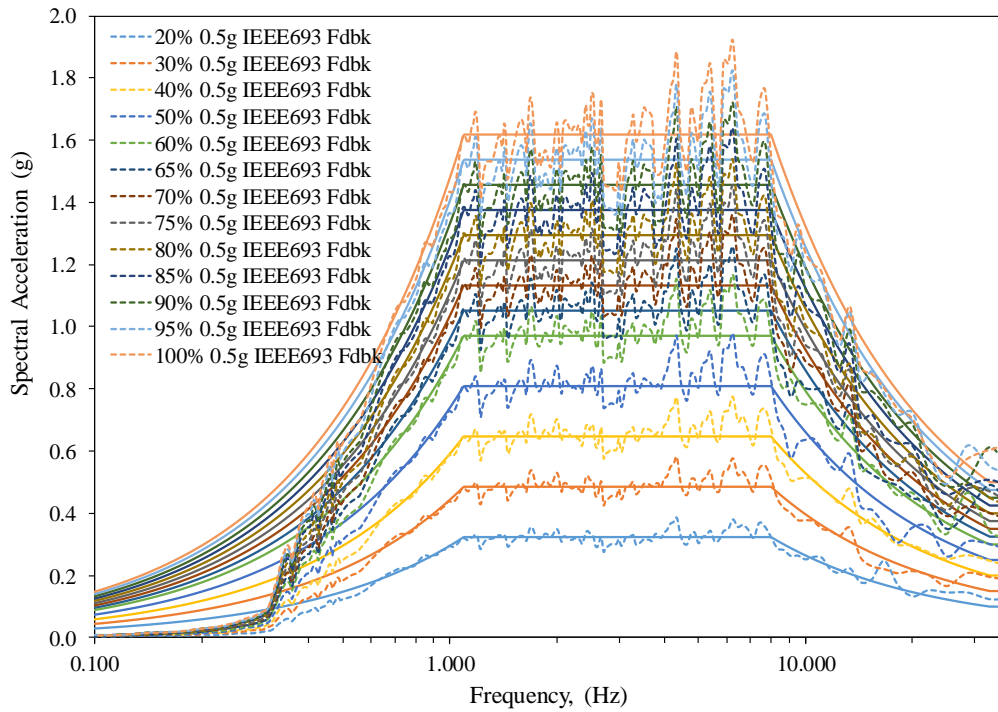


Figure 13-6: Hysteretic Device – Response Spectrum Y

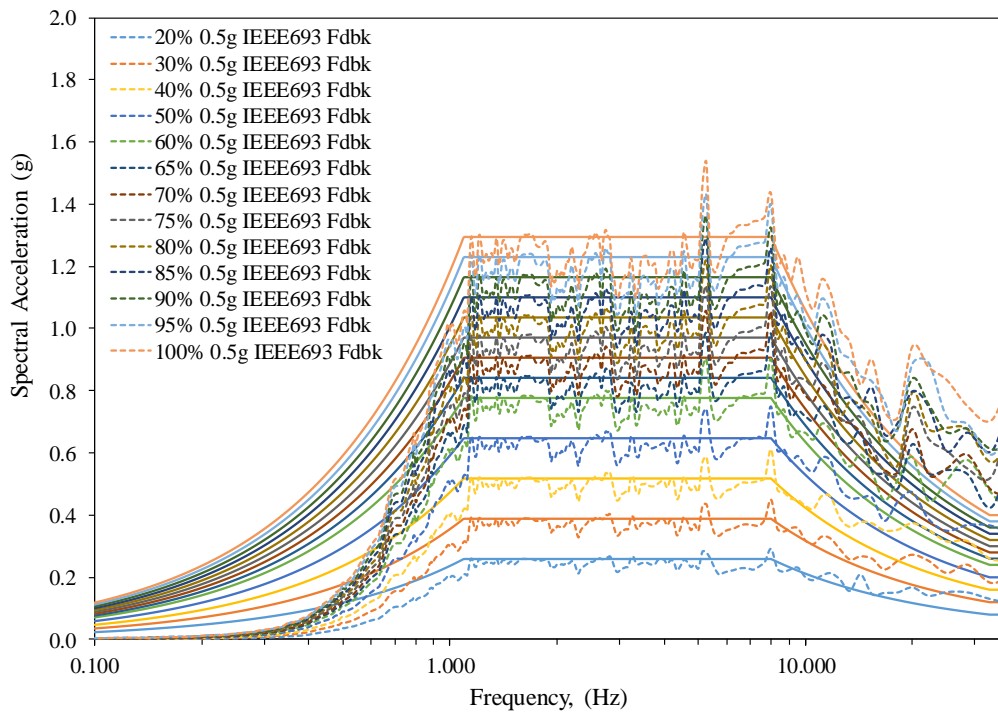


Figure 13-7: Hysteretic Device – Response Spectrum Z

13.4.2 Hysteretic Device System Damping & Free Vibration

Utilizing the same methods discussed in 13.3.2, Viscous Damper System Damping & Free Vibration, the elastic damping and fundamental frequency was determined for the rocking system with hysteretic devices. The average fundamental frequency in the X-direction was 0.80Hz using a pulse excitation and 0.78Hz using white noise excitation. Similarly, the average fundamental frequency for the Y-direction was 0.70Hz using a pulse excitation and 0.68Hz using white noise. Elastic damping X and Y components were 0.66% and 0.87% respectively. A complete summary of the system identification properties are presented in Table 13-24.

Table 13-24: UFP Retrofit Damping and Fundamental Frequency

	% Motion	Motion Name	Retrofit Device	Pulse Free Vibration				White Noise		
				Fundamental Frequency (Hz)		Elastic Damping		Fundamental Frequency (Hz)		
				x	y	x	y	x	y	z
Pre	20	0.5g IEE693 tQke	Hysteretic	0.95	0.80	0.77%	1.20%	0.95	0.80	28.19
Pre	30	0.5g IEE693 tQke	Hysteretic	0.84	0.73	0.76%	0.97%	0.87	0.71	27.38
Pre	40	0.5g IEE693 tQke	Hysteretic	0.81	0.71	0.64%	1.04%	0.82	0.70	27.25
Pre	50	0.5g IEE693 tQke	Hysteretic	0.79	0.68	0.73%	0.98%	0.80	0.66	25.49
Pre	60	0.5g IEE693 tQke	Hysteretic	0.76	0.66	0.56%	0.83%	0.73	0.64	24.49
Pre	65	0.5g IEE693 tQke	Hysteretic	0.75	0.66	0.58%	0.90%	0.73	0.64	24.97
Pre	70	0.5g IEE693 tQke	Hysteretic	0.74	0.65	0.68%	0.99%	0.73	0.64	24.49
Pre	75	0.5g IEE693 tQke	Hysteretic	0.75	0.66	0.56%	0.82%	0.73	0.64	24.50
Pre	80	0.5g IEE693 tQke	Hysteretic	0.75	0.66	0.58%	0.58%	0.73	0.64	24.50
Pre	85	0.5g IEE693 tQke	Hysteretic	0.77	0.68	0.66%	0.76%	0.73	0.67	27.39
Pre	90	0.5g IEE693 tQke	Hysteretic	0.77	0.68	0.65%	0.66%	0.73	0.64	24.97
Pre	95	0.5g IEE693 tQke	Hysteretic	0.79	0.70	0.77%	1.06%	0.82	0.68	27.25
Pre	100	0.5g IEE693 tQke	Hysteretic	0.80	0.70	0.59%	0.82%	0.68	0.68	27.39
Pre	100	0.5g IEE693 tQke	Hysteretic	0.93	0.80	-	-	0.93	0.80	-
Pre	100	0.5g IEE693 Rdm	Hysteretic	0.80	0.70	0.57%	0.93%	0.68	0.68	27.39
Pre	120	0.5g IEE693 Rdm	Hysteretic	0.81	0.70	0.58%	0.87%	0.82	0.68	27.25
Pre	140	0.5g IEE693 Rdm	Hysteretic	0.81	0.70	0.65%	0.75%	0.80	0.68	24.50
Pre	160	0.5g IEE693 Rdm	Hysteretic	0.85	0.73	0.87%	0.72%	0.82	0.71	27.39
Average Response				0.80	0.70	0.66%	0.87%	0.78	0.68	26.16

Supplemental figures demonstrating the damping for each case shown in Table 13-24 are provided in Appendix G. The calculated damping values are integrated into the plots through the bounded curves in Appendix G.

13.4.3 Hysteretic Device System Response

Similar to the metrics discussed for the viscous damper retrofit, this section summarizes the results obtained from testing for the rocking system with hysteretic devices. Summarized in Table 13-25, Table 13-26, and Table 13-27 are the absolute maximum acceleration values obtained during testing. Magnitudes are shown for each accelerometer location along the specimen length. The magnitudes do not all occur at the same instance during the ground motion but are maximums presented during the ground

motion. The 100% 0.5g IEEE693 motions were performed twice, one case considered virgin hysteretic devices denoted “*”, while the other 100% case was conducted post all preceding motion levels.

Table 13-25: Hysteretic Device – System X Absolute Maximum Acceleration

		% of IEEE693 0.5g Motion															
		20%	30%	40%	50%	60%	65%	70%	75%	80%	85%	90%	95%	100%	100%*		
X - Absolute Maximum Acceleration (g)		0.51	0.70	0.72	0.79	1.10	1.14	1.09	1.01	1.12	1.06	1.09	1.16	1.13	1.22	351	Location (in)
		0.42	0.54	0.59	0.61	0.68	0.81	0.82	0.78	0.81	0.81	0.81	0.88	0.92	0.96	322	
		0.39	0.48	0.54	0.54	0.63	0.69	0.68	0.70	0.68	0.71	0.76	0.81	0.85	0.87	304 1/2	
		0.34	0.40	0.47	0.48	0.55	0.59	0.56	0.59	0.56	0.59	0.65	0.68	0.76	0.72	285 1/2	
		0.32	0.39	0.43	0.46	0.53	0.53	0.54	0.60	0.54	0.60	0.62	0.69	0.71	0.69	268 1/2	
		0.31	0.41	0.43	0.48	0.55	0.57	0.56	0.63	0.58	0.65	0.66	0.69	0.77	0.73	254	
		0.30	0.42	0.44	0.49	0.67	0.64	0.60	0.64	0.64	0.67	0.66	0.73	0.78	0.76	235	
		0.28	0.43	0.43	0.49	0.58	0.67	0.67	0.65	0.66	0.69	0.67	0.74	0.72	0.74	214 1/2	
		0.30	0.45	0.43	0.49	0.68	0.71	0.71	0.71	0.72	0.72	0.71	0.76	0.73	0.76	199	
		0.30	0.47	0.43	0.50	0.68	0.72	0.78	0.81	0.67	0.75	0.73	0.74	0.79	0.84	182	
		0.30	0.50	0.40	0.56	0.71	0.73	0.79	0.79	0.71	0.80	0.82	0.79	0.82	0.87	163	
		0.28	0.49	0.38	0.58	0.64	0.70	0.81	0.72	0.74	0.77	0.83	0.79	0.91	0.88	146	
		0.26	0.47	0.38	0.62	0.71	0.68	0.76	0.72	0.76	0.83	0.83	0.78	0.89	0.84	127	
		0.23	0.49	0.41	0.66	0.85	0.73	0.72	0.78	0.89	0.86	0.86	0.91	1.09	0.98	91	
		0.14	0.18	0.24	0.29	0.36	0.38	0.40	0.54	0.50	0.50	0.53	0.53	0.73	0.60	1 1/8	
		0.14	0.18	0.23	0.28	0.34	0.38	0.38	0.40	0.42	0.45	0.50	0.52	0.56	0.56	0	

*virgin hysteretic device

Figure 13-8 show graphically the maximum acceleration results from Table 13-25 (20%, 50%, 75%, 100%, and 100%*). From the figure, visible increases in maximum acceleration are seen up to 151 inches from the system base and from 228 inches-304-1/2 inches. The graphic demonstrates how using just a single acceleration magnitude location near the CG (215-1/4”) will significantly misrepresent the system’s response. If actual acceleration is compared along the specimen length for the same time instance, not only are magnitudes of acceleration different along the specimen, but the direction of acceleration also varies as the system undergoes higher modes.

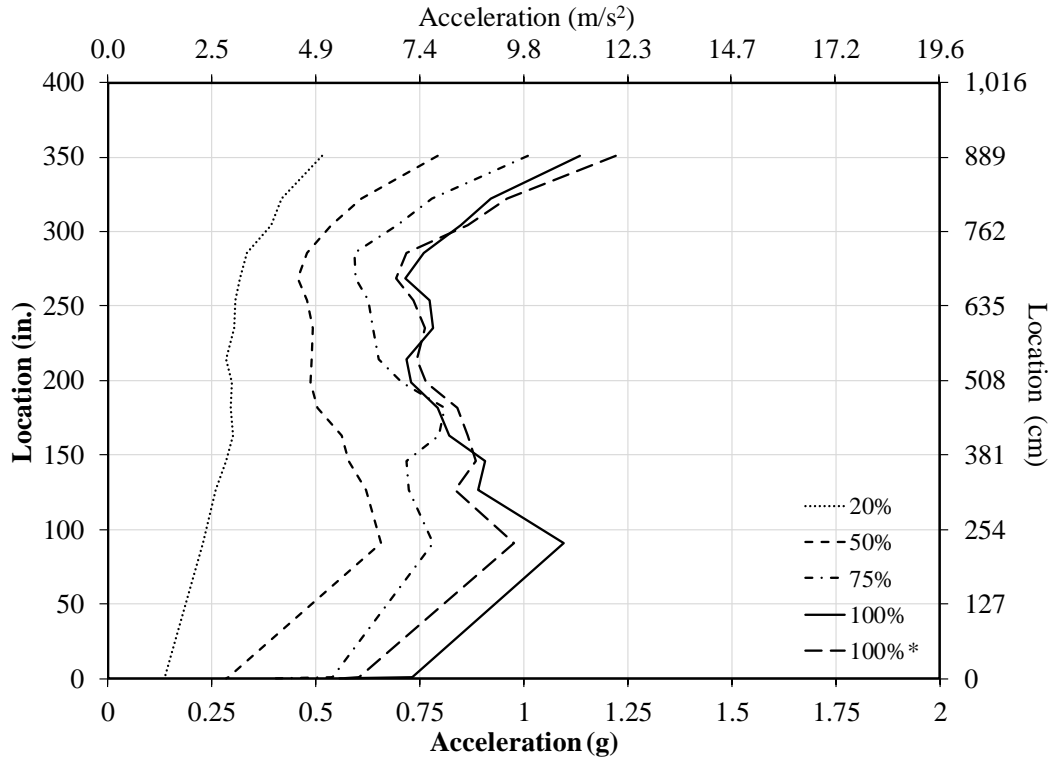


Figure 13-8: Hysteretic Device – System X Absolute Maximum Acceleration Plot

Table 13-26: Hysteretic Device – System Y Absolute Maximum Acceleration

		% of IEE693 0.5g Motion														
		20%	30%	40%	50%	60%	65%	70%	75%	80%	85%	90%	95%	100%	100%*	
Y - Absolute Maximum Acceleration (g)		0.57	0.69	0.73	0.77	1.08	1.20	1.12	1.04	1.05	1.10	1.10	1.30	1.57	1.50	351
		0.46	0.57	0.64	0.68	0.86	0.87	0.91	0.90	0.89	0.92	0.99	1.04	1.23	1.22	322
		0.37	0.49	0.57	0.61	0.73	0.75	0.75	0.77	0.76	0.82	0.85	0.87	0.96	0.99	304 1/2
		0.32	0.40	0.50	0.55	0.66	0.66	0.65	0.69	0.70	0.72	0.76	0.76	0.77	0.81	285 1/2
		0.32	0.40	0.46	0.50	0.60	0.63	0.63	0.65	0.70	0.70	0.73	0.76	0.74	0.78	268 1/2
		0.33	0.41	0.45	0.48	0.63	0.63	0.63	0.66	0.81	0.70	0.72	0.78	0.79	0.81	254
		0.34	0.43	0.45	0.49	0.72	0.77	0.69	0.65	0.88	0.77	0.76	0.92	0.91	0.90	235
		0.34	0.44	0.49	0.57	0.79	0.90	0.78	0.80	0.90	0.80	0.86	1.00	1.08	0.97	214 1/2
		0.34	0.44	0.51	0.57	0.80	0.92	0.75	0.73	0.86	0.81	0.79	0.94	1.03	1.07	199
		0.33	0.43	0.52	0.61	0.79	0.91	0.82	0.75	0.81	0.79	0.89	1.04	1.24	1.06	182
		0.33	0.44	0.56	0.61	0.85	0.87	0.79	0.77	0.73	0.80	0.82	0.96	1.10	1.06	163
		0.31	0.42	0.54	0.64	0.88	0.92	0.83	0.83	0.79	0.79	0.85	0.91	1.09	1.11	146
		0.30	0.40	0.53	0.61	0.90	0.94	0.83	0.83	0.86	0.80	0.94	0.93	1.05	1.11	127
		0.21	0.40	0.41	0.66	0.66	0.66	0.72	0.80	0.93	0.86	0.88	0.98	1.11	1.04	91
		0.14	0.18	0.24	0.29	0.36	0.38	0.40	0.54	0.50	0.50	0.53	0.53	0.73	0.60	1 1/8
	0.10	0.15	0.20	0.24	0.29	0.31	0.33	0.35	0.37	0.40	0.43	0.45	0.47	0.46	0	

*virgin hysteretic device

Similar acceleration trends were exhibited by the system in the Y-direction as discussed for the X-direction. Throughout the central portion of the system the acceleration maximums are near constant, while the values at the top of the structure and near the CT-pedestal interface significantly increase. The maximum magnitudes for 20%, 50%, 75%, 100% and 100%* from Table 13-26 are shown in Figure 13-9.

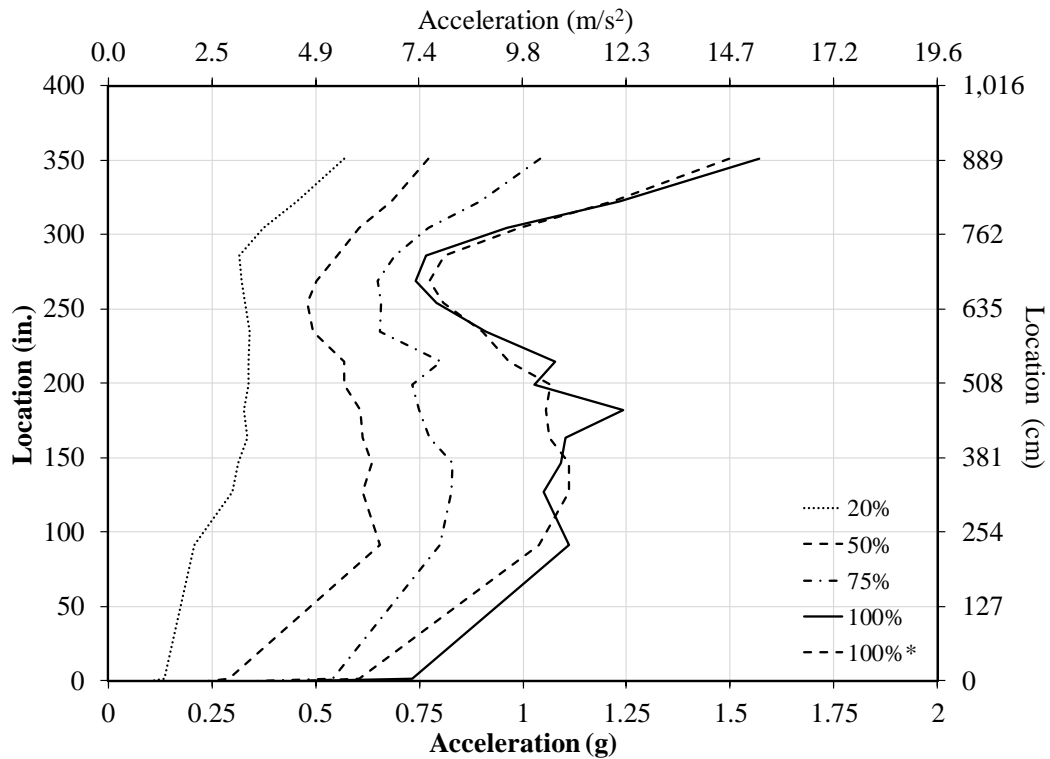


Figure 13-9: Hysteretic Device – System Y Absolute Maximum Acceleration Plot

Slight amplifications were detected in the z-direction accelerations; base accelerations could be compared to accelerations along the length of the specimen using Table 13-27. Due to slight angle change in the accelerometer during rocking, a portion of the acceleration detected is likely due to accelerometer tilt rather than acceleration amplification in the z-direction or base slapping.

Table 13-27: Hysteretic Device – System Z Absolute Maximum Acceleration

		% of IEEE693 0.5g Motion														
		20%	30%	40%	50%	60%	65%	70%	75%	80%	85%	90%	95%	100%	100%*	
Z - Absolute Maximum Acceleration (g)		0.13	0.22	0.27	0.33	0.39	0.47	0.48	0.63	0.56	0.72	0.61	0.68	0.72	0.78	351
		0.13	0.22	0.27	0.34	0.38	0.47	0.48	0.64	0.56	0.70	0.63	0.68	0.73	0.77	322
		0.13	0.22	0.27	0.32	0.39	0.47	0.48	0.63	0.54	0.69	0.62	0.68	0.73	0.77	304 1/2
		0.13	0.22	0.27	0.32	0.39	0.47	0.48	0.63	0.54	0.69	0.63	0.69	0.72	0.77	285 1/2
		0.14	0.21	0.26	0.33	0.39	0.45	0.49	0.63	0.54	0.66	0.63	0.70	0.72	0.76	268 1/2
		0.13	0.22	0.28	0.33	0.40	0.47	0.49	0.62	0.55	0.67	0.62	0.67	0.72	0.77	254
		0.13	0.21	0.28	0.34	0.41	0.45	0.49	0.62	0.55	0.65	0.64	0.68	0.71	0.77	235
		0.13	0.22	0.28	0.33	0.40	0.46	0.49	0.61	0.56	0.63	0.63	0.68	0.70	0.81	214 1/2
		0.12	0.21	0.28	0.34	0.39	0.45	0.49	0.58	0.55	0.63	0.63	0.68	0.71	0.81	199
		0.13	0.21	0.27	0.31	0.39	0.46	0.49	0.57	0.56	0.63	0.64	0.68	0.71	0.81	182
		0.13	0.21	0.28	0.32	0.38	0.46	0.49	0.55	0.54	0.61	0.64	0.68	0.70	0.83	163
		0.13	0.20	0.28	0.33	0.41	0.46	0.49	0.56	0.58	0.62	0.64	0.68	0.70	0.80	146
		0.12	0.20	0.27	0.33	0.40	0.46	0.49	0.53	0.55	0.60	0.64	0.69	0.70	0.74	127
		0.12	0.21	0.27	0.31	0.43	0.46	0.47	0.53	0.56	0.63	0.62	0.64	0.68	0.69	91
		0.12	0.19	0.28	0.34	0.48	0.63	0.50	0.57	0.55	0.66	0.58	0.65	0.68	0.63	1 1/8
		0.11	0.18	0.24	0.29	0.36	0.41	0.44	0.46	0.49	0.51	0.55	0.61	0.63	0.63	0

*virgin hysteretic device

A visual representation of 20%, 50%, 75%, 100%, and 100%* z-direction acceleration magnitudes are presented in Figure 13-10. At low level excitations, minimal amplification is exhibited by the system. As the amplitude of the input motion increases, larger increases in acceleration occur in the z-direction. The largest increase in acceleration is 29% seen in the virgin 100% 0.5g IEEE693 test case.

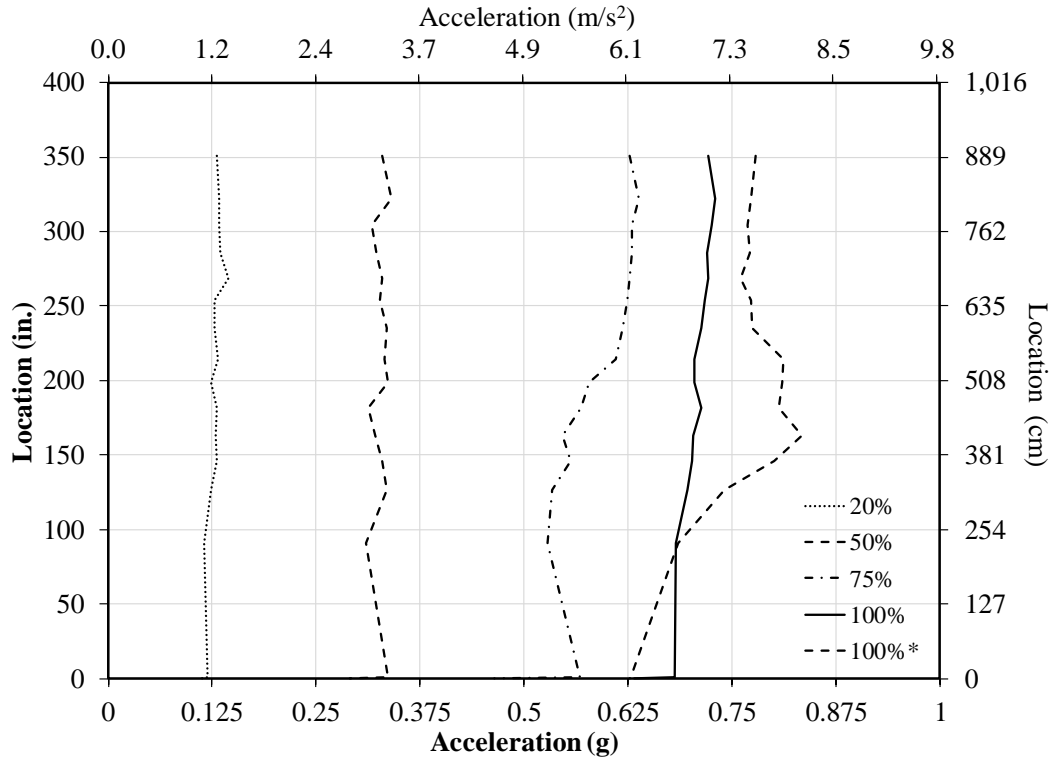


Figure 13-10: Hysteretic Device – System Y Absolute Maximum Acceleration Plot

Shear and moment measured directly and indirectly provide a more informative metric compared to maximum instantaneous acceleration because of higher mode effects. Using each acceleration reading along the specimen, base shear and moment for each instance of the motion was determined using the methods discussed in 12.1, Instrumentation. Both the direct strain and indirect acceleration approaches presented similar magnitude shear and moment values. For the 100% motions, the virgin device test case presented lower moments. The maximum X-moment and Y-moment using the strain method was 1070 kip-in and 1095 kip-in respectively for the non-virgin devices. Using the same method for the virgin cases, the maximum X-moment was 984 kip-in and 1047 kip-in for the virgin 100% motion. Utilizing the indirect acceleration method for the non-virgin case, the maximum X-moment was 1174 kip-in and 1134 kip-in for the Y-

direction. For the virgin case, the indirect method suggested a maximum X-moment of 1098 kip-in and maximum y-moment of 1109 kip-in. Generally, the mass-acceleration method resulted in 5%-10% greater moment magnitudes for the cases discussed. Using the nominal yield strength and section modulus, yield initiation is expected at 1188 kip-in. Maximum flexure resulted in the X'-direction with a moment of 1436 kip-in where pedestal yielding would occur even with the retrofit.

Table 13-28: Hysteretic Device – 20-65% System Absolute Maximum Reactions

Absolute Max Reaction	Method	% of IEEE693 0.5g Motion					
		20%	30%	40%	50%	60%	65%
Base Moment X	Strain	481	578	647	669	796	831
Base Moment Y	Strain	465	584	719	795	879	934
Base Moment X'	Strain	518	609	779	789	917	999
Base Moment Y'	Strain	403	556	698	537	541	544
Base Moment X	Accel.	513	616	725	757	863	872
Base Moment Y	Accel.	498	621	762	819	923	977
Base Shear X	Accel.	2.0	2.7	3.0	3.1	3.5	3.5
Base Shear Y	Accel.	2.1	2.7	3.1	3.3	4.2	4.3
CT-Inter. X Moment	Accel.	354	432	500	490	580	607
CT Inter. Y Moment	Accel.	342	435	523	559	656	671
CT Inter. X Shear	Accel.	1.8	2.4	2.7	2.7	3.2	3.2
CT Inter. Y Shear	Accel.	0.7	1.2	1.6	1.9	2.1	2.4

Moment (kip-in); Shear (kips)

(See Figure 12-2, Strain Gauge Placement for (X,Y) & (X',Y'))

Table 13-29: Hysteretic Device – 70-100% System Absolute Maximum Reactions

Absolute Max Reaction	Method	% of IEEE693 0.5g Motion								
		70%	75%	80%	85%	90%	95%	100%	100%*	
Base Moment X	Strain	825	821	771	839	887	962	1070	984	Moment (kip-in); Shear (kips)
Base Moment Y	Strain	947	996	1005	1021	1093	1055	1095	1047	
Base Moment X'	Strain	1046	1121	1158	1223	1348	1325	1436	1341	
Base Moment Y'	Strain	605	706	801	882	946	932	910	921	
Base Moment X	Accel.	872	856	878	941	996	1050	1174	1098	
Base Moment Y	Accel.	955	1005	1043	1046	1125	1082	1134	1109	
Base Shear X	Accel.	3.4	3.5	3.6	4.1	4.2	4.4	4.9	4.7	
Base Shear Y	Accel.	4.3	4.4	4.3	4.7	4.8	5.0	5.2	5.1	
CT-Inter. X Moment	Accel.	596	616	598	618	667	705	796	768	
CT Inter. Y Moment	Accel.	669	692	688	706	758	755	788	805	
CT Inter. X Shear	Accel.	3.2	3.2	3.3	3.6	3.7	3.9	4.4	4.1	
CT Inter. Y Shear	Accel.	2.6	2.9	2.9	3.3	3.1	3.7	4.2	4.9	

*virgin hysteretic device

(See Figure 12-2, Strain Gauge Placement for (X,Y) & (X',Y'))

Relative displacement between the shake table and key locations on the specimen were determined and summarized in Table 13-30 and Table 13-31. The virgin 100% case had a maximum displacement of 22.38 inches at the top of the structure and 13.02 inches at the C.G. location. For the same motion, with non-virgin UFPs, the system experienced 24.56 inches of displacement at the top of the structure and 14.26 inches at the C.G.. The tables summarize the maximum displacement in both directions of motion at the CT-pedestal interface, C.G. of the specimen, and top of the specimen. A complete set of moment-displacement plots for 20%, 50%, 75%, and 100% motions are located in Appendix J.

Table 13-30: Hysteretic Device – System Maximum Displacement 20-70% Motions

Location	Location from Base (in.)	% of IEEE693 0.5g Motion							Displacement (in.)
		20%	30%	40%	50%	60%	65%	70%	
Top of Pedestal X	91 1/2	1.29	1.62	2.11	2.27	2.70	2.85	2.78	
Top of Pedestal Y	91 1/2	1.11	1.43	2.05	2.69	3.29	3.53	3.70	
CG X	215	3.64	4.52	5.81	6.12	7.40	7.78	7.59	
CG Y	216 1/2	3.16	4.08	5.65	7.26	8.78	9.45	9.91	
Top of Specimen X	352 1/2	6.38	7.92	10.15	10.64	12.87	13.51	13.14	
Top of Specimen Y	352 1/2	5.51	7.15	9.79	12.47	15.10	16.26	17.03	

Table 13-31: Hysteretic Device – System Maximum Displacement 75-100% Motions

Location	Location from Base (in.)	% of IEEE693 0.5g Motion							Displacement (in.)
		75%	80%	85%	90%	95%	100%	100%*	
Top of Pedestal X	91 1/2	2.70	3.26	3.75	4.33	4.82	5.52	5.02	
Top of Pedestal Y	91 1/2	3.85	4.10	4.37	4.67	4.91	5.26	5.07	
CG X	215	7.32	8.51	9.76	11.20	12.43	14.26	12.93	
CG Y	216 1/2	10.32	10.73	11.38	12.14	12.76	13.64	13.02	
Top of Specimen X	352 1/2	12.71	14.77	16.90	19.34	21.43	24.56	22.38	
Top of Specimen Y	352 1/2	17.78	18.37	19.38	20.60	21.60	23.05	21.88	

*virgin hysteretic device

The rocking system with hysteretic devices presented true self-centering with minimal permanent drift. One instance presented a permanent drift value of 0.14 inch that was considered negligible compared to the system maximum displacement amplitude and structure height. All residual displacements are summarized in Table 13-32 and Table 13-33.

Table 13-32: Hysteretic Device – System Residual Displacement 20-70% Motions

Location	Location from Base (in.)	% of IEEE693 0.5g Motion							Displacement (in.)
		20%	30%	40%	50%	60%	65%	70%	
Top of Pedestal X	91 1/2	-0.03	-0.01	0.00	0.01	0.02	0.01	0.00	
Top of Pedestal Y	91 1/2	0.00	0.01	0.04	-0.02	0.01	0.01	0.00	
CG X	215	-0.08	-0.03	0.00	0.03	0.04	0.02	0.00	
CG Y	216 1/2	-0.03	0.01	0.08	-0.05	0.02	0.01	-0.01	
Top of Specimen X	352 1/2	-0.14	-0.06	0.01	0.06	0.07	0.01	0.00	
Top of Specimen Y	352 1/2	0.02	-0.01	0.00	0.00	0.01	0.02	0.02	

Table 13-33: Hysteretic Device – System Residual Displacement 75-100% Motions

Location	Location from Base (in.)	% of IEEE693 0.5g Motion							Displacement (in.)
		75%	80%	85%	90%	95%	100%	100%*	
Top of Pedestal X	91 1/2	0.01	0.00	0.02	0.01	0.00	-0.01	0.01	
Top of Pedestal Y	91 1/2	0.00	0.01	0.01	0.02	0.01	0.01	0.04	
CG X	215	0.01	-0.02	0.02	0.02	0.00	-0.03	0.02	
CG Y	216 1/2	0.01	0.00	0.04	0.02	0.03	0.03	0.12	
Top of Specimen X	352 1/2	0.00	-0.03	0.03	0.03	0.01	-0.05	0.01	
Top of Specimen Y	352 1/2	-0.01	0.00	0.01	-0.01	0.00	0.01	-0.02	

*virgin hysteretic device

The pedestal was instrumented with 8 strain gauges as outlined in 12.1, Instrumentation. Most strain pairs presented values less than the yield strain of $1450\mu\epsilon$, but the NW-SE strain pair. The NW-SE strain pair experienced strains of $1892\mu\epsilon$ - $2240\mu\epsilon$ for the 0.5g 100% IEEE693 motions.

Table 13-34: Hysteretic Device – Pedestal Absolute Maximum Strain

Pedestal Strain ($\mu\epsilon$)	% of IEEE693 0.5g Motion													
	20%	30%	40%	50%	60%	65%	70%	75%	80%	85%	90%	95%	100%	100%*
North Gauge	547	707	917	1016	1116	1182	1197	1243	1252	1262	1338	1277	1303	1235
South Gauge	596	749	928	946	1003	1076	1104	1134	1167	1181	1241	1288	1335	1253
NE Gauge	547	768	1021	781	742	789	772	909	1039	1206	1322	1214	1140	1274
SW Gauge	537	750	1048	678	807	781	867	1052	1220	1368	1484	1454	1426	1430
East Gauge	458	576	656	684	699	724	747	744	777	830	884	960	1094	1001
West Gauge	588	719	798	831	997	1045	1041	1035	975	1043	1078	1078	1179	1087
SE Gauge	745	883	1161	1161	1332	1341	1375	1519	1605	1737	1820	1923	2134	1892
NW Gauge	758	873	1086	1188	1368	1501	1584	1703	1770	1894	2101	2054	2240	2085

*virgin hysteretic device

The high strains above $1450\mu\epsilon$ caused minor pedestal yielding which could be seen by examining the residual pedestal strains shown in Table 13-35. For all motions above 70% where the max strain values exceeded the yielding strain, the sensors exhibited larger residual strains.

Table 13-35: Hysteretic Device – Pedestal Residual Strain

Pedestal Strain ($\mu\epsilon$)	% of IEEE693 0.5g Motion													
	20%	30%	40%	50%	60%	65%	70%	75%	80%	85%	90%	95%	100%	100%*
North Gauge	6	0	5	0	-1	3	7	8	12	17	30	7	24	3
South Gauge	3	-1	4	-2	-3	-2	0	2	8	10	8	17	42	2
NE Gauge	-4	-1	-4	-5	-2	0	2	1	1	0	13	-2	17	-3
SW Gauge	-2	-3	-1	-1	1	-2	-3	-2	0	5	5	0	8	-2
East Gauge	-4	2	-1	0	0	1	0	0	-2	7	11	20	27	6
West Gauge	-6	1	0	5	7	4	1	7	9	20	32	10	17	3
SE Gauge	6	4	4	1	1	0	0	1	0	14	16	32	45	18
NW Gauge	4	2	4	5	3	5	5	16	19	32	58	23	37	17

*virgin hysteretic device

Examining bracket slip allows for a better understanding of the device displacement results. Shown in Table 13-36 are the individual device bracket slip values. When bracket slip occurs, the UFP is not deformed and efficient energy dissipation does not occur. Examining the SW-S device, slip initiated at early stages and continued throughout the testing sequence. Torque verification was not performed on the slip-critical bracket, leading to slip in the bracket. In reality, torque verification would not likely happen between an initial subduction zone (mega thrust) event and the aftershocks. The rocking system with hysteretic devices was tested with 3 out of 4 dampers fully engaged.

Table 13-36: Hysteretic Device – UFP Bracket Slip

Device Slip (in.)	% of IEEE693 0.5g Motion													
	20%	30%	40%	50%	60%	65%	70%	75%	80%	85%	90%	95%	100%	100%*
NE-N	0.004	0.009	0.012	0.008	0.009	0.013	0.014	0.014	0.015	0.015	0.016	0.016	0.017	0.015
SE-S	0.005	0.006	0.013	0.016	0.018	0.019	0.019	0.017	0.016	0.016	0.017	0.019	0.023	0.023
SW-S	0.015	0.023	0.032	0.039	0.049	0.064	0.066	0.072	0.081	0.097	0.158	0.306	0.399	0.371
NW-N	0.003	0.004	0.009	0.011	0.012	0.013	0.013	0.013	0.012	0.013	0.017	0.019	0.022	0.018

*virgin hysteretic device

The bracket slip is reflected in the UFP displacement results presented in Table 13-37. The bracket connection continued to loosen as demonstrated by the device

displacement data. Comparing the magnitude of displacement in all devices for the 100% motion, the SW device displacements was roughly 30% of the SE and NW displacement, and 50% of the NE displacement.

Table 13-37: Hysteretic Device – UFP Absolute Maximum Displacement

Device Dispalcement	% of IEEE693 0.5g Motion													
	20%	30%	40%	50%	60%	65%	70%	75%	80%	85%	90%	95%	100%	100%*
NE	0.132	0.198	0.360	0.369	0.512	0.599	0.671	0.732	0.819	0.885	0.954	1.012	1.101	1.069
SE	0.155	0.211	0.373	0.507	0.756	0.869	0.972	1.045	1.180	1.267	1.362	1.512	1.602	1.553
SW	0.204	0.252	0.349	0.451	0.579	0.610	0.641	0.649	0.678	0.659	0.614	0.534	0.574	0.500
NW	0.218	0.283	0.479	0.494	0.671	0.784	0.863	0.933	1.063	1.220	1.399	1.520	1.698	1.589

*virgin hysteretic device

After each motion was complete, the self-centering mechanism along with the self-weight plumbed the system. The hysteretic devices were yielded back to their original, however possessing residual forces, to plumb the system. Demonstrated in Table 13-38 is the systems ability to deform the UFPs back to their original orientation and self-center the system.

Table 13-38: Hysteretic Device – UFP Residual Displacement

Device Dispalcement	% of IEEE693 0.5g Motion													
	20%	30%	40%	50%	60%	65%	70%	75%	80%	85%	90%	95%	100%	100%*
NE	-0.010	-0.002	0.010	-0.001	0.006	0.003	-0.001	0.000	-0.002	0.003	0.001	0.001	-0.002	0.015
SE	-0.001	0.000	0.004	0.012	0.008	0.004	0.003	0.002	0.002	0.004	0.004	0.008	0.011	0.012
SW	0.007	0.002	0.000	0.008	0.014	0.006	0.012	0.008	0.006	0.024	0.068	0.069	0.037	-0.011
NW	0.003	0.002	0.012	0.000	0.007	0.007	0.004	0.005	0.005	0.009	0.013	0.015	0.019	0.027

*virgin hysteretic device

Device forces were measured directly through the anchoring rod for the UFP sets. Modeling and design assumed pure flexural contribution of the UFP. Under rocking, slight torsional resistance and axial resistance could have contributed to increased the device force. While under dynamic motion, torsion, axial, and flexure may contribute to UFP resistance, when re-centering the system, combined shear-flexure action controls the

UFP response. The UFP maximum force ranged from 7 kips-8.3 kips in the 4 devices; all device maximum forces are reported in Table 13-39.

Table 13-39: Hysteretic Device – UFP Set Maximum Force

Device Force (kips)	% of IEEE693 0.5g Motion													
	20%	30%	40%	50%	60%	65%	70%	75%	80%	85%	90%	95%	100%	100%*
NE Device	5.07	5.21	6.23	6.29	6.65	7.01	7.11	7.18	7.32	7.28	7.35	7.38	7.60	7.90
SE Device	5.04	5.92	6.61	6.73	7.35	7.66	7.34	7.00	6.73	6.83	7.00	7.11	7.28	7.95
SW Device	3.56	3.96	4.97	4.59	5.31	5.36	5.52	5.46	5.42	5.47	6.23	6.32	7.00	7.09
NW Device	4.33	5.06	6.14	6.32	6.89	7.01	7.24	7.27	7.32	7.59	7.50	7.48	7.71	8.32

*virgin hysteretic device

The BeS linear load for the specified Belleville spring is 12.76 kips. Since one damper was minimally engaging, the BeS system experienced higher forces than expected. For the 100% motions with non-virgin UFPs, the PT force exceeded 12.76 kips causing the BeS washers to permanently deform and pre-tension force to be lost. The largest loss in pre-tension force was 8.3% in the 100% non-virgin test case. Shown in Table 13-40 is the maximum force experienced by the PT member. Table 13-41 compares the initial PT load to the final PT load,. Decreases in PT load are caused by slight shifting in the system base or PT yielding. Although the load exceeded the linear load, the design specified is expected to perform without exceedance with all 4 UFP sets engaged.

Table 13-40: Hysteretic Device – Maximum PT Force

PT Force (kips)	% of IEEE693 0.5g Motion													
	20%	30%	40%	50%	60%	65%	70%	75%	80%	85%	90%	95%	100%	100%*
PT North	4.60	4.89	5.68	6.09	6.86	7.71	8.29	8.83	9.50	9.92	10.45	10.85	11.45	11.20
PT East	4.41	4.71	5.30	5.85	7.06	7.42	7.41	7.80	8.45	8.97	9.48	10.40	11.08	10.95
PT South	4.38	4.90	5.65	6.78	8.01	8.56	8.94	9.18	9.93	10.31	10.58	11.53	11.85	11.64
PT West	4.72	5.06	6.00	6.19	6.56	6.81	7.11	7.93	8.69	9.69	10.72	11.81	13.02	12.61

*virgin hysteretic device

Minimal loss in PT force was presented for the system when exposed to motions below 80%. Less than 3% PT loss was exhibited by all motions from 20%-80%. For motions above 80%, generally, less than 5% PT loss was presented by the system, although one instance exceeded 5% loss.

Table 13-41: Hysteretic Device – % PT Force Loss Post Motion

PT Force Loss (kips)	% of IEEE693 0.5g Motion													
	20%	30%	40%	50%	60%	65%	70%	75%	80%	85%	90%	95%	100%	100%*
PT North	-1.4%	-0.4%	-0.6%	-0.6%	-1.2%	-2.0%	-1.6%	-1.2%	-1.2%	-3.3%	-2.0%	-3.4%	-4.2%	-3.3%
PT East	-1.9%	-0.4%	-0.6%	0.0%	-1.2%	-0.6%	0.0%	-0.6%	-1.2%	-1.9%	-1.2%	-2.9%	-3.1%	-1.4%
PT South	0.0%	-0.4%	-1.5%	-0.6%	-2.1%	-1.9%	-0.8%	-1.0%	-1.4%	-2.7%	-2.2%	-4.8%	-4.2%	-2.5%
PT West	-1.1%	0.0%	-0.9%	-1.1%	-0.7%	-0.9%	-0.6%	-1.7%	-0.9%	-2.5%	-3.0%	-4.3%	-8.3%	-3.9%

*virgin hysteretic device

Displacement in the system increased as the input motion amplitude was increased. System displacement primarily consisted of flexure and rotation of the structure due to rocking. The maximum base uplift was manifested by the structure for the non-virgin 100% 0.5g IEEE693 motion, see Table 13-42. A vertical uplift of 1.49 inches was measured by the LVDT located in the center of the west base plate edge. The north, east, and south sides measured 1.37 inches, 1.13 inches, and 1.28 inches respectively. Using virgin hysteretic devices, uplift reductions of 2%-8% were exhibited by the system. Using virgin UFPs changes the behavior of the initial loop of the hysteresis, starting at zero rather than maximum negative pre-compressed load. The differences in device response could easily be distinguished when comparing the force-displacement curves in Appendix J.

Table 13-42: Hysteretic Device – Pedestal Rocking Uplift

Uplift (in.)	% of IEEE693 0.5g Motion													
	20%	30%	40%	50%	60%	65%	70%	75%	80%	85%	90%	95%	100%	100%*
Base PL Uplift N	0.18	0.24	0.40	0.45	0.65	0.78	0.86	0.93	1.02	1.10	1.19	1.26	1.37	1.34
Base PL Uplift E	0.14	0.21	0.32	0.41	0.63	0.67	0.65	0.63	0.72	0.80	0.89	1.03	1.13	1.10
Base PL Uplift S	0.17	0.23	0.38	0.56	0.76	0.85	0.92	0.96	1.06	1.10	1.15	1.25	1.28	1.21
Base PL Uplift W	0.20	0.27	0.43	0.46	0.52	0.56	0.58	0.70	0.85	0.99	1.17	1.31	1.49	1.37

*virgin hysteretic device

While slight base plate translations occur during the motion, no residual base plate displacement was presented for any of the test cases. A contributing factor to the horizontal displacements measured was the base rocking. The UFPs out-of-plane stiffness helped prevent base translation. Summarized in Table 13-43 are the magnitudes of the maximum translation measured on all corners of the pedestal base plate. Shown in Table 13-44 are the residual translations, where all values measured were in the instrument noise range.

Table 13-43: Hysteretic Device – Maximum Base Plate Slip

Device Uplift (in.)	% of IEEE693 0.5g Motion													
	20%	30%	40%	50%	60%	65%	70%	75%	80%	85%	90%	95%	100%	100%*
Base PL Slip NE-X	0.02	0.02	0.03	0.04	0.06	0.06	0.05	0.05	0.06	0.06	0.06	0.06	0.07	0.07
Base PL Slip SE-X	0.04	0.03	0.04	0.04	0.06	0.08	0.08	0.08	0.08	0.08	0.09	0.11	0.13	0.14
Base PL Slip SW-X	0.03	0.03	0.05	0.06	0.04	0.05	0.07	0.06	0.09	0.08	0.10	0.12	0.14	0.11
Base PL Slip NW-X	0.02	0.03	0.04	0.05	0.06	0.07	0.07	0.07	0.08	0.08	0.10	0.12	0.14	0.12
Base PL Slip NE-Y	0.04	0.04	0.05	0.05	0.06	0.08	0.09	0.09	0.10	0.11	0.12	0.13	0.15	0.14
Base PL Slip SE-Y	0.03	0.03	0.04	0.05	0.08	0.09	0.10	0.10	0.11	0.13	0.13	0.14	0.15	0.13
Base PL Slip SW-Y	0.02	0.03	0.05	0.07	0.09	0.10	0.10	0.10	0.11	0.12	0.12	0.13	0.12	0.12
Base PL Slip NW-Y	0.02	0.03	0.04	0.05	0.05	0.07	0.07	0.09	0.10	0.10	0.12	0.12	0.14	0.12

*virgin hysteretic device

Table 13-44: Hysteretic Device – Relative Base Plate Movement Pre-Post Motion

Device Uplift (in.)	% of IEEE693 0.5g Motion													
	20%	30%	40%	50%	60%	65%	70%	75%	80%	85%	90%	95%	100%	100%*
Base PL Slip NE-X	0.00	0.00	0.00	0.00	0.00	0.00	0.00	-0.01	0.00	-0.01	0.00	0.00	-0.01	0.00
Base PL Slip SE-X	-0.02	-0.01	-0.01	0.00	-0.01	-0.01	0.00	-0.01	0.00	-0.01	0.00	0.00	0.00	-0.01
Base PL Slip SW-X	0.02	0.01	0.01	0.00	0.01	0.01	0.00	0.01	0.00	0.01	0.00	0.00	0.00	0.02
Base PL Slip NW-X	0.00	0.00	0.00	0.00	0.01	0.00	0.00	0.01	0.00	0.01	0.00	0.00	0.01	0.01
Base PL Slip NE-Y	-0.03	-0.02	-0.02	-0.02	-0.01	0.00	-0.01	0.00	-0.01	0.00	0.00	0.00	0.00	0.01
Base PL Slip SE-Y	0.03	0.02	0.02	0.02	0.01	0.00	0.01	0.00	0.01	0.00	0.00	-0.01	0.00	0.00
Base PL Slip SW-Y	0.01	0.01	0.02	0.01	0.00	0.00	0.00	0.00	0.01	0.00	0.00	0.00	0.01	0.00
Base PL Slip NW-Y	-0.01	-0.01	-0.01	-0.01	0.00	0.00	-0.01	0.01	-0.01	0.00	0.00	0.00	-0.01	0.01

*virgin hysteretic device

13.5 Non-Retrofitted

13.5.1 Non-Retrofitted Table Response Spectrum

The non-retrofitted system was exposed to three complete ground motions prior to pedestal strains exceeding $2500 \mu\epsilon$. Amplitudes of 20%, 30%, and 40% of the 0.5g IEEE693 record were used to excite the system. When the system was exposed to the 50% 0.5g IEEE693 motion, pedestal strains exceeded $2500\mu\epsilon$ set for the shake table limit. Shown in Figure 13-11, Figure 13-12, and Figure 13-13 is a comparison between the 0.5g IEEE693 design spectrum and table response spectrum. For the horizontal directions, the table performed well near the fundamental frequency, 1.13Hz-1.18Hz. More error is seen in the incomplete 50% motion compared to the other executed motions. Significant undershooting of the design spectrum was produced by the incomplete motion in the vertical direction.

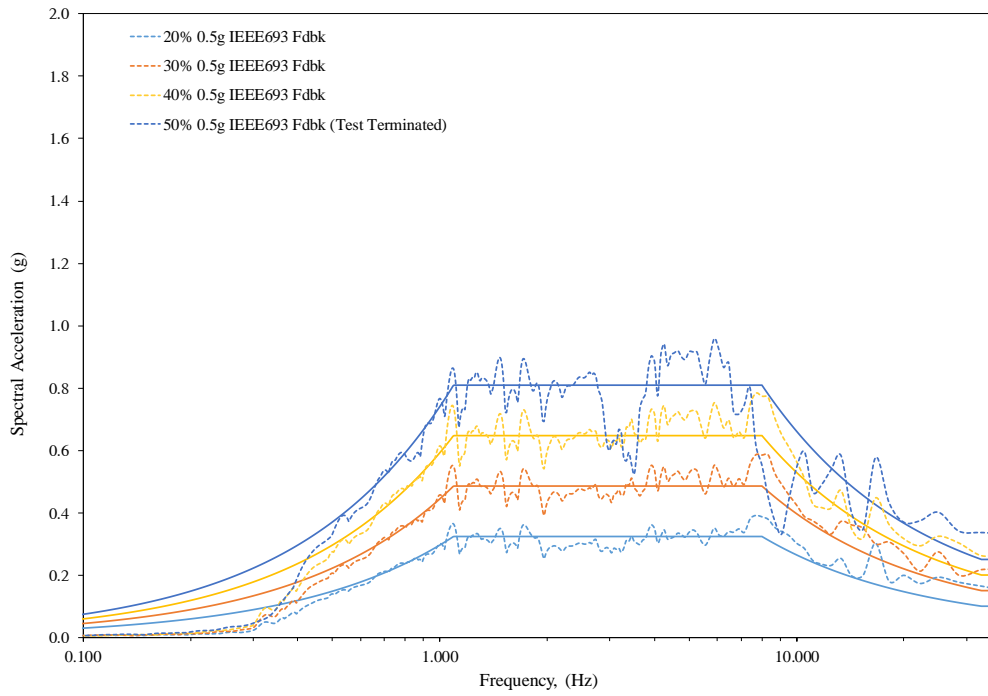


Figure 13-11: Non-Retrofitted – Response Spectrum X

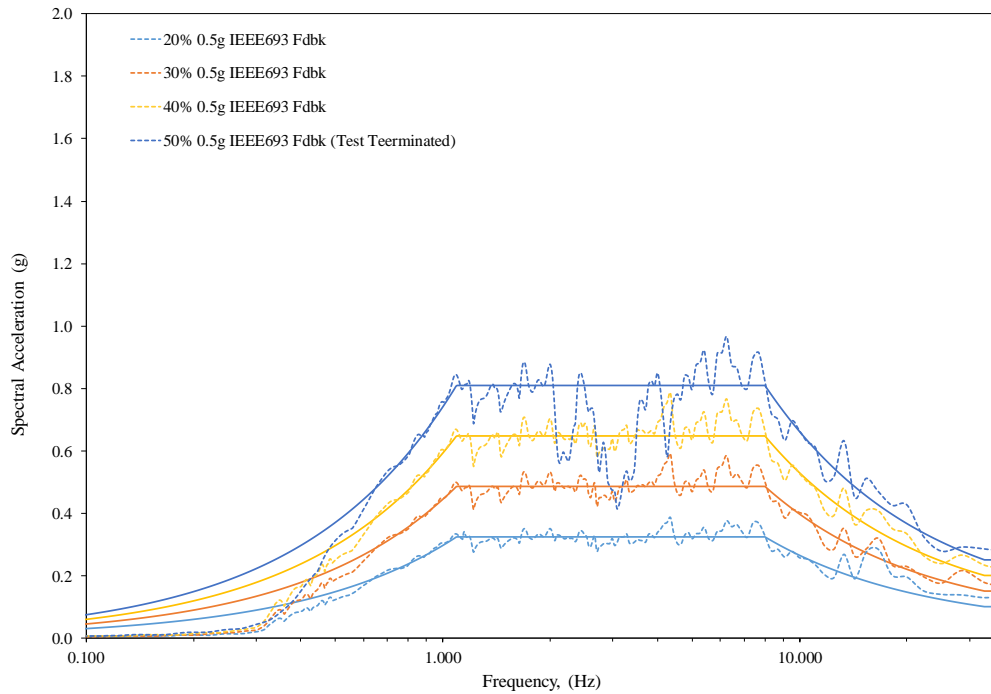


Figure 13-12: Non-Retrofitted– Response Spectrum Y

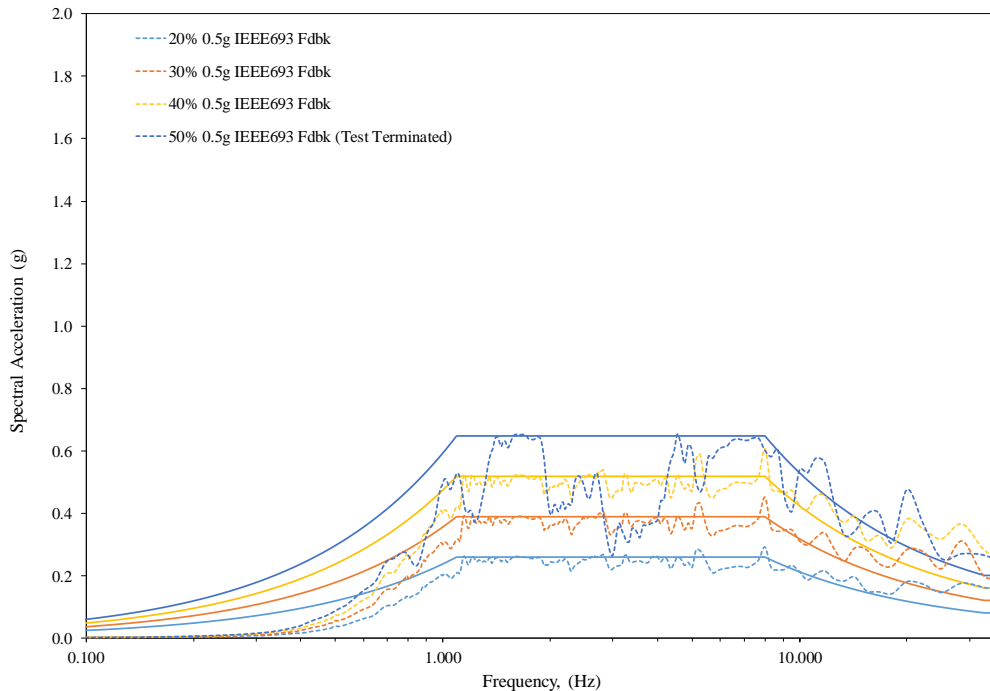


Figure 13-13: Non-Retrofitted– Response Spectrum Z

13.5.2 Non-Retrofitted System Damping & Free Vibration

The non-retrofitted system has a fundamental frequency between 1.13Hz-1.18Hz in the horizontal directions. Using pulse excitation, the X-direction fundamental frequency was 1.13Hz. Similarly, exciting the structure via a pulse, the Y-direction had a fundamental frequency of 1.18Hz. Using white noise, the structure had a fundamental frequency of 1.18Hz in both horizontal directions. The average vertical fundamental frequency was 28.8Hz. The non-retrofitted mass system has minimal elastic damping, estimated to be 0.32%-0.35%. A complete summary of the individual pulses and white noise results are shown in Table 13-45. Free vibration plots for each test case are presented in Appendix K.

Table 13-45: Non-Retrofitted System Damping and Fundamental Frequency

	% Motion	Motion Name	Retrofit Device	Pulse Free Vibration				White Noise		
				Fundamental Frequency (Hz)		Elastic Damping		Fundamental Frequency (Hz)		
				x	y	x	y	x	y	z
Pre	20	0.5g IEE693 tQke	None	1.13	1.18	0.35%	0.31%	1.18	1.18	27.39
Pre	30	0.5g IEE693 tQke	None	1.13	1.18	0.34%	0.29%	1.18	1.18	29.50
Pre	40	0.5g IEE693 tQke	None	1.13	1.17	0.32%	0.33%	1.17	1.17	29.50
Pre	50	0.5g IEE693 tQke	None	1.13	1.17	0.35%	0.33%	-	-	-
Post	50	0.5g IEE693 tQke	None	1.13	1.17	0.36%	0.37%	-	-	-
Average Response				1.13	1.18	0.35%	0.32%	1.18	1.18	28.80

13.5.3 Non-Retrofitted System Response

The non-retrofitted system manifested accelerations at the top of the structure exceeding 1g for motions 40% and above. Large amplifications were demonstrated by the system in the horizontal directions. Minimal vertical amplification was produced by the system because of the directional stiffness. Maximum acceleration values are reported in Table 13-46, Table 13-47, and Table 13-48.

Table 13-46: Non-Retrofitted – System X Absolute Maximum Acceleration

		% of IEE693 0.5g Motion				Location (in)
		20%	30%	40%	50%	
X - Absolute Maximum Acceleration (g)		0.67	0.77	1.12	1.38	351
		0.60	0.67	0.95	1.18	322
		0.56	0.64	0.88	1.08	304 1/2
		0.54	0.62	0.86	1.01	285 1/2
		0.49	0.57	0.79	0.95	268 1/2
		0.47	0.53	0.76	0.91	254
		0.42	0.46	0.68	0.81	235
		0.39	0.45	0.67	0.81	214 1/2
		0.36	0.39	0.59	0.73	199
		0.33	0.35	0.53	0.67	182
		0.27	0.31	0.52	0.61	163
		0.25	0.29	0.49	0.59	146
		0.23	0.27	0.46	0.52	127
		0.19	0.23	0.39	0.43	91
		0.13	0.19	0.25	0.31	1 1/8
	0.14	0.18	0.25	0.31	0	

Table 13-47: Non-Retrofitted – System Y Absolute Maximum Acceleration

		% of IEEE693 0.5g Motion				Location (in)
		20%	30%	40%	50%	
Y - Absolute Maximum Acceleration (g)		0.31	0.41	1.06	1.06	351
		0.26	0.36	0.83	0.80	322
		0.23	0.31	0.70	0.70	304 1/2
		0.20	0.28	0.61	0.65	285 1/2
		0.18	0.26	0.56	0.65	268 1/2
		0.18	0.26	0.56	0.67	254
		0.19	0.25	0.55	0.67	235
		0.19	0.27	0.62	0.76	214 1/2
		0.19	0.26	0.58	0.67	199
		0.20	0.25	0.55	0.66	182
		0.19	0.25	0.59	0.68	163
		0.19	0.24	0.54	0.65	146
		0.18	0.24	0.57	0.63	127
		0.17	0.22	0.72	0.73	91
		0.14	0.18	0.45	0.48	1 1/8
	0.10	0.14	0.44	0.46	0	

Table 13-48: Non-Retrofitted – System Z Absolute Maximum Acceleration

		% of IEEE693 0.5g Motion				Location (in)
		20%	30%	40%	50%	
Z - Absolute Maximum Acceleration (g)		0.15	0.20	0.25	0.23	351
		0.13	0.19	0.26	0.21	322
		0.13	0.17	0.27	0.20	304 1/2
		0.15	0.20	0.26	0.21	285 1/2
		0.12	0.21	0.26	0.22	268 1/2
		0.16	0.20	0.24	0.23	254
		0.12	0.19	0.26	0.20	235
		0.14	0.20	0.25	0.22	214 1/2
		0.11	0.19	0.26	0.19	199
		0.14	0.20	0.25	0.22	182
		0.11	0.19	0.26	0.20	163
		0.15	0.21	0.25	0.21	146
		0.11	0.21	0.26	0.20	127
		0.14	0.21	0.26	0.20	91
		0.12	0.20	0.25	0.18	1 1/8
	0.11	0.19	0.24	0.18	0	

The non-retrofitted case exhibited extremely high moments in all directions, Table 13-49. For the partial 50% motion maximum moments were as follows: X-moment was 1752 kip-in, the Y-moment was 1231 kip-in, the X²-moment was 1059 kip-in, and the

Y'-moment was 2141 kip-in. Yielding occurred during the 40% and 50%, the residual strain values obtained are shown in Table 13-53.

Table 13-49: Non-Retrofitted – 20-50% System Absolute Maximum Reactions

Absolute Max Reaction	Method	% of IEEE693 0.5g Motion			
		20%	30%	40%	50%
Base Moment X	Strain	768	880	1338	1752
Base Moment Y	Strain	847	1198	1046	1231
Base Moment X'	Strain	494	754	913	1059
Base Moment Y'	Strain	941	1188	1551	2141
Base Moment X	Accel.	820	938	1306	1547
Base Moment Y	Accel.	902	1255	1109	1207
Base Shear X	Accel.	3.1	3.5	5.0	5.9
Base Shear Y	Accel.	3.4	4.6	4.3	4.6
Moment CT Interface X	Accel.	540	621	861	1040
Moment CT Interface Y	Accel.	595	834	739	820
Shear CT Interface X	Accel.	2.9	3.3	4.7	5.6
Shear CT Interface Y	Accel.	1.2	1.4	1.6	1.6

Moment (kip-in); Shear (kips)

With the bolted base, the flexible system displaced 10.2 inches in the X-direction and 8.0 inches in the Y-direction during the partial 50% motion. All maximum displacement values for the non-retrofitted test cases are summarized in Table 13-50. After the free vibration stopped, the system presented only 0.045 inch of permanent displacement at the top of the structure. Maximum residual displacements for both horizontal directions at three specimen locations are shown in Table 13-51.

Table 13-50: Non-Retrofitted – System Maximum Displacement 20-50% Motions

Location	Location from Base (in.)	% of IEEE693 0.5g Motion			
		20%	30%	40%	50%
Top of Pedestal X	91 1/2	0.721	0.852	1.236	1.521
Top of Pedestal Y	91 1/2	0.780	1.143	1.033	1.196
CG X	215	2.608	3.044	4.480	5.454
CG Y	216 1/2	2.910	4.203	3.789	4.310
Top Displacement X	352 1/2	4.921	5.731	8.369	10.238
Top Displacement Y	352 1/2	5.456	7.890	7.020	8.092

Displacement (in.)

Table 13-51: Non-Retrofitted – System Residual Displacement 20-50% Motions

Location	Location from Base (in.)	% of IEEE693 0.5g Motion				Displacement (in.)
		20%	30%	40%	50%	
Top of Pedestal X	91 1/2	-0.008	-0.014	-0.013	-0.017	
Top of Pedestal Y	91 1/2	-0.001	0.003	-0.001	0.001	
CG X	215	-0.014	-0.037	-0.035	-0.023	
CG Y	216 1/2	0.001	0.001	0.010	0.011	
Top Displacement X	352 1/2	-0.030	-0.073	-0.051	-0.045	
Top Displacement Y	352 1/2	0.007	-0.022	0.020	-0.008	

Extremely high strains were obtained in the non-retrofitted system significantly surpassing the nominal yield strain. For the incomplete 50% 0.5g IEEE693 motion, the system had maximum strains ranging from $1168 \mu\epsilon$ - $2710 \mu\epsilon$. All maximum strain values are reported in Table 13-52 for the tested cases without retrofit. Permanent strains are reported in Table 13-53 for the test cases.

Table 13-52: Non-Retrofitted – Pedestal Absolute Maximum Strain

Pedestal Strain ($\mu\epsilon$)	% of IEEE693 0.5g Motion			
	20%	30%	40%	50%
North Gauge	925	1367	1129	1340
South Gauge	992	1388	1237	1444
NE Gauge	1127	1429	1912	2710
SW Gauge	1061	1382	1833	2350
East Gauge	812	941	1416	1860
West Gauge	858	995	1409	1835
SE Gauge	948	1344	1160	1444
NW Gauge	544	818	1008	1168

Table 13-53: Non-Retrofitted – Pedestal Residual Strain

Pedestal Strain ($\mu\epsilon$)	% of IEEE693 0.5g Motion			
	20%	30%	40%	50%
North Gauge	-1	11	17	43
South Gauge	-2	-15	-6	11
NE Gauge	4	-21	-26	-73
SW Gauge	9	-26	-33	-15
East Gauge	-4	1	5	-13
West Gauge	-3	-8	7	61
SE Gauge	-13	0	-2	9
NW Gauge	-18	2	-13	-11

The non-retrofitted system produced high anchor loads ranging from 36 kips-62 kips. The overturning moment is resisted through a moment couple at the base of the structure. The anchors were torqued subjecting them to an initial load. The initial loads of the anchors are conveyed in Table 13-54. As the system is excited, the load in the anchors increase when the lateral forces produce a higher overturning moments than the initial pre-loaded anchor couple resists. The maximum experienced anchor loads are shown in Table 13-55.

Table 13-54: Initial Anchor Loads

Anchor Force (kips)	% of IEEE693 0.5g Motion			
	20%	30%	40%	50%
NW	12.1	11.2	9.4	8.8
SW	12.0	10.1	8.7	7.2
SE	23.5	21.8	19.2	17.8
NE	21.8	19.2	16.9	14.8

Table 13-55: Maximum Anchor Loads

Anchor Force (kips)	% of IEEE693 0.5g Motion			
	20%	30%	40%	50%
NW	24.8	29.9	33.2	36.0
SW	34.8	41.8	50.9	57.3
SE	31.7	39.2	38.6	38.5
NE	41.1	46.3	54.2	62.1

14.0 NUMERICAL MODEL VS. EXPERIMENTAL RESULTS

Numerical model outputs for XYZ, X-direction, Y-direction, and Z-direction simultaneously, 0.5g PGA IEEE693 motions were compared to the experimental response of the system. For all retrofitted cases, the models underestimated the system displacements. In fabrication, the pedestal stiffener welding caused a concave profile in the surface of the base plate. The concave surface caused premature rocking and a significantly lower initial elastic stiffness. Due to existing gaps around the exterior edge of the base plate, the initial structure stiffness was reduced and no clear transition was exhibited when rocking initiated. Premature rocking due to the base plate geometry resulted in larger system displacements, acting as if the pre-tension force was lower. As introduced in 6.1, Pre-Tension Force, the parametric study suggested that a reduced pre-tension force results in larger system displacements. Since rocking did not occur at the exterior edge until high lateral forces, less moment was required to cause rocking in the experimental work.

14.1 Viscous Damper Experimental Comparison to Numerical

Figure 14-1 and Figure 14-2 illustrate the experimental and numerical moment-displacement hysteresis for the rocking system with Taylor viscous dampers. From the numerical work, the maximum X-displacement at the top of the structure was 11.25 inches with an associated moment of 636 kip-in. The experimental results had a displacement of 21.71 inches and an associated moment of 834.9 kip-in. The discrepancies in the initial stiffness of the systems are clearly demonstrated in Figure 14-1 and Figure 14-2. The experimental results had a maximum displacement that was

93% larger than the numerical model output. The numerical model under-estimated the maximum moment in the pedestal by 31%.

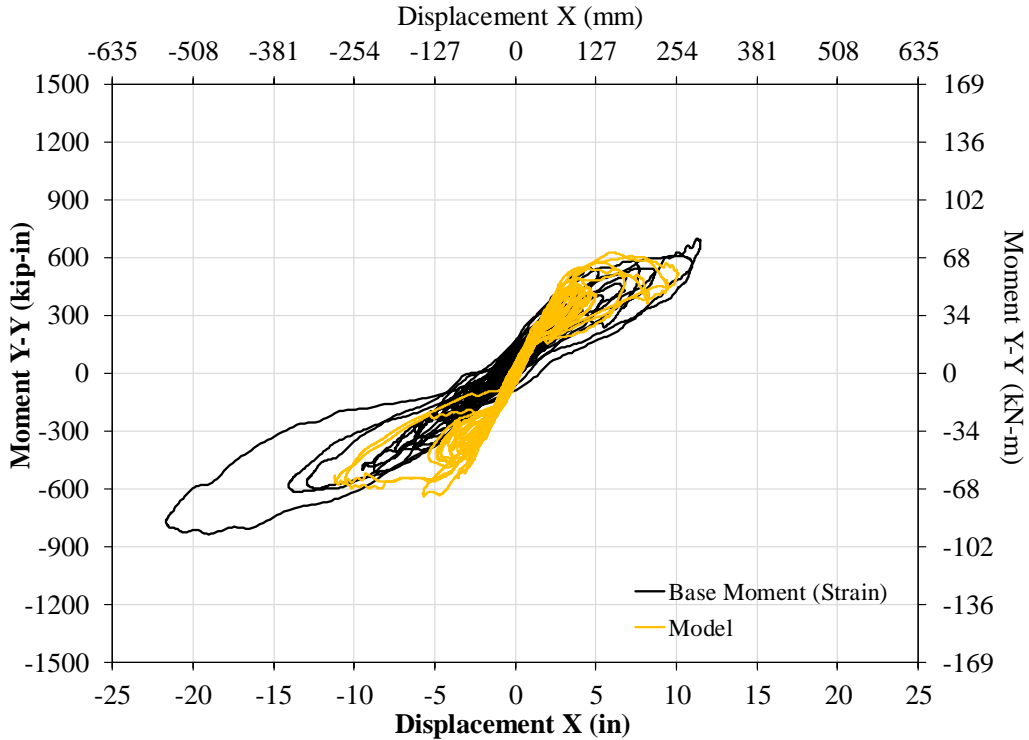


Figure 14-1: Viscous Damper – 100% - X Experimental vs. Numerical Comparison

Comparing the numerical and experimental response for the Y-direction of the system, less error between the model and the experimental results was present. A maximum moment of 731 kip-in was obtained through SAP2000 analysis compared with the experimental moment of 853 kip-in. The experimental maximum moment obtained for the X-X-moment was 18% greater than the model output. From SAP2000 output, the Y-direction maximum displacement exhibited by the system was 15.91 inches compared to 21.24 inches from experimental instrumentation. System top displacement in the Y-direction was 34% larger than the estimated displacement by the SAP2000 model.

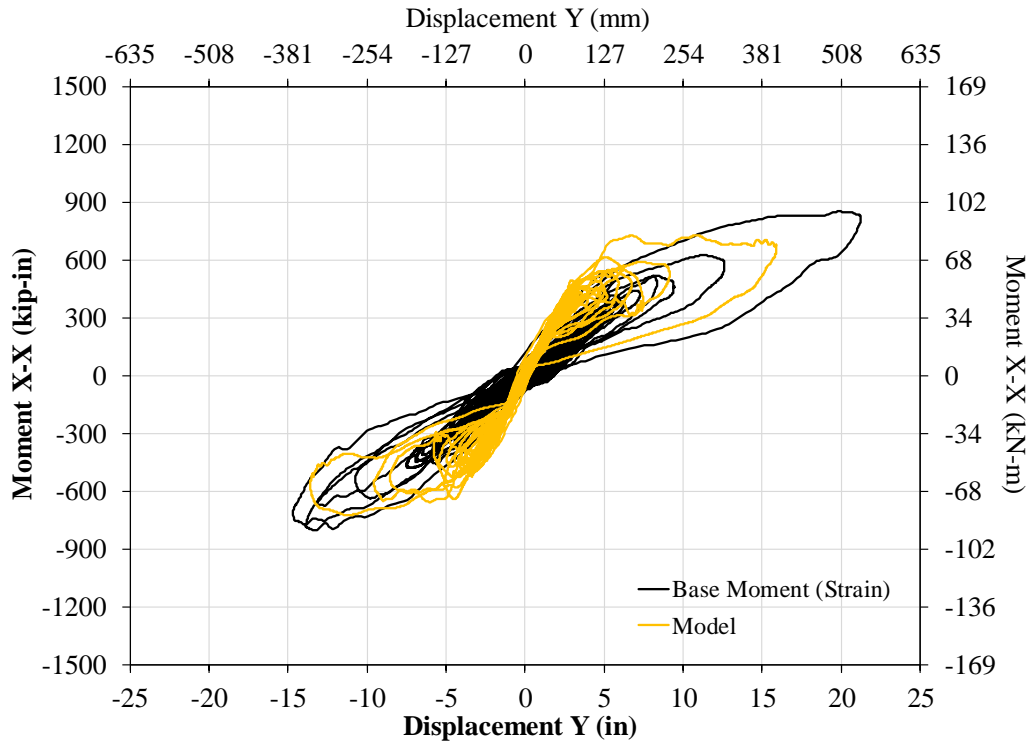


Figure 14-2: Viscous Damper -100% -Y Experimental vs. Numerical Comparison

14.2 Hysteretic Experimental Comparison to Numerical

In addition to the premature rocking due to the base plate geometry, the hysteretic test cases only fully engaged 3 out of 4 of the UFP sets as discussed in 13.4.3, Hysteretic Device System Response. With all four UFP sets fully engaging, energy dissipation would increase and structure drift would be reduced.

Shown in Figure 14-3 and Figure 14-4 are comparisons between the numerical and experimental results for the rocking system with hysteretic energy dissipaters. From numerical analysis, the defined system had a maximum top X-displacement of 14.78 inches and a maximum associated moment of 804 kip-in. The instrumentation from the 3-D virgin UFP test measured 22.38 inches of X-displacement at the specimen top. The

maximum Y-Y base moment measured by the calibrated strain gauges was 984 kip-inches.

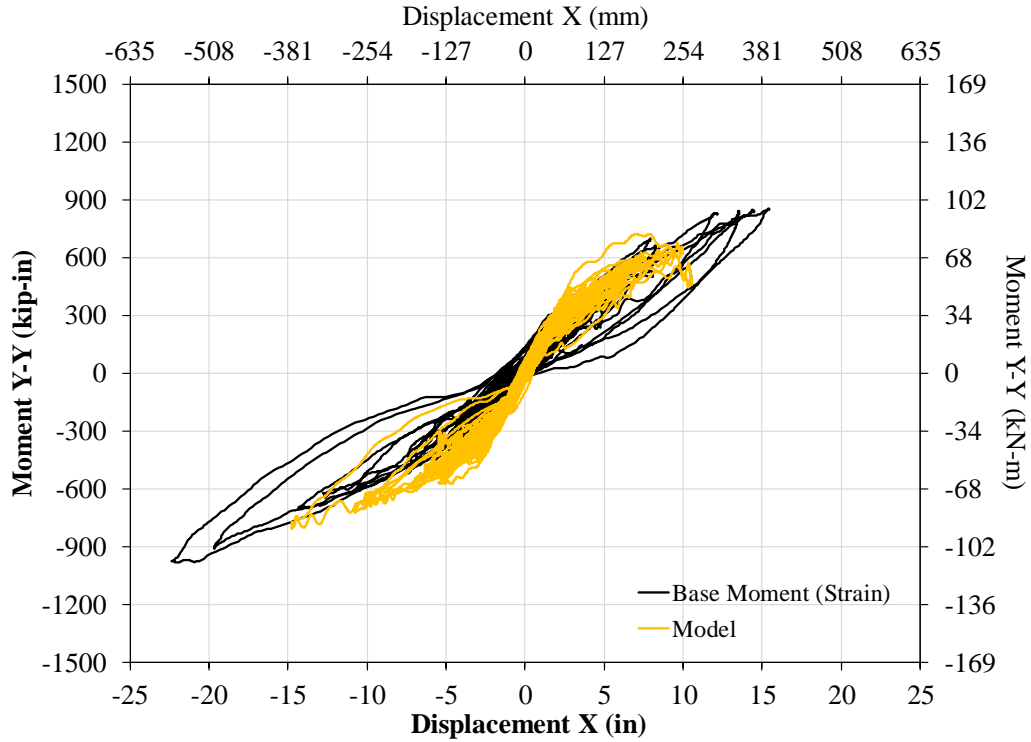


Figure 14-3: Hysteretic Device – 100% - X Experimental vs. Numerical Comparison

Examining Figure 14-4, the maximum Y-displacement was 16.08 inches and 23.05 inches for the numerical and experimental respectively. The experimental results with 3 out of 4 UFP sets engaging resulted in 43% larger displacements than the numerical model predicted. The maximum X-X-moments were 810 kip-in and 1047 kip-in for the numerical and experimental respectively.

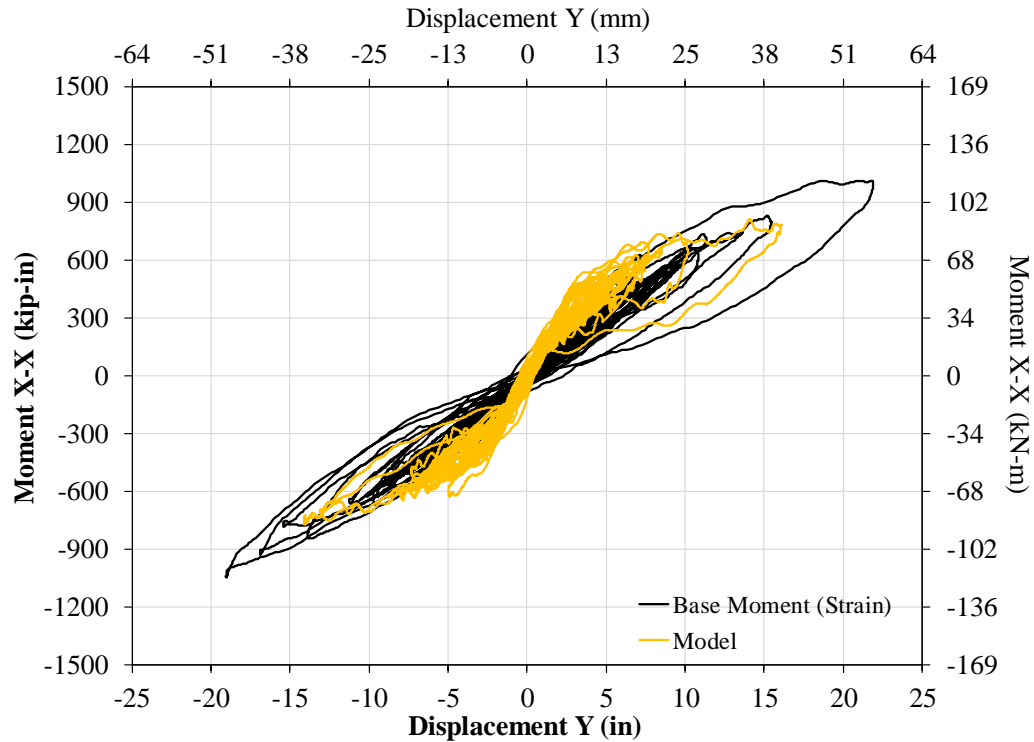


Figure 14-4: Hysteretic Device – 100% - Y Experimental vs. Numerical Comparison

14.3 Non-Retrofitted Experimental Comparison to Numerical

Unlike the retrofitted cases, the bolted non-retrofitted case was not affected by the geometric imperfection of the base plate. The stiffness of the numerical model compared to the experimental results was near identical. Consistently, the numerical model underestimated the maximum displacement and reactions in the system. The numerical models were constructed assuming 2% elastic damping while the actual full steel structure had less than 0.4% elastic damping. Both methods for determining moment in the experimental system are plotted along with the numerical output in Figure 14-5 and Figure 14-6.

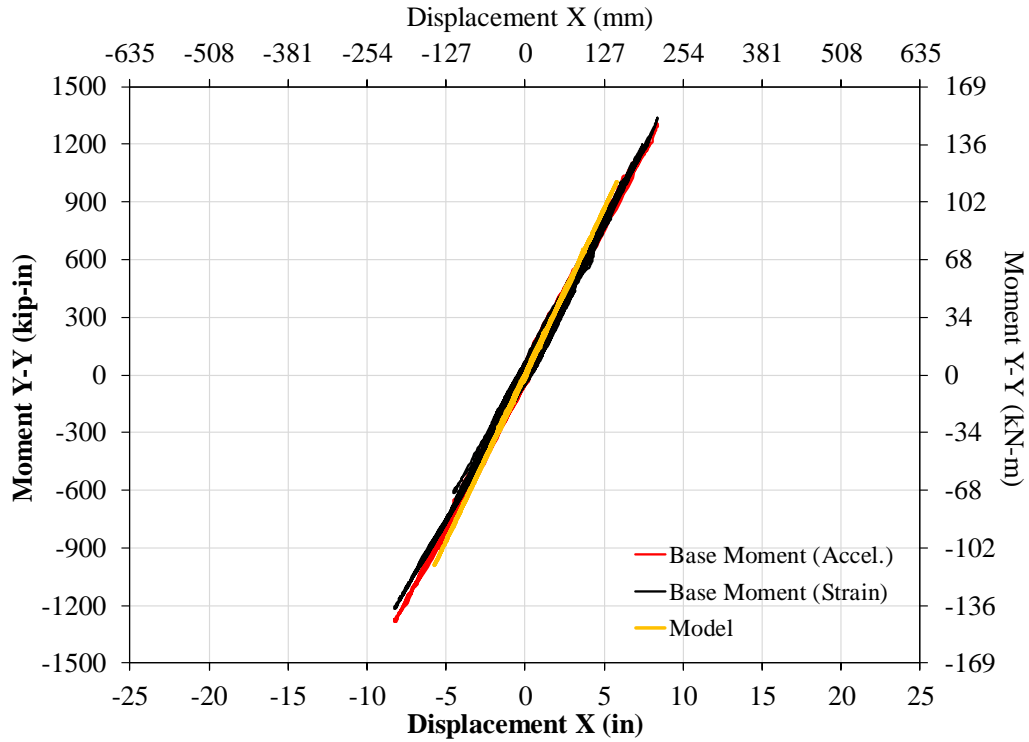


Figure 14-5: Non-Retrofitted – 40% - X Experimental vs. Numerical Comparison

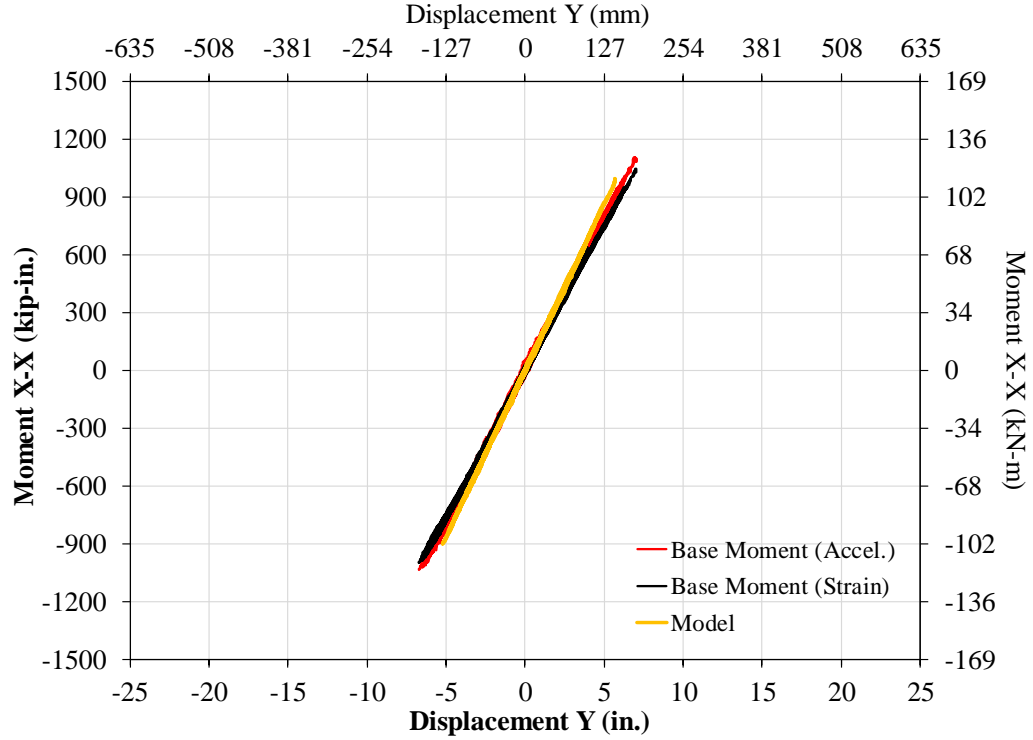


Figure 14-6: Non-Retrofitted – 40% - Y Experimental vs. Numerical Comparison

15.0 ECONOMIC COMPARISON

Both retrofit measures consistently presented repeatable self-centering behavior. Summarized in the following section are the costs for each current transformer retrofit. Both retrofit measures economic comparisons exclude the cost of installation labor. Labor required for each retrofit installation is near equal and are neglected in the economical comparison.

Portrayed in Figure 15-1 and Table 15-1 are the costs of each component required for the self-centering system with viscous dampers. The total cost of the viscous damper retrofit components is \$16,900 of which \$10,000 is the cost of the four Taylor viscous dampers.

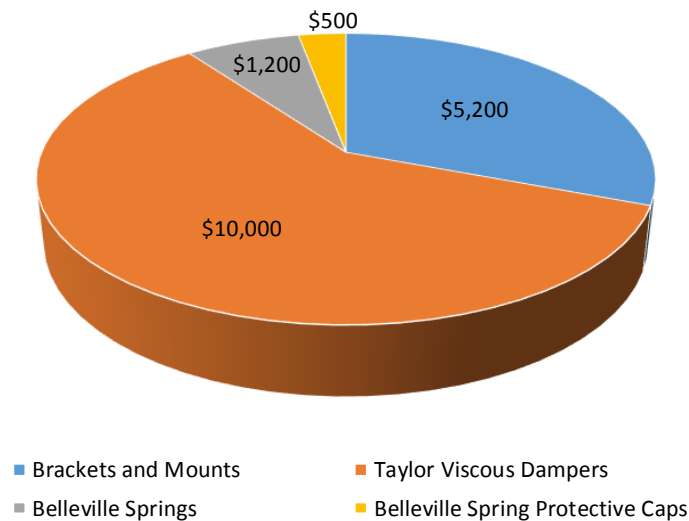


Figure 15-1: Viscous Damper Retrofit Cost

Table 15-1: Viscous Damper Retrofit Cost Summary

Component	Additional Details	Cost
Brackets and Mounts	Set of 4	\$5,200
Taylor Viscous Dampers	Set of 4	\$10,000
Belleville Springs	Set of 144 - 4 Stacks of 36	\$1,200
Belleville Spring Protective Caps	Set of 4	\$500
Total Retrofit Cost		\$16,900

The self-centering retrofit with hysteretic devices has a material cost of \$3,820. The attachment brackets cost 47% of the total retrofit. A complete breakdown of each component of the retrofit is shown in Figure 15-2 and Table 15-2.

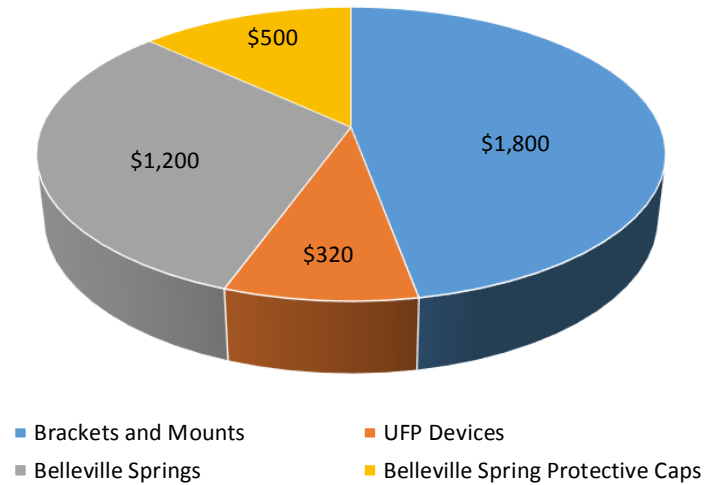


Figure 15-2: Hysteretic Device Retrofit Cost

Table 15-2: Hysteretic Device Retrofit Cost Summary

Component	Additional Details	Cost
Brackets and Mounts	Set of 4	\$1,800
UFP Devices	Set of 8	\$320
Belleville Springs	Set of 144 - 4 Stacks of 36	\$1,200
Belleville Spring Protective Caps	Set of 4	\$500
Total Retrofit Cost		\$3,820

16.0 FULL-SCALE RETROFIT COMPARISON AND SUMMARY

Both retrofit concepts have been shown to demonstrate effectiveness as compared to the non-retrofitted case. Damping and fundamental frequency for all three test cases are shown in Table 16-1. As previously discussed, base plate imperfections caused instant softening of the elastic structure in the retrofitted cases, however that can be readily mitigated with design specifications or installation procedures. Comparing the fundamental frequency in the retrofitted cases to the non-retrofitted case, 25-40% decrease in fundamental frequency occurs when the system is retrofitted. When the system is retrofitted with viscous dampers, any displacement engages the dampers. With an 1/8 inch gap between the base plate edge and the “foundation”, any load on the system engages the dampers. The viscous damper retrofit increases the elastic damping of the system from 0.35% - 1.22% in the X-direction and 0.32% - 1.84% in the Y-direction. The UFP device is displacement-dependent and energy dissipation occurs only when the yield displacement of 0.093 inch is exceeded. The self-centering system with hysteretic devices presented 0.66% damping in the X-direction and 0.87% damping in the Y-direction.

Table 16-1: Damping and Fundamental Frequency Comparison

Retrofit Device	Pulse Free Vibration				White Noise		
	Fundamental Frequency (Hz)		Elastic Damping (%)		Fundamental Frequency (Hz)		
	x	y	x	y	x	y	z
Viscous	0.86	0.75	1.22%	1.84%	0.85	0.75	26.35
Hysteretic	0.80	0.70	0.66%	0.87%	0.78	0.68	26.16
None Retrofitted	1.13	1.18	0.35%	0.32%	1.18	1.18	28.80

Both retrofits methods significantly reduced demand on the CT-interface and pedestal moments compared to the non-retrofitted system. Presented in Figure 16-1 and Figure 16-2 are comparisons between the two retrofit types and the non-retrofitted

structure. The response of the retrofitted cases excited by the 100% 0.5g PGA IEEE693 tQke motion is compared to the response of the non-retrofitted system excited by a 40% 0.5g PGA IEEE693 tQke motion. Comparing the viscous damper retrofit to the hysteretic device retrofit, minor differences in system response were presented. Viscous dampers act out of phase with system displacement and generally the shape of the system response is significantly different than that of hysteretic devices. The combination of the self-centering and elliptical viscous damper response generally results with higher forces near zero displacement. Since the system tested was extremely flexible, the viscous dampers did not significantly outperform the hysteretic devices. The differences are marginal which would not be the case for a stiff system.

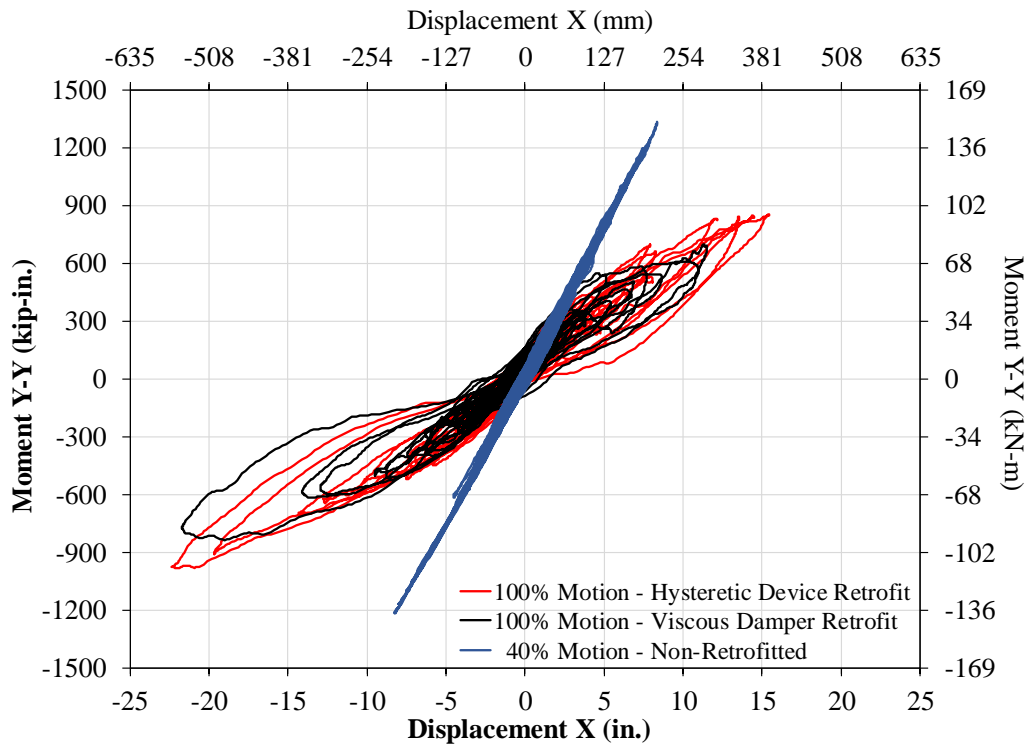


Figure 16-1: X - Retrofitted System Compared to Non-Retrofitted System

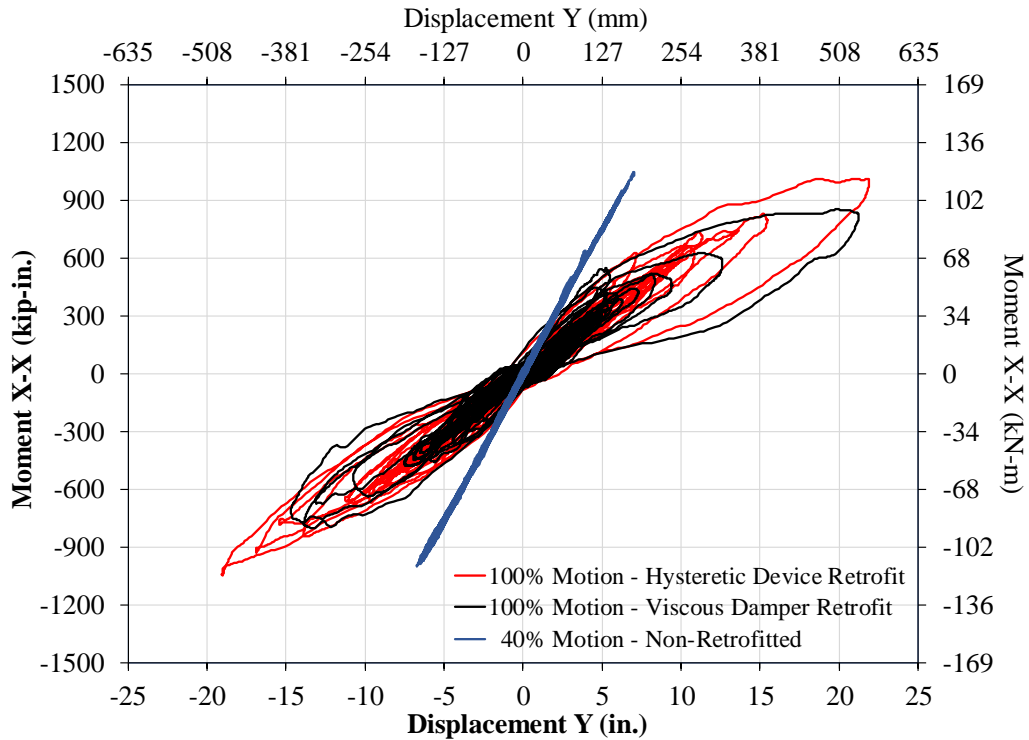


Figure 16-2: Y - Retrofitted System Compared to Non-Retrofitted System

The viscous damper retrofit was most effective in limiting displacement and decreasing system forces, but only marginally compared to the hysteretic retrofit. The UFP performance difference would likely be even less if all 4 UFP sets were fully engaged and energy dissipation was maximized. Comparing the X-direction response (100% motion), the viscous damper retrofit had a maximum moment of 835 kip-in and a top X-displacement of 21.70 inches, while the hysteretic device retrofit had a maximum base moment of 984 kip-in and a top X-displacement of 22.38 inches. The non-retrofitted system had a maximum base moment of 1338 kip-in and a maximum X-displacement of 8.37 inches for the 40% motion. Significant pedestal yielding and damage to the CT is expected if the 100% motion excites the non-retrofitted system.

Similar trends were exhibited in the Y-direction system response (100% motion). The viscous damper retrofit experienced a maximum moment of 853 kip-in and a top Y-displacement of 21.4 inches. The structure retrofitted with UFPs had a maximum measured X-X-moment of 1047 kip-in and a Y-displacement of 21.88 inches. The non-retrofitted structure excited by the 40% motion manifested 1046 kip-in moment and 7.02 inches of top displacement.

Extreme reductions in the anchor forces were presented in the retrofitted cases. The retrofit distributed the loads on the foundation into 8 anchors and a rocking edge compared to the non-retrofitted system which uses a 4 bolt moment couple to resist overturning. For the retrofitted cases, the energy dissipating device anchors are limited to the maximum device capacity. For the 100% IEEE693 retrofitted cases the device anchor were all below 9 kips while in the non-retrofitted system the anchor loads were 30-54 kips for the 40% motion. Nominal yield of the anchors is expected for any loads over 28 kips. The rocking structure does impose a concentrated line load along the length of the rocking edge, but the distribution of the load produces little concern.

Viscous damper retrofit showed significantly more benefit for the PSU scaled system than for the full-scale system. The full-scale results suggest that the gain in benefit compared to the high costs associated with viscous damper procurement is minimal. The hysteretic device retrofit economically shows significant favorability at only 23% the cost of the viscous damper retrofit.

17.0 RECOMMENDATIONS

Current Transformer retrofit is highly effective in mitigating seismic ground motion. The high demands imposed on the CT-pedestal interface and the pedestal base alone, encourage consideration of retrofit. The retrofit aims to reduce loads, but yielding may still occur in the pedestal due to its structural deficiency. The following further investigations are recommended:

- Design of a slack release system to accommodate the displacements at the top of the CT.
- Investigation on options for rerouting electrical connections at the base of the structure.
- Investigating temperature conditions and performance of devices under extreme conditions.
- Self-leveling foundation to reduce and eliminate premature rocking and decrease displacements. Having a foundation that is molded to the actual base plate will reduce premature rocking, increase initial stiffness, and result in more predictable structure response.
- Increase moment capacity of the current transformer pedestal.
- Adding additional gap opening at other locations of the structure to reduce effects of higher modes. Gap openings at the pedestal-CT interface could reduce loads further by limiting the load above the stiff pedestal.
- Investigate potential applicability of the retrofit technology on other types of substation equipment.

18.0 REFERENCES

- Aslan FRP. (2011). *Carbon Fiber Reinforced Polymer (CFRP) Bar- Aslan 200 Series*. Seward: Hughes Brothers, Inc.
- Baird, A. S. (2014). Experimental and numerical study of U-shape flexural plate (UFP) dissipators. Auckland: New Zealand Society for Earthquake Engineering 2014 Technical Conference and AGM.
- Chancellor, N. B. (2014). Chancellor, N. B., Eatherton, M. R., Roke, D. A., & Akbaş, T. (2014). Self-centering seismic lateral force resisting systems: high performance structures for the city of tomorrow. *Buildings*, 4(3), 520-548.
- CSI. (2016, January 5). *Software Verification EXAMPLE 6-008 LINK – PLASTIC WEN LINK*. Retrieved from CSI America:
<http://docs.csiamerica.com/manuals/sap2000/Verification/Analysis/Links/Problem%206-008.pdf>
- Eatherton, M. R. (2014). Design concepts for controlled rocking of self-centering steel-braced frames. *Journal of Structural Engineering*, 140.11 .
- Gu, M. W. (2015). Displacement Design Procedure for Cross Laminated Timber (CLT) Rocking Walls with Sacrificial Dampers. *Structures Congress 2015*, (pp. 2777-2791).
- Gu, M., Pang, W., & Schiff, S. (2015). Displacement Design Procedure for Cross Laminated Timber (CLT) Rocking Walls with Sacrificial Dampers. *Structures Congress 2015*. Clemson: Glenn Department of Civil Engineering.

- IEEE. (2006). *Recommended Practice for Seismic Design of Substations (IEEE693)*. New York.
- Kelly, J. M. (1972). Mechanisms of energy absorption in special devices for use in earthquake resistant structures. *Bulletin of NZ Society for Earthquake Engineering*, 63-88.
- Kelly, J. M., Skinner, R. I., & Heine, A. J. (1972). Mechanisms of Energy Absorption in Special Devices for use in Earthquake Resistant Structures. *Bulletin of the New Zealand Society for Earthquake Engineering*, 5(3).
- Pampanin, S. P. (2001). Analytical modelling of the seismic behaviour of precast concrete frames designed with ductile connections. *Journal of Earthquake*, 329–367.
- Pennucci, D. G. (2009). Displacement-Based Design of Precast Walls with Additional Dampers. *Journal of Earthquake Engineering* 13.S1, 40-65.
- Ricles, J. M. (2006). Ricles, J. M., et al. "Post-tensioned moment connections with a bottom flange friction device for seismic resistant self-centering steel MRFs. *4th International conference on earthquake engineering*.
- Schultz, A., R., M., Tadros, M., & Huo, X. (1994). Experimental Study of Joint Connections in Precast Concrete Walls. *Fifth U.S. National Conference on Earthquake Engineering* (p. Vol. II). Oakland: Earthquake Engineering Research Institute.

Seo, C.-Y. a. (2005). Ductility demands on self-centering systems. *ACI Struct. J.*, 102(2), 275–285.

19.0 APPENDIX A

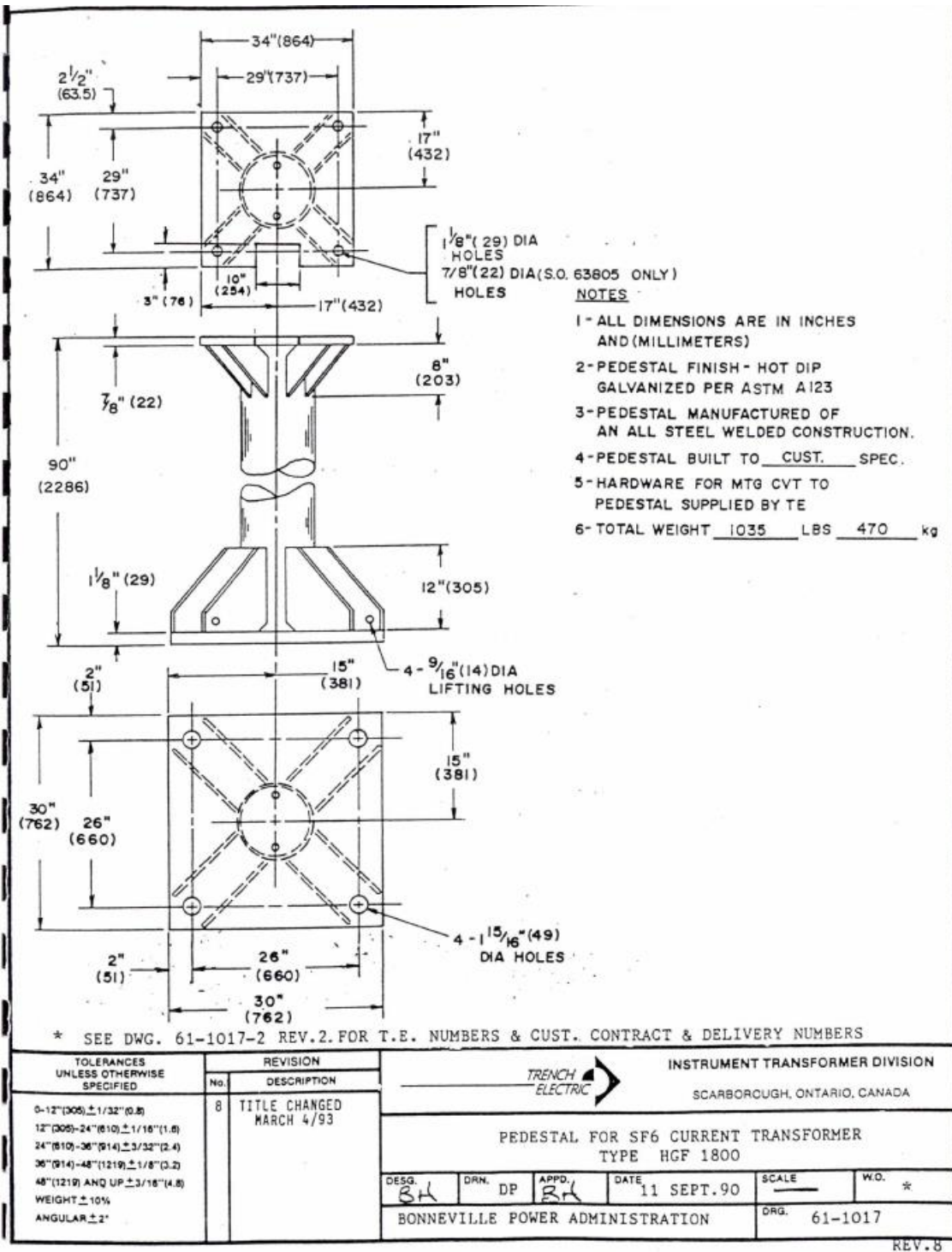


Figure 19-1: Trench Support Pedestal

20.0 APPENDIX B

EXISTING GUSSETS (NOT TO BE PROVIDED)

9/32" x 20 x 1-3/4" BOLTS W/ NUTS & WASHERS;
B7 HIGH STRENGTH OR EQUIVALENT
(TOTAL OF 16 TO BE PROVIDED)

UPPER MOUNTING BRACKET & CLEVIS
(TO BE FABRICATED)

EXISTING DAMPER (NOT TO BE PROVIDED)

LOWER MOUNTING CLEVIS
(TO BE FABRICATED)

EXISTING RODS & COUPLER
(NOT TO BE PROVIDED)

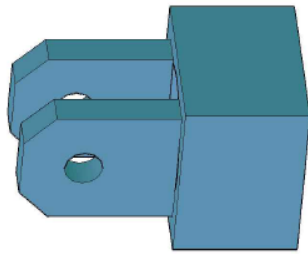
BILL OF MATERIAL

PCS	DESCRIPTION	LENGTH		MARK	WT + 3.5% FOR PAINT
		FT	IN		
4	U. MOUNT BR.	1	3	A1	98.36
4	PL 3/4x2-1/2	0	5-1/2	A1a	12.11
8	PL 3/8x2-1/2	0	8-1/4	A1b	18.16
8	PL 1/4x1	0	1-1/4	A1c	0.73
8	PL 3/8x6	0	10-1/4	A1d	54.15
8	PL 1/4x1-1/2	1	3	A1e	13.21
4	L. MOUNT CLEV.	0	2-1/2	B1	3.38
4	PL 1x1-1/2	0	1-1/2	B1a	2.64
8	PL 1/4x1	0	1-1/4	B1b	0.73

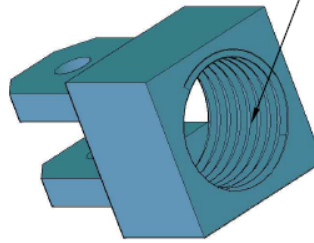
VISCOUS DAMPER COMPONENTS

GENERAL NOTES
 STEEL - ASTM A572 GR. 50
 FINISH - PAINTED GRAY
 BOLTS - ASTM A193 GR. B7
 NUTS AND WASHERS - ASTM A 194 GR. 2H

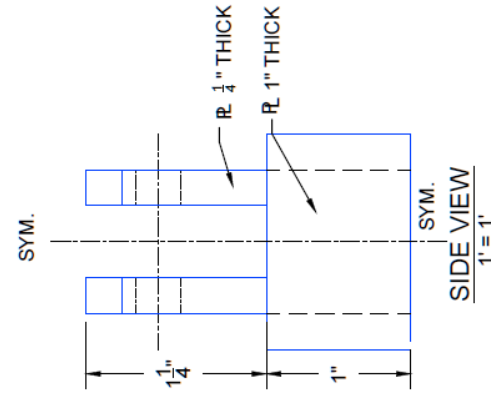
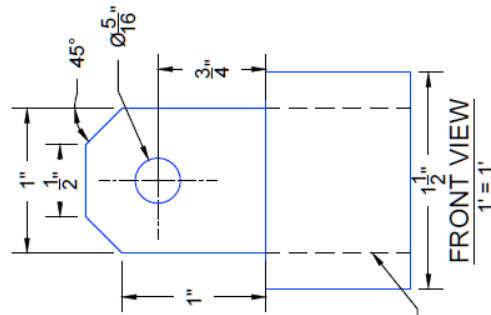
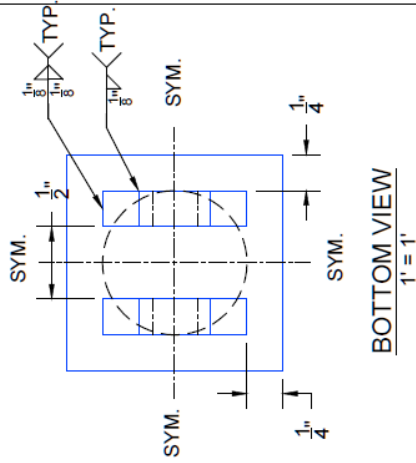
VISCOUS MOUNTS COMP.
 Designed By: Ilya Painikov
 Approved By: Rev. R4
 Units: IN. Scale: N/A Date: 2/29/2016
 Sheet: 1 OF 3



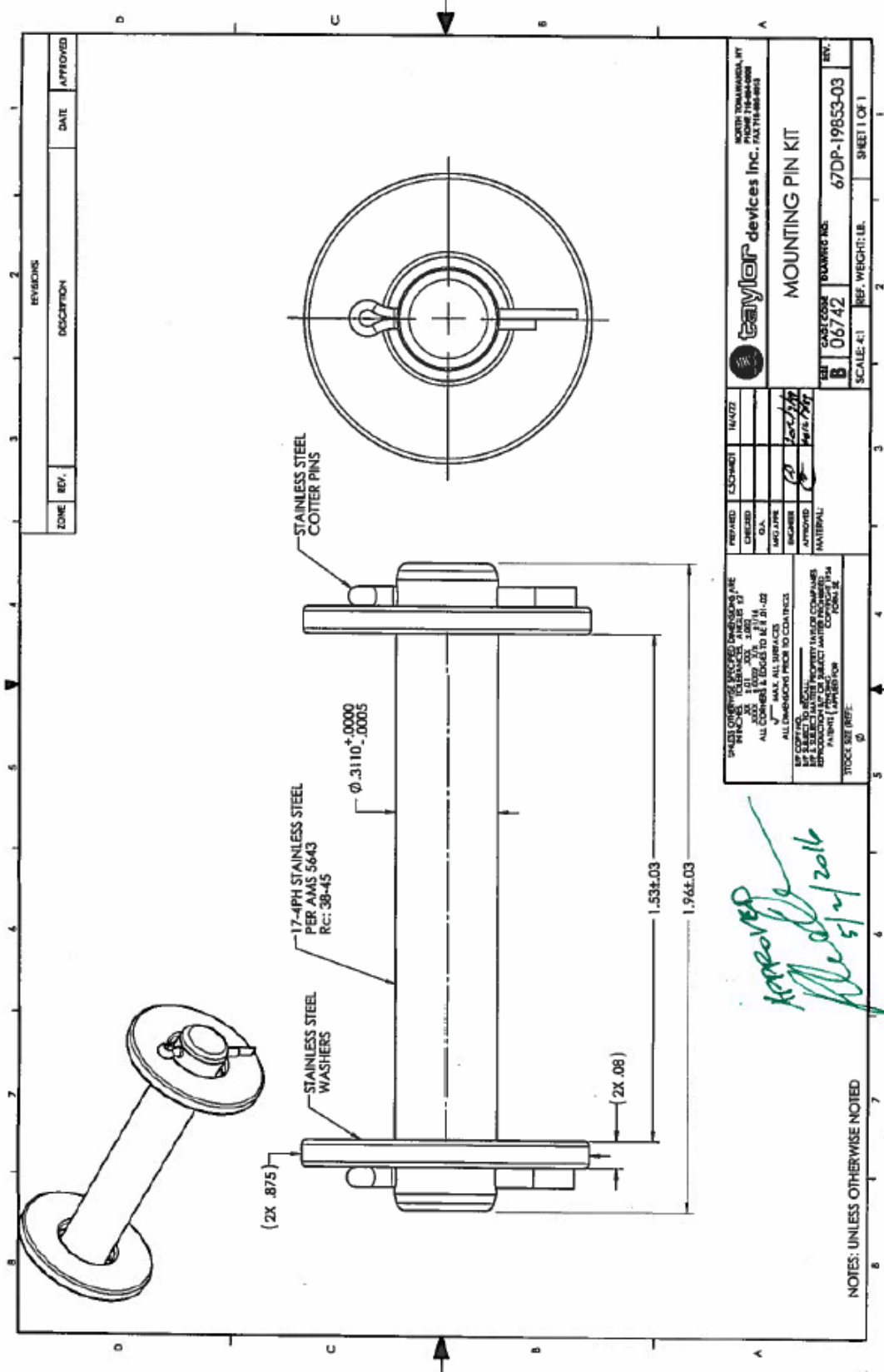
QUANTITY OF 4 TO BE PROVIDED



1"-8 UNC - 2B



LOWER MOUNTING CLEVIS	
Designed By: Ilya Palnikov	Approved By: Rev: R4
Units: IN.	Scale: N/A
Date: 2/29/2016	Sheet: 3 OF 3

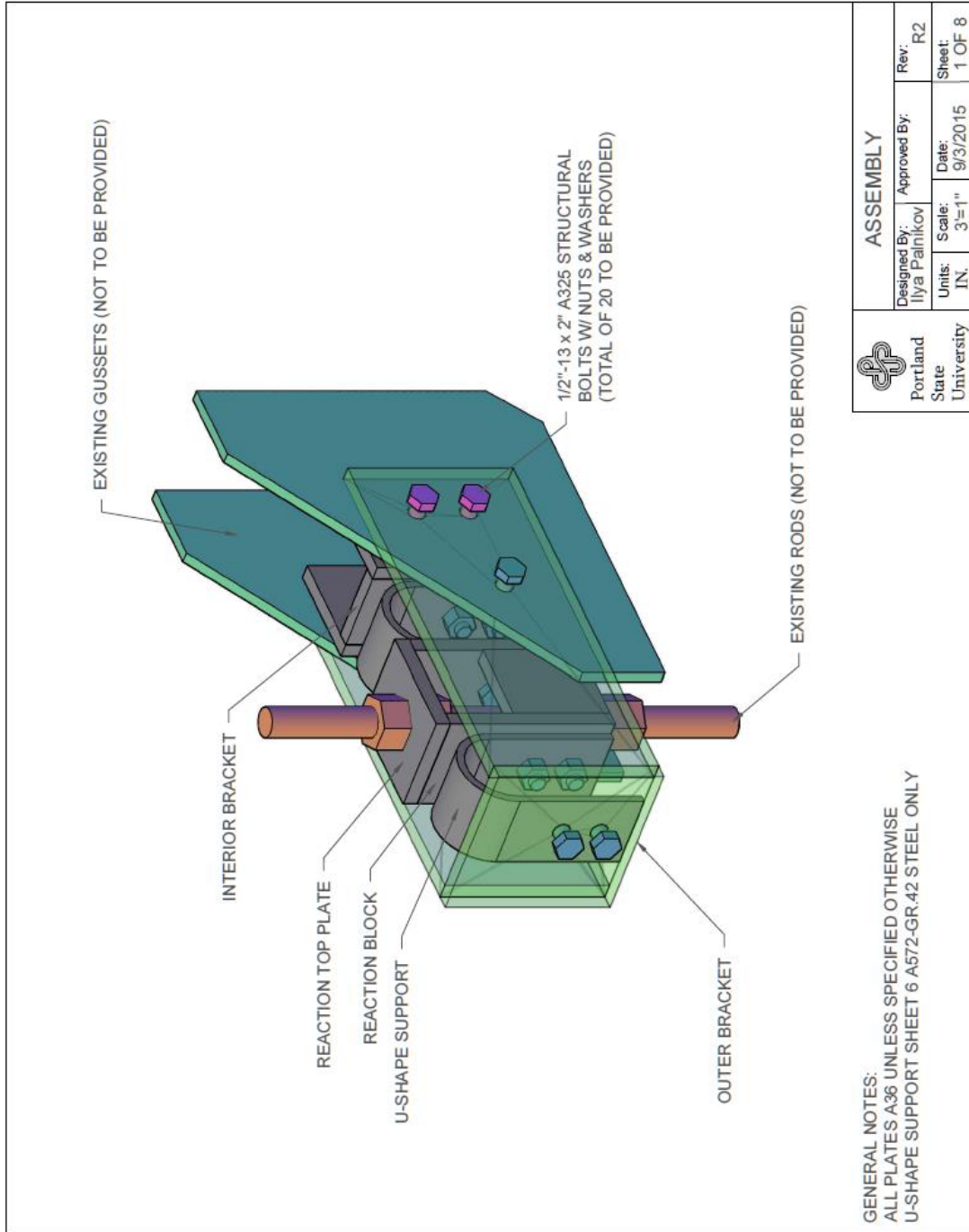


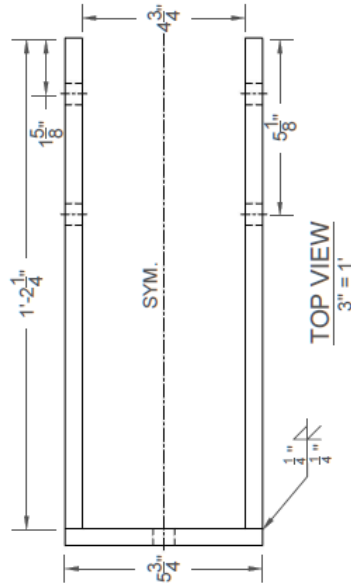
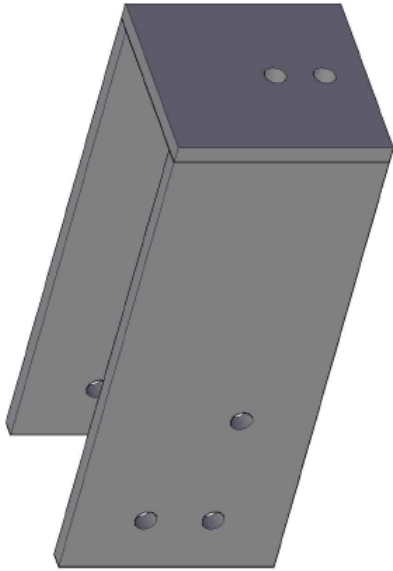
PREPARED: [] CHECKED: [] DATE: [] APPROVED: [] MATERIAL: []		16472 16472 16472 16472	NORTH TOWNSEND, VT TAYLOR DEVICES INC., FAX 774-884-8933
DIMENSIONS UNLESS OTHERWISE SPECIFIED ARE IN INCHES. TOLERANCES ARE AS FOLLOWS: ALL DIMENSIONS UNLESS OTHERWISE SPECIFIED ARE TO BE H/2. ALL DIMENSIONS TO BE TO COILS. ALL DIMENSIONS TO BE TO COILS. ALL DIMENSIONS TO BE TO COILS.		DRAWING NO. 67DP-19853-03 SCALE: 4:1 REF. WEIGHT: LB.	SHEET 1 OF 1

APPROVED
 [Signature]
 5/2/2016

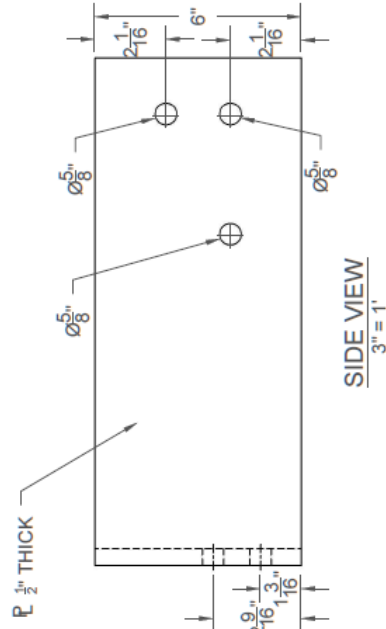
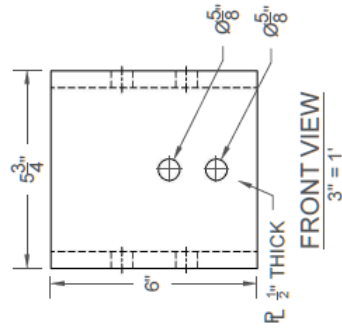
NOTES: UNLESS OTHERWISE NOTED

21.0 APPENDIX C





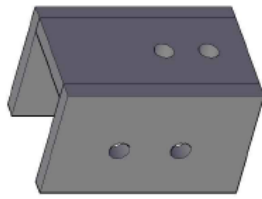
QUANTITY OF 4 TO BE PROVIDED



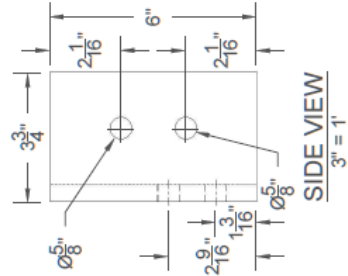
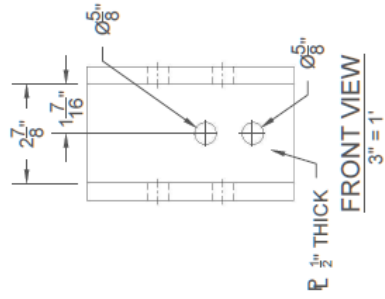
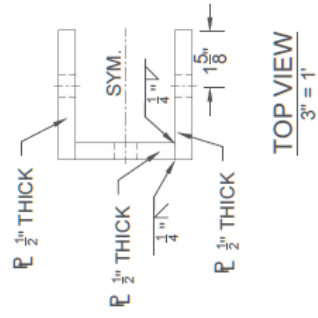
Portland
State
University

OUTER BRACKET

Designed By: Ilya Painikov	Approved By:	Rev:
Units: IN.	Scale: 3"=1"	Date: 9/3/2015
		Sheet: 2 OF 8

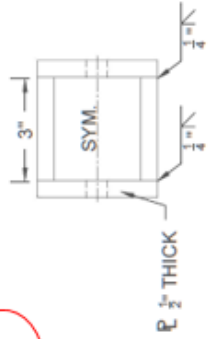
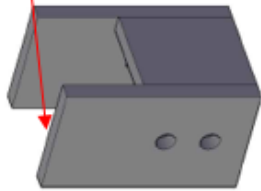


QUANTITY OF 4 TO BE PROVIDED



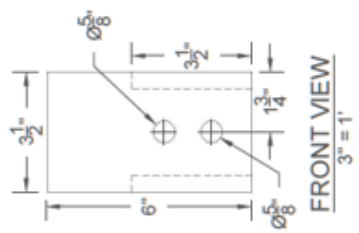
 Portland State University	INTERIOR BRACKET	
	Designed By: Ilya Palnikov	Approved By:
Units: IN.	Scale: 3"=1'	Date: 9/3/2015
		Sheet: 3 OF 8

Top PL must be welded to block pg. 5

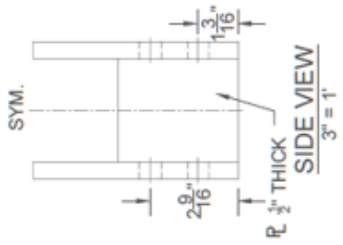


TOP VIEW
3" = 1"

QUANTITY OF 5 TO BE PROVIDED

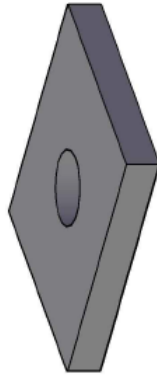


FRONT VIEW
3" = 1"

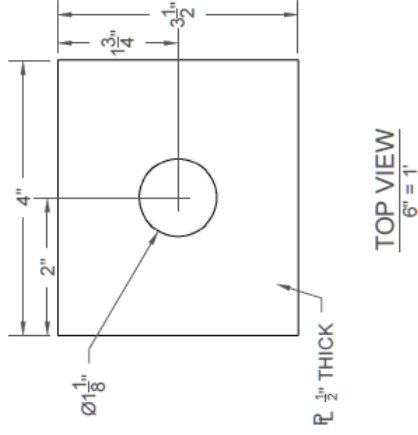


SIDE VIEW
3" = 1"

 Portland State University	REACTION BLOCK		
	Designed By: Ilya Palmikov	Approved By:	Rev: R2
	Units: IN.	Scale: 3"=1'	Date: 9/3/2015
			Sheet: 4 OF 8

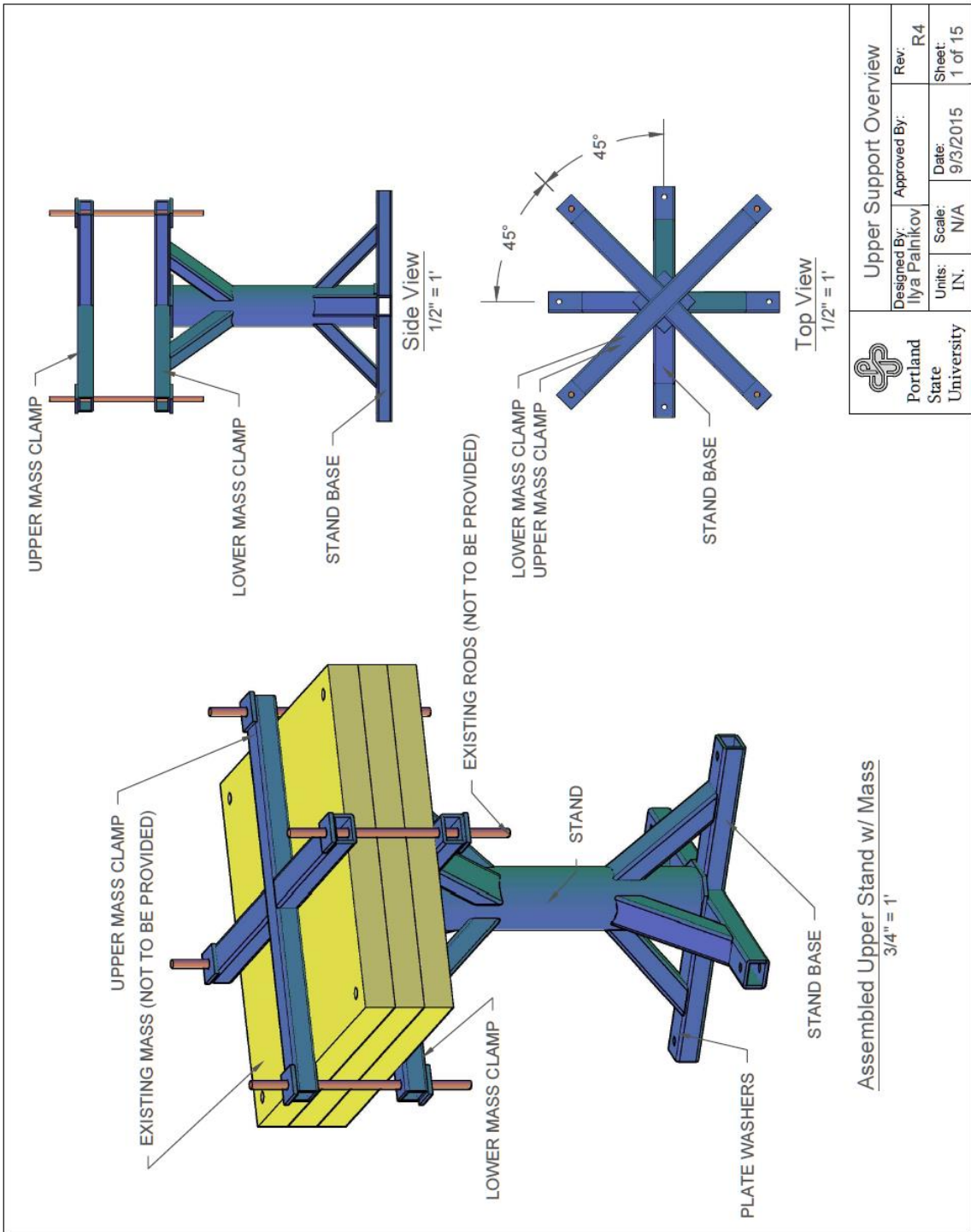


QUANTITY OF 5 TO BE PROVIDED

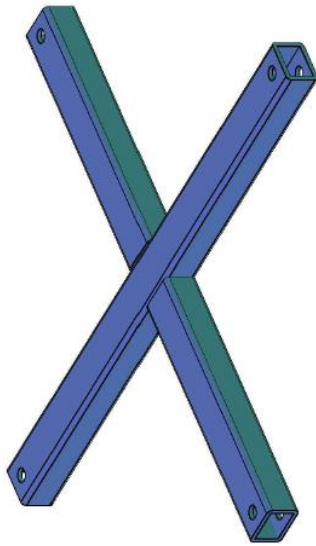


REACTION TOP PLATE			
Designed By: Ilya Palnikov	Approved By:	Rev:	R2
Units: IN.	Scale: 6"=1'	Date:	9/3/2015
		Sheet:	5 OF 8

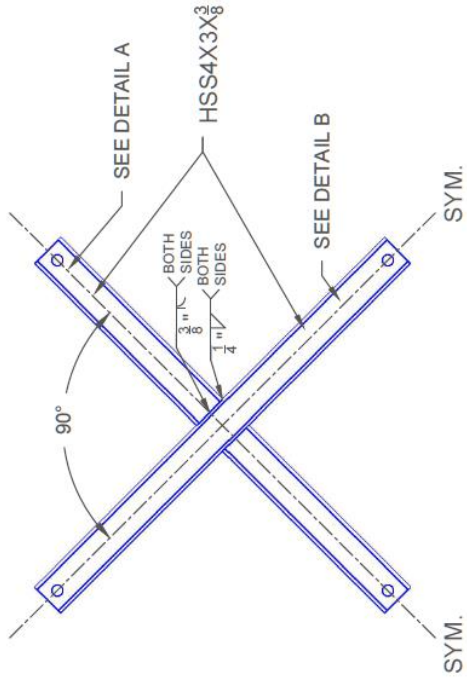
22.0 APPENDIX D



 Upper Support Overview			
Designed By:	Approved By:	Rev:	
Ilya Palnikov		R4	
Units:	Scale:	Date:	
IN.	N/A	9/3/2015	
		Sheet:	
		1 of 15	



ISOMETRIC
1" = 1'



TOP VIEW
3/4" = 1'



Portland
State
University

UPPER MASS CLAMP

Designed By: Ilya Palnikov

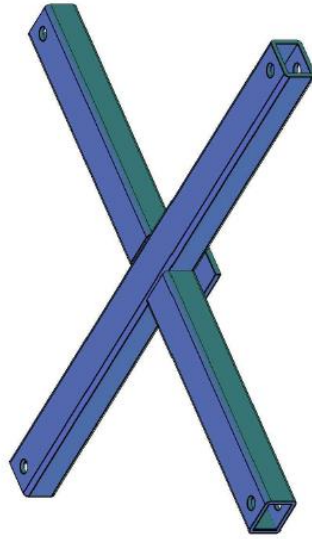
Units: IN.

Scale: N/A

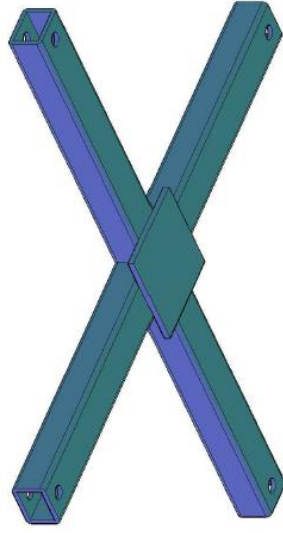
Approved By: Rev. R4

Date: 9/3/2015

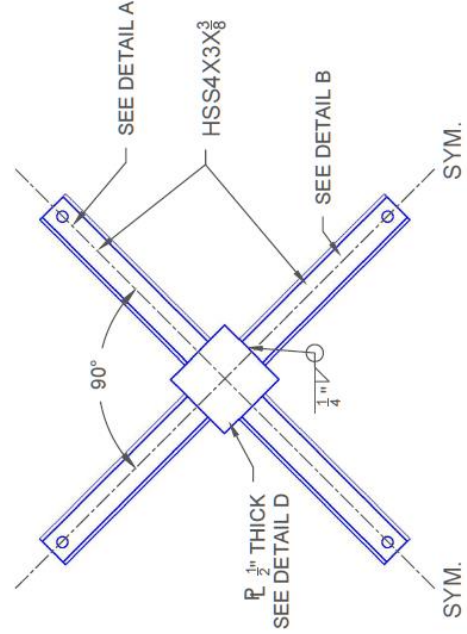
Sheet 2 of 15



TOP-ISOMETRIC
1" = 1'



BOTTOM-ISOMETRIC
1" = 1'

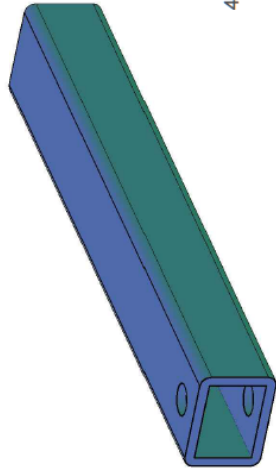


WELD ALL HSS SECTIONS TOGETHER WITH $\frac{3}{8}$ " FLARE BEVEL WELD AND $\frac{1}{4}$ " FILLET WELD COMBINATION AS SHOWN ON SHEET 2.

BOTTOM VIEW
3/4" = 1'

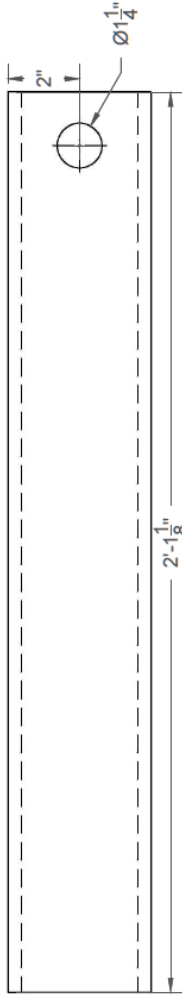


LOWER MASS CLAMP			
Designed By:	Approved By:	Rev:	R4
Ilya Palmikov		Date:	9/3/2015
Units:	Scale:	Sheet:	3 of 15
IN.	N/A		



4 TOTAL NEEDED

ISOMETRIC
1-1/2" = 1'



TOP VIEW
3" = 1'



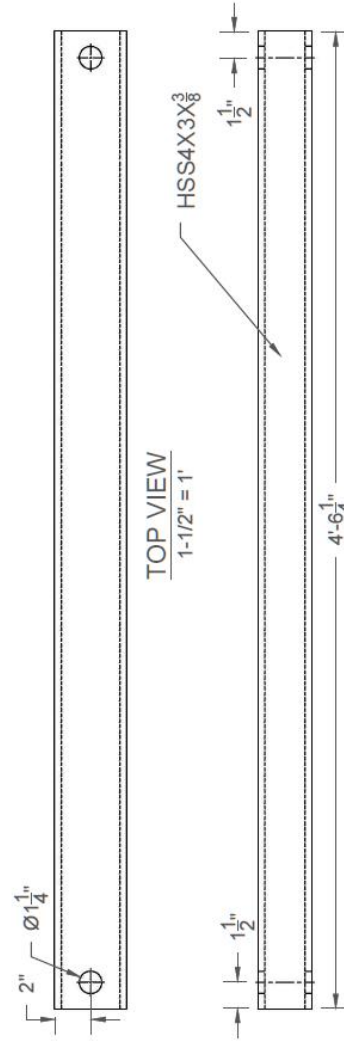
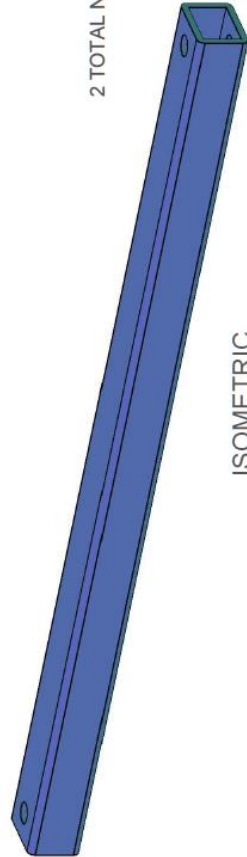
SIDE VIEW
3" = 1'



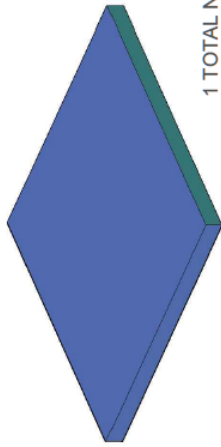
DETAIL A

Designed By: Ilya Palnikov	Approved By:	Rev:
Units: IN.	Scale: N/A	Sheet: 4 of 15
	Date: 9/3/2015	R4

2 TOTAL NEEDED

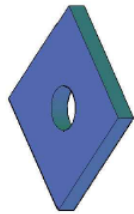
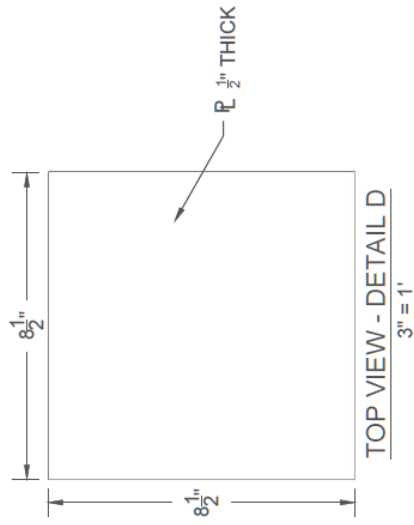


 Portland State University	DETAIL B		Rev:	R4
	Designed By: Ilya Painikov	Approved By:	Date:	9/3/2015
	Units: IN.	Scale: N/A	Sheet:	5 of 15



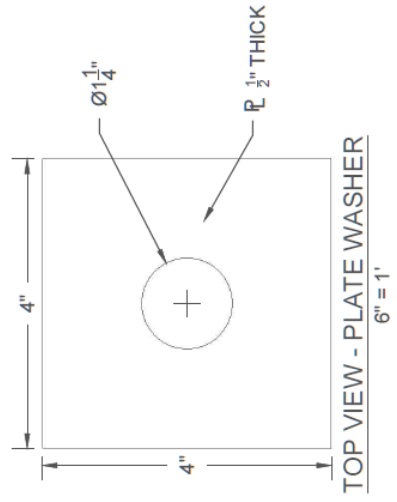
1 TOTAL NEEDED

ISOMETRIC - DETAIL D
3" = 1'



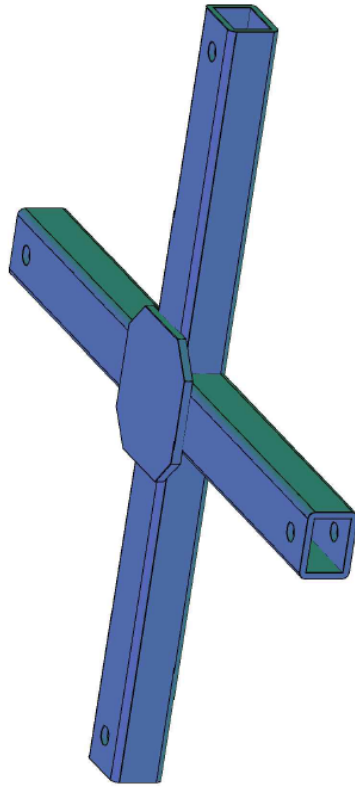
16 TOTAL NEEDED

ISOMETRIC - PLATE WASHER
3" = 1'

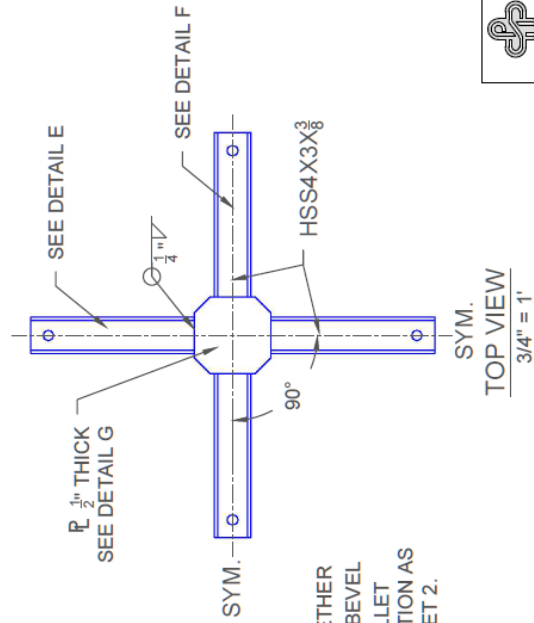


PL WASHER & DETAIL D

Designed By: Ilya Painikov	Approved By:	Rev: R4
Units: IN.	Scale: N/A	Date: 9/3/2015
		Sheet: 6 of 15



ISOMETRIC
1-1/2" = 1'

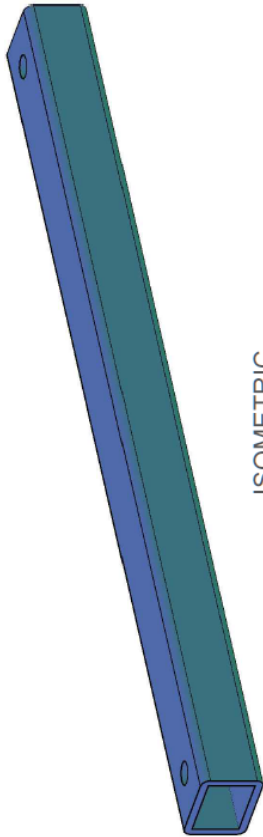


WELD ALL HSS
SECTIONS TOGETHER
WITH $\frac{3}{8}$ " FLARE BEVEL
WELD AND $\frac{1}{4}$ " FILLET
WELD COMBINATION AS
SHOWN ON SHEET 2.

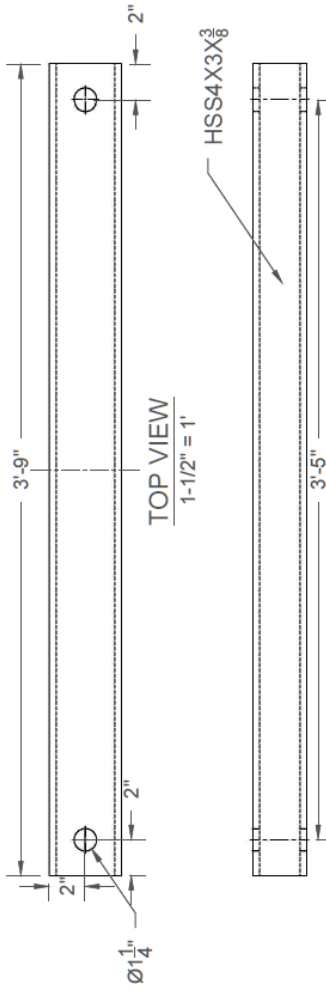


STAND BASE

Designed By: Ilya Painikov	Approved By:	Rev: R4
Units: IN.	Scale: N/A	Date: 9/3/2015
		Sheet 7 of 15



ISOMETRIC
1-1/2" = 1'



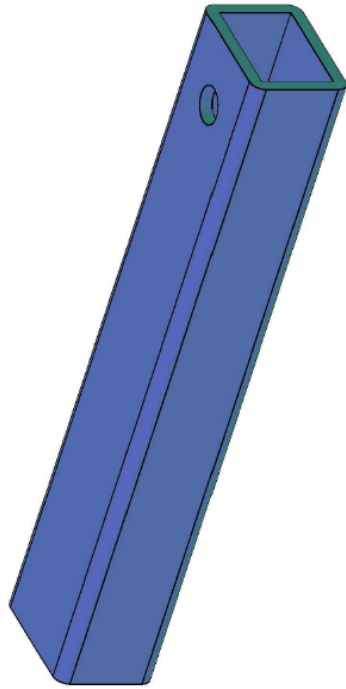
TOP VIEW
1-1/2" = 1'

SIDE VIEW
1-1/2" = 1'

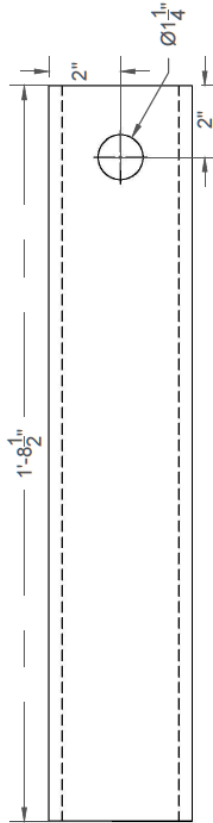


DETAIL E

Designed By: Ilya Palnikov	Approved By:	Rev: R4
Units: IN.	Scale: N/A	Date: 9/3/2015
		Sheet: 8 of 15



ISOMETRIC
3" = 1'



TOP VIEW
3" = 1'

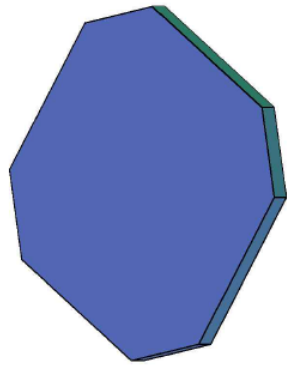


SIDE VIEW
3" = 1'

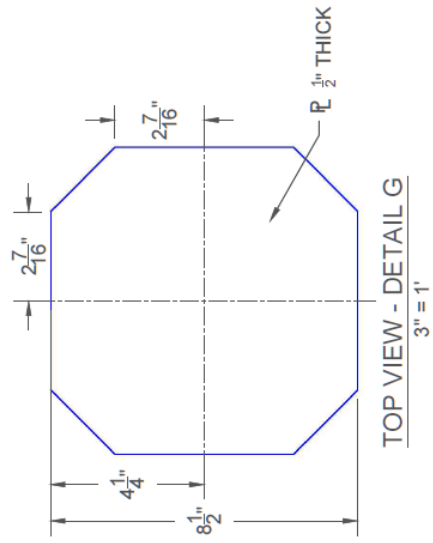


DETAIL F

Designed By: Ilya Painikov	Approved By:	Rev: R4
Units: IN.	Scale: N/A	Date: 9/3/2015
		Sheet: 9 of 15

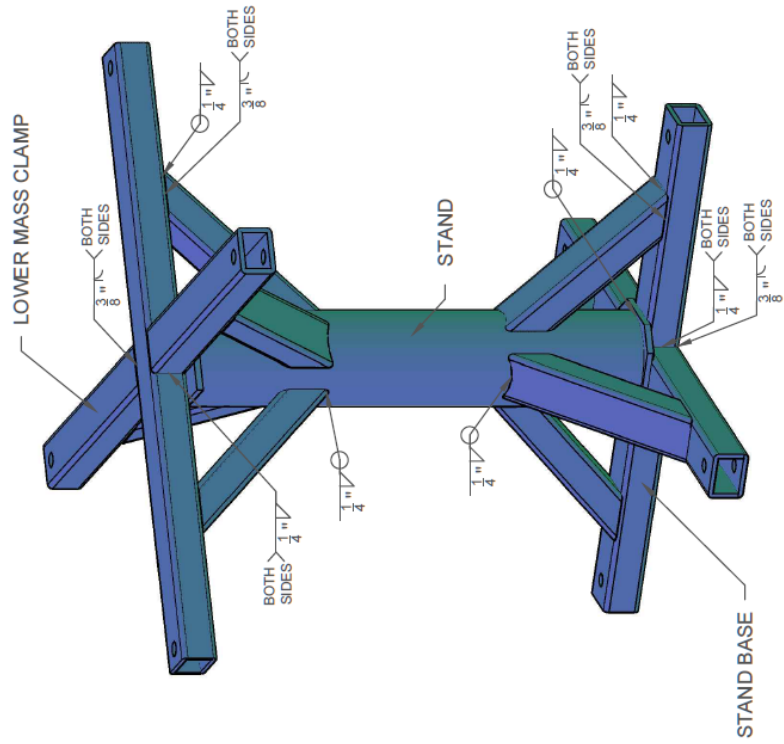


ISOMETRIC - DETAIL G
3" = 1'



DETAIL G

Designed By: Ilya Palnikov	Approved By: R4	Rev:
Units: IN.	Scale: N/A	Date: 9/3/2015
		Sheet: 10 of 15



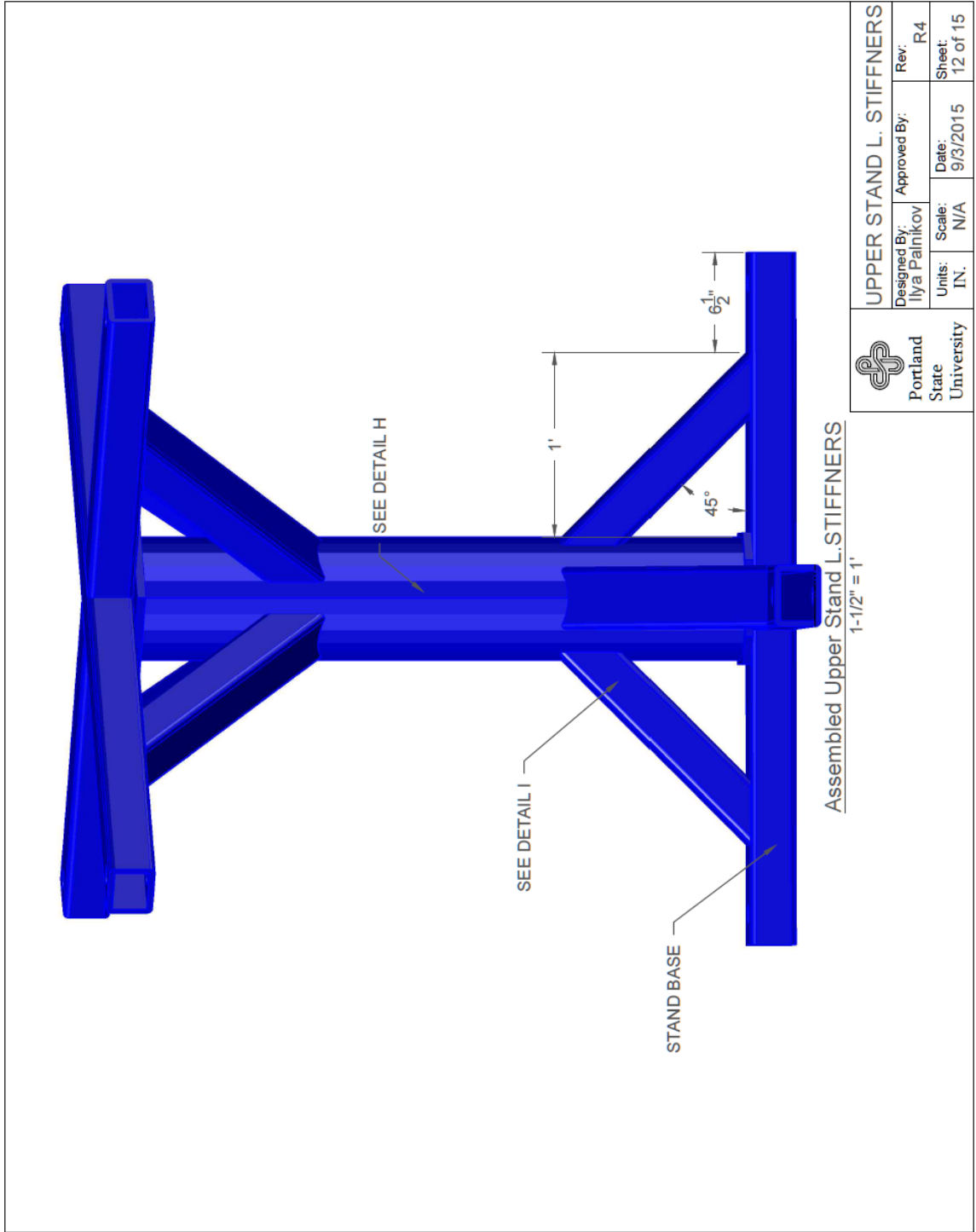
Assembled Upper Stand
1" = 1"

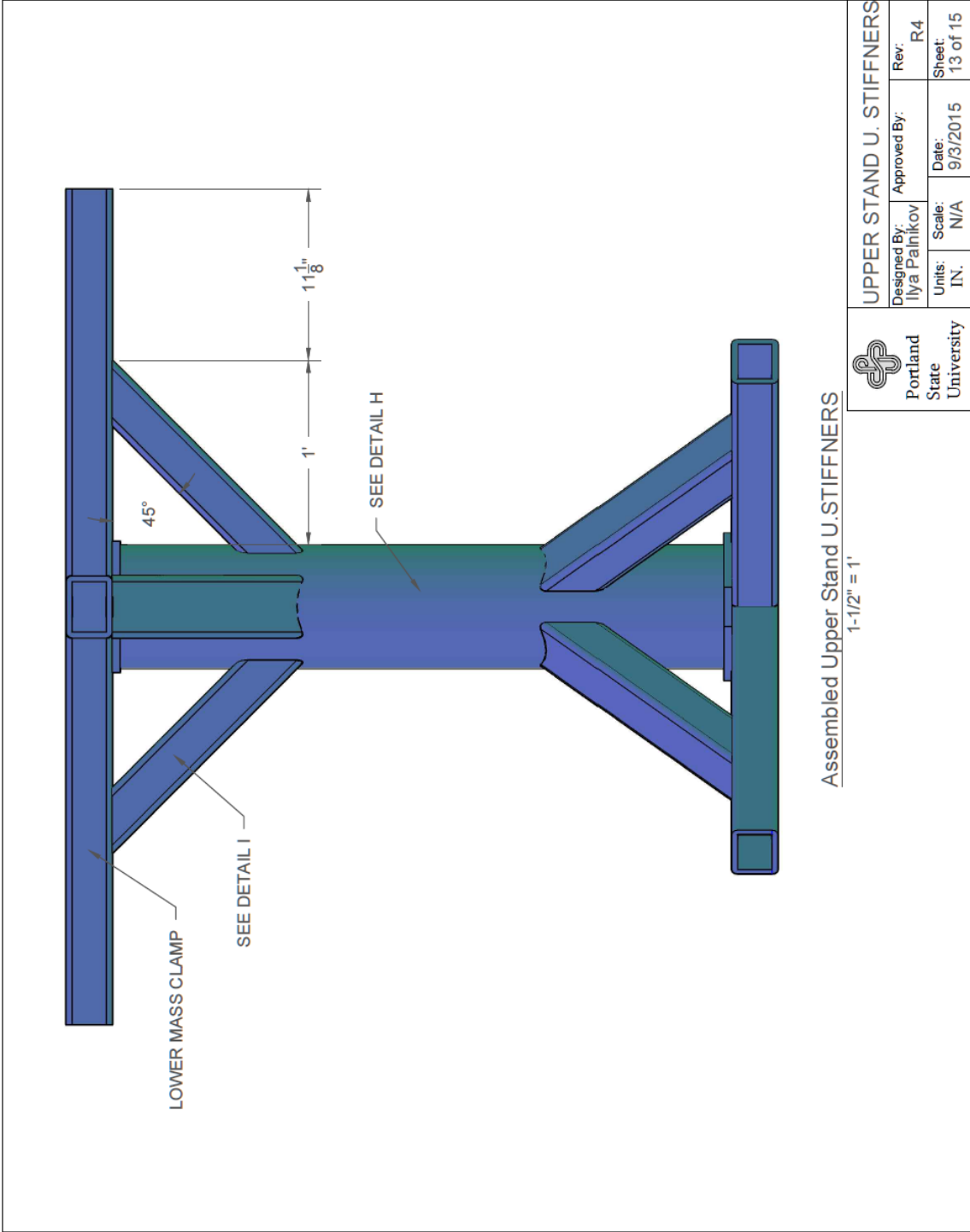


Portland State University

UPPER STAND

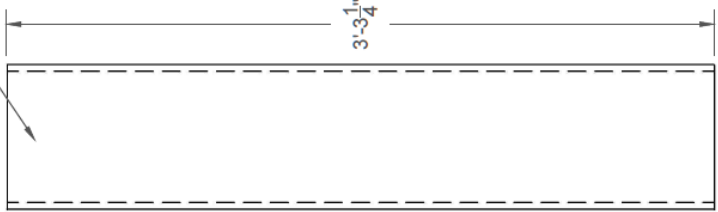
Designed By: Ilya Painikov	Approved By:	Rev: R4
Units: IN.	Scale: N/A	Date: 9/3/2015
		Sheet: 11 of 15



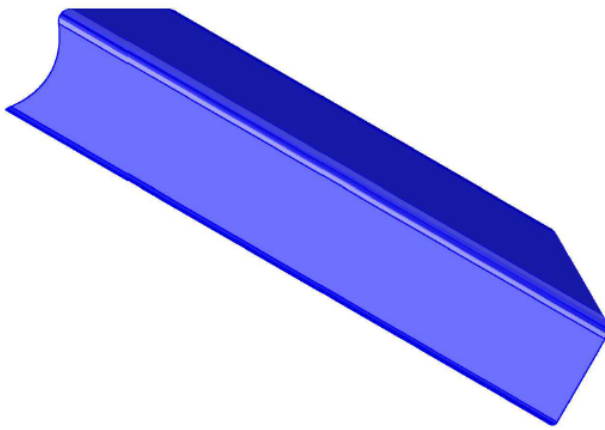


 Portland State University			
Designed By: Ilya Painikov	Approved By:	Rev: R4	UPPER STAND U. STIFFENERS
Units: IN.	Scale: N/A	Date: 9/3/2015	Sheet: 13 of 15

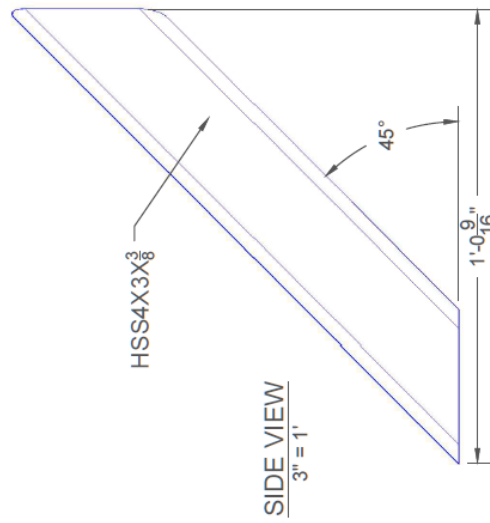
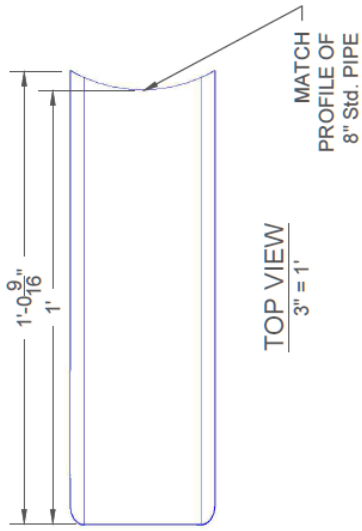
8" Std. PIPE



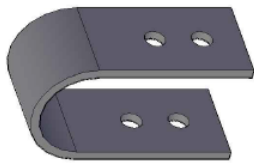
DETAIL H			
 Portland State University	Designed By: Ilya Painikov	Approved By:	Rev: R4
	Units: IN.	Scale: N/A	Date: 9/3/2015
			Sheet 14 of 15



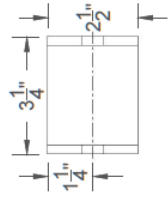
HSS STIFFNER DETAIL I
3" = 1'



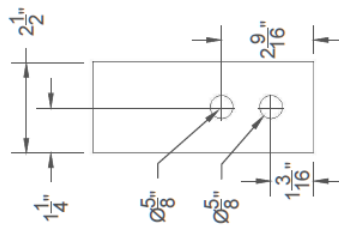
 Portland State University	DETAIL I		
	Designed By:	Approved By:	Rev:
	Iliya Palnikov		R4
	Units:	Date:	Sheet:
IN.	9/3/2015	15 of 15	
	Scale:	N/A	



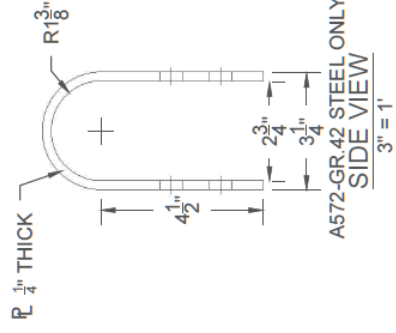
QUANTITY OF 104 TO BE PROVIDED



A572-GR.42 STEEL ONLY
TOP VIEW
3" = 1'



A572-GR.42 STEEL ONLY
FRONT VIEW
3" = 1'



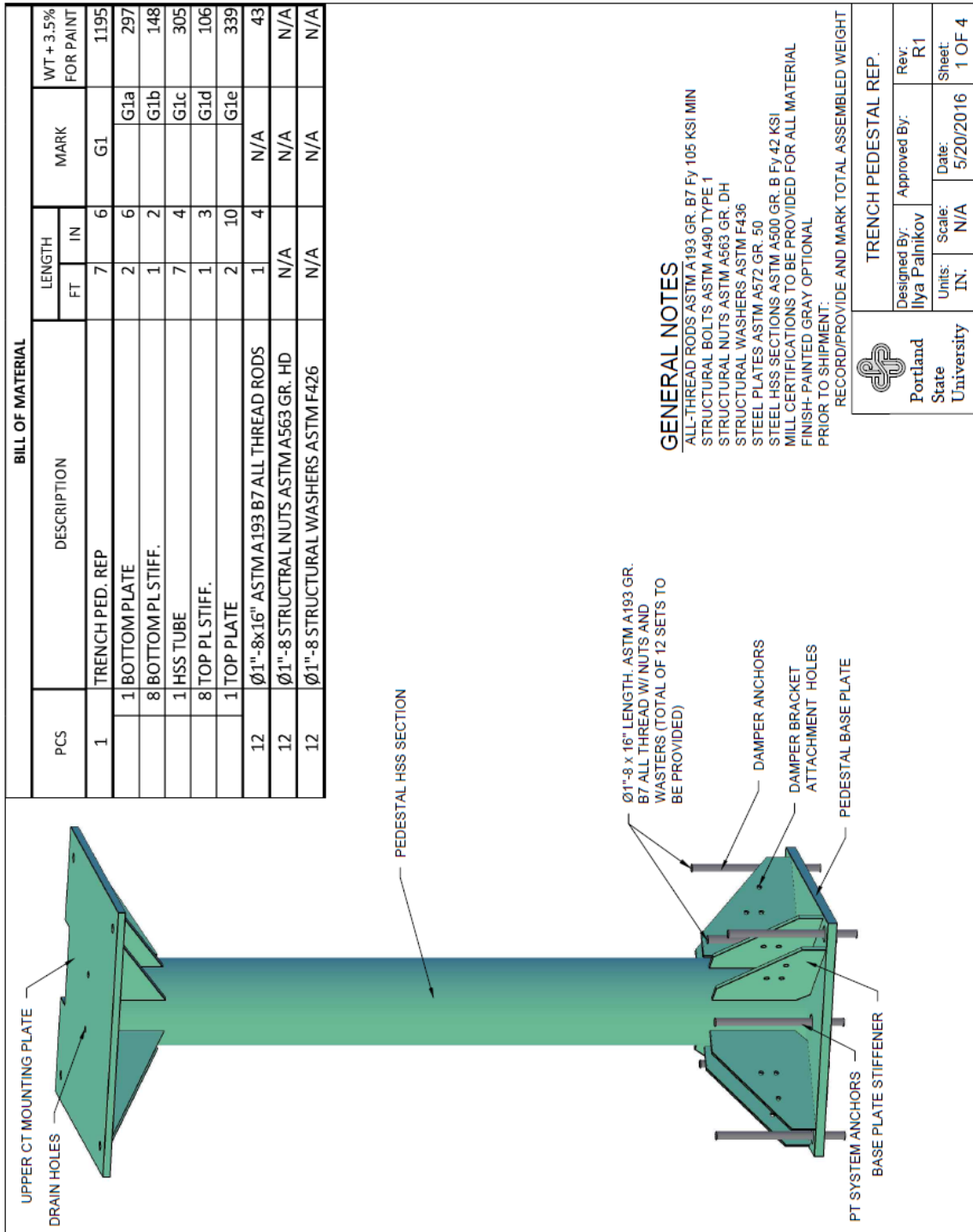
A572-GR.42 STEEL ONLY
SIDE VIEW
3" = 1'



U-SHAPE SUPPORT

Designed By: Ilya Painikov	Approved By:	Rev: R2
Units: IN.	Scale: 3"=1'	Date: 9/3/2015
		Sheet: R2

23.0 APPENDIX E



BILL OF MATERIAL

PCS	DESCRIPTION	LENGTH		MARK	WT + 3.5% FOR PAINT
		FT	IN		
1	TRENCH PED. REP	7	6	G1	1195
	1 BOTTOM PLATE	2	6	G1a	297
	8 BOTTOM PLS STIFF.	1	2	G1b	148
	1 HSS TUBE	7	4	G1c	305
	8 TOP PL STIFF.	1	3	G1d	106
	1 TOP PLATE	2	10	G1e	339
12	Ø1"-8x16" ASTM A193 B7 ALL THREAD RODS	1	4	N/A	43
12	Ø1"-8 STRUCTURAL NUTS ASTM A563 GR. HD	N/A	N/A	N/A	N/A
12	Ø1"-8 STRUCTURAL WASHERS ASTM F426	N/A	N/A	N/A	N/A

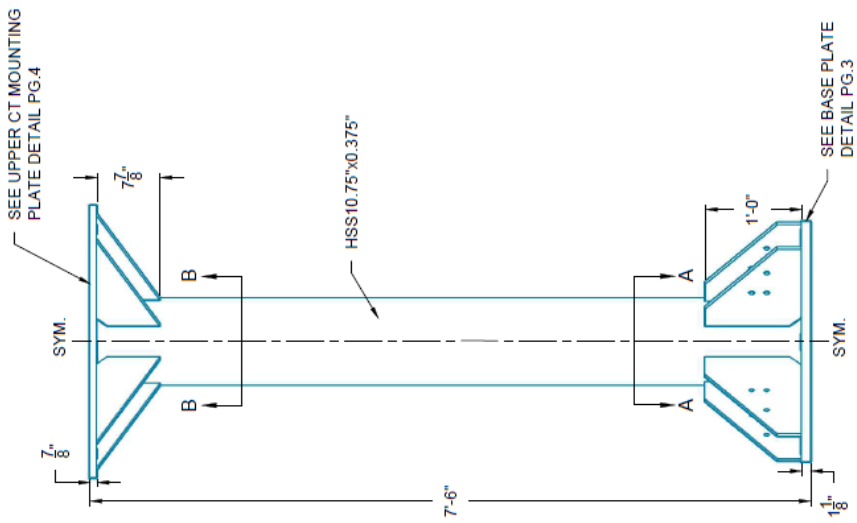
GENERAL NOTES

- ALL-THREAD RODS ASTM A193 GR. B7 Fy 105 KSI MIN
- STRUCTURAL BOLTS ASTM A490 TYPE 1
- STRUCTURAL NUTS ASTM A563 GR. DH
- STRUCTURAL WASHERS ASTM F436
- STEEL PLATES ASTM A572 GR. 50
- STEEL HSS SECTIONS ASTM A500 GR. B Fy 42 KSI
- MILL CERTIFICATIONS TO BE PROVIDED FOR ALL MATERIAL
- FINISH- PAINTED GRAY OPTIONAL
- PRIOR TO SHIPMENT:
- RECORD/PROVIDE AND MARK TOTAL ASSEMBLED WEIGHT

TRENCH PEDESTAL REP.

Designed By: Ilya Painikov
 Approved By: R1
 Units: IN. Scale: N/A Date: 5/20/2016
 Sheet: 1 OF 4

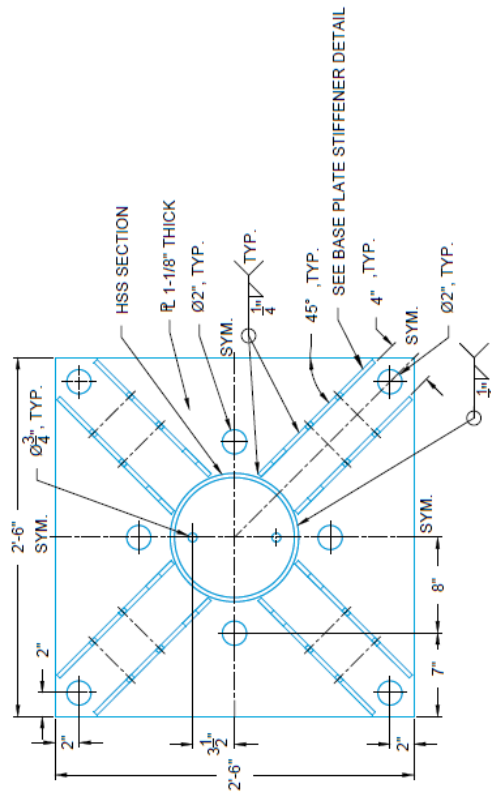
Portland State University



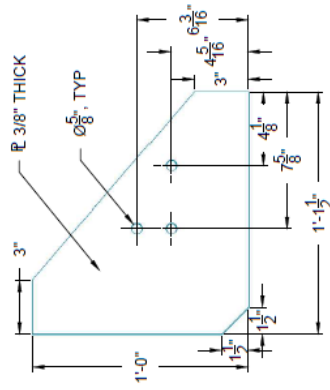
SIDE VIEW



PEDESTAL SIDE			
Designed By:	Approved By:	Rev:	
Ilya Palnikov		R1	
Units:	Scale:	Date:	
IN.	N/A	5/20/2016	
		Sheet:	2 OF 4



PEDESTAL BASE PLATE DETAIL



BASE PLATE STIFFENER

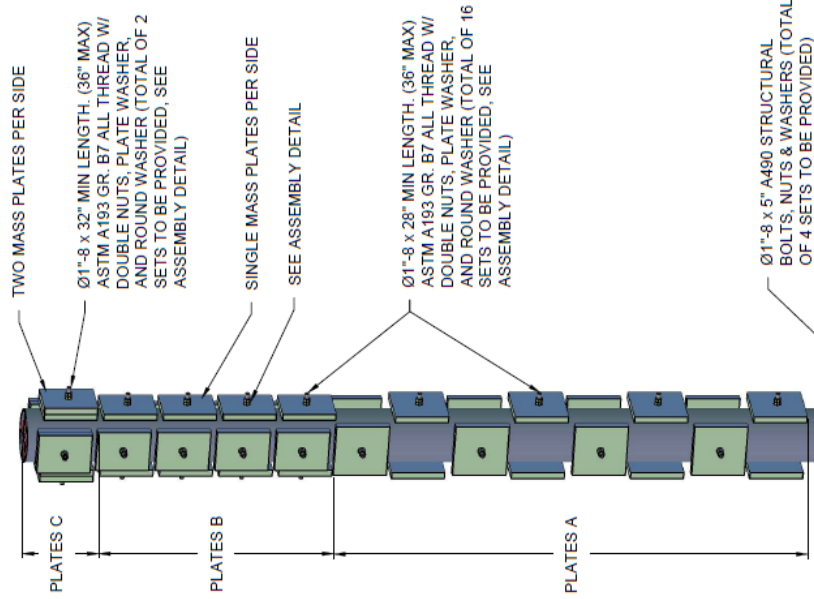


BOTTOM PEDESTAL PLATE	
Designed By: Ilya Palnikov	Approved By: R1
Units: IN.	Date: 5/20/2016
Scale: N/A	Sheet: 3 OF 4

24.0 APPENDIX F

BILL OF MATERIAL						
PCS	DESCRIPTION	LENGTH		MARK	WT + 3.5% FOR PAINT	
		FT	IN			
1	CT-HSS-STIFF	21	5 5/8	C1	1856	
1	PL 1x34	2	10	C1a	339	
8	PL 3/8x12	0	12	C1b	127	
1	HSS16x3/8	21	5 1/4	C1c	1390	
1	MASS PLATES A	2	5	D1	2404	
16	PL 2x16	1	4	D1a	2404	
1	MASS PLATES B/C	2	5	E1	2818	
24	PL 2x16	1	0.5	E1a	2818	
1	LIFTING HOOK	1	4	F1	34	
1	HSS2.5x2.5x5/16	1	4	F1a	11	
2	HSS2.5x2.5x5/16	1	4	F1b	23	
16	Ø1"-8x28" (36" MAX) ASTM A193 B7 ALL THREAD RODS	1	4	N/A	100	
2	Ø1"-8x32" (36" MAX) ASTM A193 B7 ALL THREAD RODS	1	4	N/A	14	
76	Ø1"-8 STRUCTURAL NUTS ASTM A563 GR. HD	N/A	N/A	N/A	N/A	
44	Ø1"-8 STRUCTURAL WASHERS ASTM F426	N/A	N/A	N/A	N/A	
38	PLATE WASHERS	N/A	N/A	N/A	N/A	
4	Ø1"-8x5" A490 STRUCTURAL BOLTS	N/A	N/A	N/A	N/A	
TOTAL RAW WEIGHT					7211	
RAW WEIGHT, NOT EQUAL TO WEIGHT OF FINISHED PRODUCT						

 Portland State University	TRENCH CT 226-293 MASS SYSTEM	
	Designed By: Ilya Painikov	Approved By: Date: 5/17/2016
Units: IN.	Scale: N/A	Sheet: 1 OF 7



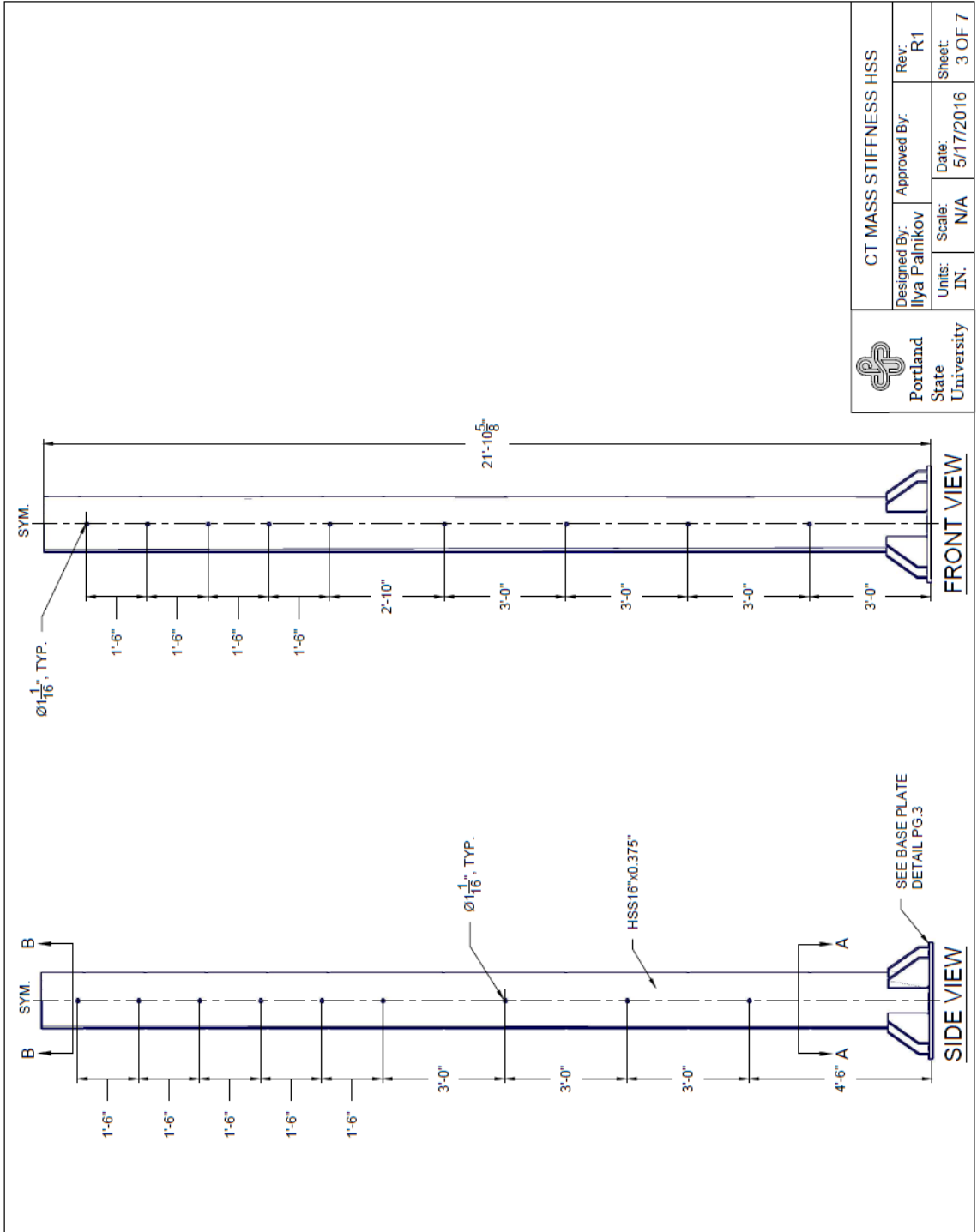
GENERAL NOTES

ALL-THREAD RODS ASTM A193 GR. B7 Fy 105 KSI MIN
 STRUCTURAL BOLTS ASTM A490 TYPE 1
 STRUCTURAL NUTS ASTM A563 GR. DH
 STRUCTURAL WASHERS ASTM F436
 STEEL PLATES ASTM A572 GR. 50
 STEEL HSS SECTIONS ASTM A500 GR. B Fy 42 KSI
 MILL CERTIFICATIONS TO BE PROVIDED FOR ALL MATERIAL
 FINISH- PAINTED GRAY OPTIONAL
 ASSEMBLE PRIOR TO SHIPMENT.
 PRE-LOAD ALL-THREAD RODS TO 12 KIPS EACH
 RECORD/PROVIDE AND MARK TOTAL ASSEMBLED WEIGHT

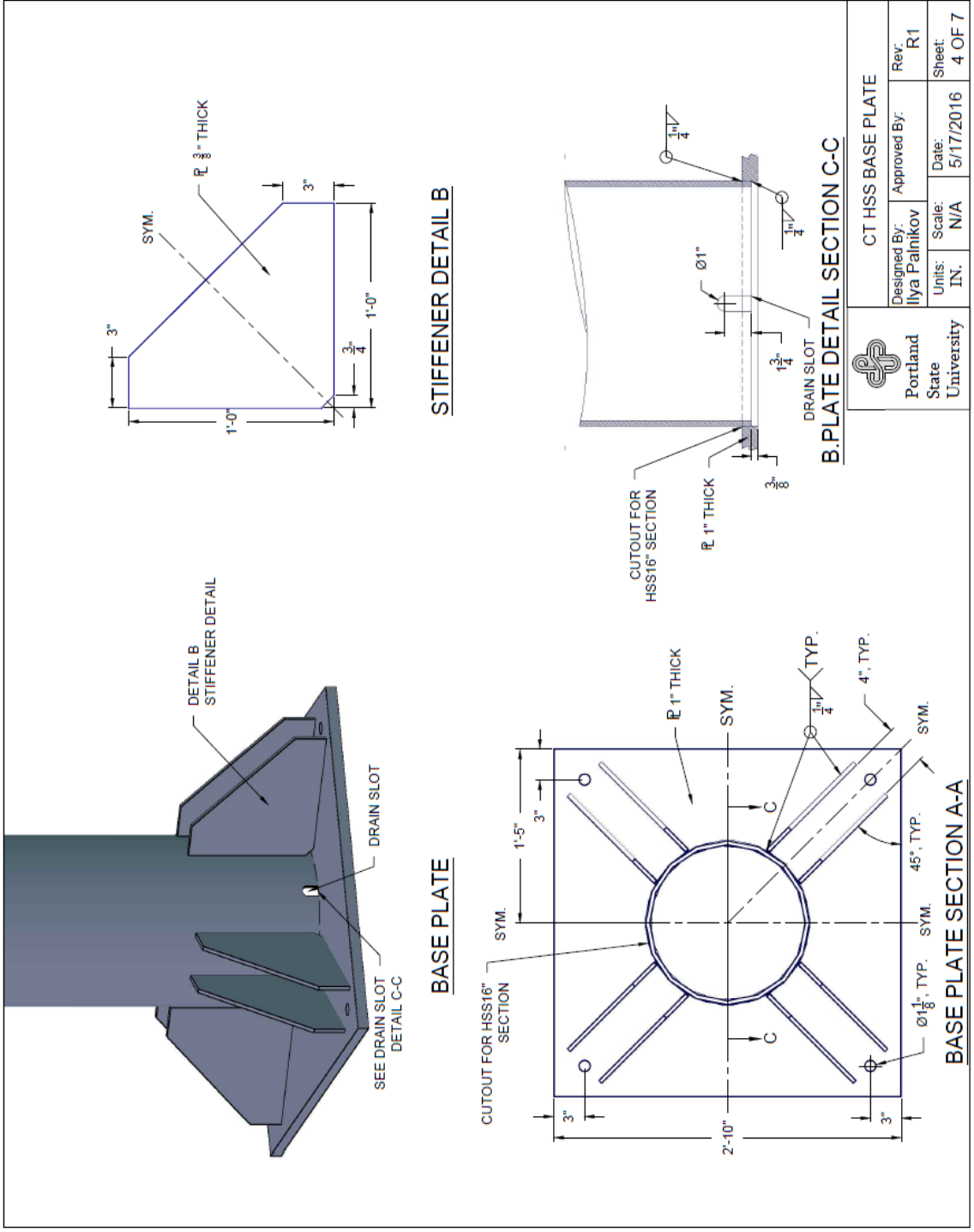


Portland
State
University

TRENCH CT 226-293 MASS SYSTEM	
Designed By: Ilya Palmikov	Approved By:
Units: IN.	Scale: N/A
Date: 5/17/2016	Rev: R1
Sheet: 2 OF 7	



CT MASS STIFFNESS HSS			
Designed By:	Approved By:	Rev:	R1
Ilya Palnikov		Sheet:	3 OF 7
Units:	Scale:	Date:	5/17/2016
IN.	N/A		



STIFFENER DETAIL B

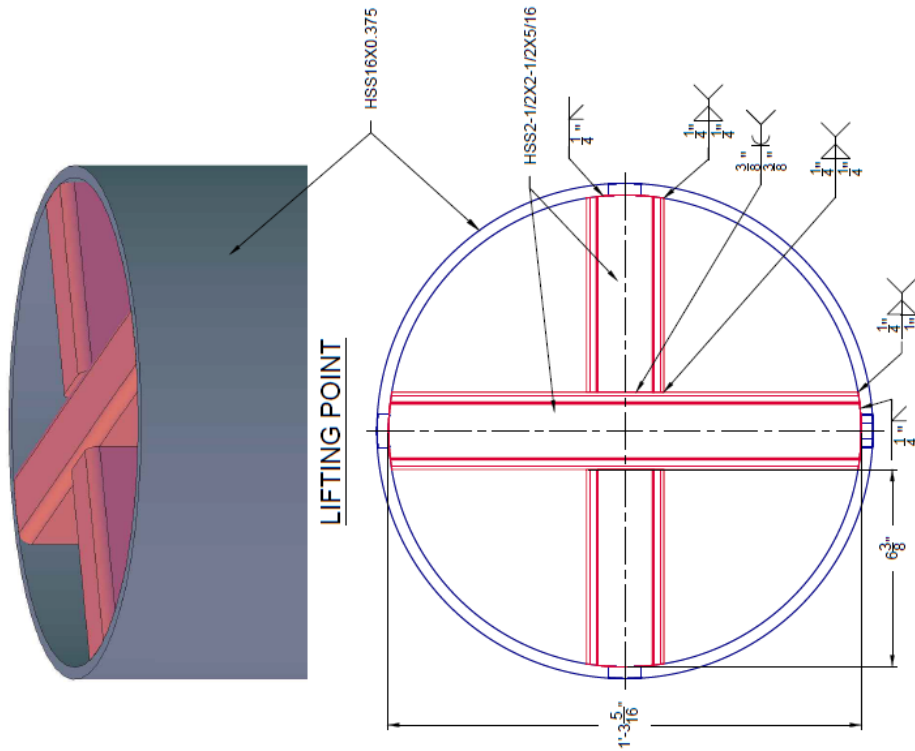
BASE PLATE

B. PLATE DETAIL SECTION C-C



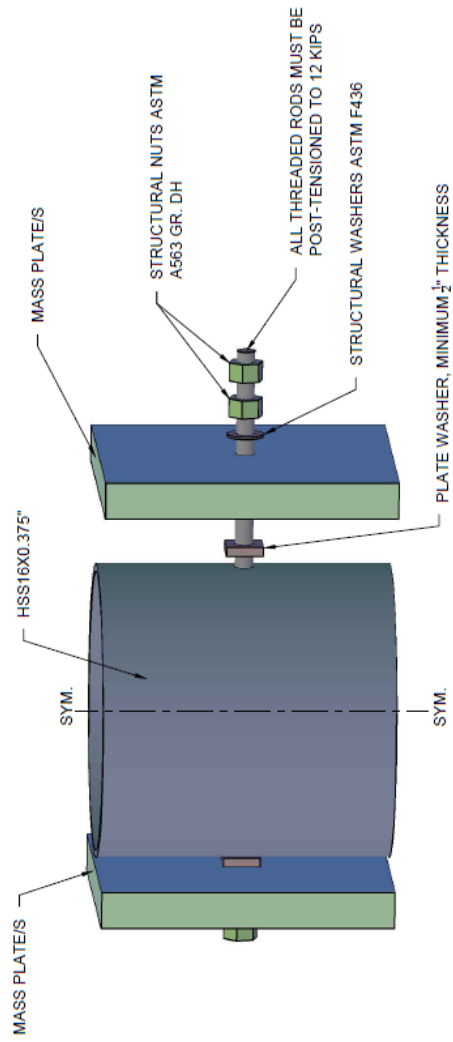
CT HSS BASE PLATE

Designed By:	Approved By:	Rev:
Ilyia Palnikov		R1
Units:	Scale:	Date:
IN.	N/A	5/17/2016
		Sheet:
		4 OF 7



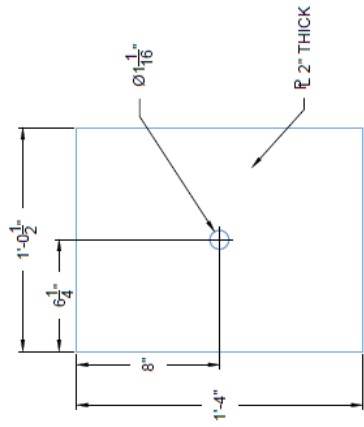
LIFTING POINT SECTION B-B

HSS LIFTING POINT			
Designed By:	Approved By:	Rev:	
Ilya Palmikov		R1	
Units:	Scale:	Date:	Sheet:
IN.	N/A	5/17/2016	5 OF 7



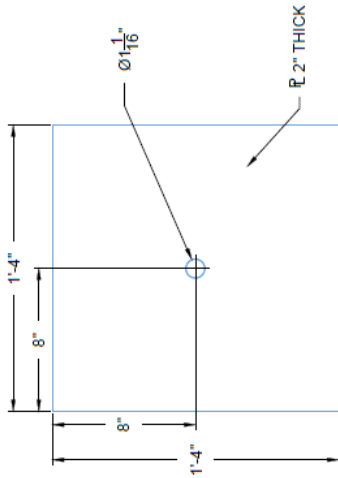
ASSEMBLY DETAIL

 Portland State University			
Designed By: Ilya Paimikov		Approved By:	
Units: IN.		Scale: N/A	
Date: 5/17/2016		Rev: R1	
Sheet: 6 OF 7		Date: 5/17/2016	



MASS PLATE B & C

QUANTITY OF 24 TO BE PROVIDED



MASS PLATE A

QUANTITY OF 16 TO BE PROVIDED

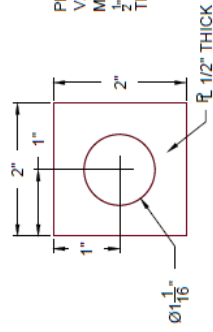


PLATE WASHER DIMENSIONS COULD VARY; PLATE WASHER THICKNESS MUST BE A MINIMUM THICKNESS OF 1/2" AND MUST ACCOMMODATE A 1" THREADED ROD

PLATE WASHER

QUANTITY OF 36 TO BE PROVIDED



Portland State University

PLATE DETAILS

Designed By:	Approved By:	Rev:
Ilyia Palnikov		R1
Units:	Scale:	Date:
IN.	N/A	5/17/2016
		Sheet:
		7 OF 7

25.0 APPENDIX G

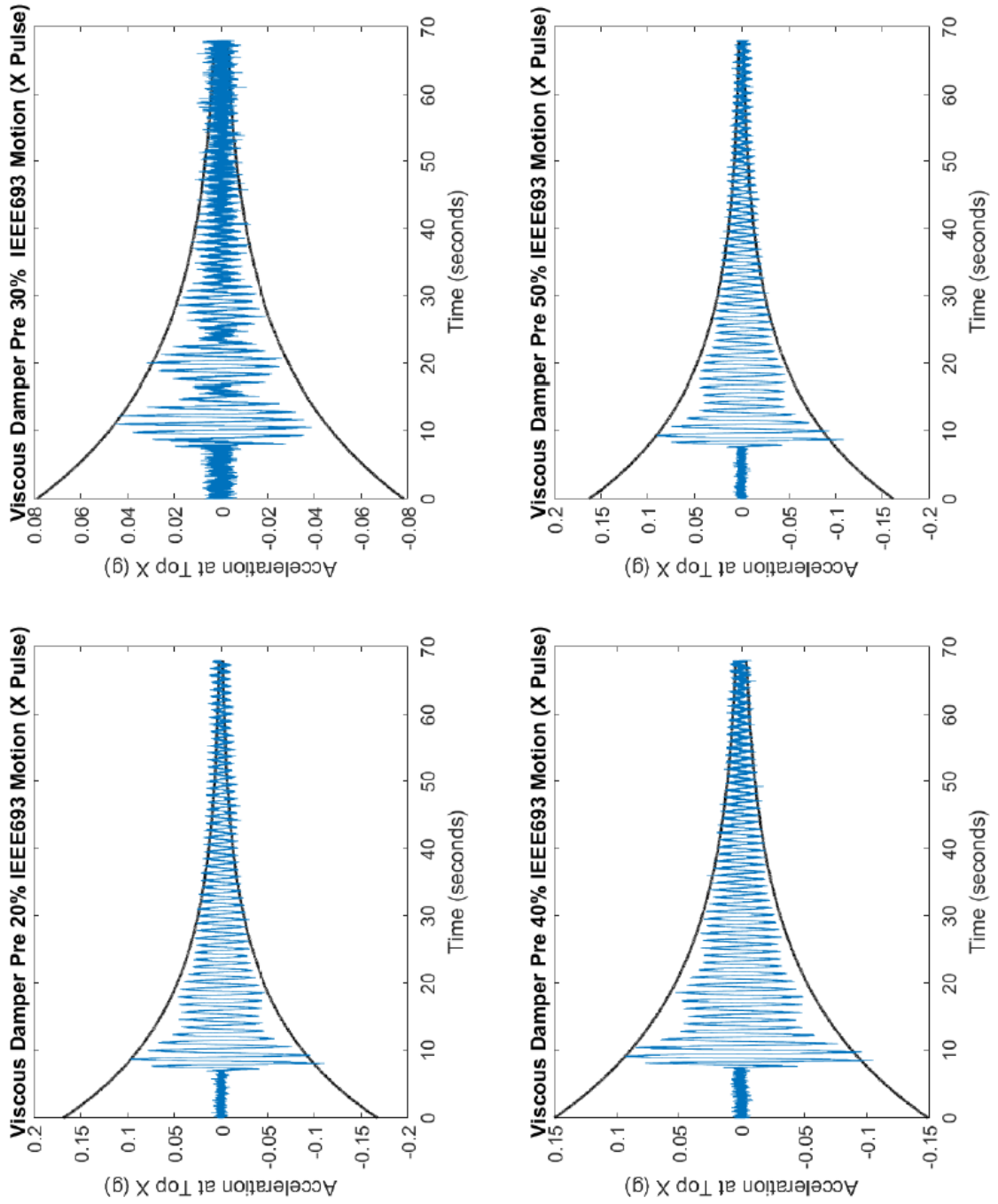


Figure 25-1: Viscous Damper Retrofit X-Damping 20-50%

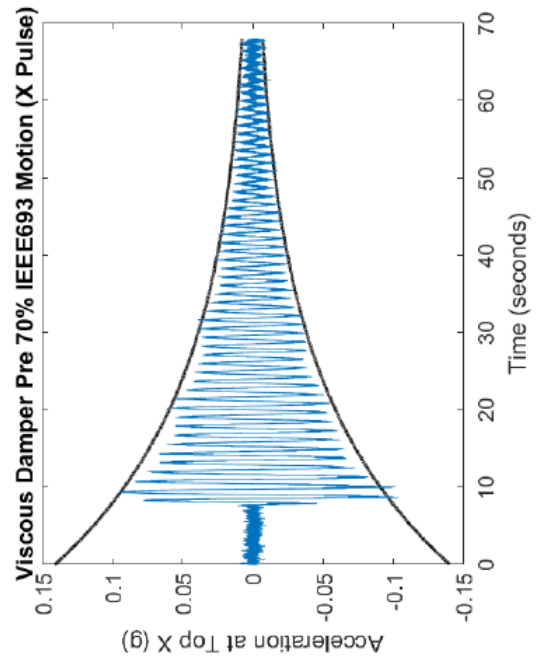
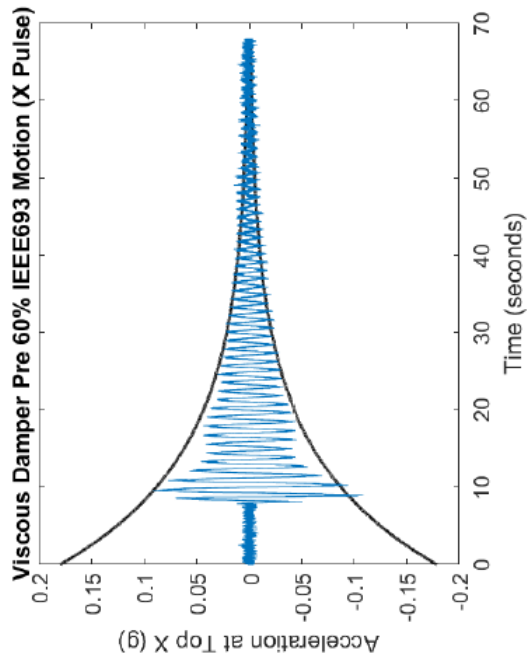
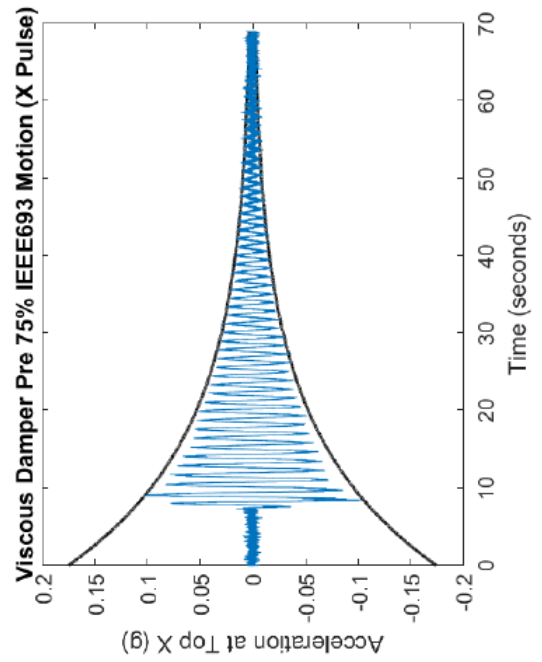
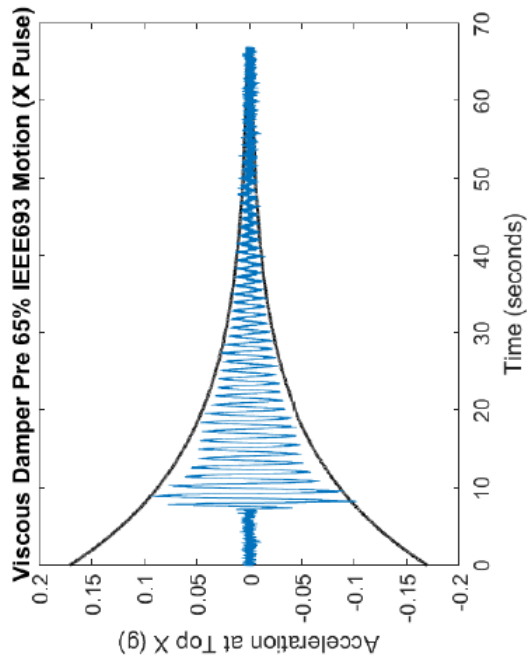


Figure 25-2: Viscous Damper Retrofit X-Damping 60-75%

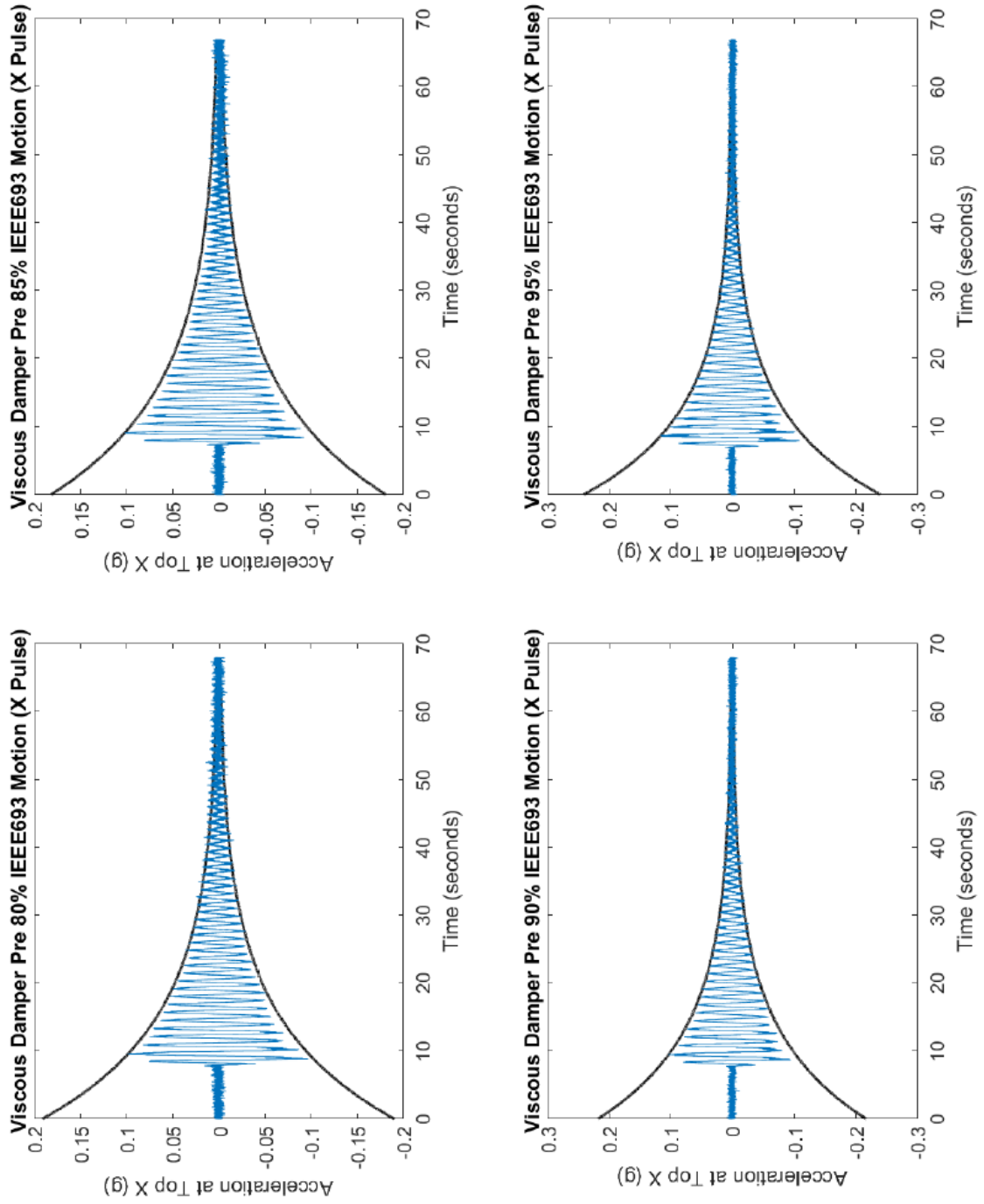


Figure 25-3: Viscous Damper Retrofit X-Damping 85-95%

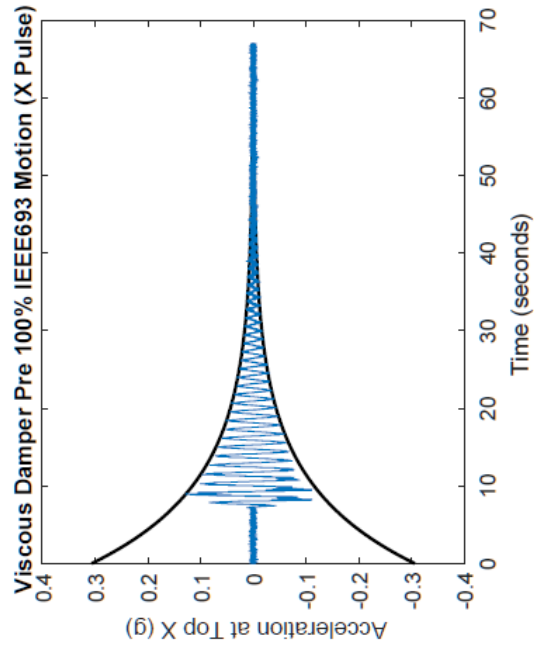


Figure 25-4: Viscous Damper Retrofit X-Damping 100%

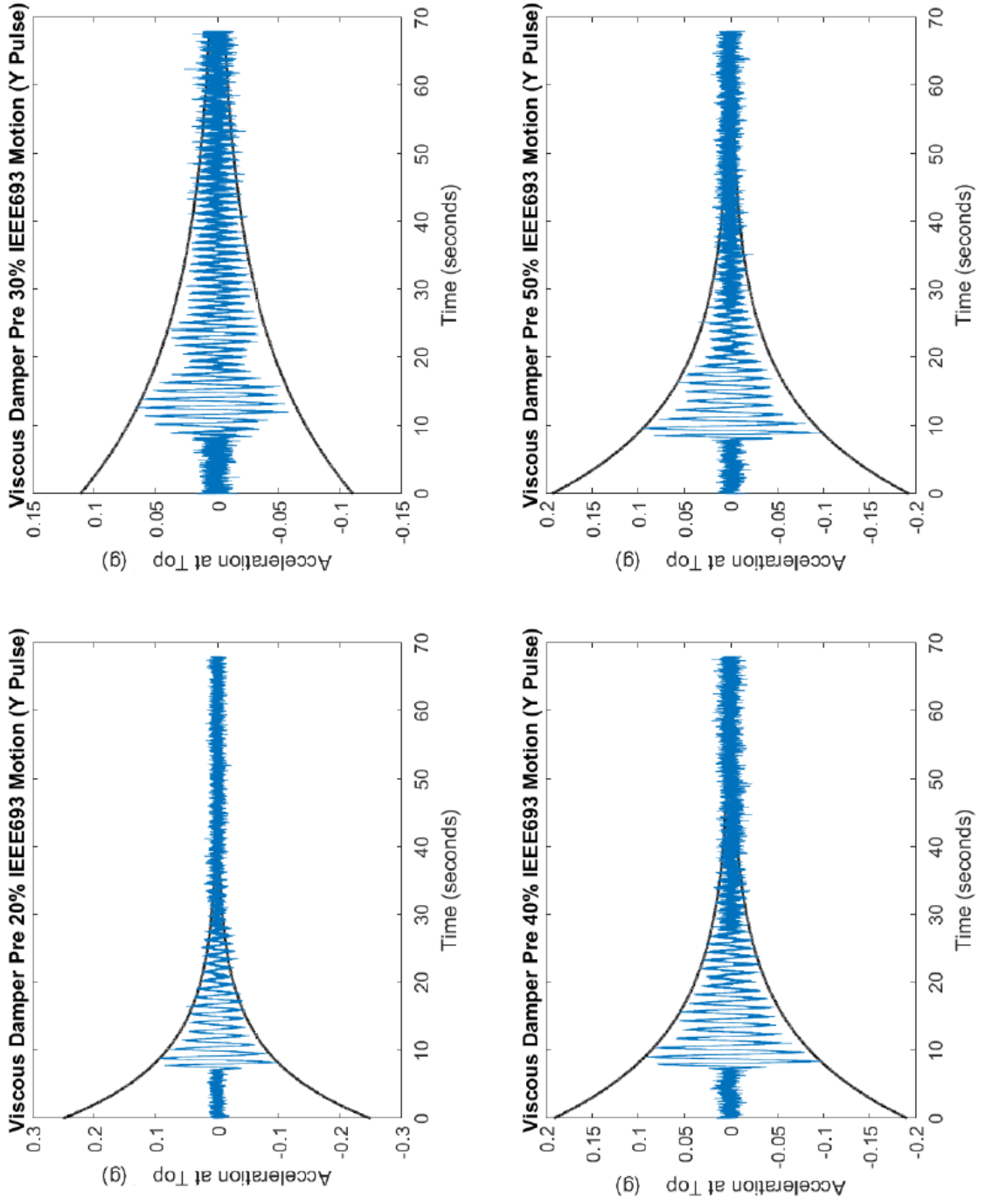


Figure 25-5: Viscous Damper Retrofit Y-Damping 20-50%

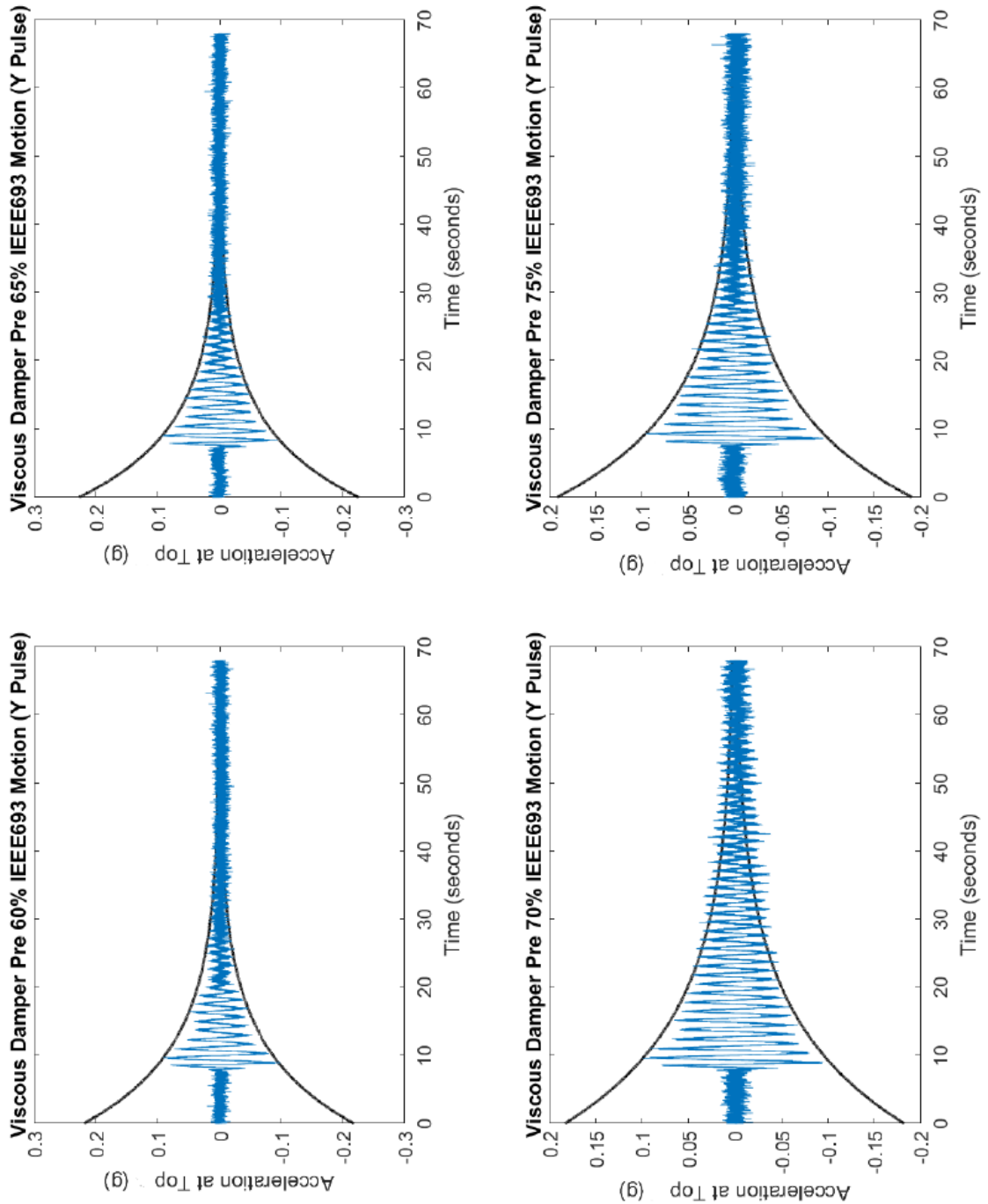


Figure 25-6: Viscous Damper Retrofit Y-Damping 60-75%

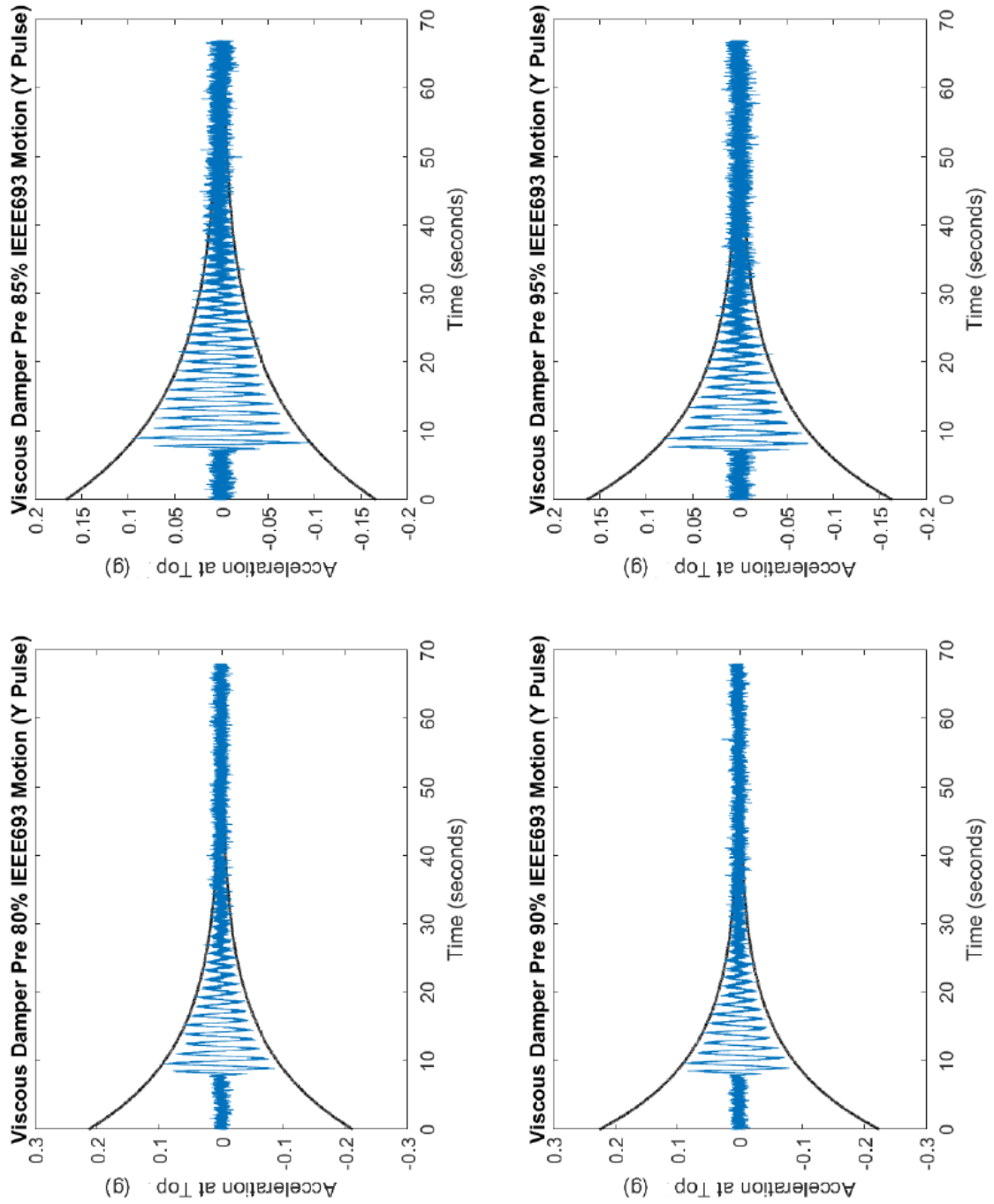


Figure 25-7: Viscous Damper Retrofit Y-Damping 80-95%

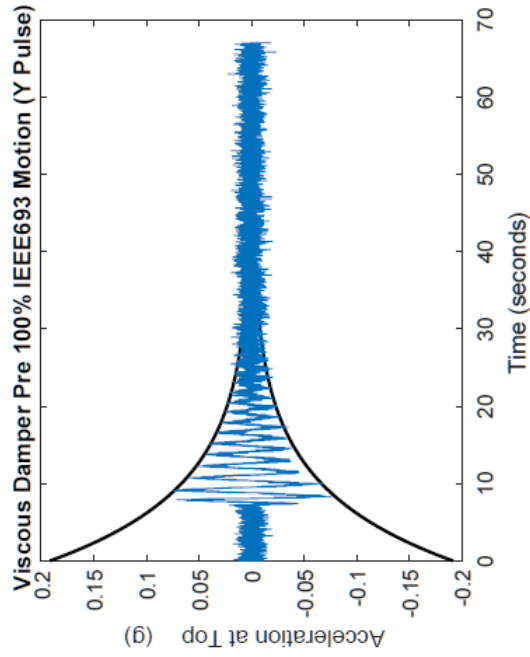


Figure 25-8: Viscous Damper Retrofit Y-Damping 100%

26.0 APPENDIX H

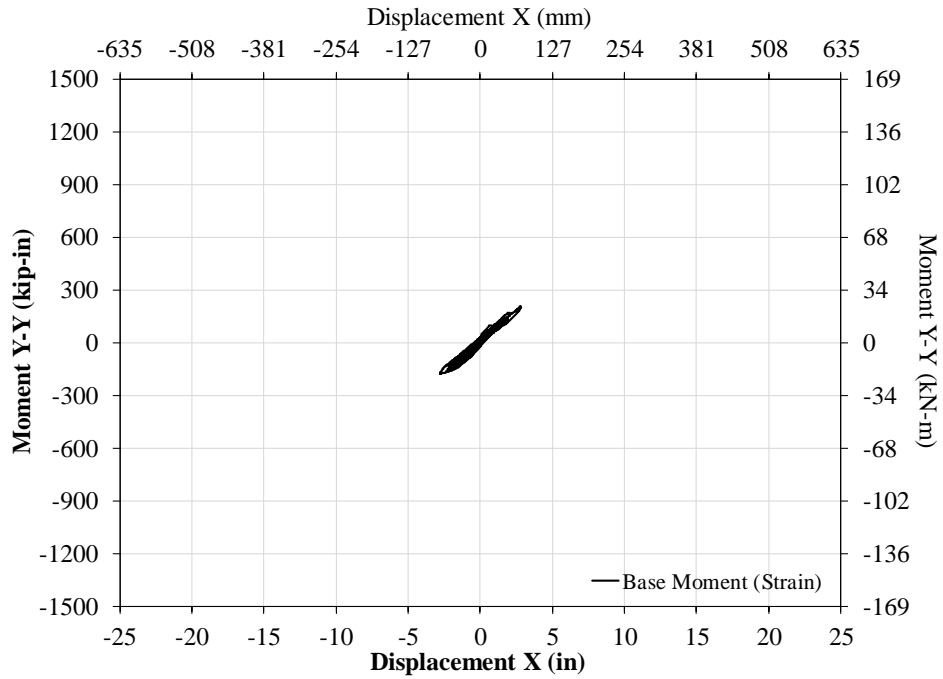


Figure 26-1: 20% 0.5g IEEE693 X-System Response w/ Viscous Dampers

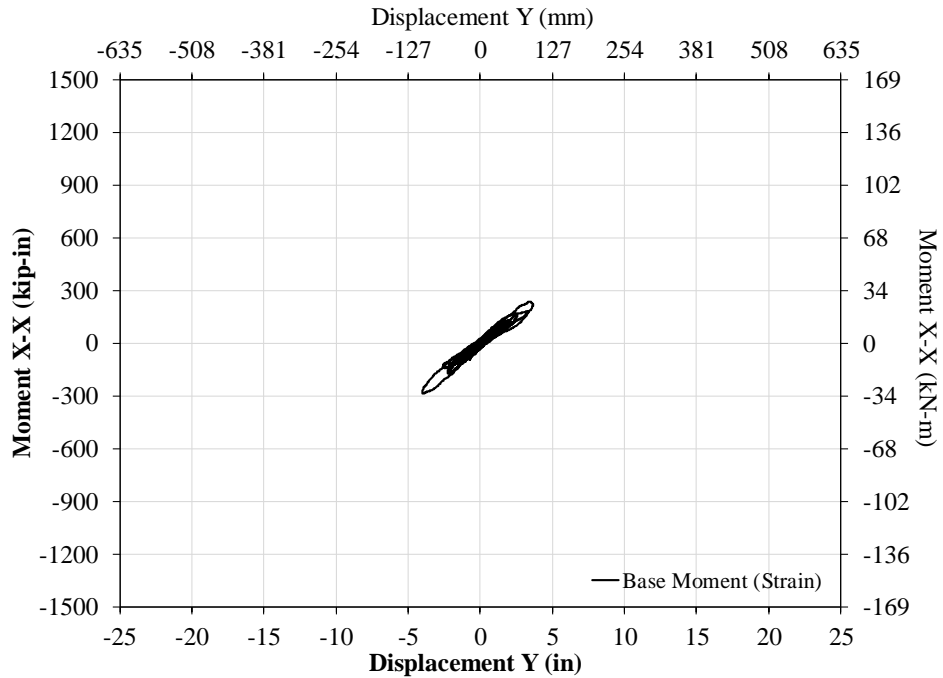


Figure 26-2: 20% 0.5g IEEE693 Y-System Response w/ Viscous Dampers

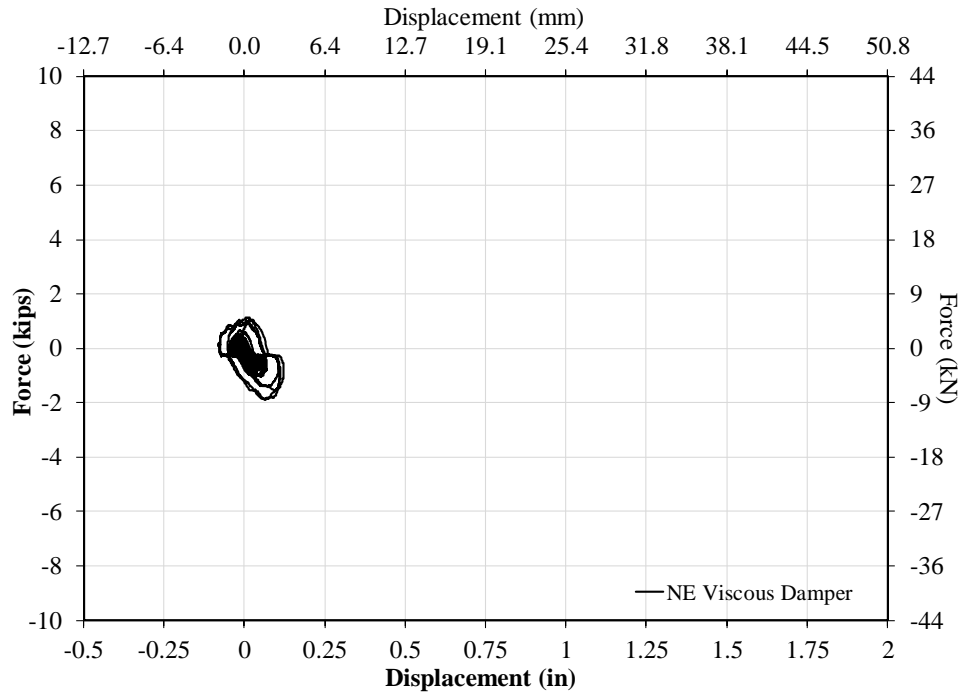


Figure 26-3: 20% 0.5g IEEE693 NE Viscous Damper Response

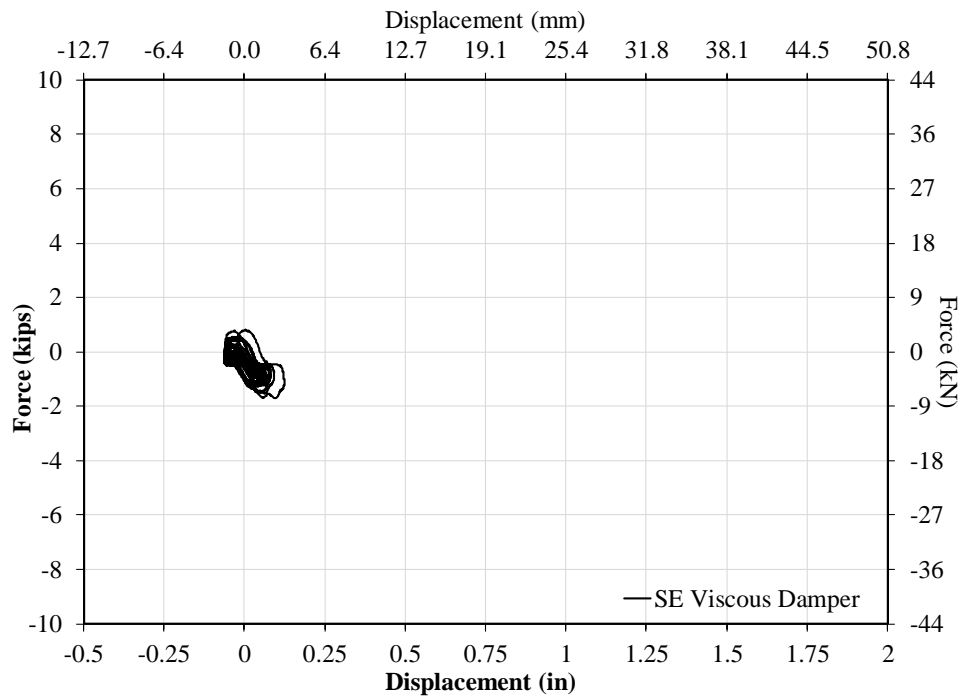


Figure 26-4: 20% 0.5g IEEE693 SE Viscous Damper Response

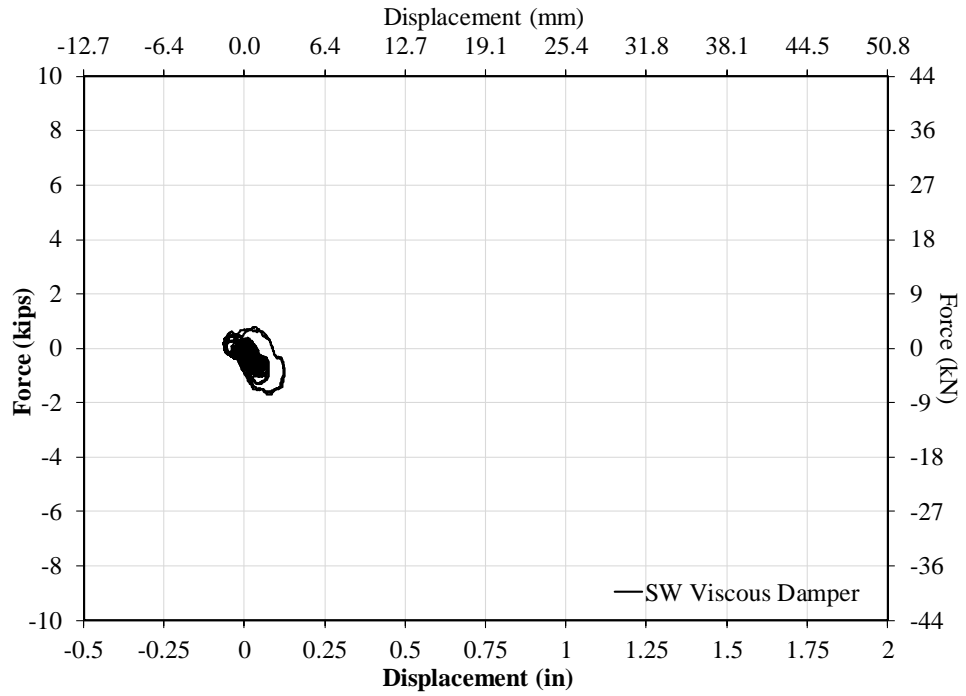


Figure 26-5: 20% 0.5g IEEE693 SW Viscous Damper Response

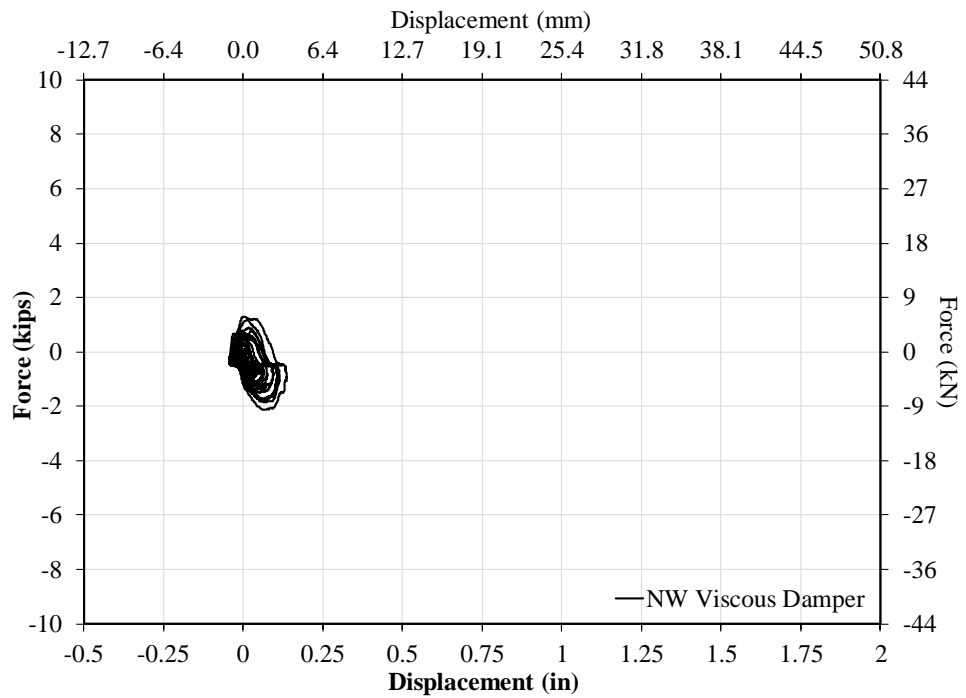


Figure 26-6: 20% 0.5g IEEE693 NW Viscous Damper Response

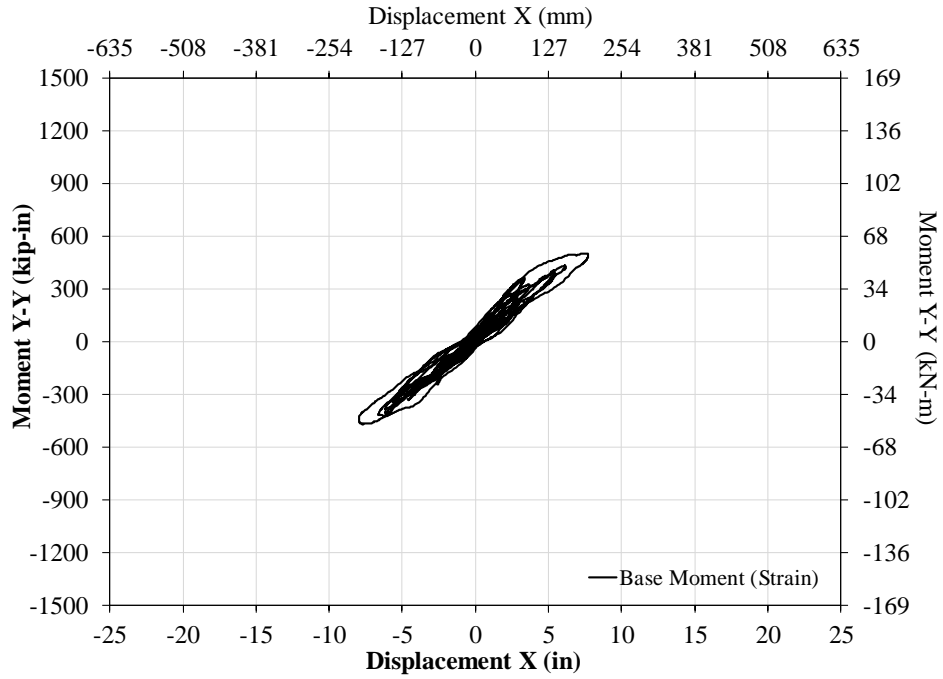


Figure 26-7: 50% 0.5g IEEE693 X-System Response w/ Viscous Devices

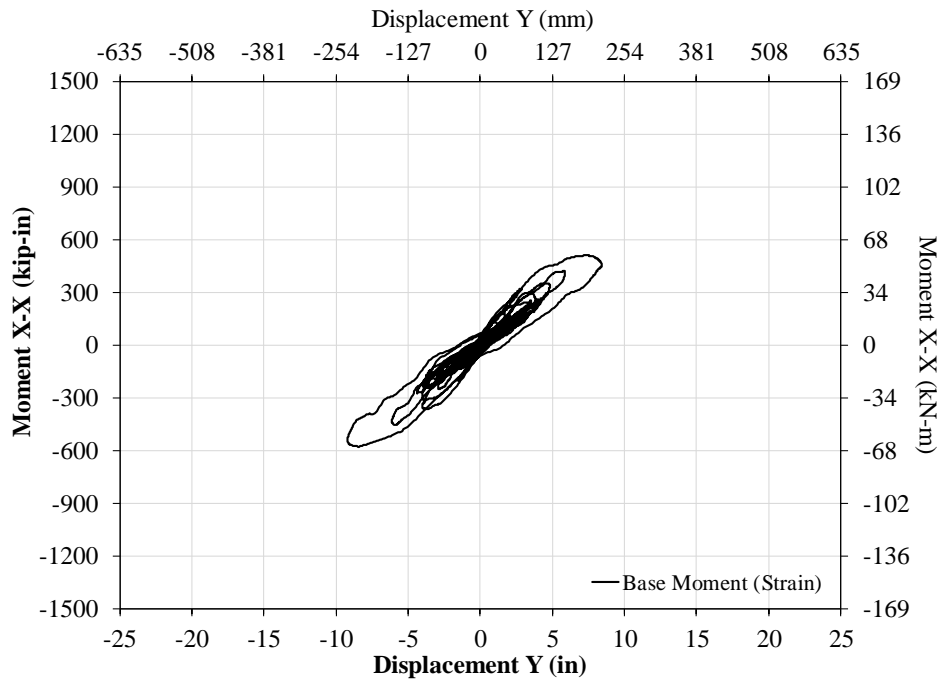


Figure 26-8: 50% 0.5g IEEE693 Y-System Response w/ Viscous Devices

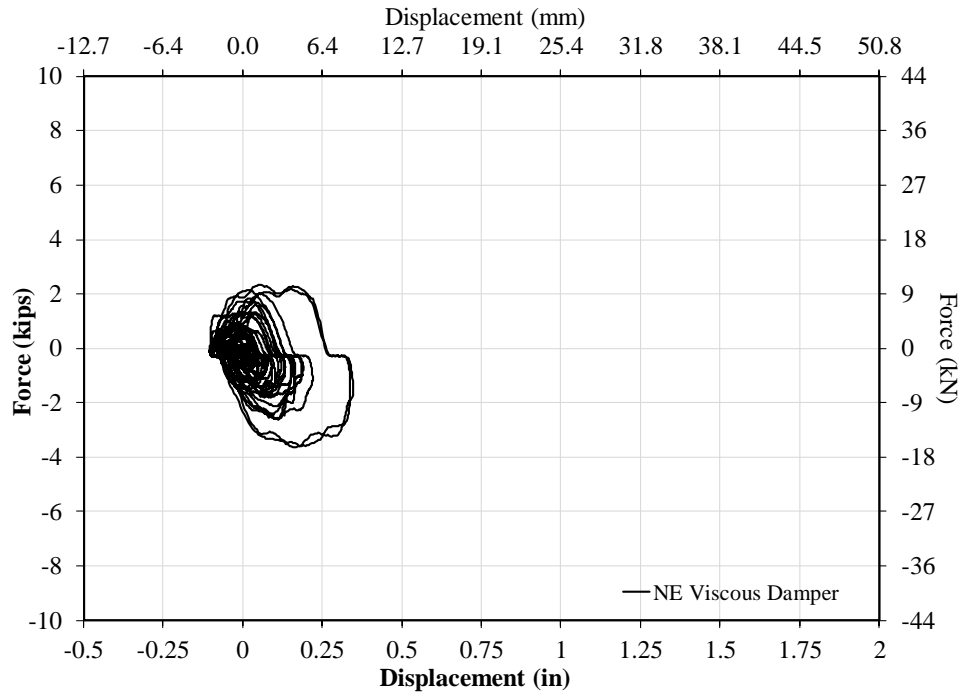


Figure 26-9: 50% 0.5g IEEE693 NE Viscous Damper Response

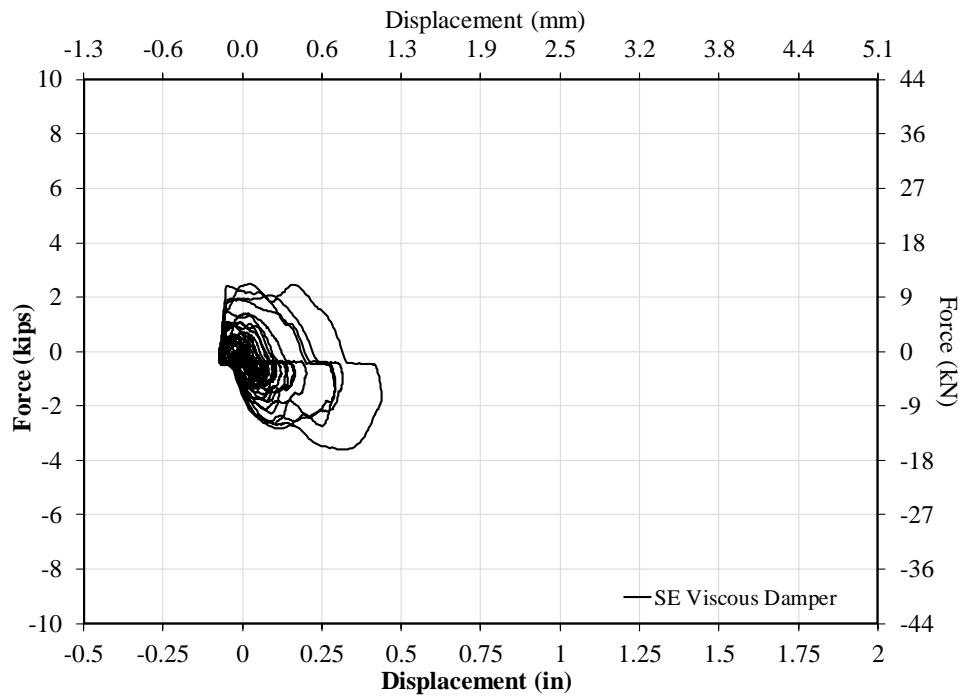


Figure 26-10: 50% 0.5g IEEE693 SE Viscous Damper Response

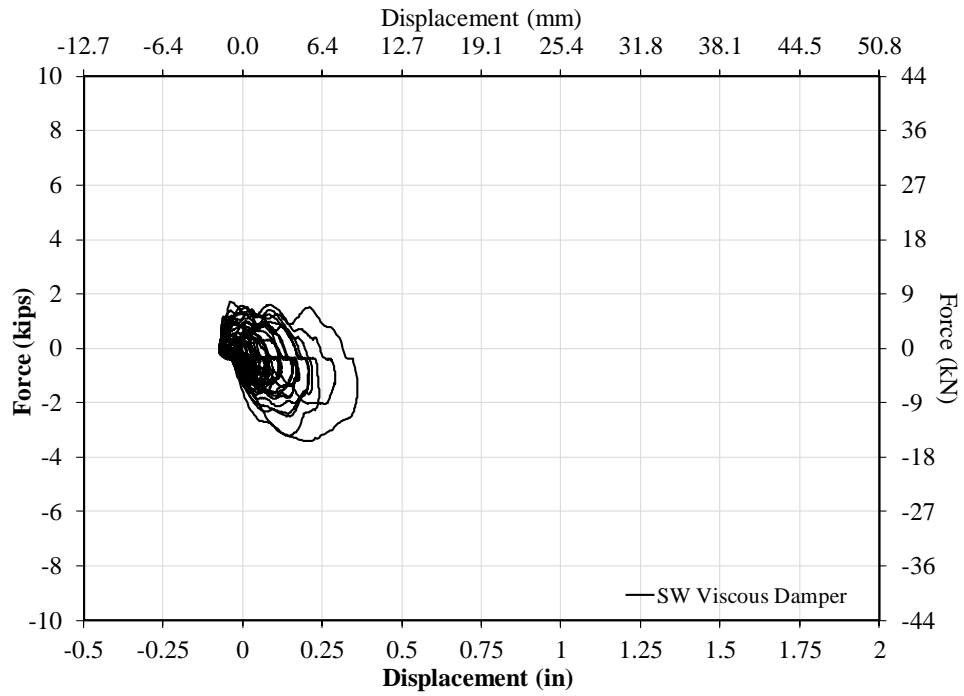


Figure 26-11: 50% 0.5g IEEE693 SW Viscous Damper Response

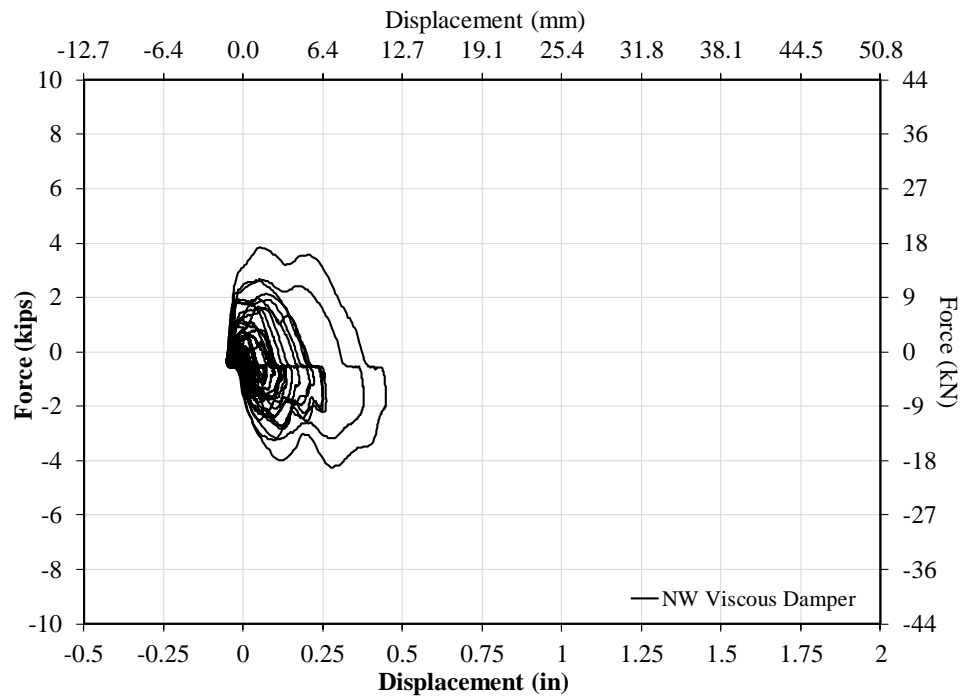


Figure 26-12: 50% 0.5g IEEE693 NW Viscous Damper Response

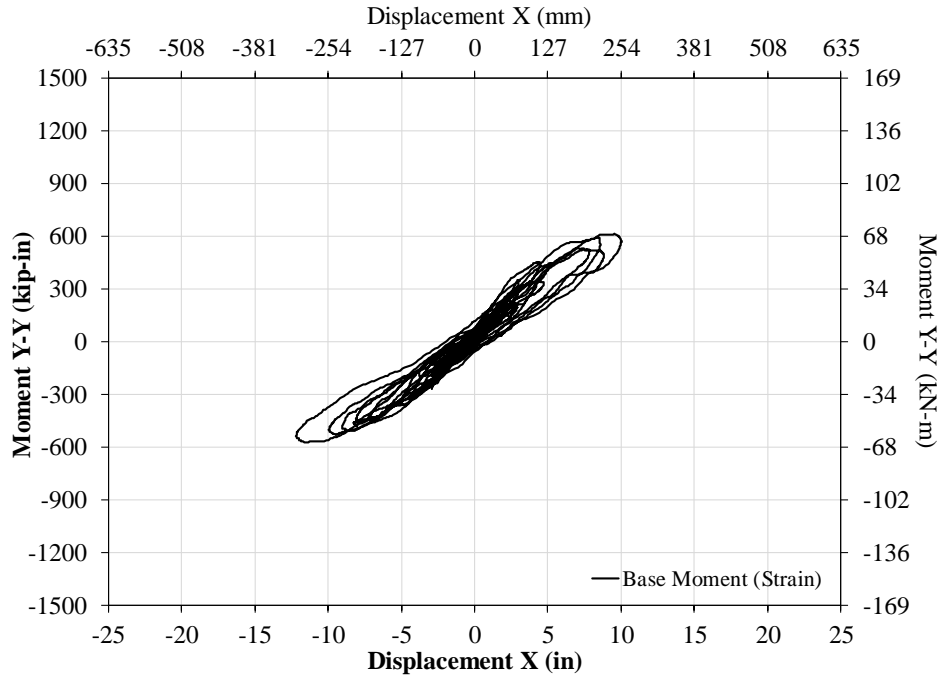


Figure 26-13: 75% 0.5g IEEE693 X-System Response w/ Viscous Devices

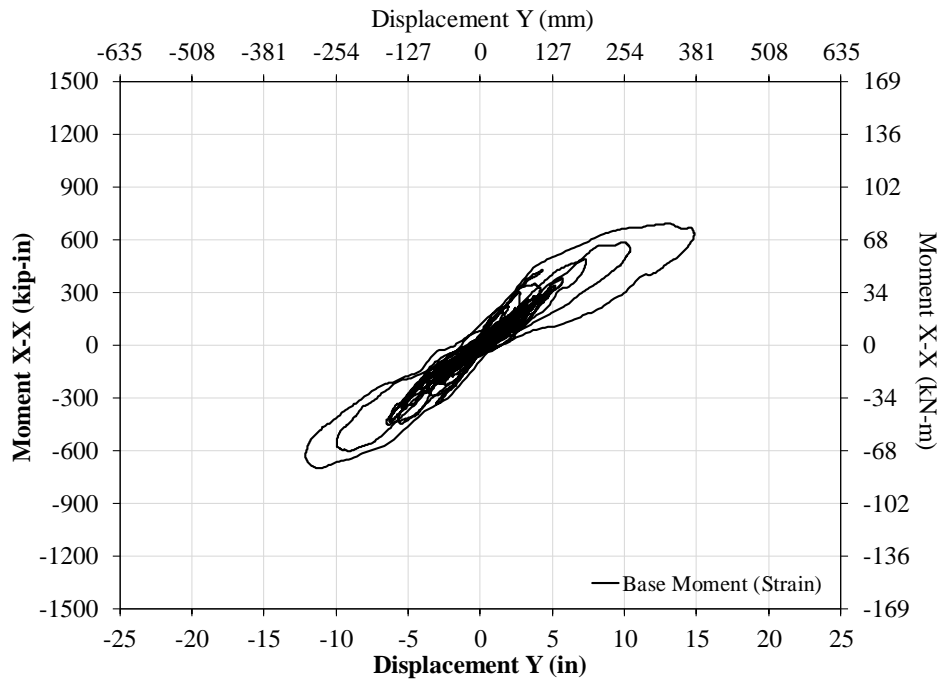


Figure 26-14: 75% 0.5g IEEE693 Y-System Response w/ Viscous Devices

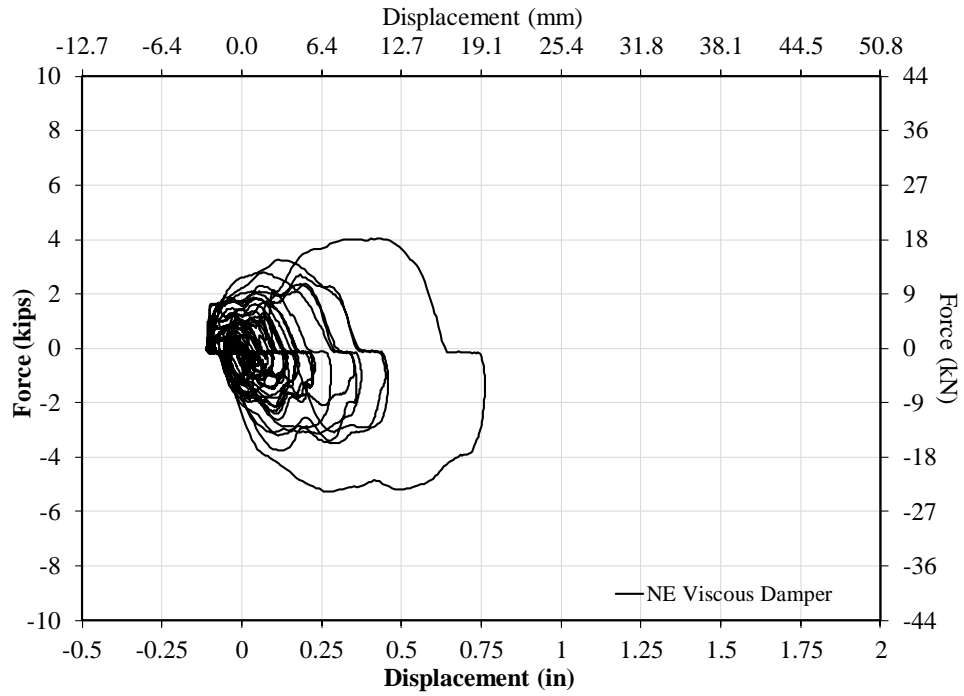


Figure 26-15: 75% 0.5g IEEE693 NE Viscous Damper Response

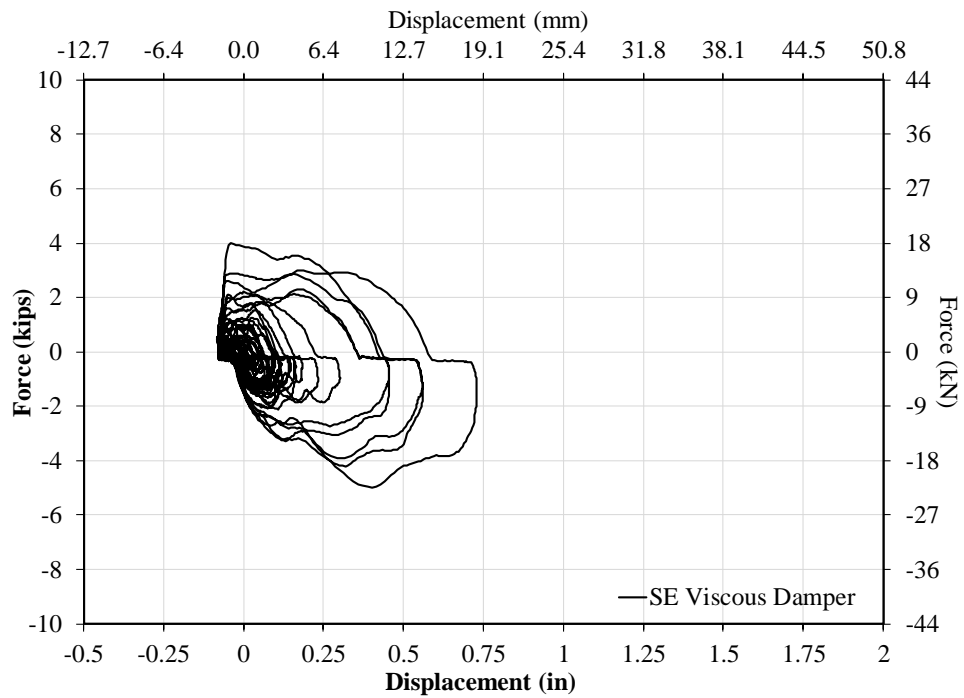


Figure 26-16: 75% 0.5g IEEE693 SE Viscous Damper Response

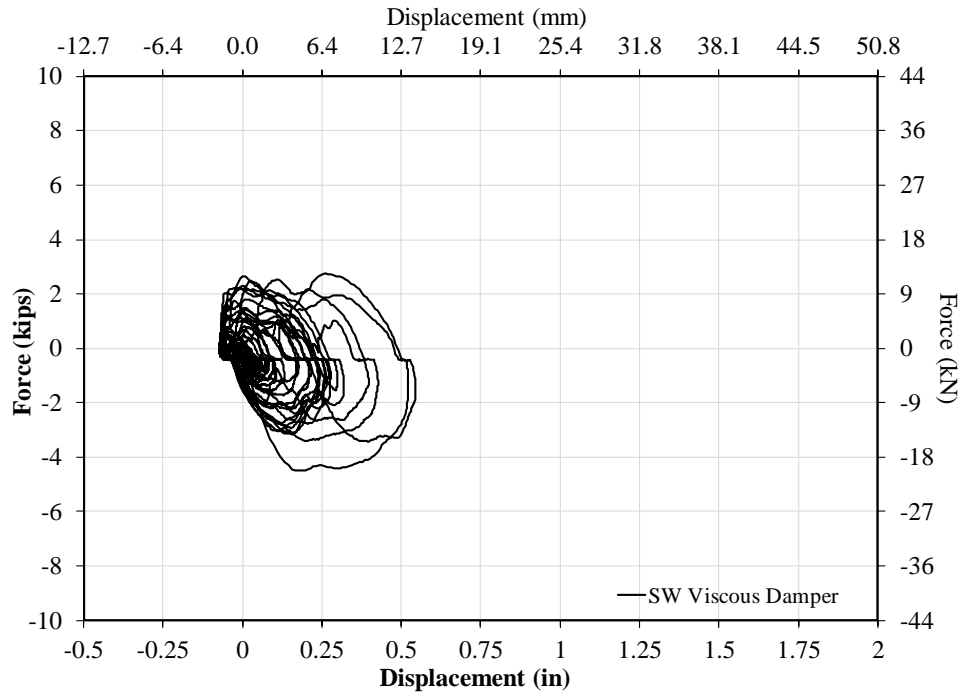


Figure 26-17: 75% 0.5g IEEE693 SW Viscous Damper Response

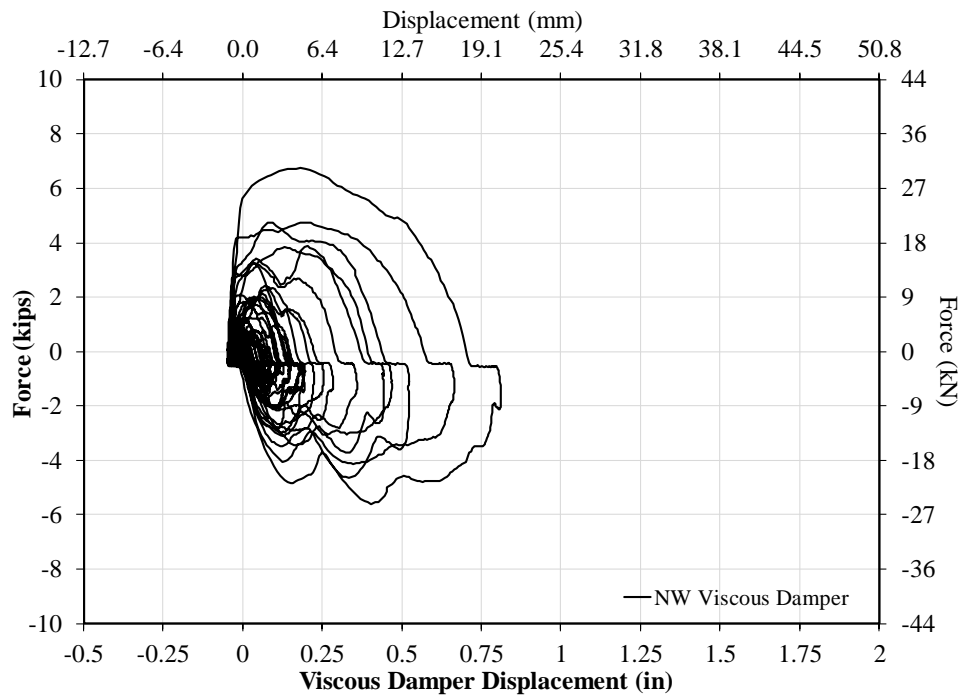


Figure 26-18: 75% 0.5g IEEE693 NW Viscous Damper Response

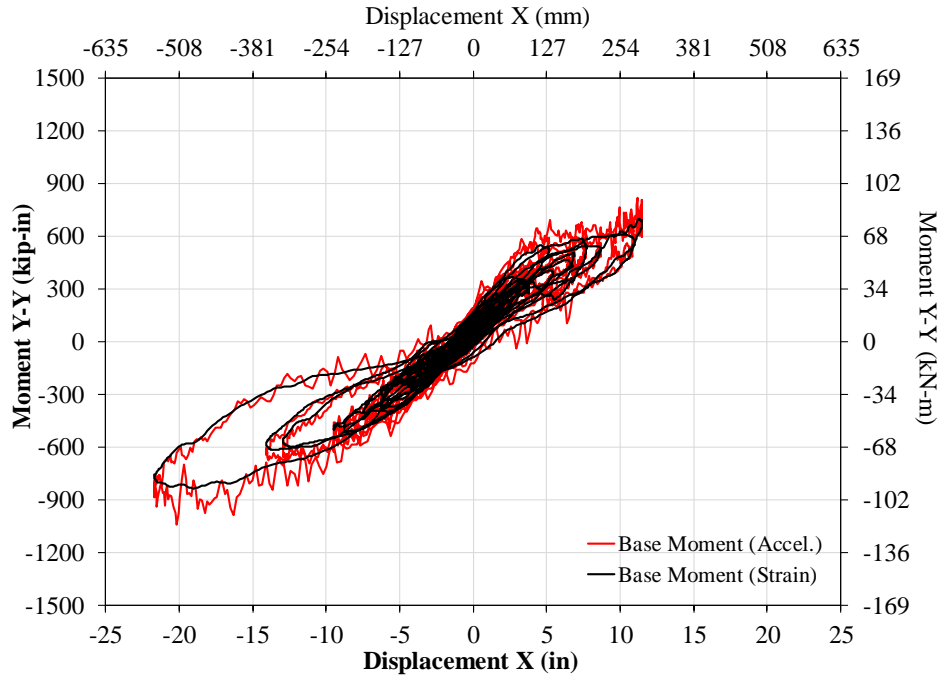


Figure 26-19: 100% 0.5g IEEE693 X-System Response w/ Viscous Dampers

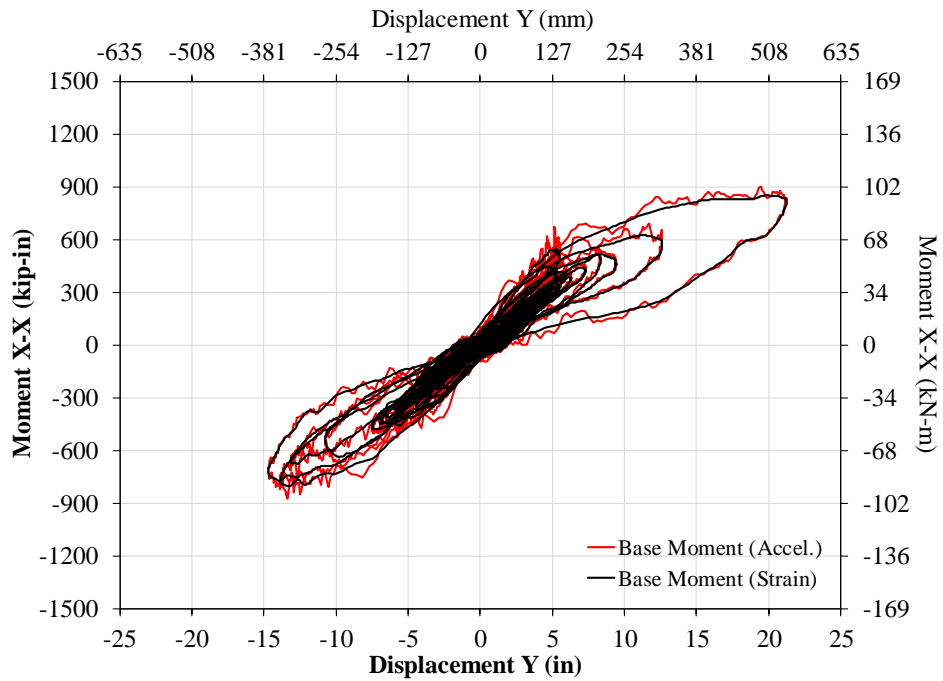


Figure 26-20: 100% 0.5g IEEE693 Y-System Response w/ Viscous Dampers

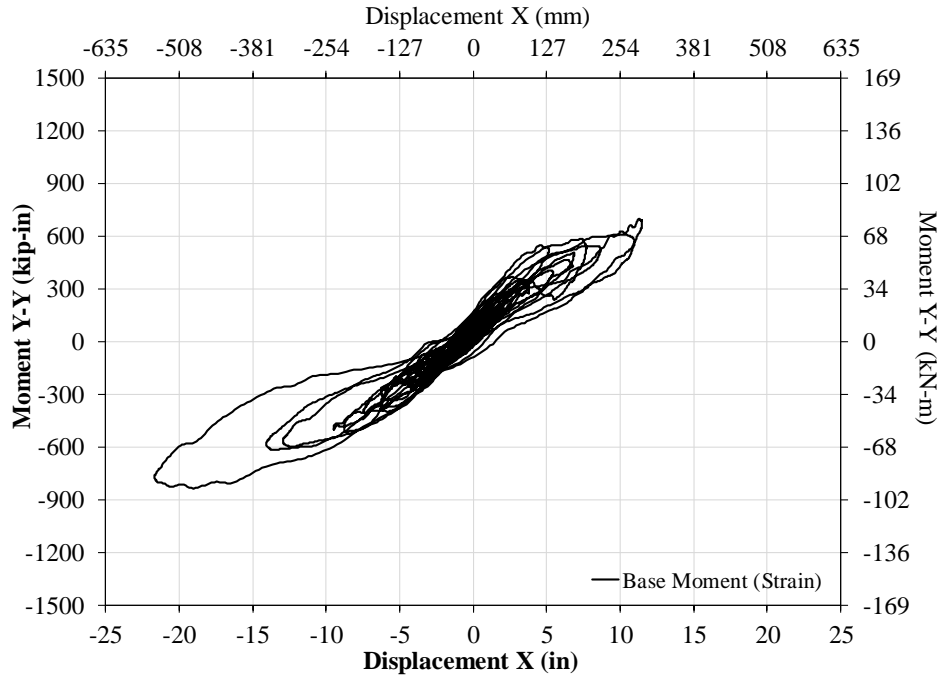


Figure 26-21: 100% 0.5g IEEE693 X-System Response w/ Viscous Dampers

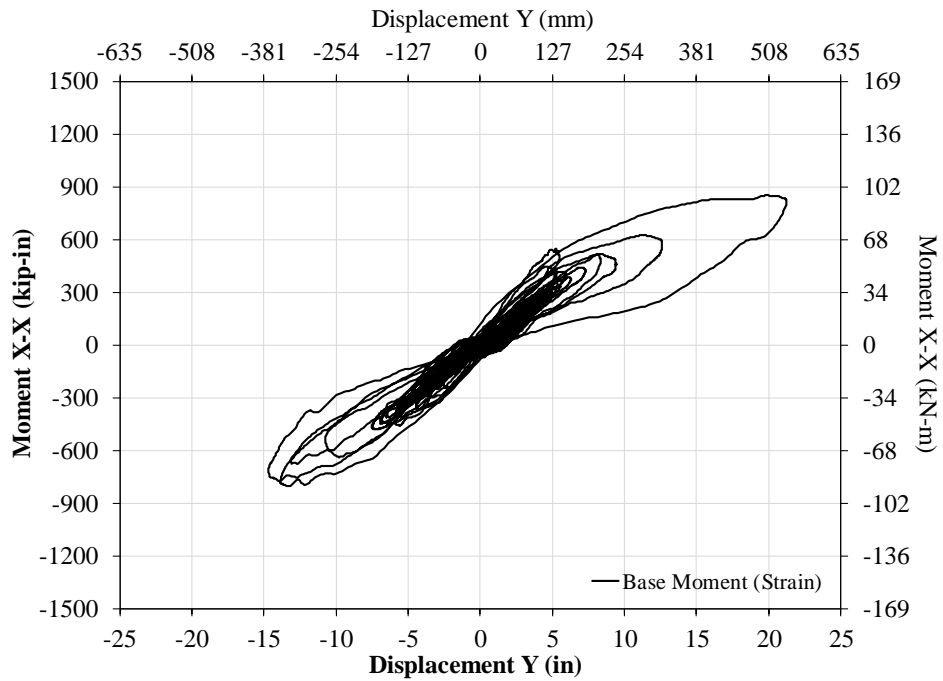


Figure 26-22: 100% 0.5g IEEE693 Y-System Response w/ Viscous Dampers

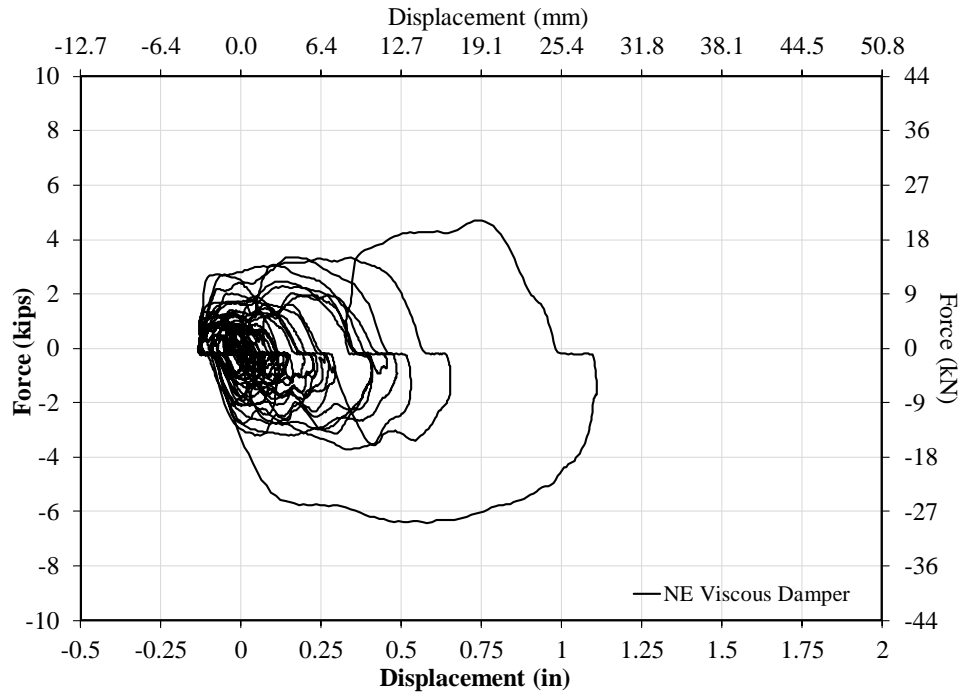


Figure 26-23: 100% 0.5g IEEE693 NE Viscous Damper Response

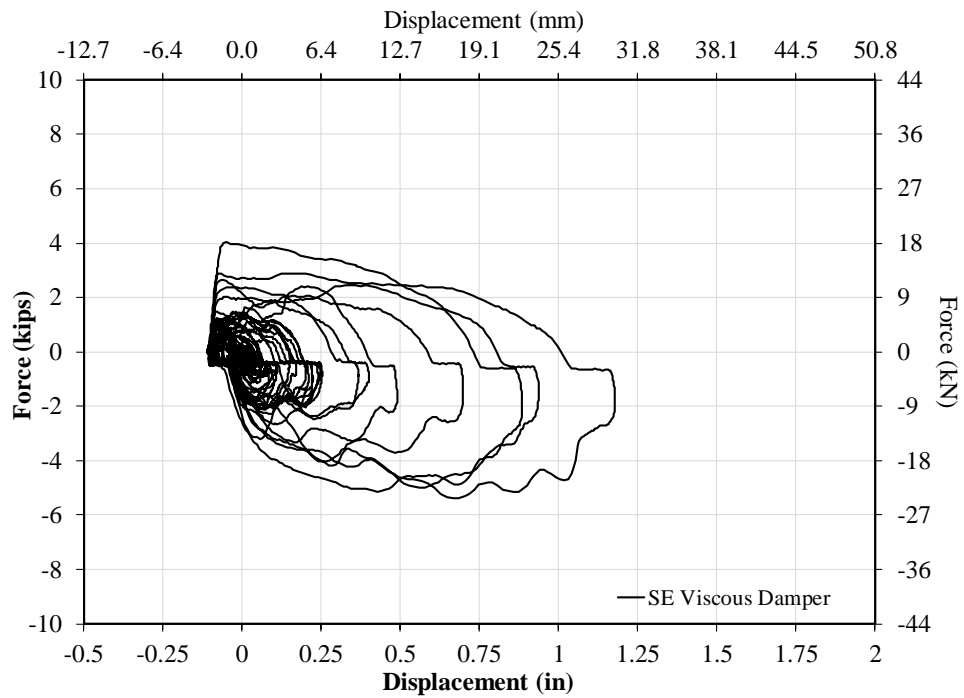


Figure 26-24: 100% 0.5g IEEE693 SE Viscous Damper Response

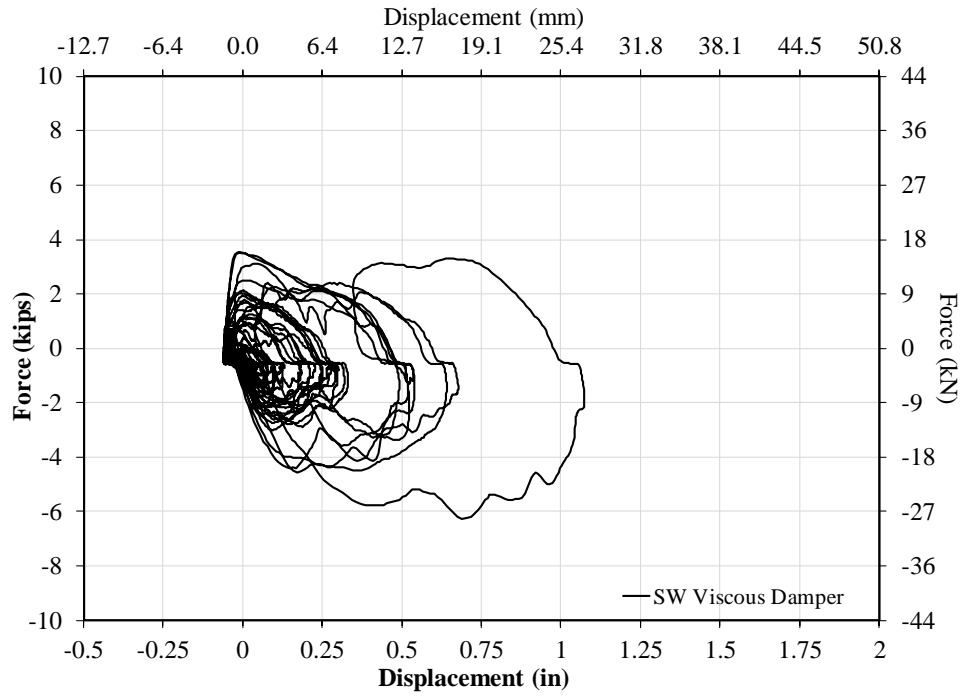


Figure 26-25: 100% 0.5g IEEE693 SW Viscous Damper Response

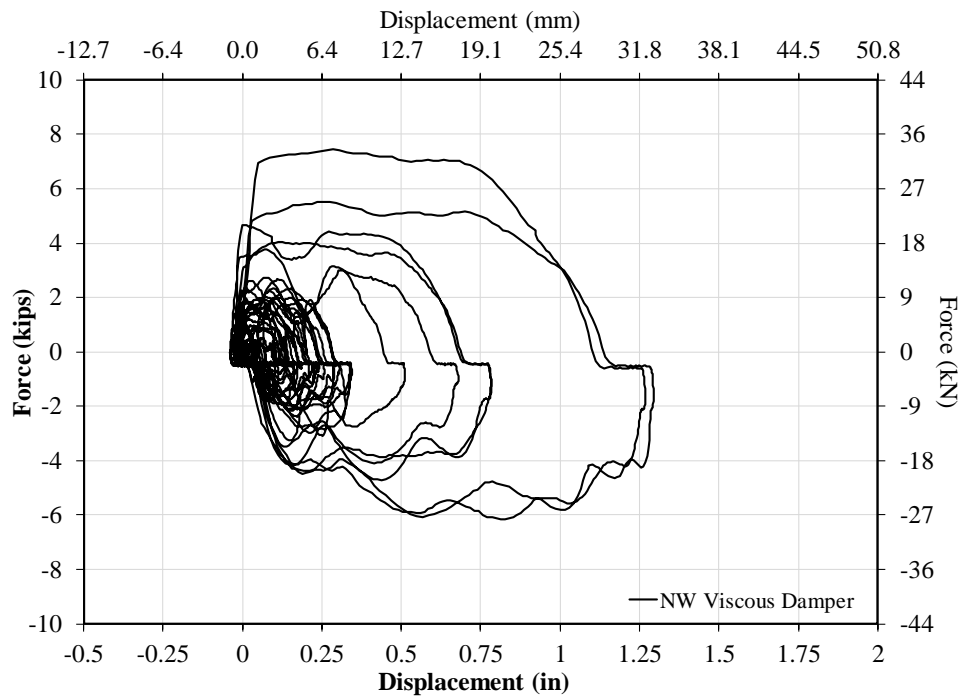


Figure 26-26: 100% 0.5g IEEE693 NW Viscous Damper Response

27.0 APPENDIX I

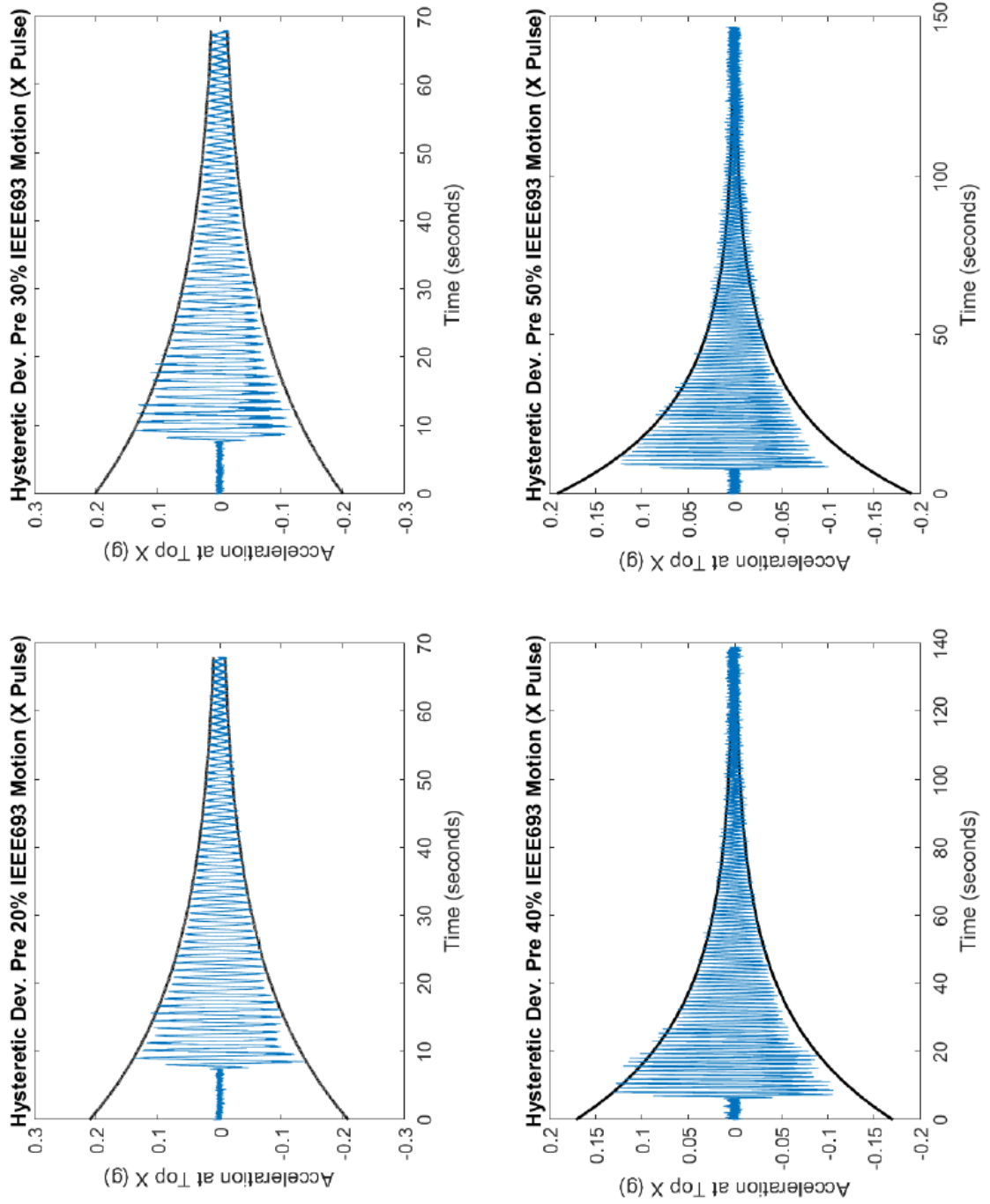


Figure 27-1: Hysteretic Device Retrofit X-Damping 20-50%

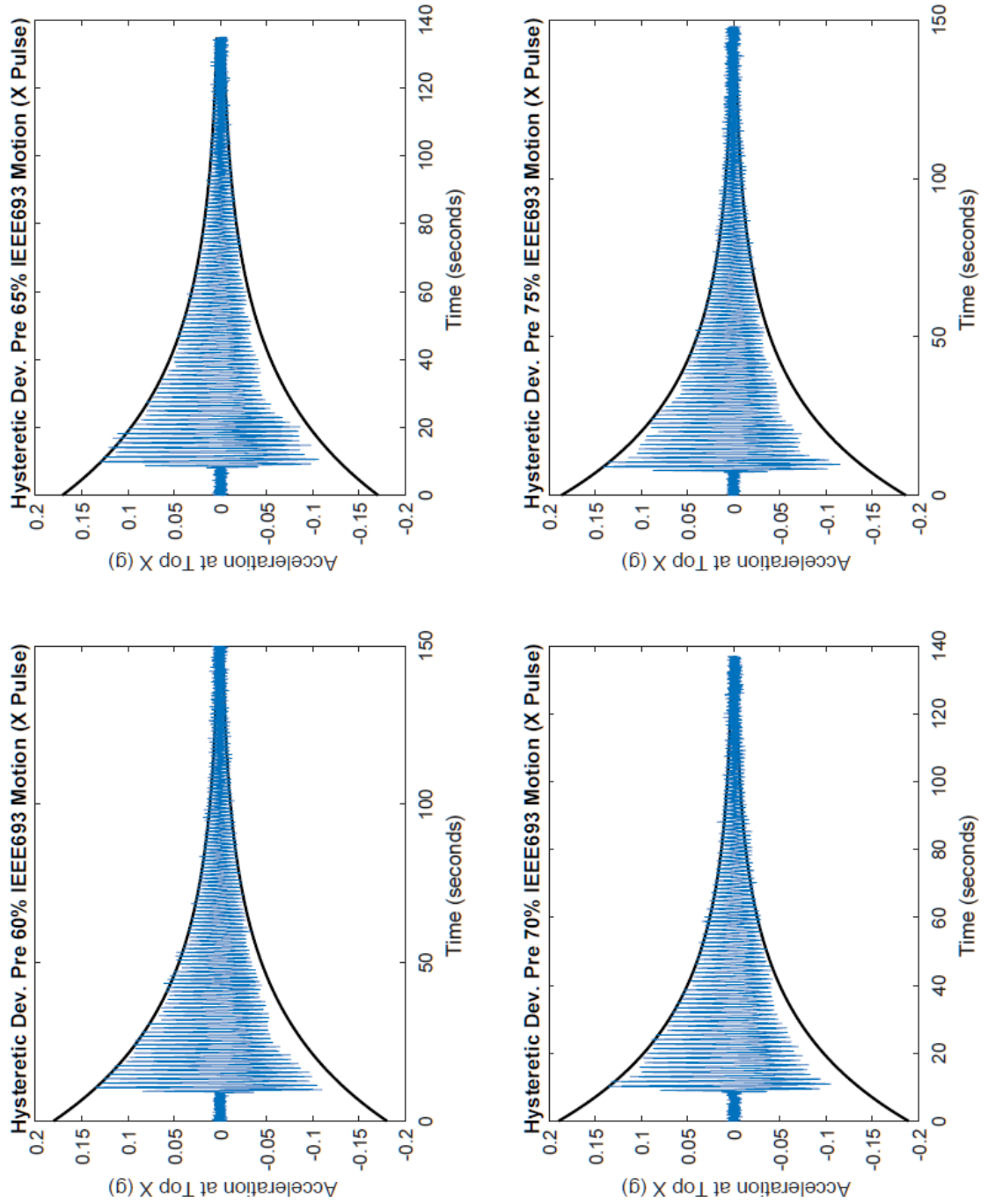


Figure 27-2: Hysteretic Device Retrofit X-Damping 60-75%

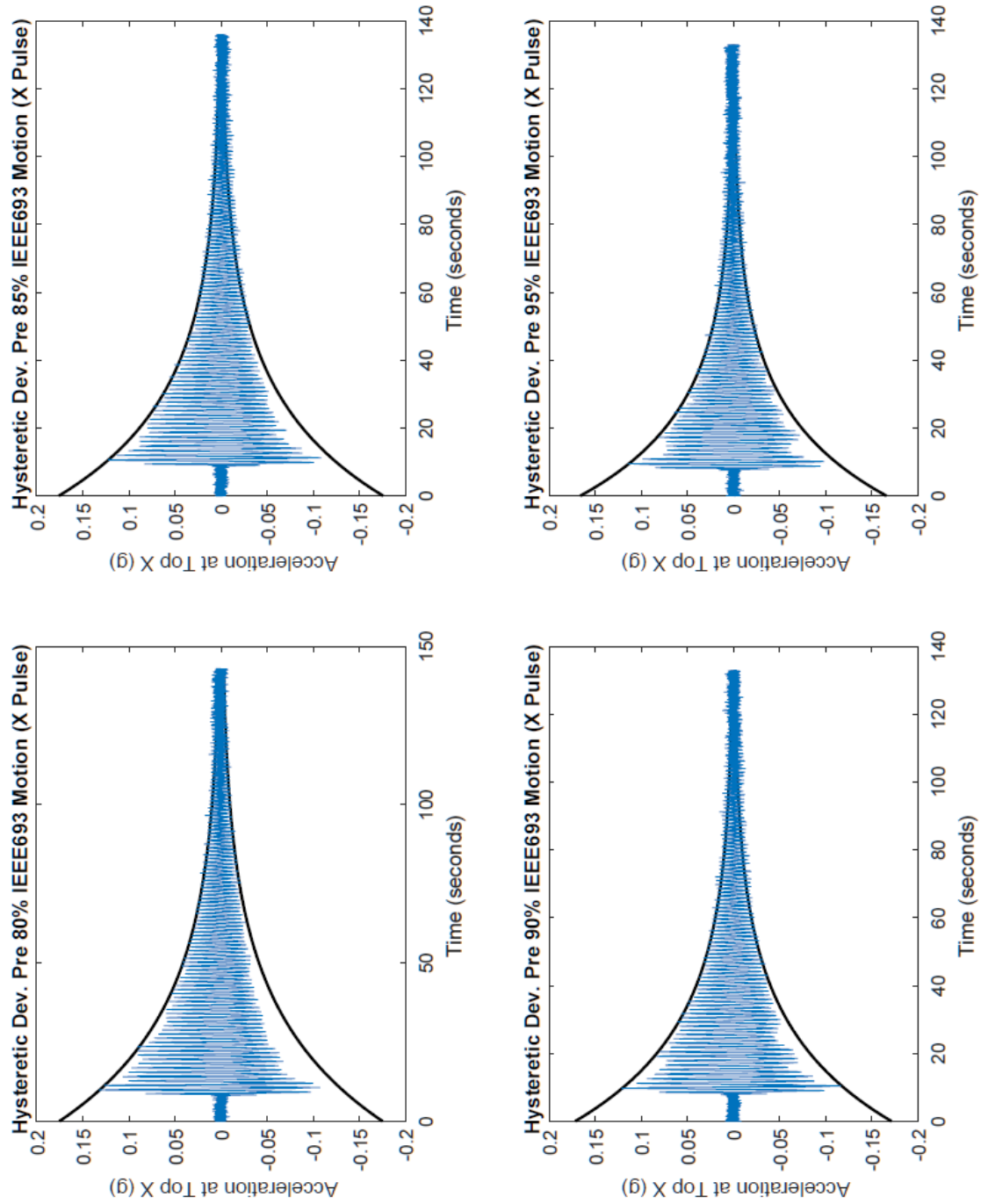


Figure 27-3: Hysteretic Device Retrofit X-Damping 80-95%

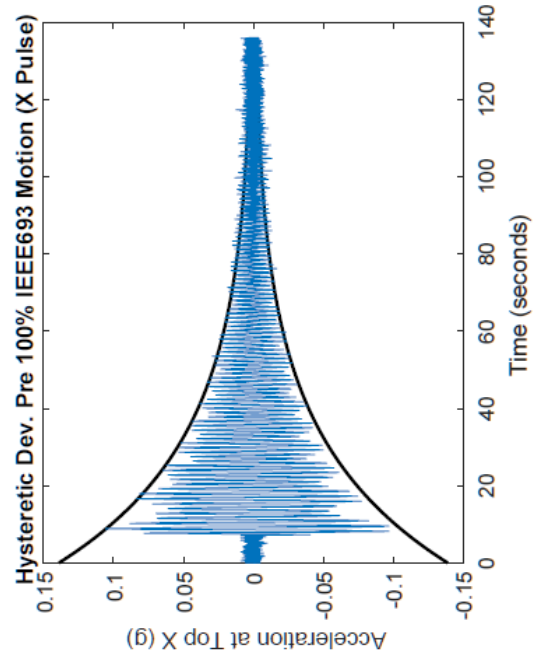


Figure 27-4: Hysteretic Device Retrofit X-Damping 100%

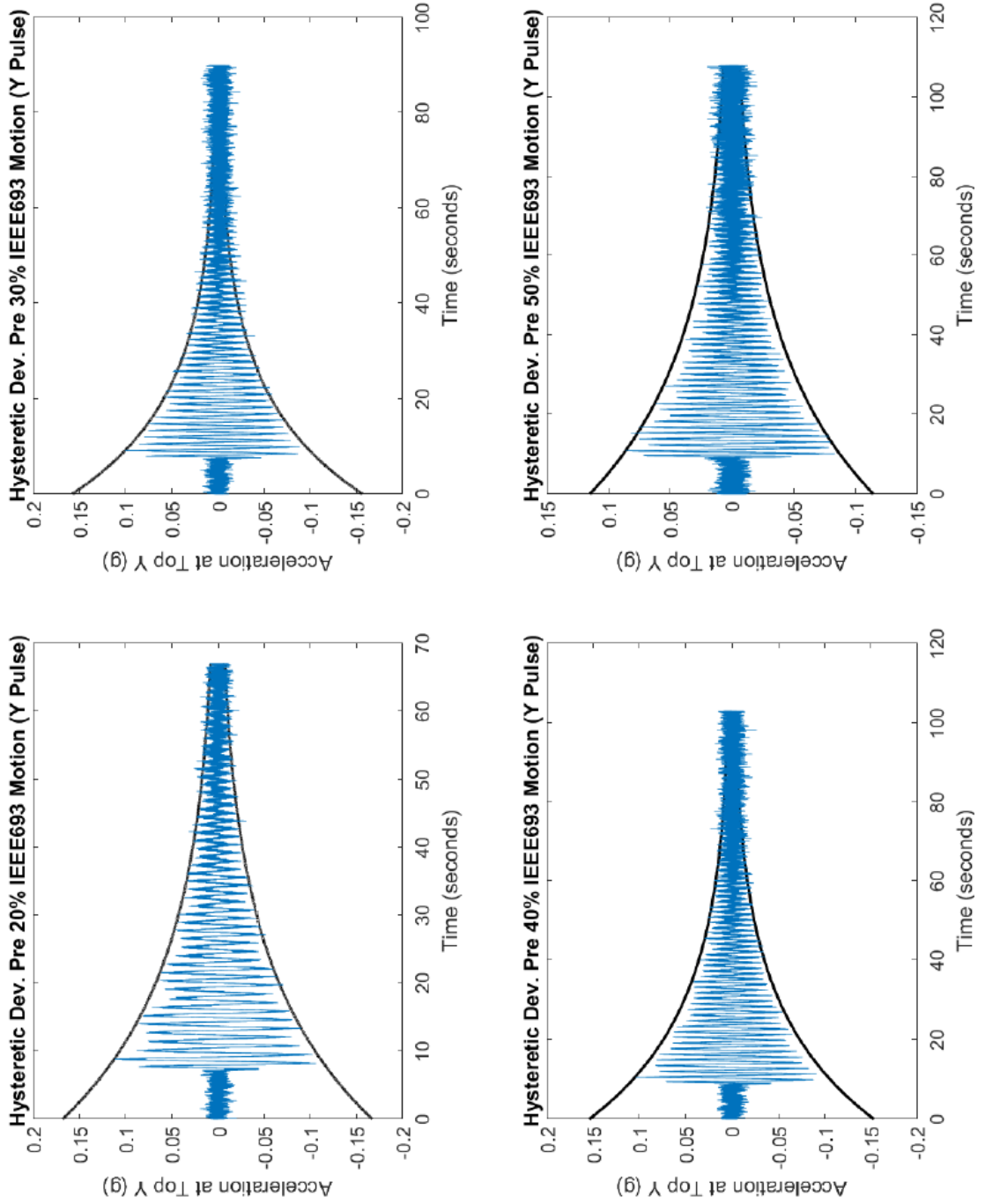


Figure 27-5: Hysteretic Device Retrofit Y-Damping 20-50%

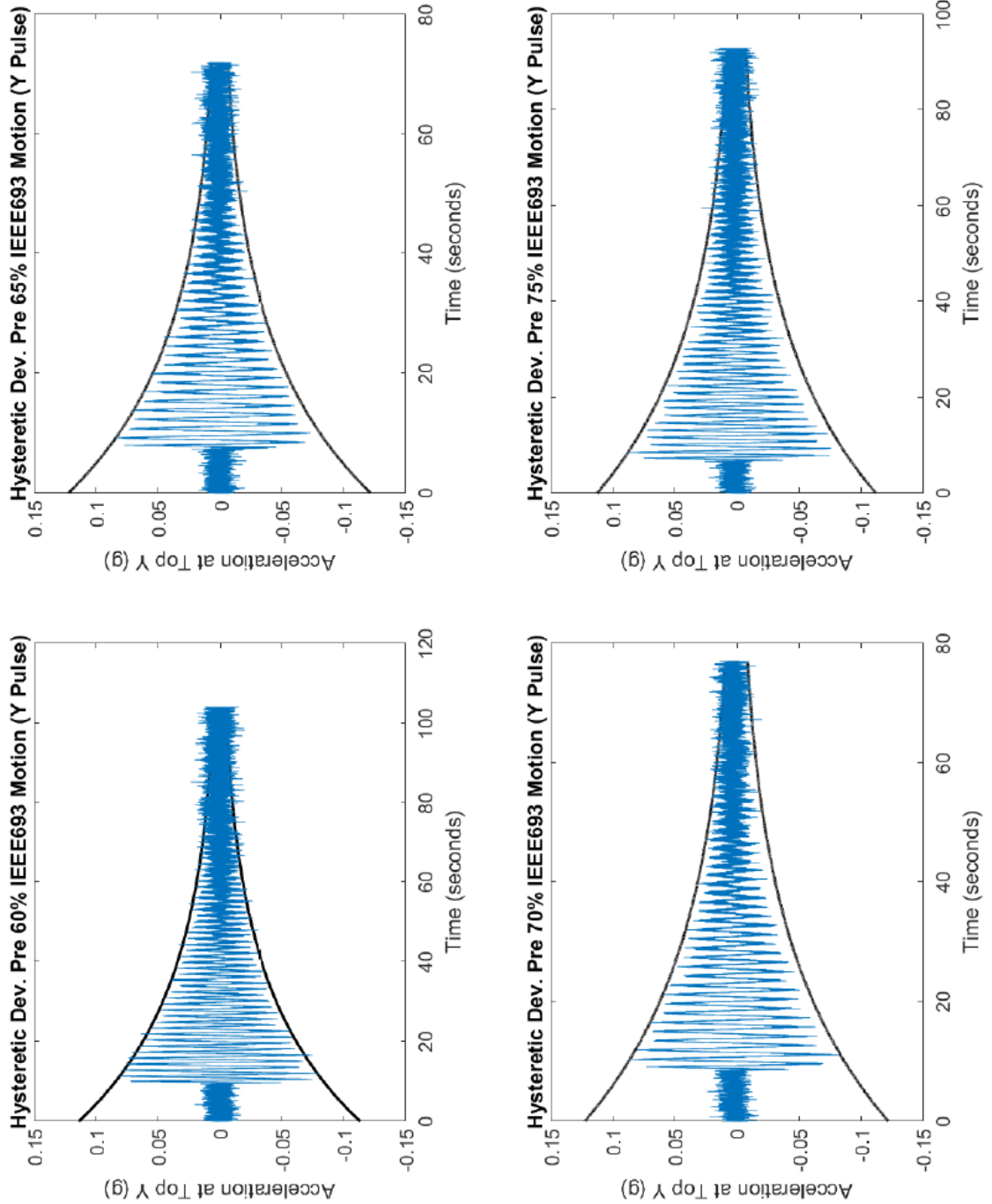


Figure 27-6: Hysteretic Device Retrofit Y-Damping 60-75%

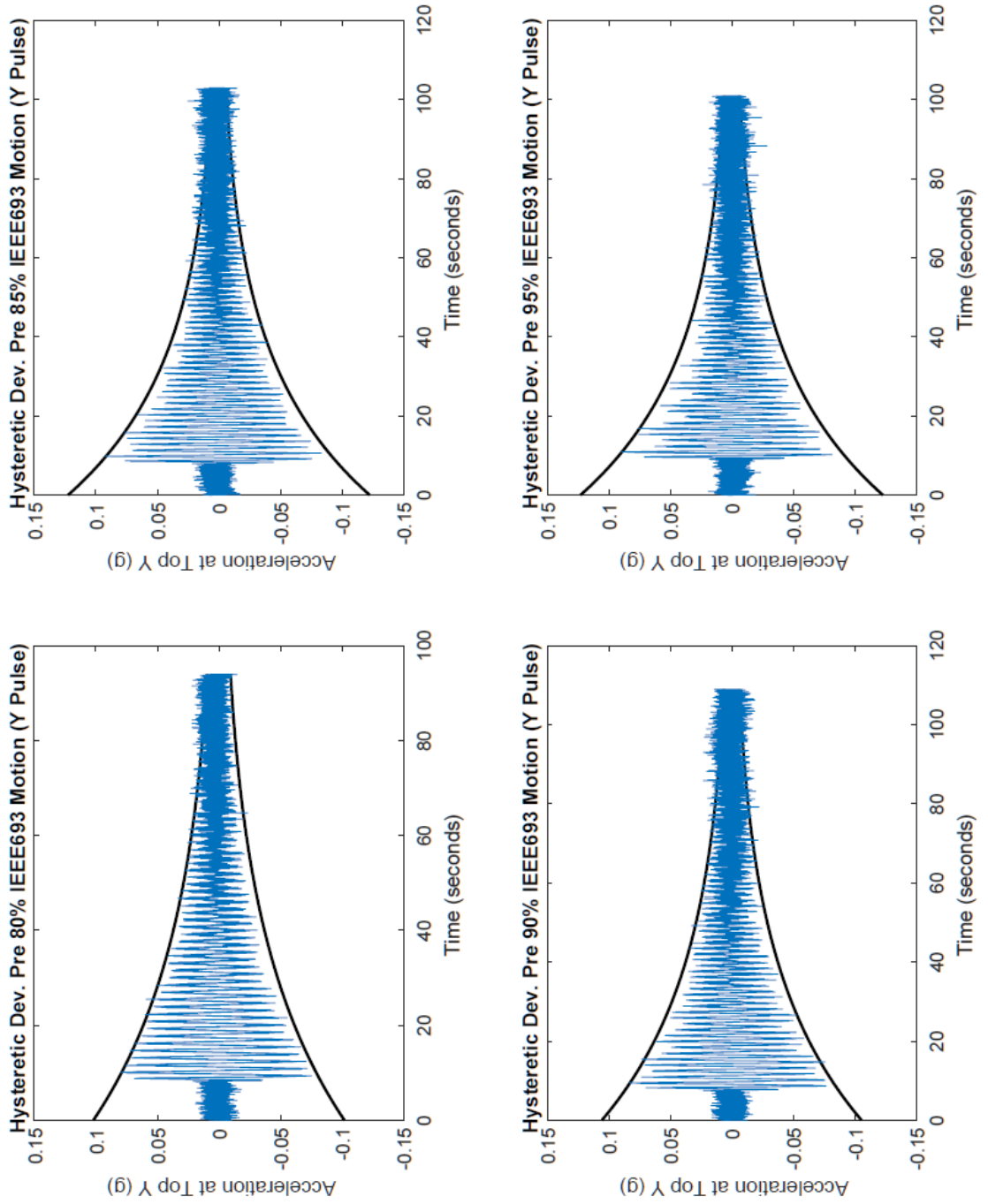


Figure 27-7: Hysteretic Device Retrofit Y-Damping 80-95%

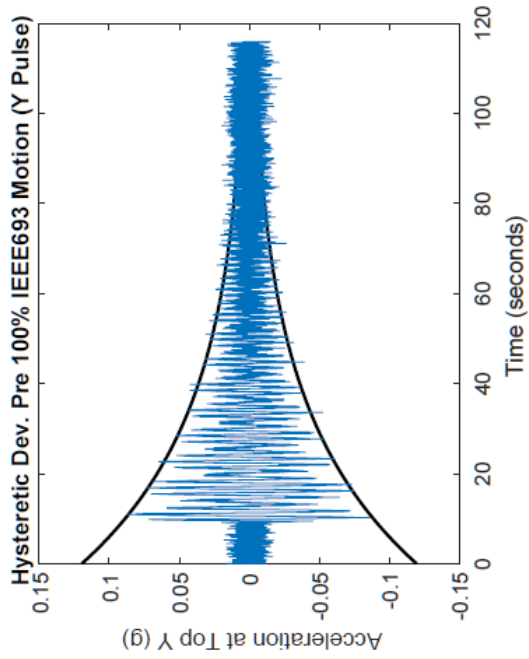


Figure 27-8: Hysteretic Device Retrofit Y-Damping 100%

28.0 APPENDIX J

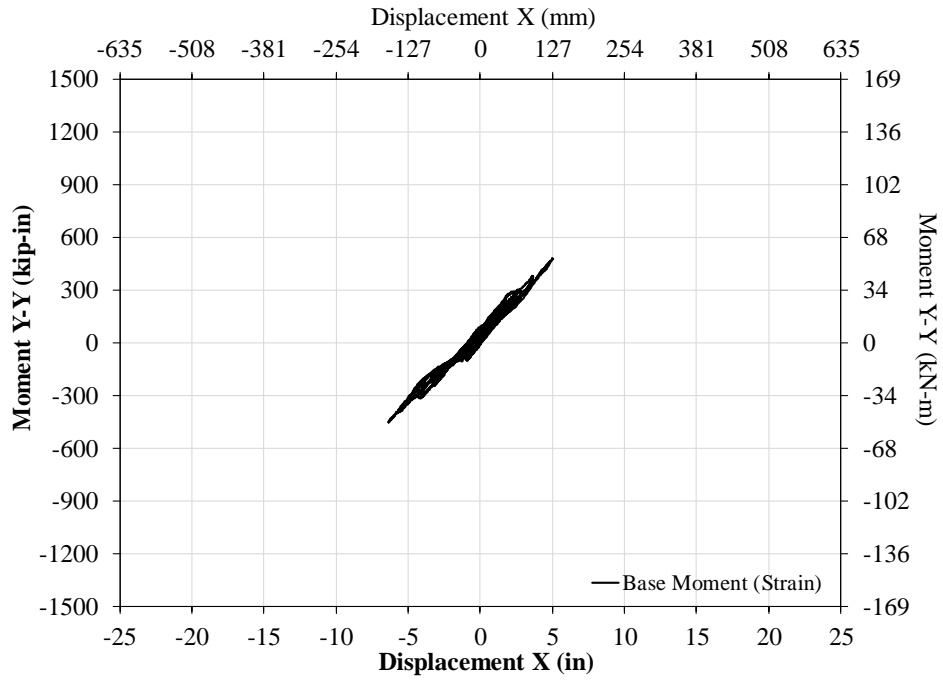


Figure 28-1: 20% 0.5g IEEE693 X-System Response w/ Hysteretic Device

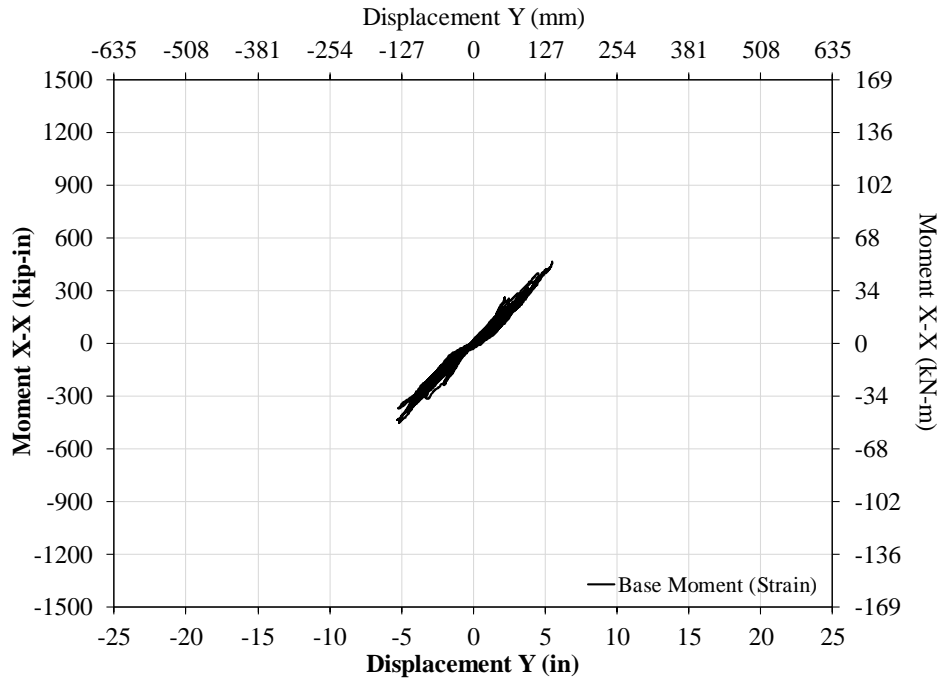


Figure 28-2: 20% 0.5g IEEE693 X-System Response w/ Hysteretic Device

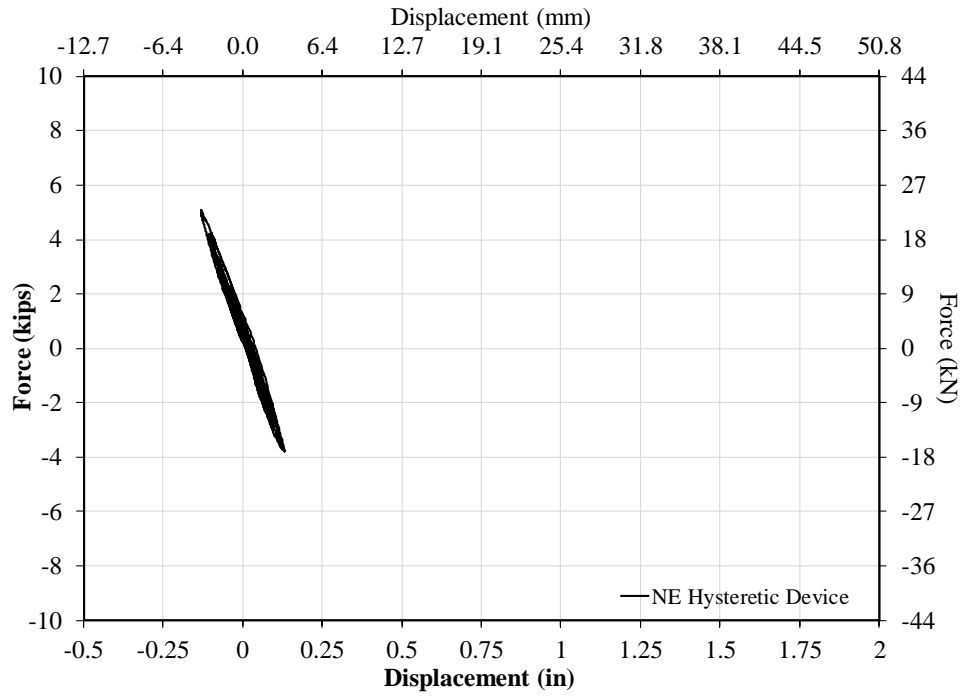


Figure 28-3: 20% 0.5g IEEE693 NE Hysteretic Device Response

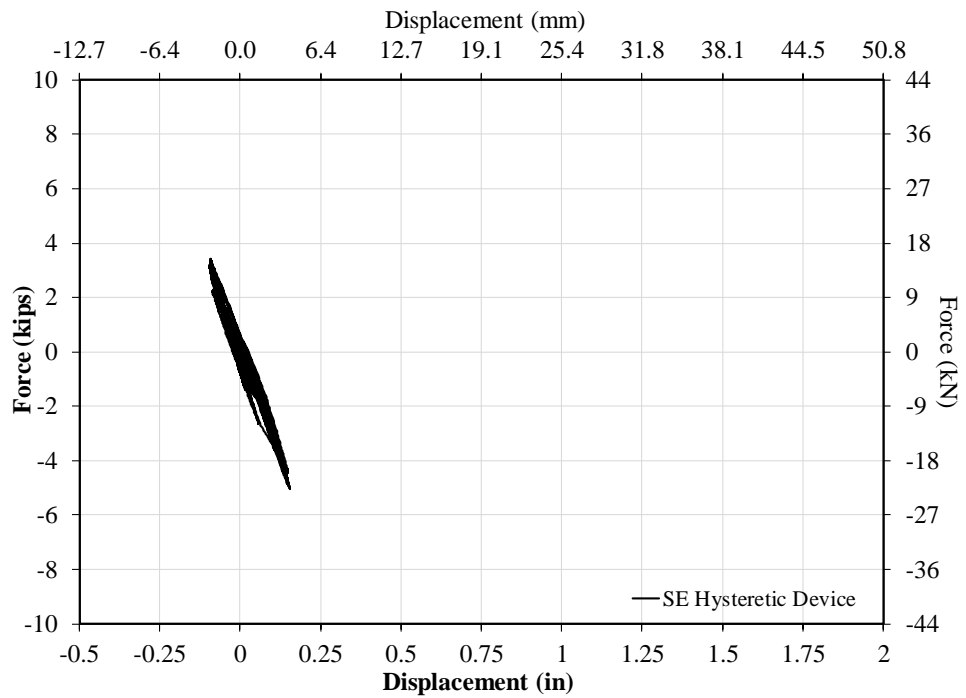


Figure 28-4: 20% 0.5g IEEE693 SE Hysteretic Device Response

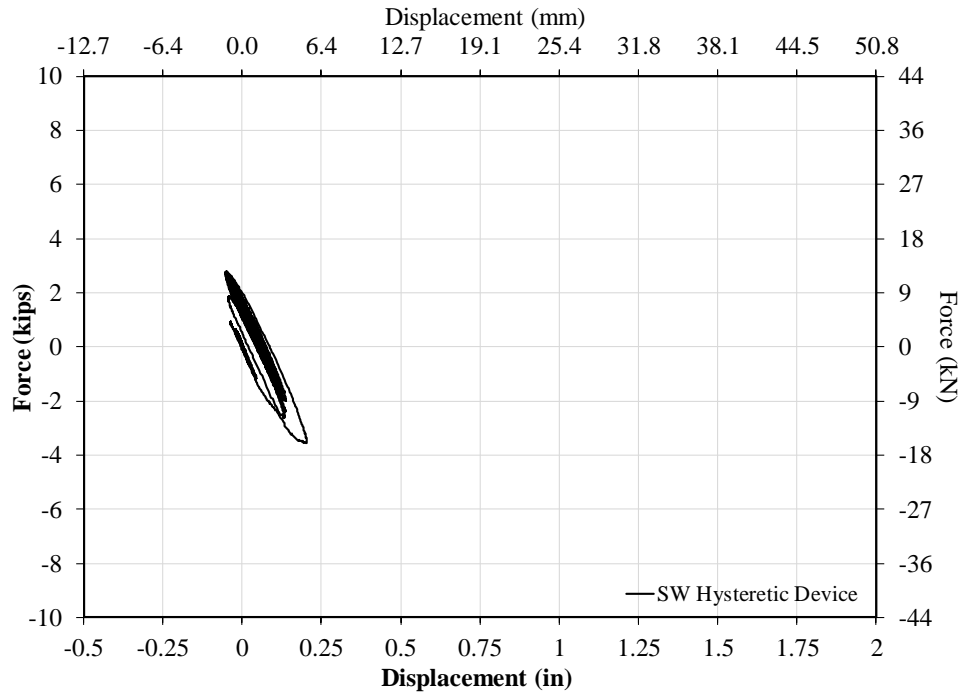


Figure 28-5: 20% 0.5g IEEE693 SW Hysteretic Device Response

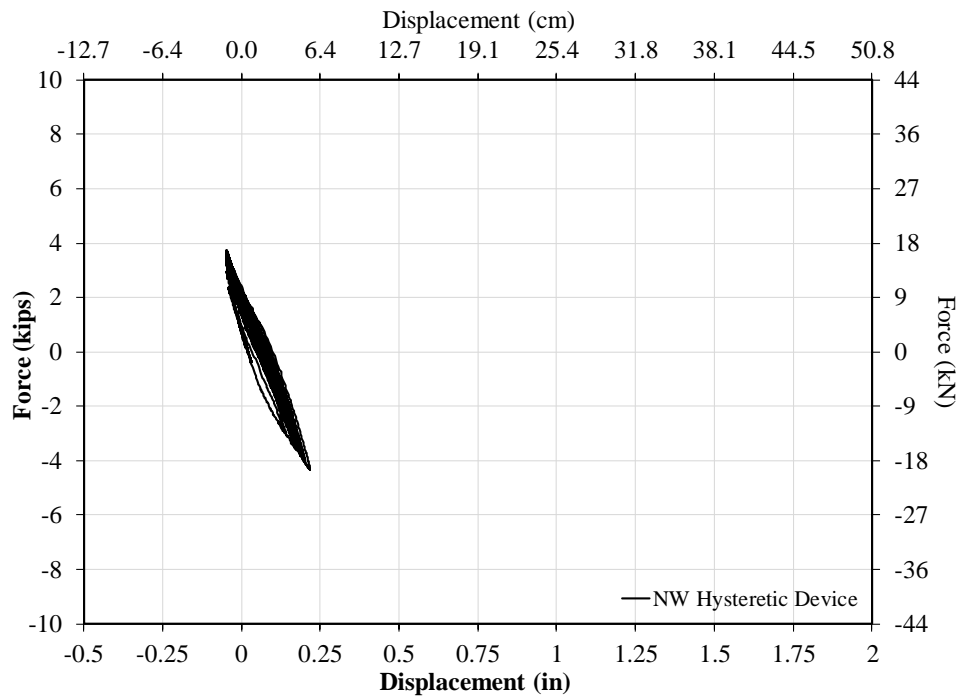


Figure 28-6: 20% 0.5g IEEE693 NW Hysteretic Device Response

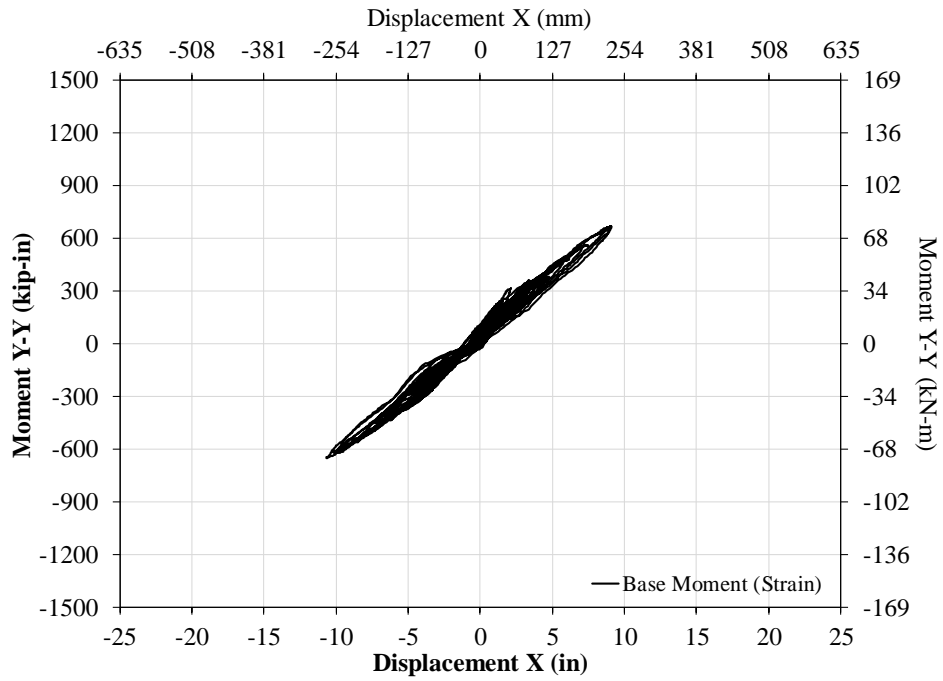


Figure 28-7: 50% 0.5g IEEE693 X-System Response w/ Hysteretic Device

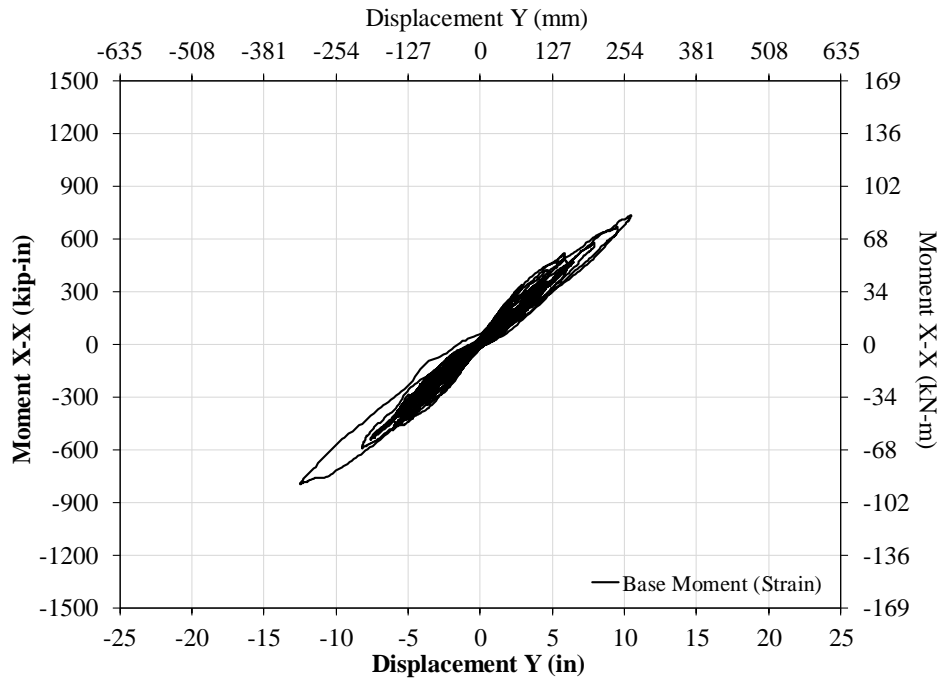


Figure 28-8: 50% 0.5g IEEE693 Y-System Response w/ Hysteretic Device

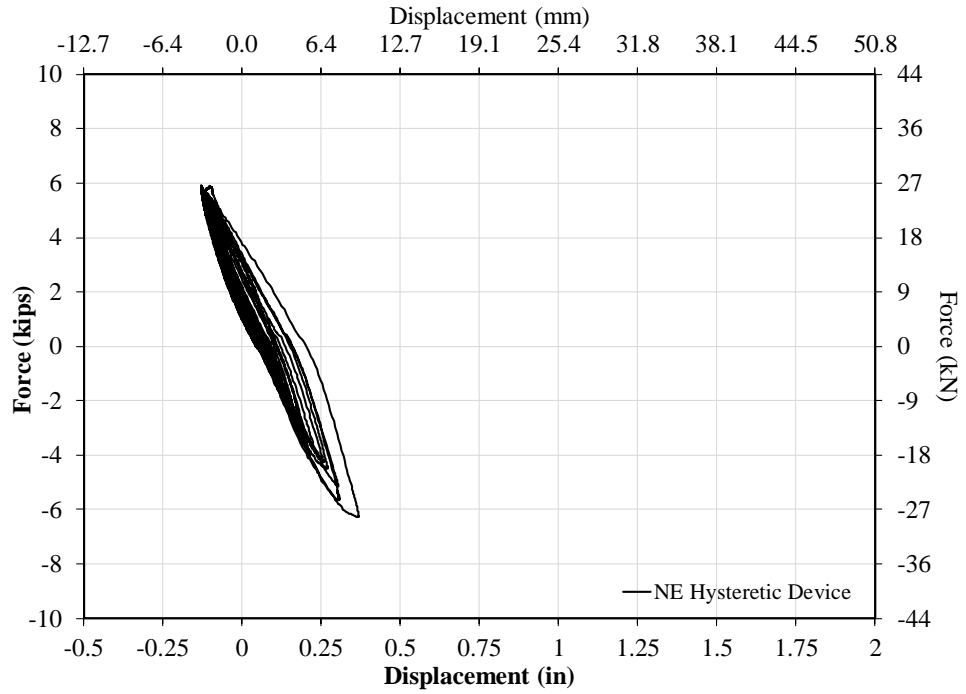


Figure 28-9: 50% 0.5g IEEE693 NE Hysteretic Device Response

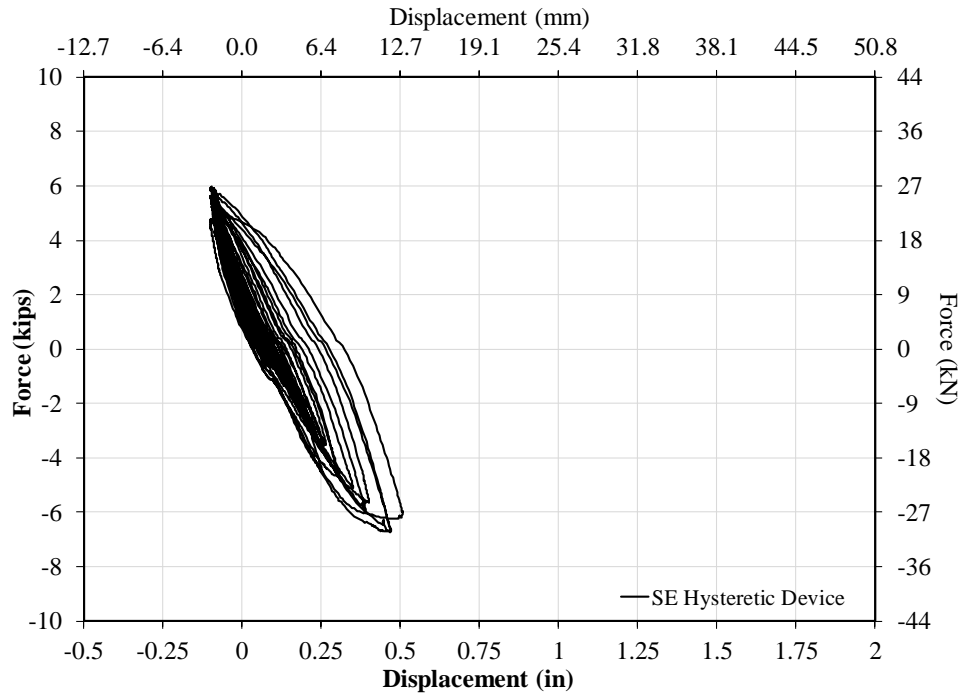


Figure 28-10: 20% 0.5g IEEE693 SE Hysteretic Device Response

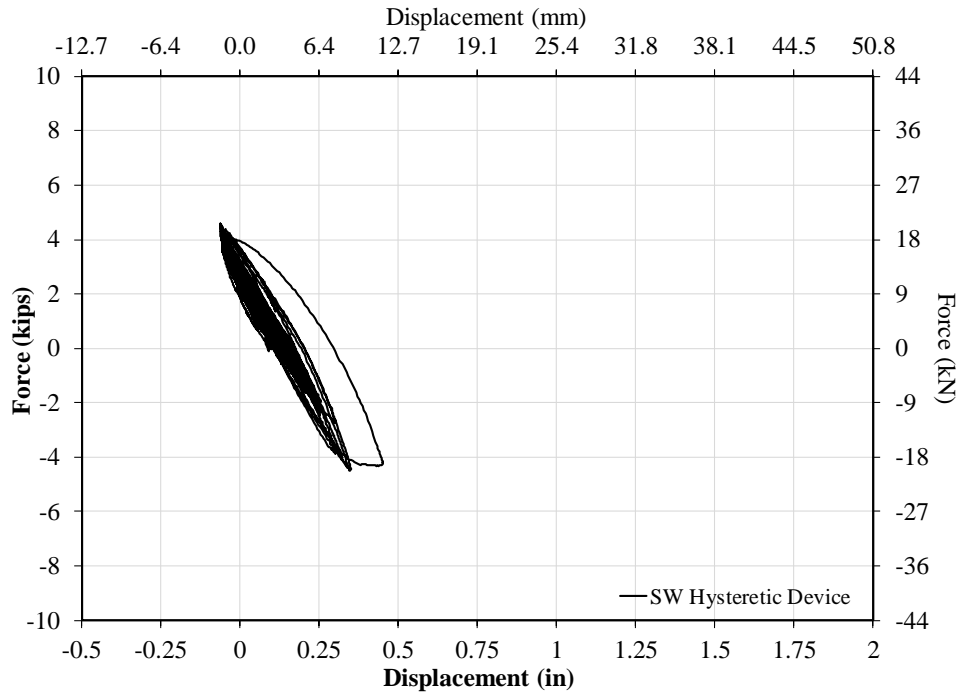


Figure 28-11: 50% 0.5g IEEE693 SW Hysteretic Device Response

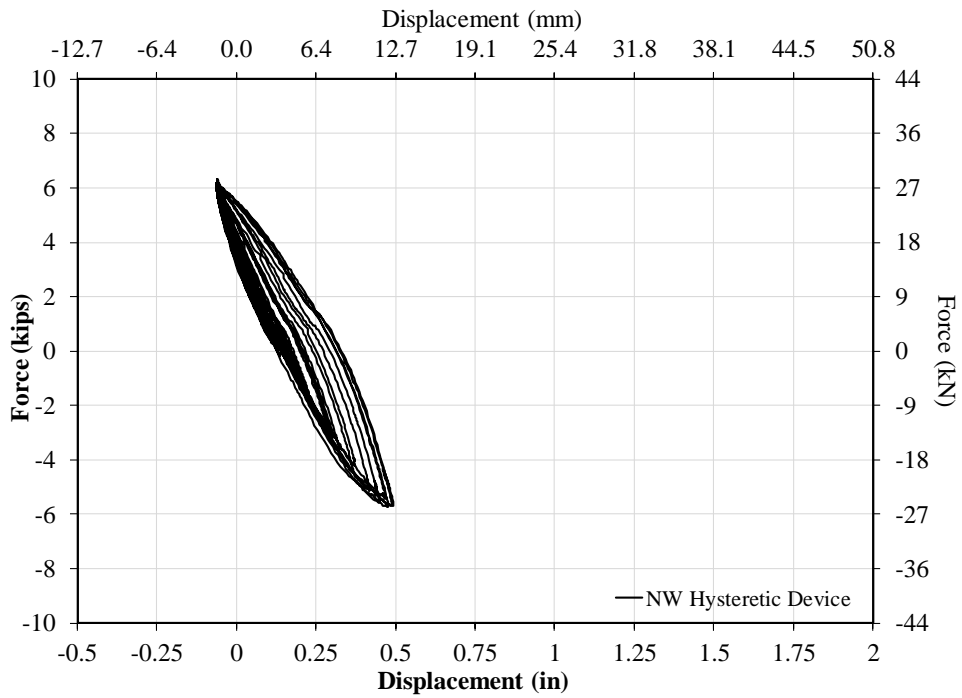


Figure 28-12: 50% 0.5g IEEE693 NW Hysteretic Device Response

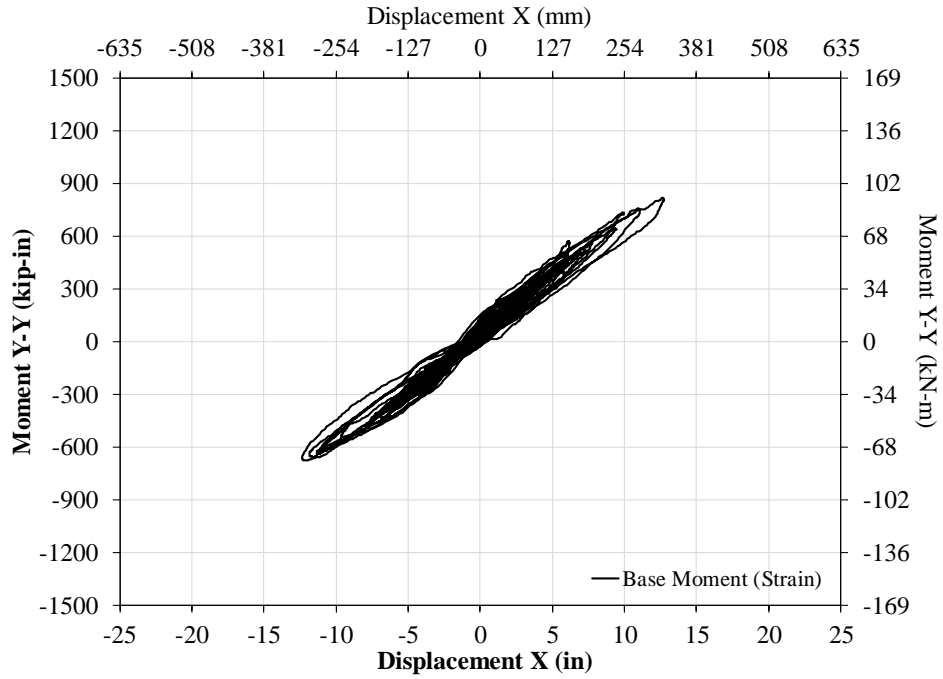


Figure 28-13: 75% 0.5g IEEE693 X-System Response w/ Hysteretic Device

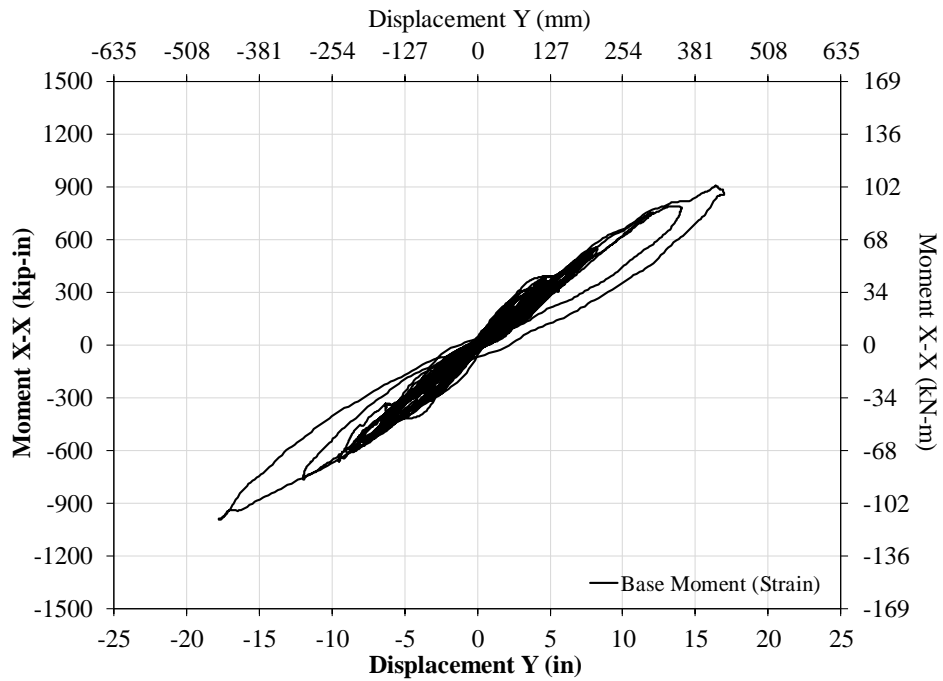


Figure 28-14: 75% 0.5g IEEE693 Y-System Response w/ Hysteretic Device

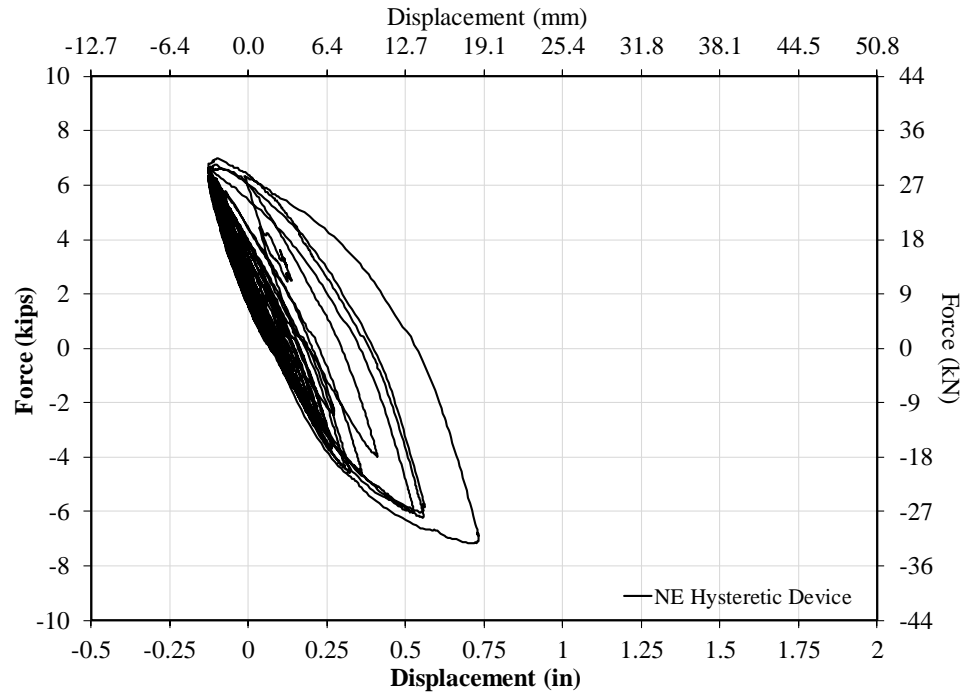


Figure 28-15: 75% 0.5g IEEE693 NE Hysteretic Device Response

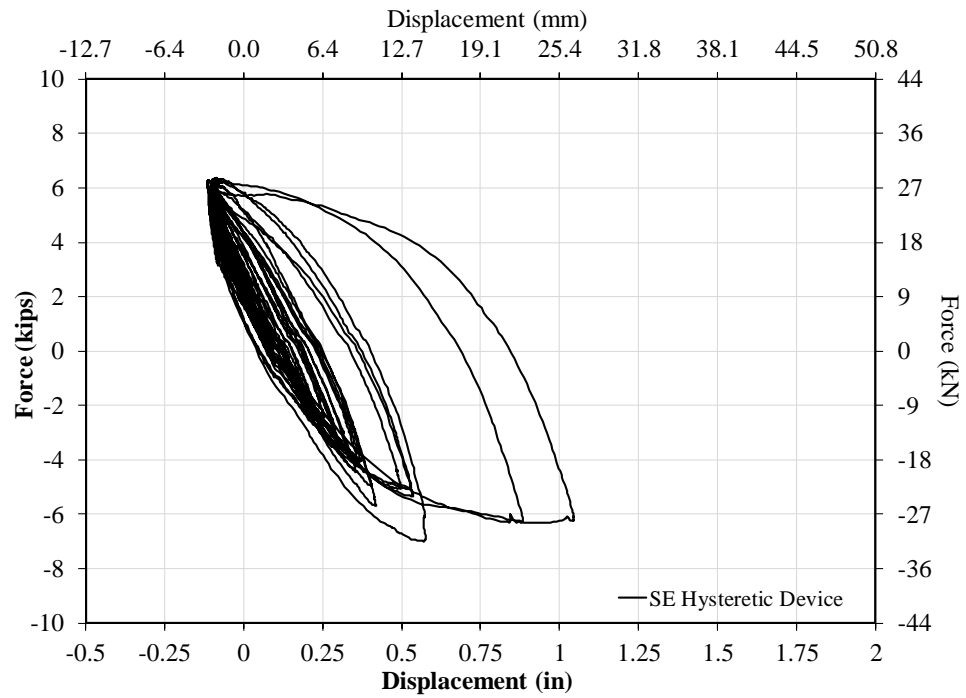


Figure 28-16: 75% 0.5g IEEE693 SE Hysteretic Device Response

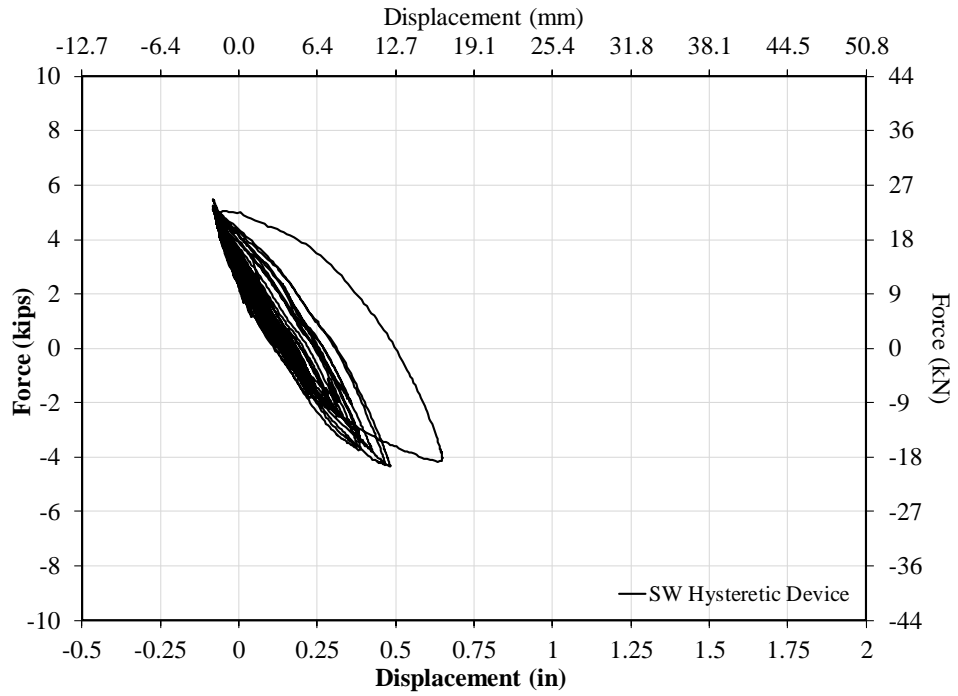


Figure 28-17: 75% 0.5g IEEE693 SW Hysteretic Device Response

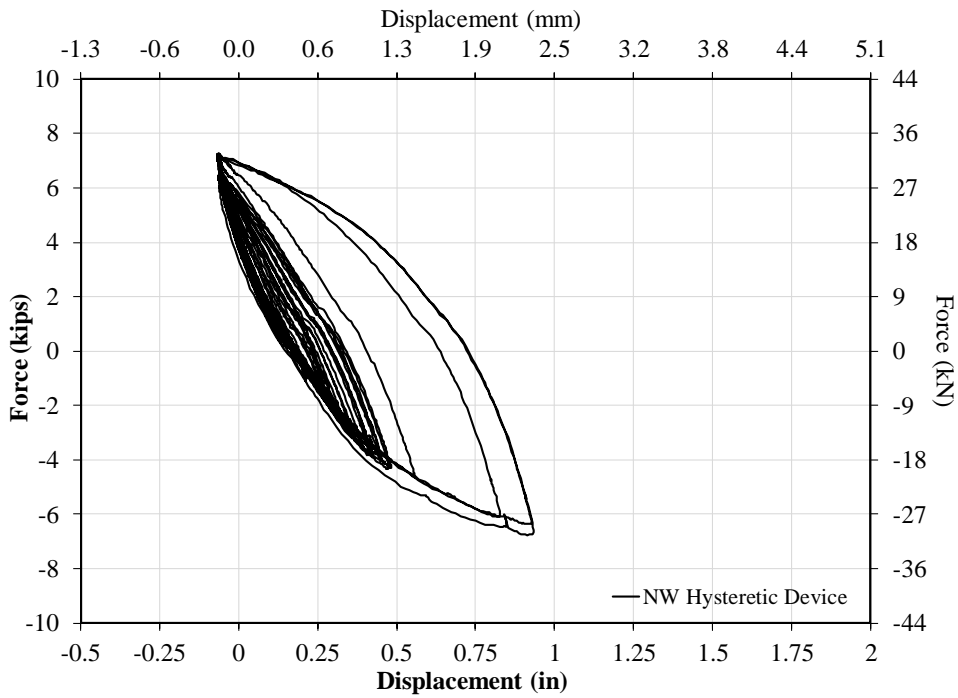


Figure 28-18: 75% 0.5g IEEE693 NW Hysteretic Device Response

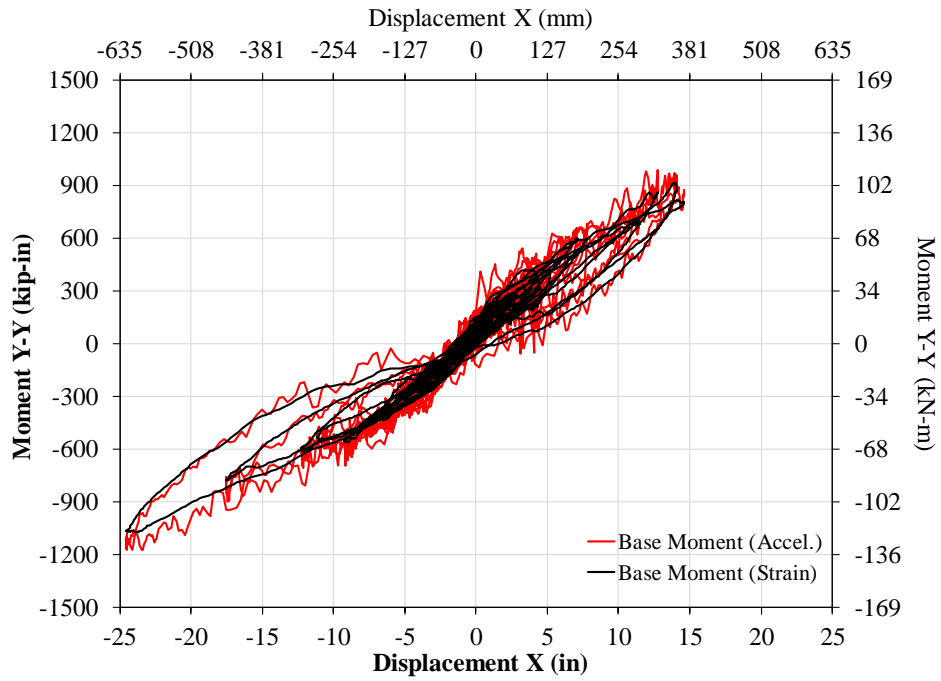


Figure 28-19: 100% 0.5g IEEE693 X-System Response w/ Hysteretic Device

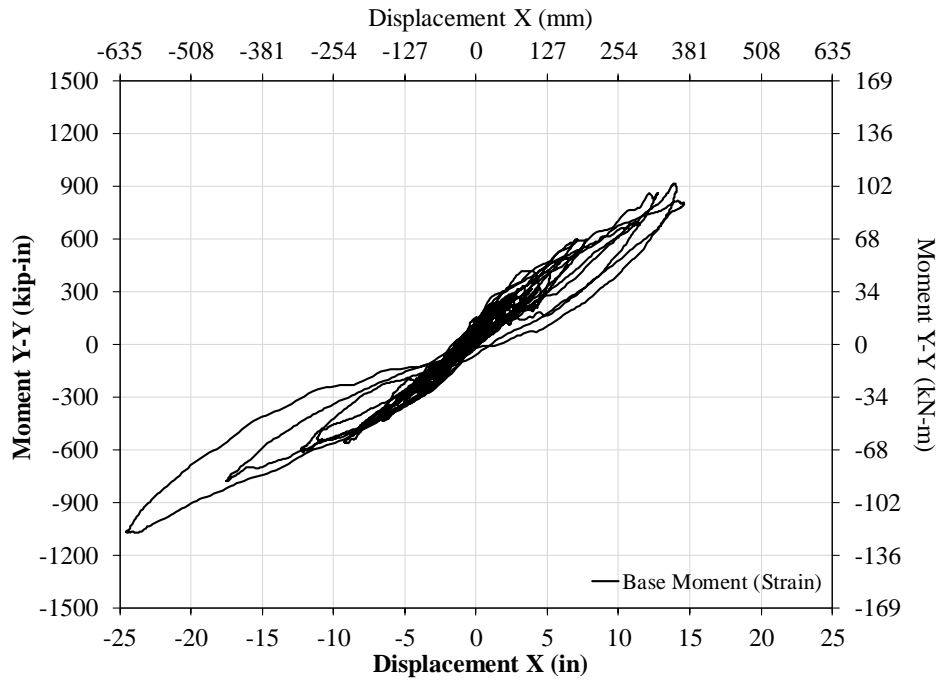


Figure 28-20: 100% 0.5g IEEE693 X-System Response w/ Hysteretic Device

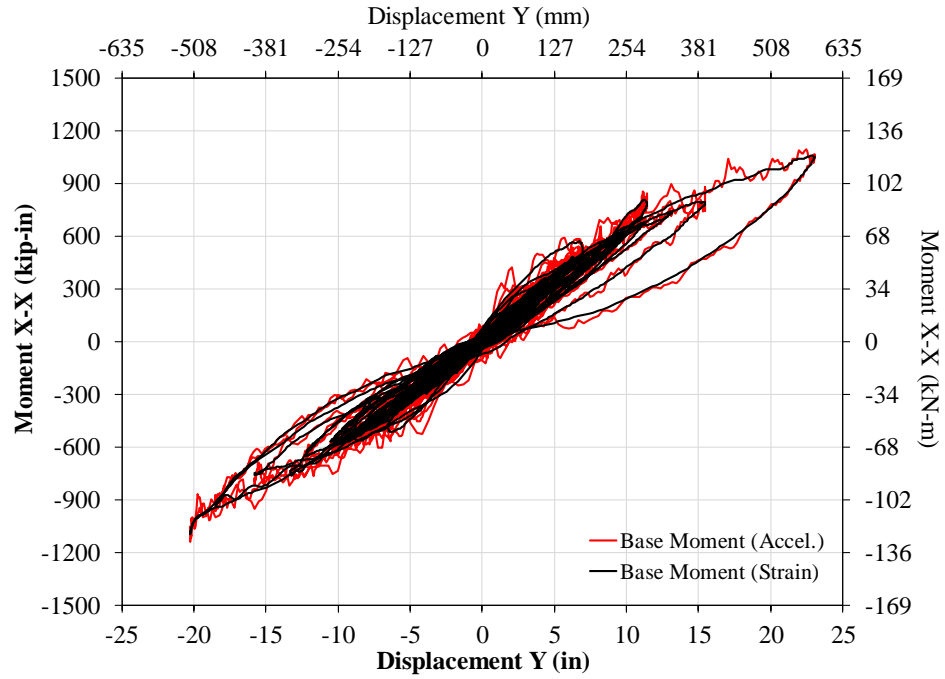


Figure 28-21: 100% 0.5g IEEE693 Y-System Response w/ Hysteretic Device

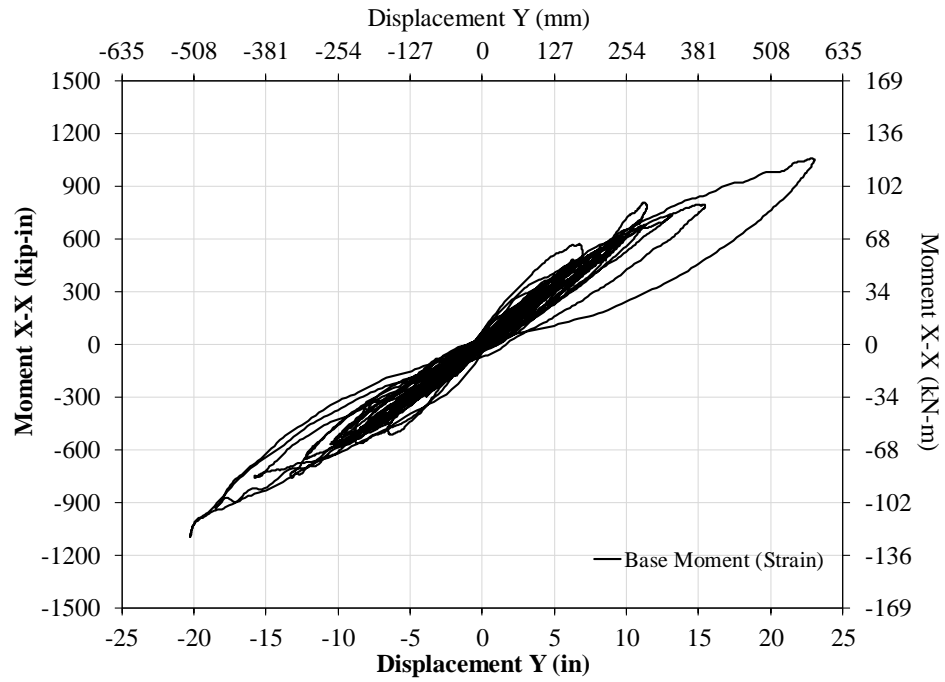


Figure 28-22: 100% 0.5g IEEE693 Y-System Response w/ Hysteretic Device

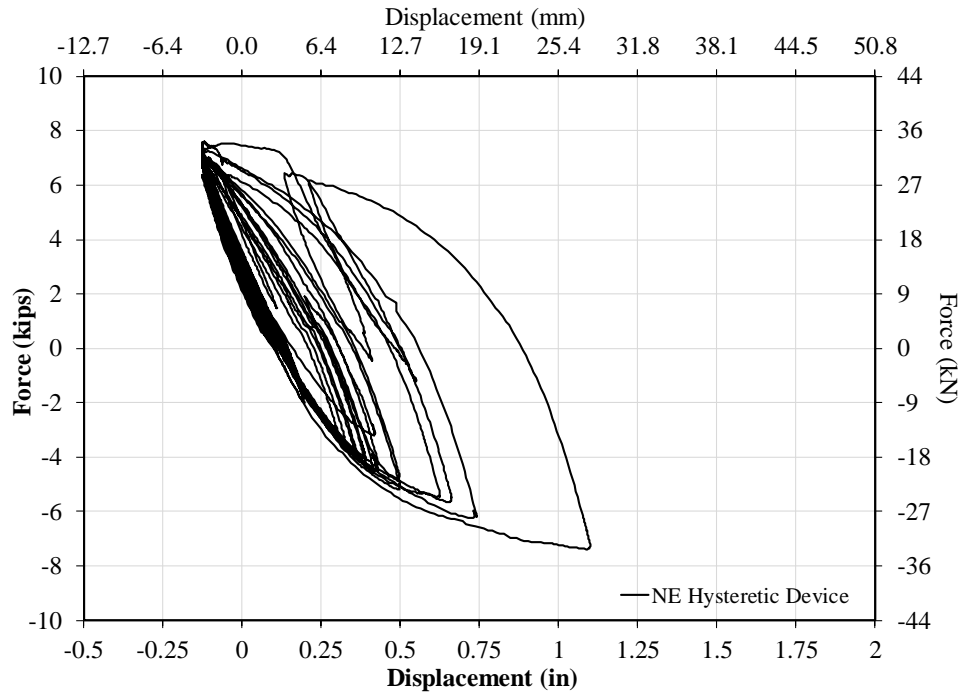


Figure 28-23: 100% 0.5g IEEE693 NE Hysteretic Device Response

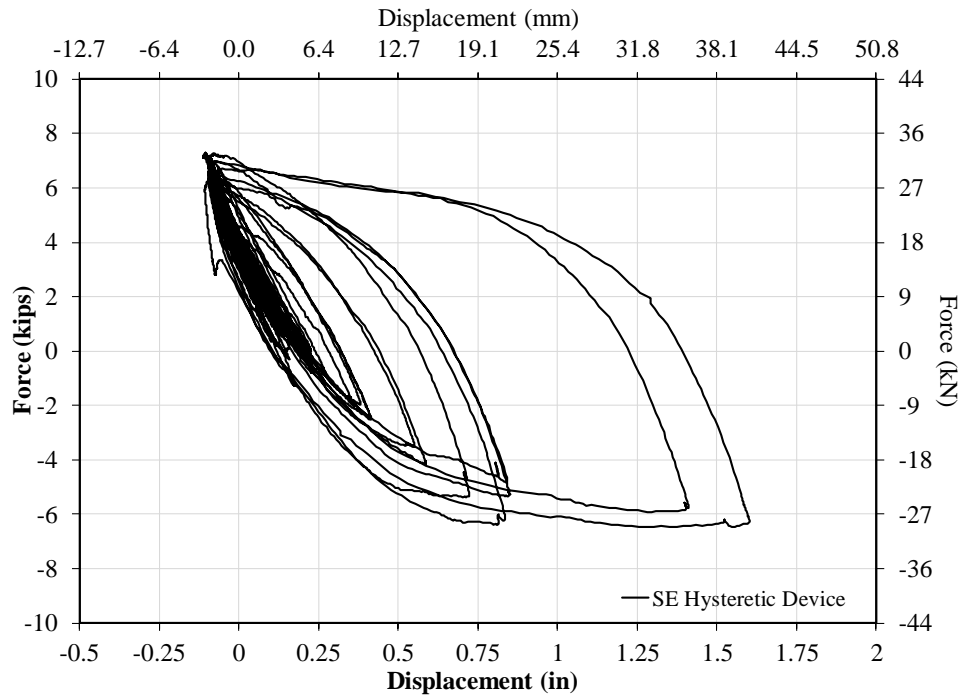


Figure 28-24: 100% 0.5g IEEE693 SE Hysteretic Device Response

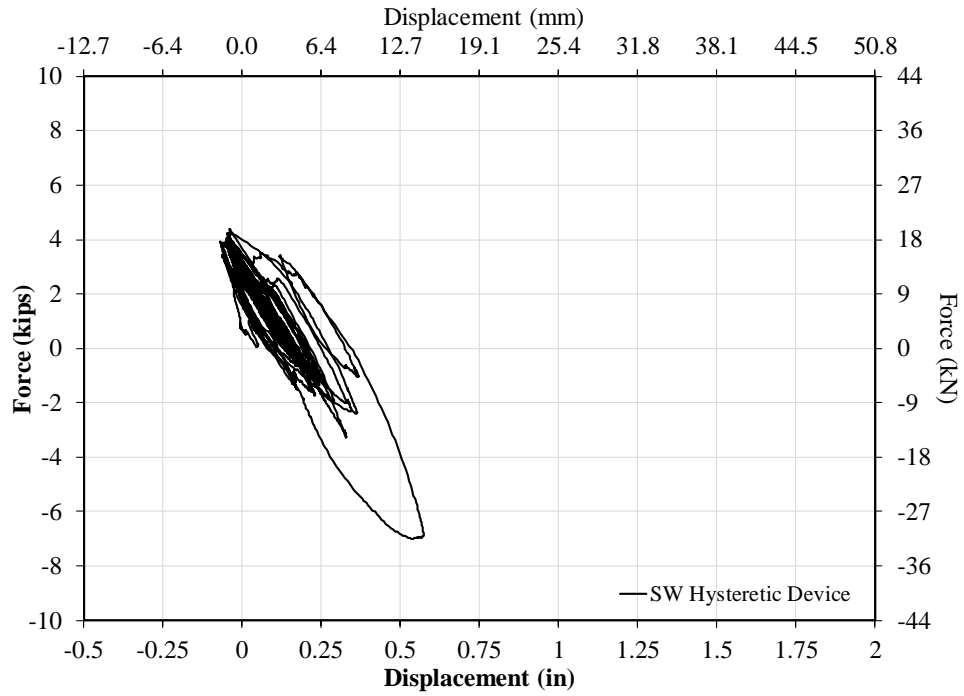


Figure 28-25: 100% 0.5g IEEE693 SW Hysteretic Device Response

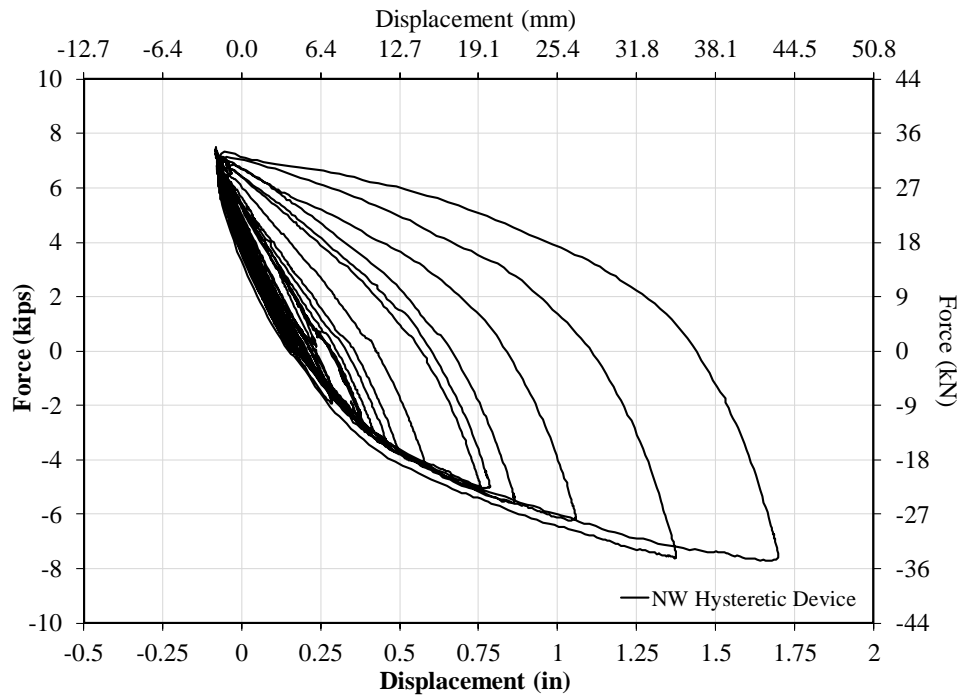


Figure 28-26: 100% 0.5g IEEE693 NW Hysteretic Device Response

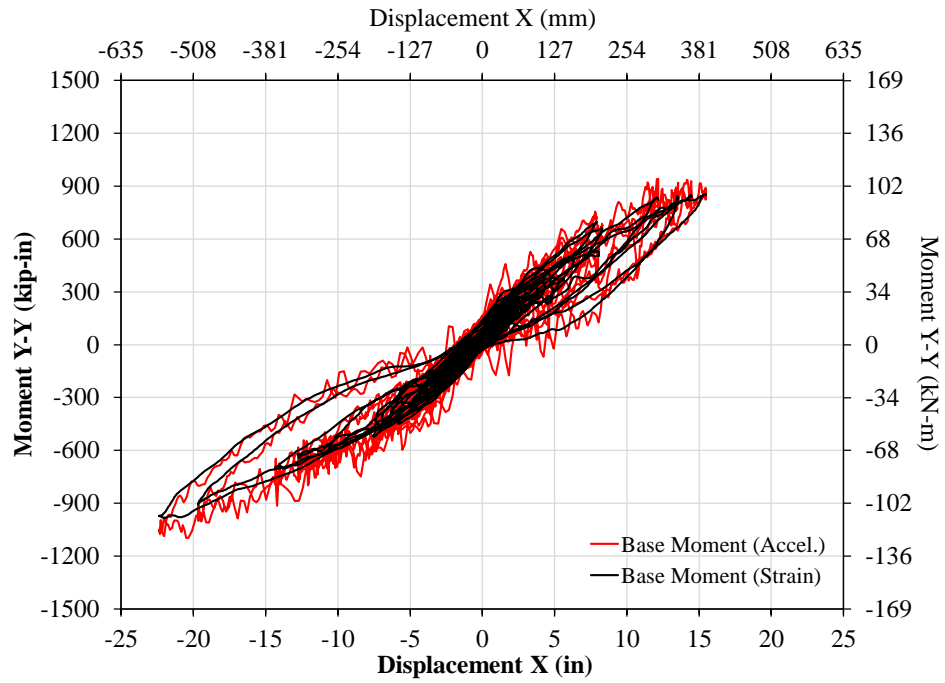


Figure 28-27: 100% 0.5g IEEE693 X-System Response w/ Virgin Hysteretic Device

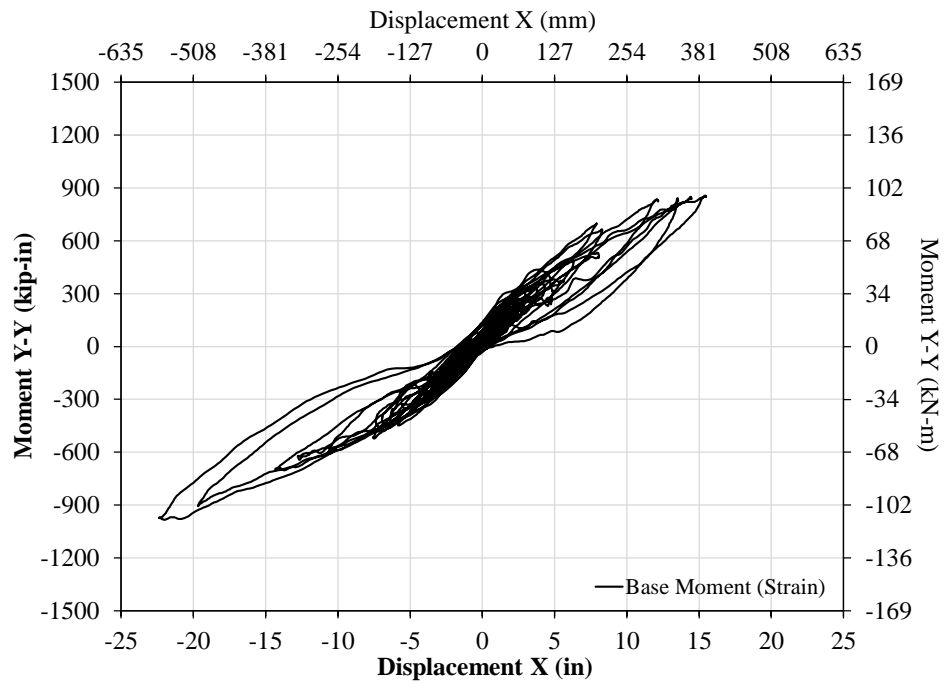


Figure 28-28: 100% 0.5g IEEE693 X-System Response w/ Virgin Hysteretic Device

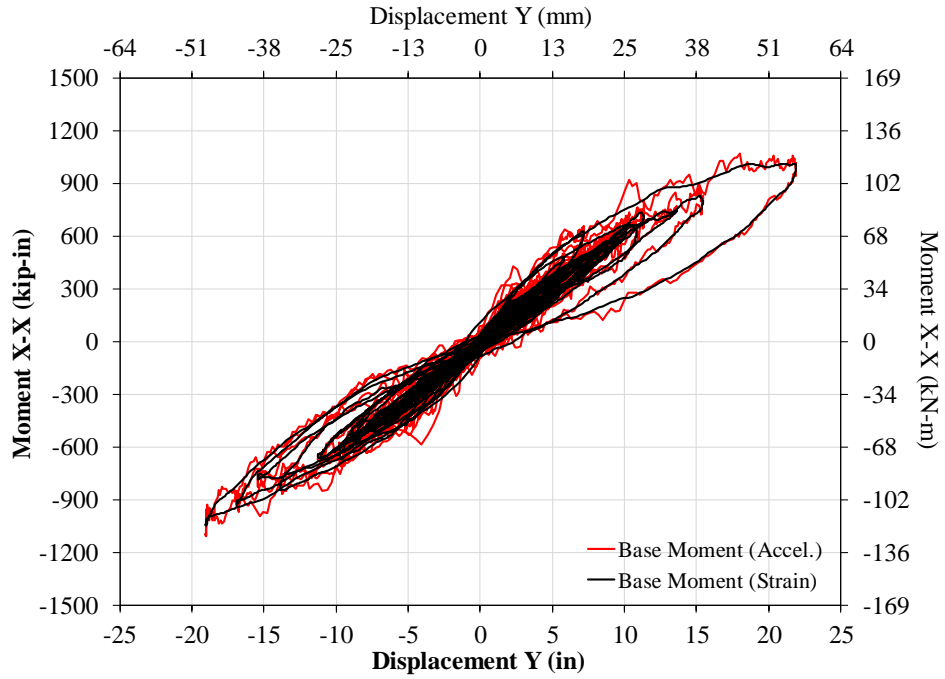


Figure 28-29: 100% 0.5g IEEE693 Y-System Response w/ Virgin Hysteretic Device

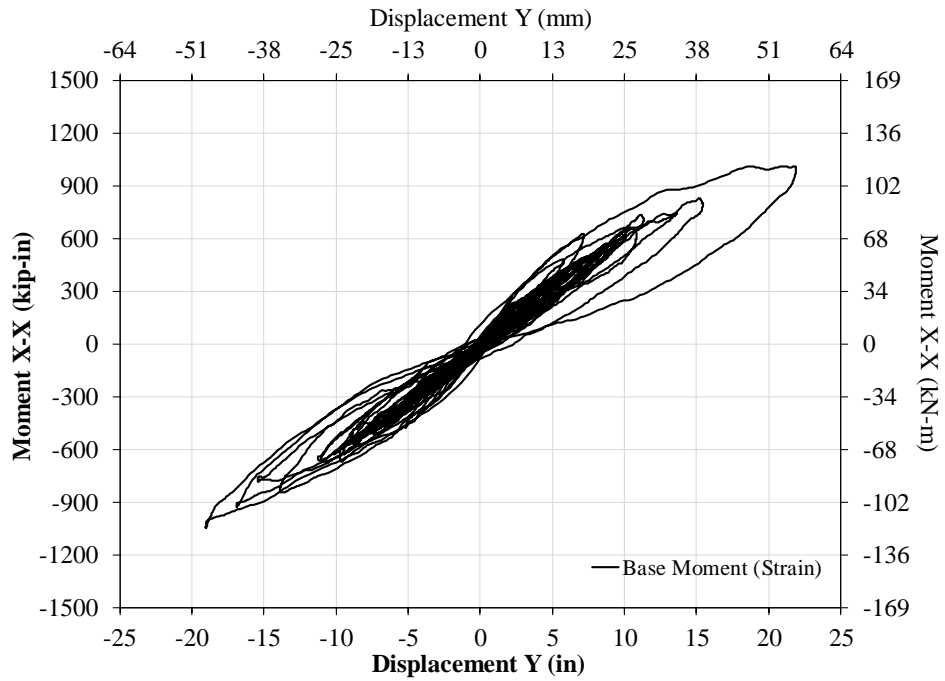


Figure 28-30: 100% 0.5g IEEE693 Y-System Response w/ Virgin Hysteretic Device

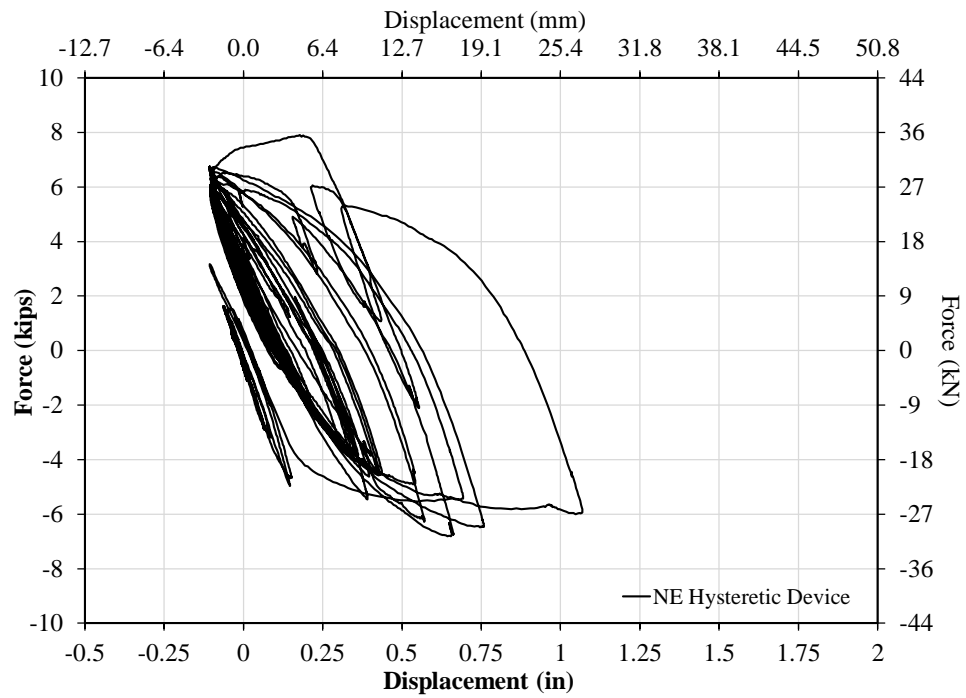


Figure 28-31: 100% 0.5g IEEE693 NE Virgin Hysteretic Device Response

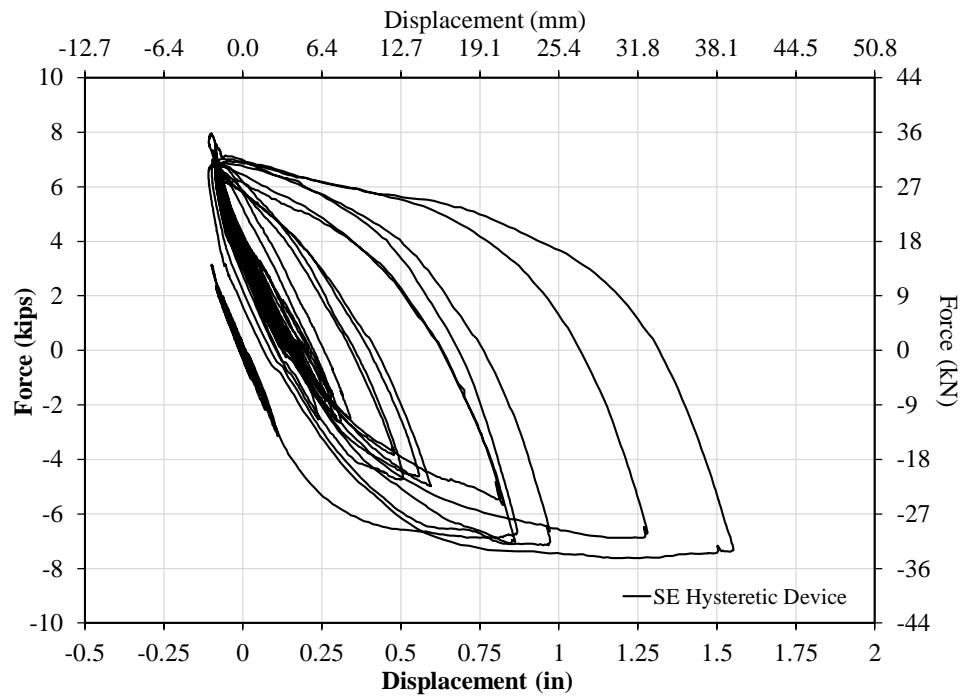


Figure 28-32: 100% 0.5g IEEE693 SE Virgin Hysteretic Device Response

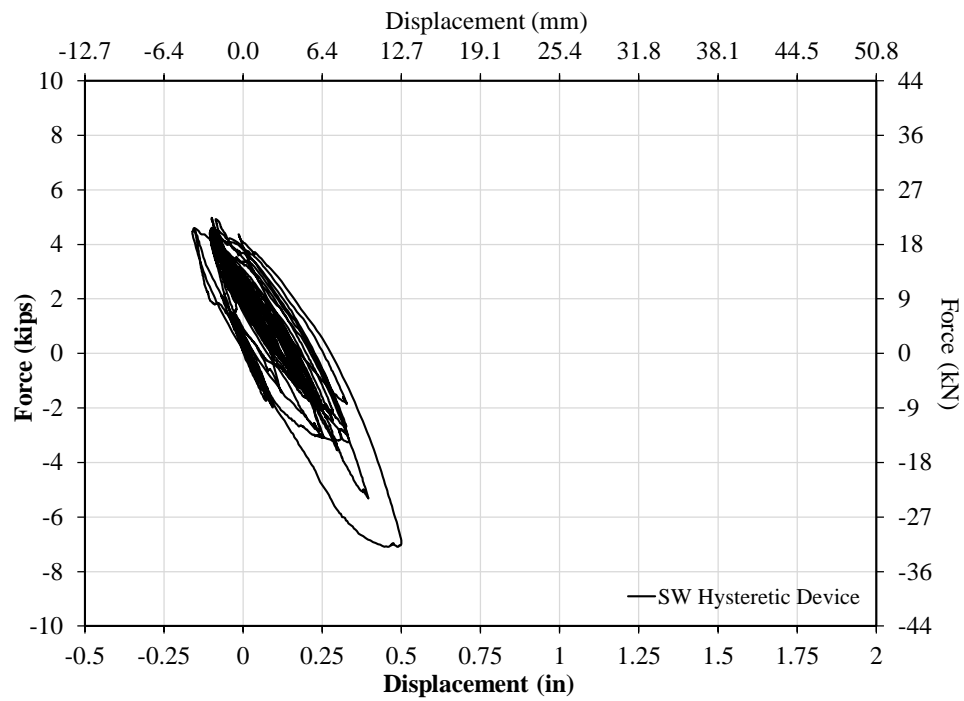


Figure 28-33: 100% 0.5g IEEE693 NE SW Virgin Hysteretic Device Response

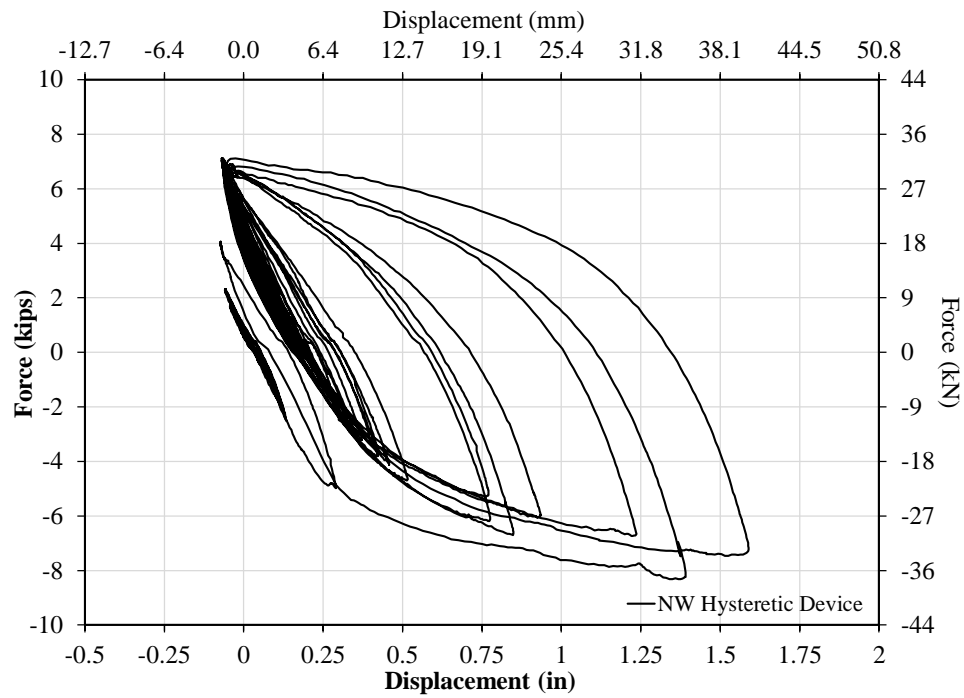


Figure 28-34: 100% 0.5g IEEE693 NW Virgin Hysteretic Device Response

29.0 APPENDIX K

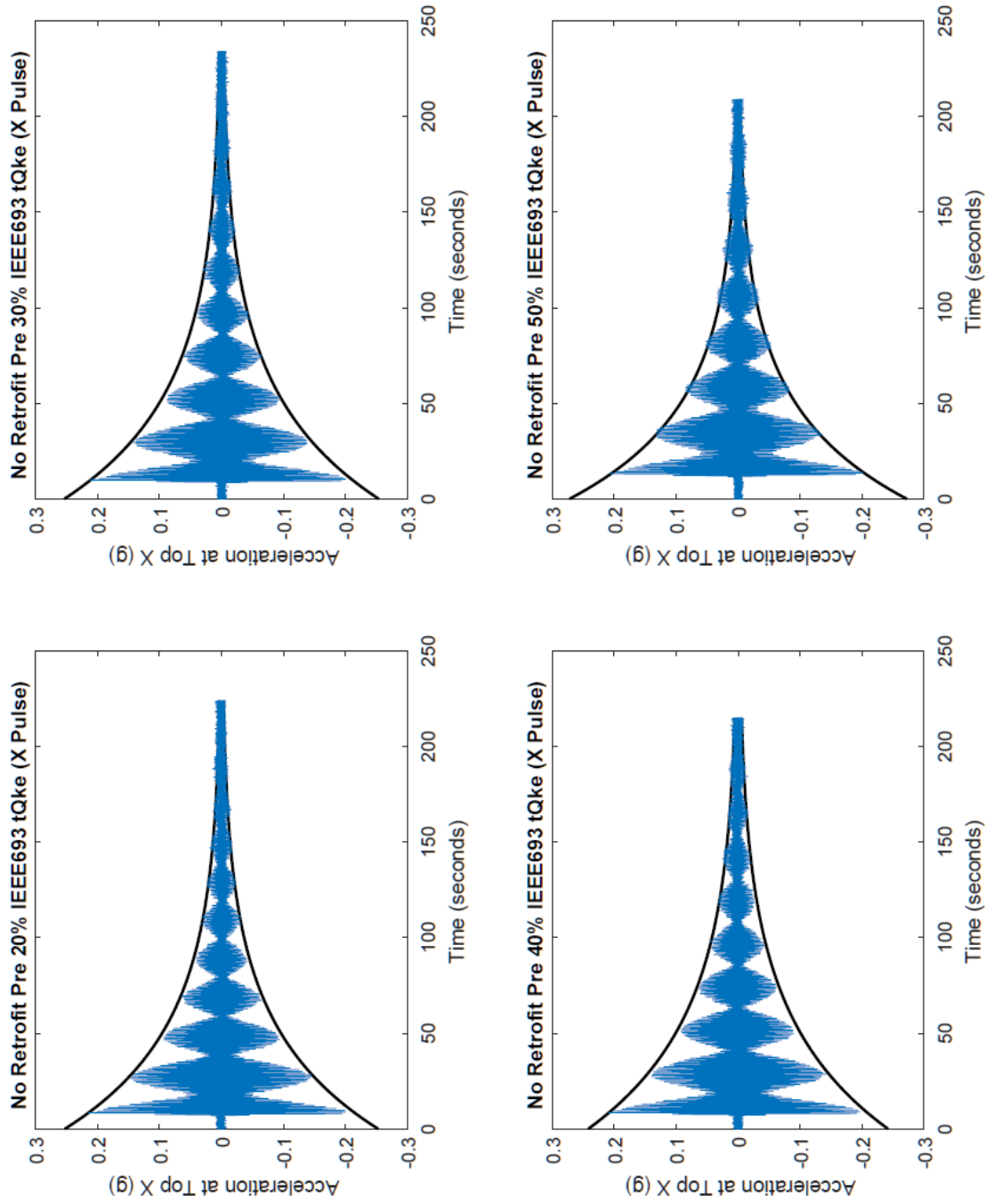


Figure 29-1: Non-Retrofitted X-Damping 20-50%

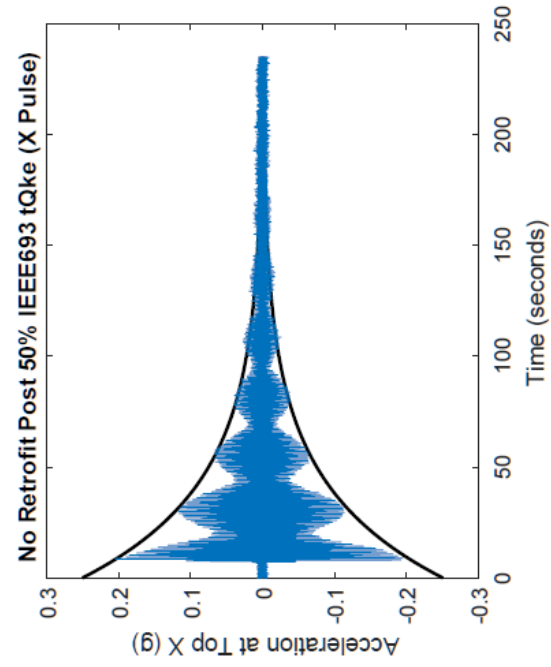


Figure 29-2: Non-Retrofitted X-Damping 50%

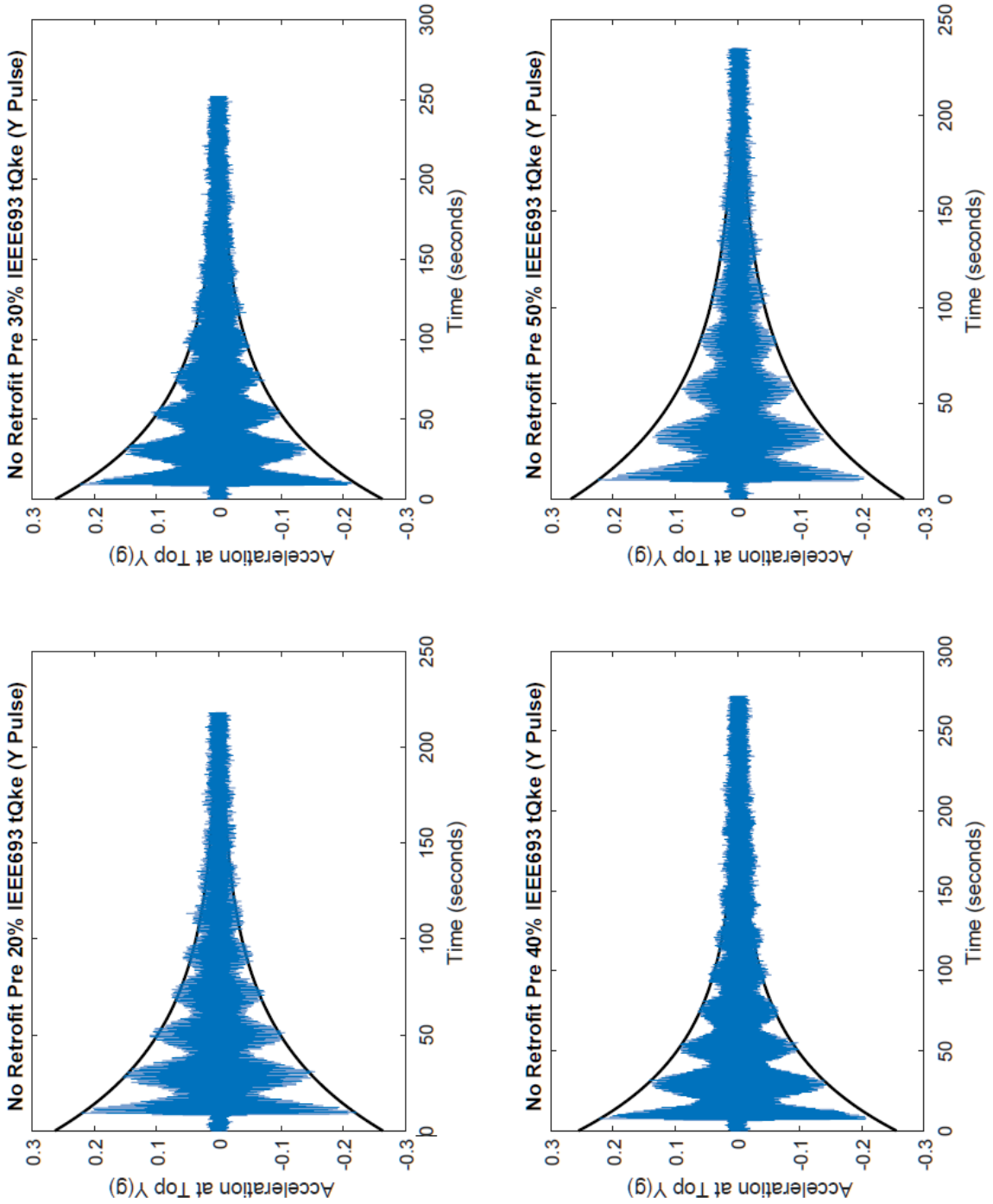


Figure 29-3: Non-Retrofitted Y-Damping 20-50%

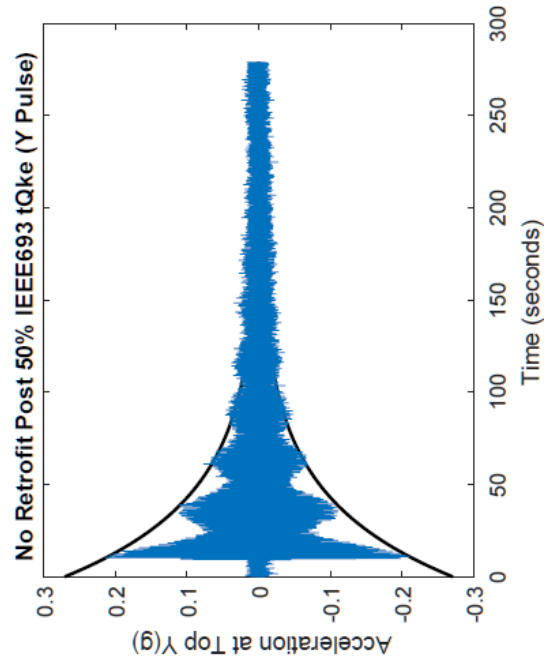


Figure 29-4: Non-Retrofitted Y-Damping 50%

30.0 APPENDIX L

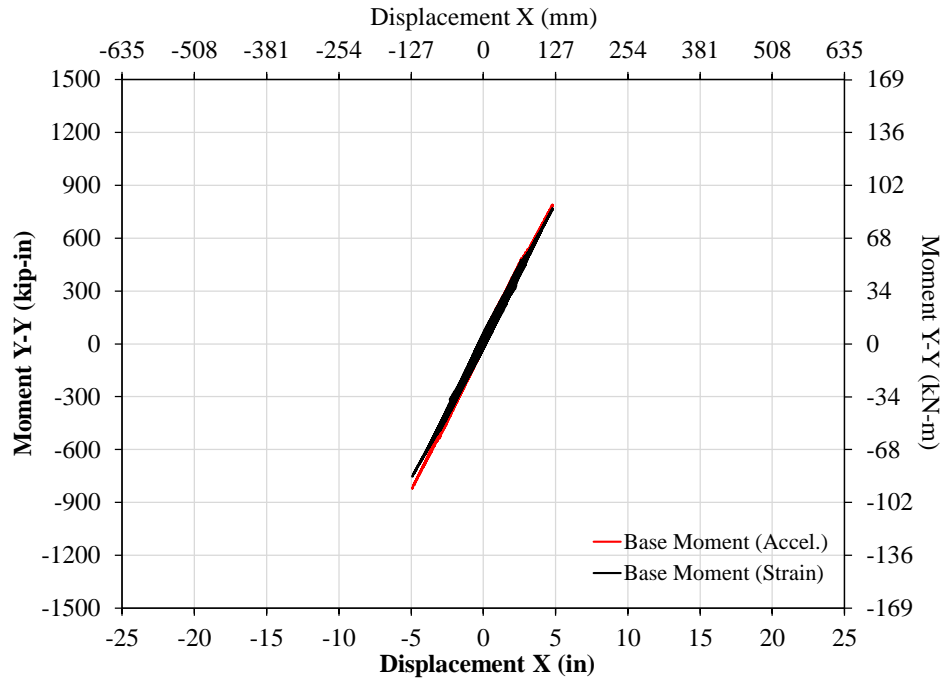


Figure 30-1: 20% 0.5g IEEE693 Non-Retrofitted X-System Response

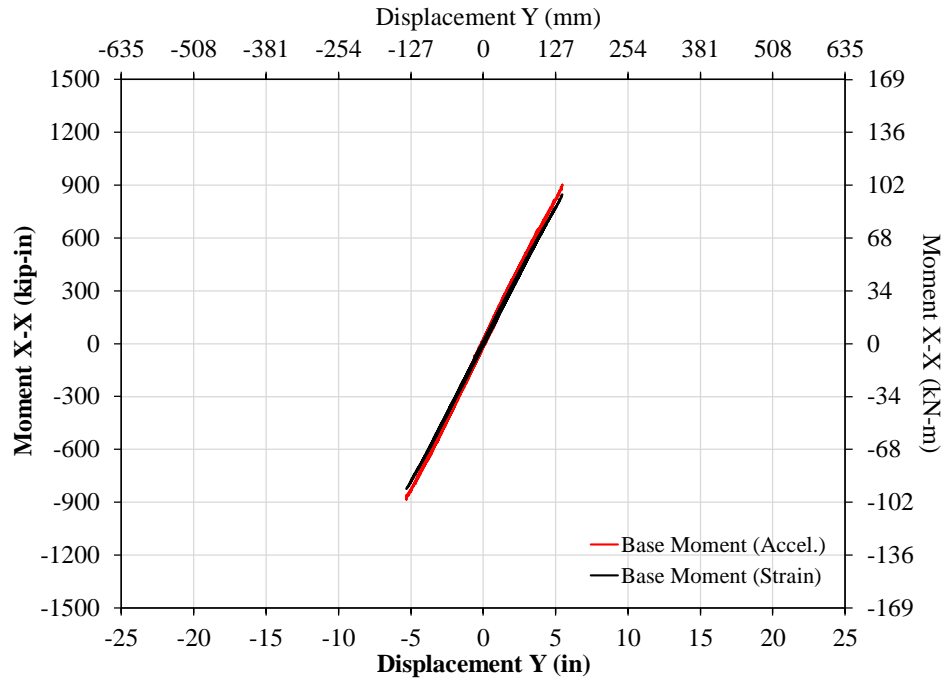


Figure 30-2: 20% 0.5g IEEE693 Non-Retrofitted Y-System Response

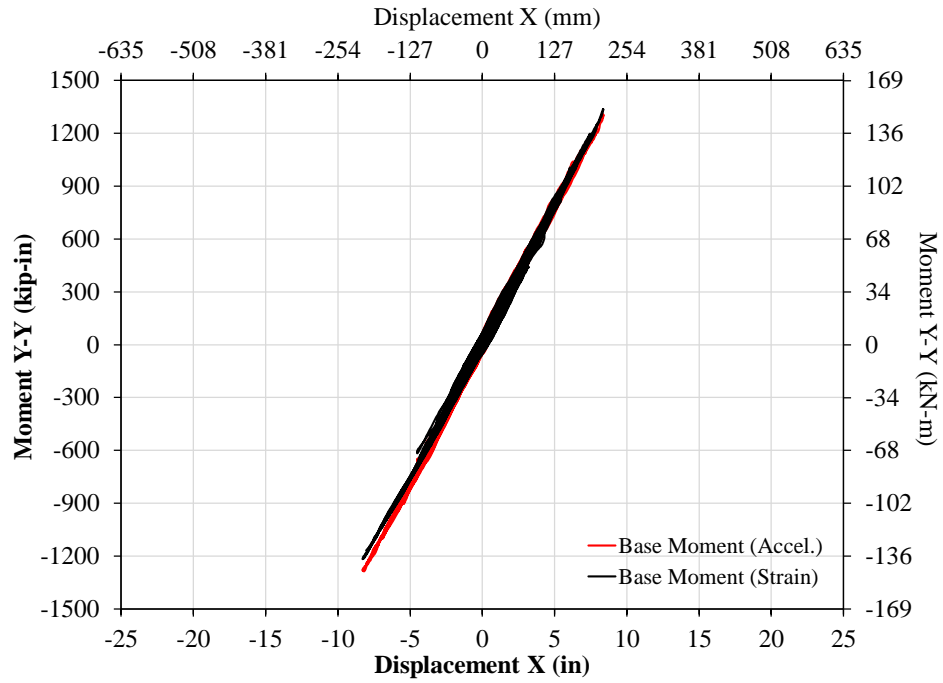


Figure 30-3: 40% 0.5g IEEE693 Non-Retrofitted X-System Response

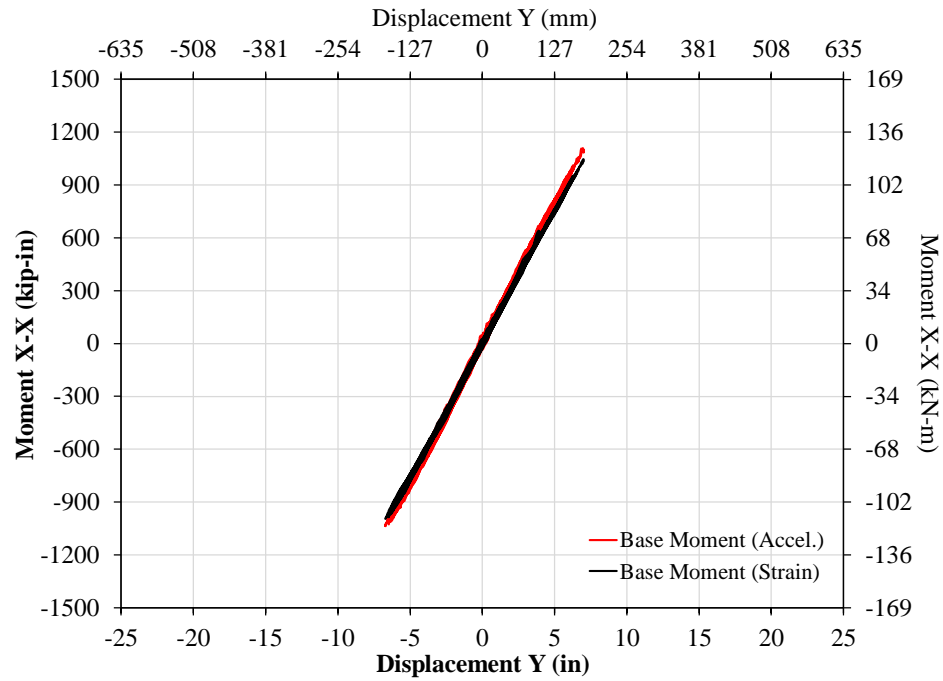


Figure 30-4: 40% 0.5g IEEE693 Non-Retrofitted Y-System Response